

Princetonlaan 6  
3584 CB Utrecht  
P.O. Box 80015  
3508 TA Utrecht  
The Netherlands

[www.tno.nl](http://www.tno.nl)

T +31 88 866 42 56  
F +31 88 866 44 75

## TNO report

**TNO 2019 R11635**

# CO<sub>2</sub> storage feasibility in the P18-2 depleted gas field

Date	October 2019
Author(s)	Filip Neele Ton Wildenborg Kees Geel Daniel Loeve Lies Peters Siavash Kahrobaei Thibault Candela Mariëlle Koenen Paul Hopmans Kaj van der Valk Bogdan Orlic Vincent Vandeweijer

\*

Copy no	
No. of copies	
Number of pages	232 (incl. appendices)
Number of appendices	
Sponsor	
Project name	P18-2 storage study
Project number	060.35859

All rights reserved.

No part of this publication may be reproduced and/or published by print, photoprint, microfilm or any other means without the previous written consent of TNO.

In case this report was drafted on instructions, the rights and obligations of contracting parties are subject to either the General Terms and Conditions for commissions to TNO, or the relevant agreement concluded between the contracting parties. Submitting the report for inspection to parties who have a direct interest is permitted.

© 2019 TNO

## Summary

### *Objective*

This study presents the results from a CO<sub>2</sub> storage feasibility study on the P18-2 depleted gas field that is located in the Netherlands offshore. The aim of the study was to understand the risks associated with injecting CO<sub>2</sub> into the field, to outline injection strategies that lead to safe and secure storage and, finally, to propose an approach to risk management and monitoring during injection. The results from this study are to form the geoscientific basis for a CO<sub>2</sub> storage permit application.

### *Background*

The study was carried out for the Porthos consortium that plans to transport CO<sub>2</sub> from several industrial sources in the Port of Rotterdam to three P18 fields operated by Taqa: P18-2, P18-4 and P18-6. TAQA already obtained a storage permit for the P18-4 field in 2013, with the aim to store CO<sub>2</sub> for the ROAD project, with a mass of about 5 Mt. However, the ROAD project was cancelled in 2017.

The Porthos consortium builds onto the work done by the ROAD project. The consortium plans to transport and store an amount of CO<sub>2</sub> that is larger than the 5 Mt target of the ROAD project and, hence, will need storage capacity in addition to that offered by the already permitted P18-4 field. Operated from the same P18-A platform and also close to the end of production, the P18-2 and P18-6 fields represent a maximum storage capacity 32.3 Mt and 1.5 Mt (in both cases for a final reservoir pressure of just under original gas pressure). The current study is directed to the P18-2 field only.

In 2010 already a CO<sub>2</sub> storage feasibility study of the P18 fields was done. The present study provides an update for the P18-2 field based on new data and improved methods and workflows to investigate the response of the depleted field to injection of CO<sub>2</sub>.

### *Study approach*

The requirements for a CO<sub>2</sub> storage permit application are set out in the Dutch Mining Act which was amended in 2011 to include a transposition of the EU Storage Directive (EU, 2009). The results presented in this report cover the requirements described in the EU Storage Directive. The present study follows a workflow that was developed in a consortium of several EU Member States, building on combined experience in CO<sub>2</sub> storage feasibility assessments.

The workflow is risk-based, with the aim to understand the site-specific risks associated with CO<sub>2</sub> storage, to reduce them to a level that is as low as reasonably possible through site-specific design of injection scenarios and to develop a monitoring program and mitigation plan aimed at the most relevant, remaining risks.

### *Overall conclusion regarding storage of CO<sub>2</sub> in the P18-2 field*

The overall conclusion of the study is that CO<sub>2</sub> can be stored safely and securely in the P18-2 field. The CO<sub>2</sub> can be injected into the field in a way that is safe; during and after the end of injection, the P18-2 field will retain the CO<sub>2</sub> securely. There is no reason to assume that CO<sub>2</sub> could migrate out of the field after proper decommissioning of the injection wells after the end of injection.

### *Managing relevant risks*

The identified risks that are related to the potential leakage of CO<sub>2</sub> out of the P18-2 storage complex during or after CO<sub>2</sub> injection have been studied in detail and classified in a risk register. Most of the risks have been classified as 'low', with 'very low likelihood' that a small ('nil to negligible') amount of CO<sub>2</sub> that could migrate out of the reservoir; this corresponds with the lowest possible risk class. The remaining risks, with slightly higher likelihood and/or consequence, are related to (1) lateral CO<sub>2</sub> migration out of the storage reservoir, (2) the integrity of the wells in the field and (3) the stability of the faults in the storage system.

- (1) Simulation of the flow of CO<sub>2</sub> during injection into the storage formations shows that there is a possibility for the CO<sub>2</sub> to move into the attached water-filled formation, but remain within the storage complex. Simulations show that when CO<sub>2</sub> injection is stopped before the initial reservoir natural gas pressure is reached, the CO<sub>2</sub> will be retained within the original gas-filled reservoir formation and will not leave the storage complex.
- (2) Analysis of available data on the integrity of the wells in the P18-2 field shows that a workover is required for each of the potential injection wells to make them suitable for CO<sub>2</sub> storage operations or to decommission them. Once these are performed, the risk of CO<sub>2</sub> leaking along the wells, based on pre-injection status, is considered low.

The initial low reservoir pressure leads to low temperature of the injected CO<sub>2</sub> at the bottom of the well, causing significant temperature gradients in the well. This might lead to de-bonding of well liner (casing) and cement, potentially allowing leakage pathways to form (microannuli) for CO<sub>2</sub>. However, only when the pressure in the reservoir is above hydrostatic pressure could CO<sub>2</sub> enter these micro-annuli and potentially migrate into overlying aquifers. Therefore, the pressure in the reservoir is to be maximized at hydrostatic pressure, to reduce the likelihood of CO<sub>2</sub> flowing through these micro-annuli to small to negligible.

- (3) The cold CO<sub>2</sub> is injected into the reservoir formations, where it will create a low-temperature zone around the injection wells. If this zone reaches faults that are present in the reservoir, fault stability is affected; at the same time, faults become more stable during the injection process due to re-pressurizing the reservoir. Monitoring of injection rate and temperature is required to track the pressure and temperature development in the reservoir and ensure that faults remain stable. All analysis points to small to negligible probability of fault reactivation; the caprock of 450 m to 750 m thick, fault destabilization will not lead to CO<sub>2</sub> movement through the caprock.

### *Recommendations*

- (1) In the study presented here the modelling of the injection process was performed with an isothermal reservoir simulator that could not simultaneously handle pressure and temperature variations in the reservoir. The impact of the low temperature of the injected CO<sub>2</sub> was estimated through the use of an additional simulator and analytical approaches and of scenarios that emphasise potential effects. While the results obtained thus far are considered sufficient for the assessment of the risks associated with CO<sub>2</sub> storage, detailed coupled

modelling of pressure and temperature in the storage formations is required prior to the start of injection. This is needed for pressure and temperature predictions that are sufficiently reliable for the management of the injection process and for the interpretation of monitoring data.

- (2) The aim of the present study was to provide the basis for a storage permit application, by understanding the current status of the storage formations, the caprock, the faults and the wells, and their response to the injection of CO<sub>2</sub>. The study established that conditions can be found under which CO<sub>2</sub> can be injected and stored safely and securely in the P18-2 field. The study did not aim to arrive at a complete and detailed description of these conditions. Such an 'operational plan' for CO<sub>2</sub> injection into the P18-2 field will be required prior to the start of injection, as a basis for the detailed monitoring plan and for the operational management of the injection process. The present study is the first step towards the P18-2 operational plan.

# Contents

	<b>Summary .....</b>	<b>2</b>
<b>1</b>	<b>Introduction .....</b>	<b>8</b>
<b>2</b>	<b>Reading guide .....</b>	<b>10</b>
2.1	Definitions .....	10
<b>3</b>	<b>Methodology .....</b>	<b>12</b>
3.1	Legal background .....	12
3.2	Feasibility study .....	12
3.3	Risk assessment.....	13
<b>4</b>	<b>P18-2 field overview .....</b>	<b>17</b>
4.1	Introduction .....	17
4.2	Geological description .....	17
4.3	Caprock .....	22
4.4	Naturally sealing formations .....	25
4.5	Overview of wells.....	26
<b>5</b>	<b>Injection scenario .....</b>	<b>28</b>
5.1	Injection wells and well completion.....	28
5.2	CO <sub>2</sub> supply scenarios .....	28
5.3	CO <sub>2</sub> quality.....	29
5.4	Summary of injection conditions.....	30
<b>6</b>	<b>Evaluation of reservoir performance and integrity .....</b>	<b>31</b>
6.1	Introduction .....	31
6.2	Setup of injection simulations .....	31
6.3	CO <sub>2</sub> storage capacity and CO <sub>2</sub> dispersion .....	32
6.4	Temperature development in the reservoir .....	44
6.5	Chemical interactions .....	52
6.6	Conclusions .....	55
<b>7</b>	<b>Fault stability.....</b>	<b>57</b>
7.1	Introduction .....	57
7.2	Fault stability: pressure effect.....	57
7.3	Fault stability: temperature effect .....	63
7.4	Fault stability: geochemical effects.....	68
7.5	Conclusions .....	71
<b>8</b>	<b>Caprock integrity .....</b>	<b>72</b>
8.1	Introduction .....	72
8.2	Pressure effect on caprock integrity .....	72
8.3	Temperature effect on caprock integrity .....	72
8.4	Geochemical effects .....	74
8.5	Conclusions .....	76
<b>9</b>	<b>Well integrity .....</b>	<b>78</b>
9.1	Introduction .....	78

9.2	Status of the well barriers .....	79
9.3	Influence of cooling on well cement.....	102
9.4	Well abandonment.....	115
9.5	Conclusions .....	116
<b>10</b>	<b>P18-2 storage site and storage complex.....</b>	<b>118</b>
10.1	Introduction .....	118
10.2	Definitions in the Netherlands Mining Law and the EU Storage Directive .....	118
10.3	Definition of the storage site .....	119
10.4	Definition of the storage complex .....	119
10.5	Differences with the P18-4 storage complex definition .....	121
10.6	Barriers .....	121
<b>11</b>	<b>Migration paths .....</b>	<b>123</b>
11.1	Introduction .....	123
11.2	Available data and workflow .....	123
11.3	Geological model of the overburden.....	124
11.4	Migration scenarios.....	126
11.5	Methods .....	127
11.6	Results .....	127
11.7	Present day hydrocarbon migration.....	131
11.8	Conclusions .....	132
<b>12</b>	<b>Risk assessment and preventative measures.....</b>	<b>133</b>
12.1	Reservoir .....	134
12.2	Caprock .....	136
12.3	Fault zones .....	138
12.4	Wells .....	140
12.5	Conclusion .....	143
<b>13</b>	<b>Monitoring and corrective measures plan .....</b>	<b>145</b>
13.1	Introduction .....	145
13.2	Foundation of the monitoring and corrective measures plan .....	146
13.3	Philosophy of the monitoring plan .....	150
13.4	Interpretation.....	154
13.5	The monitoring plan .....	155
13.6	Conclusion .....	160
<b>14</b>	<b>Conclusions .....</b>	<b>162</b>
<b>15</b>	<b>References .....</b>	<b>164</b>
<b>16</b>	<b>Appendix A. compliance with EU Storage Directive site characterisation and assessment .....</b>	<b>169</b>
16.1	Data collection (step 1).....	169
16.2	Building the 3-D static geological earth model (step 2) .....	170
16.3	Characterisation of storage dynamic behaviour, sensitivity characterisation, risk assessment (step 3) .....	171
<b>17</b>	<b>Appendix B. Subsurface model descriptions .....</b>	<b>174</b>
17.1	Static model .....	174
17.2	Seismic interpretation .....	174

17.3	Time-depth conversion .....	176
17.4	Petrel model building .....	176
17.5	Differences with 2010 model and implications .....	192
17.6	Adjustments made to the static model.....	195
17.7	Dynamic model.....	196
17.8	History Match of the dynamic model .....	203
17.9	Geomechanical model.....	217
17.10	Well degradation model.....	221
<b>18</b>	<b>Appendix C. Risk Register.....</b>	<b>223</b>
<b>19</b>	<b>Appendix D. Monitoring Plan .....</b>	<b>227</b>

# 1 Introduction

This report presents the results of a study into the technical feasibility of storing CO<sub>2</sub> in the depleted offshore gas field P18-2. This field is one of several fields in the P18 cluster. The Porthos consortium<sup>1</sup> is developing plans for a multi-user CO<sub>2</sub> transport and storage network that connects industrial emitters of CO<sub>2</sub> in the Rotterdam harbour area with geological storage capacity in the Dutch sector of the North Sea. The consortium is targeting the P18 cluster as the first candidate for CO<sub>2</sub> storage. Operation of the network is planned for 2022 / 2023<sup>2</sup>.

The Porthos network is still in its planning stage and no certainty exists at this point in time about the supply of CO<sub>2</sub>. A recent study of the P18 gas field cluster suggested that the fields P18-2, P18-4 and P18-6 together can accommodate a supply rate of the order of 2-3 Mt/yr (million tonnes per year) and possibly up to 5 Mt/yr (Vandeweyer et al., 2011). With a combined storage capacity of about 37 Mt, storage at a rate of 2-3 Mt/yr could continue for about 15 years.

The P18-4 gas field has a CO<sub>2</sub> storage permit in place. This permit was awarded irrevocably in 2013. The P18-4 field was planned to be part of the “Rotterdam afvang en opslag demonstratieproject” (ROAD), which aimed to capture CO<sub>2</sub> at a coal-fired power plant at the Maasvlakte, compress the CO<sub>2</sub> and transport it by offshore pipeline to the P18-A platform, located at a distance of about 20 km from the Maasvlakte. The ROAD project was cancelled in 2017; all close-out reports are available online (ROAD, 2018).

The Porthos consortium now builds onto the ROAD legacy. The Porthos network is planned to be a multi-user transport and storage network, building up to much higher CO<sub>2</sub> supply rates than those considered in the ROAD project. In addition, the Porthos network has a longer horizon. This means that more depleted gas fields are required for storage, in addition to P18-4. The first candidates are the P18-2 and, potentially, the P18-6 gas fields.

The starting point of the present study was the storage feasibility study of the P18 cluster that was performed under the CATO-2 R&D programme (Vandeweyer et al., 2011). While the scope of that study was the entire P18 complex – including the P18-2, P18-4 and P18-6 compartments – the focus of the analyses was on the P18-4 structure. The P18-4 storage feasibility study was used in a storage permit application that resulted in the permit granted in 2013. The analyses of the P18-2 and P18-6 compartments presented by Vandeweyer et al. (2011) were not sufficient for a subsequent storage permit application for these compartments.

This report presents the results of a technical CO<sub>2</sub> storage feasibility study of the P18-2 structure. The aim of the feasibility is to identify risks for the containment of CO<sub>2</sub> in the storage complex, how to minimize those risks and the best way to monitor remaining risks. The study, which extends the analyses and results of the CATO-2 study by using the latest production data and deploying state-of-the-art

---

<sup>1</sup> See <https://rotterdamccus.nl/>.

<sup>2</sup> See Notitie Reikwijdte en Detailniveau – Rotterdam CCUS Project (Porthos), available at <https://www.rvo.nl/sites/default/files/2019/02/Porthos%20concept%20NRD%20-%20versie%20finaal.pdf>

workflows and tools, will provide the necessary input for a CO<sub>2</sub> storage permit application under the Dutch Mining Act and a 'Milieu Effect Rapportage'(MER) (which is a required element for the permit application). In 2011, the Dutch Mining Act transposed the EU Storage Directive (EU, 2009), thus ensuring that a storage permit application submitted under the Dutch Mining Act will comply with European legislation concerning CO<sub>2</sub> storage.

## 2 Reading guide

This report presents the results of a technical CO<sub>2</sub> storage feasibility study for the P18-2 depleted gas field. The setup of the report is as follows.

Sections 3 through 5 set the scene for the storage feasibility study. Section 3 introduces the risk-based approach taken in assessing the feasibility of storing CO<sub>2</sub> in the P18-2 field. The geological setting of the P18-2 field is described in Section 4. Section 5 describes some of the key boundary conditions and assumptions used in the study: the CO<sub>2</sub> supply profile until 2035, as well as the preliminary approach to the injection process. The latter includes the number of wells that are assumed to be used. Section 5 also provides a brief summary of relevant results from a flow assurance study that was performed previously; this includes the conditions of the CO<sub>2</sub> at the bottom of the injection wells, which follow from the modelling of CO<sub>2</sub> flow from the compression station, through a subsea pipeline and down the injection well. These conditions are used in the present study as the starting point for the modelling of the behaviour of the CO<sub>2</sub> inside the reservoir.

Sections 6 through 11 present the results from the storage feasibility analysis. The behaviour of CO<sub>2</sub> in the reservoir and its effect on the temperature and pressure distribution is presented in Section 6. Sections 7 and 8 discuss the impact of injecting CO<sub>2</sub> on reservoir and caprock integrity and stability of the faults within and bounding the reservoir. Well integrity is covered in Section 9, evaluating the current status of the wells and discussing simulation results on the effect of CO<sub>2</sub> injection on the long-term structural integrity. Section 10 defines the storage site and storage complex and contains a description of the barriers in the storage site to CO<sub>2</sub> migration. Section 11 presents an analysis of potential migration of CO<sub>2</sub>, if it leaves the storage complex. All results are pulled together in Section 12 to assess the risks associated with injecting CO<sub>2</sub> into the P18-2 field.

Section 13, finally, outlines the system that will be designed to monitor the injection process and the behaviour of the CO<sub>2</sub> in the subsurface.

### 2.1 Definitions

The following definitions are used throughout this document.

<b>Block</b>	An area on a map (e.g., block P18)
<b>License areas</b>	Part or all of a block (e.g., P18a)
<b>Field</b>	A bounded structure where the hydrocarbons were discovered and produced from and includes the sealing faults, rocks, gas-water contact (GWC) and other structural elements (e.g., P18-2)
<b>Reservoir</b>	Part of the field where the reservoir fluids are contained and where the CO <sub>2</sub> will be stored, i.e. the porous rock
<b>Compartment</b>	Part of a field and includes the bounding elements, (e.g. three compartments in P18-2 field)
<b>Storage Site</b>	Defined under the CO <sub>2</sub> Storage Directive and under the Dutch Mining Act and includes the storage reservoir and the wellbores penetrating the storage reservoir

<b>Storage Complex</b>	Includes the storage reservoir, the wellbores penetrating the reservoir and the surrounding and bounding formations and faults which make up the storage field.
<b>Migration of CO<sub>2</sub></b>	Movement out of the storage reservoir but remaining in the storage complex
<b>Leakage of CO<sub>2</sub></b>	Under the CO <sub>2</sub> Storage Directive means movement of CO <sub>2</sub> out of the storage complex
<b>Emission of CO<sub>2</sub></b>	Under the ETS Directive (ETS directive, 2009) means escape of CO <sub>2</sub> from the storage site to the atmosphere or the water column
<b>Injection facilities</b>	Include well completions and wellheads; <i>not</i> included are other facilities on the platform, nor the platform itself.

## 3 Methodology

### 3.1 Legal background

This technical CO<sub>2</sub> storage feasibility study has the aim to provide the basis for a permit application for CO<sub>2</sub> storage in the P18-2 field. The Dutch Mining Act sets out the requirements for a storage permit application. A transposition of the EU Storage Directive (EU, 2009) was included in the Mining Act in 2011<sup>3</sup>. Previous work on the P18-4 field (Vandeweyer et al., 2011) resulted in a successful application for a CO<sub>2</sub> storage permit, proving that the workflow used provided a basis that was both sufficiently detailed and complete.

The present study follows the workflow that was used by Vandeweyer et al. (2011), and that was described in detail by Nepveu et al. (2015), who combined experience from several EU Member States in CO<sub>2</sub> storage feasibility assessments. The workflow covers the full list of requirements set out in Annex II of the EU Storage Directive (EU, 2009). Section 16 shows the link between the elements of site characterisation mentioned in Annex I of the EU Storage Directive and the present report.

### 3.2 Feasibility study

The workflow is risk-based and site specific, with the aim to understand the storage risks involved, to reduce them to a level that is as low as reasonably possible through site-specific design of injection scenarios and to develop a monitoring program aimed at monitoring and managing the most relevant, remaining risks.

This study uses the workflow described by Nepveu et al. (2015). Figure 3-1 illustrates this workflow.

- Phase 1 of the workflow represents a screening study, to find one or multiple sites that meet selection criteria, such as location, storage capacity or expected cost of storage.
- Phase 2 of the workflow represents the detailed CO<sub>2</sub> storage feasibility study that is presented in this report, for the P18-2 depleted gas field. The first part of phase 2 is a 'quick scan' of available data. The purpose of the quick scan is to identify the key risks to storage and 'showstoppers', if any, before entering the detailed assessment, which represents the second part of phase 2. This detailed assessment is shown in the diagram in the figure as the central, large rectangle labelled 'RA' (risk assessment), with several disciplines revolving around the RA. This is the key element of a storage feasibility assessment, with several disciplines analysing the response of the storage system on the injection of CO<sub>2</sub>.

In the present case, screening was already completed and outside the scope of this report. In addition, a 'quick scan' of available data was already performed in a previous study of the P18 gas fields (Vandeweyer et al., 2011). No showstoppers were identified for the P18-2 field. However, as the previous study was focused on the P18-4 depleted gas field, the detailed assessment of the P18-2 was incomplete;

---

<sup>3</sup> See <https://www.nlog.nl/en/licences-and-legislation> for links to relevant government internet sites.

the present report repeats the previous assessment with improved tools and experience where possible and fills the gaps where needed.

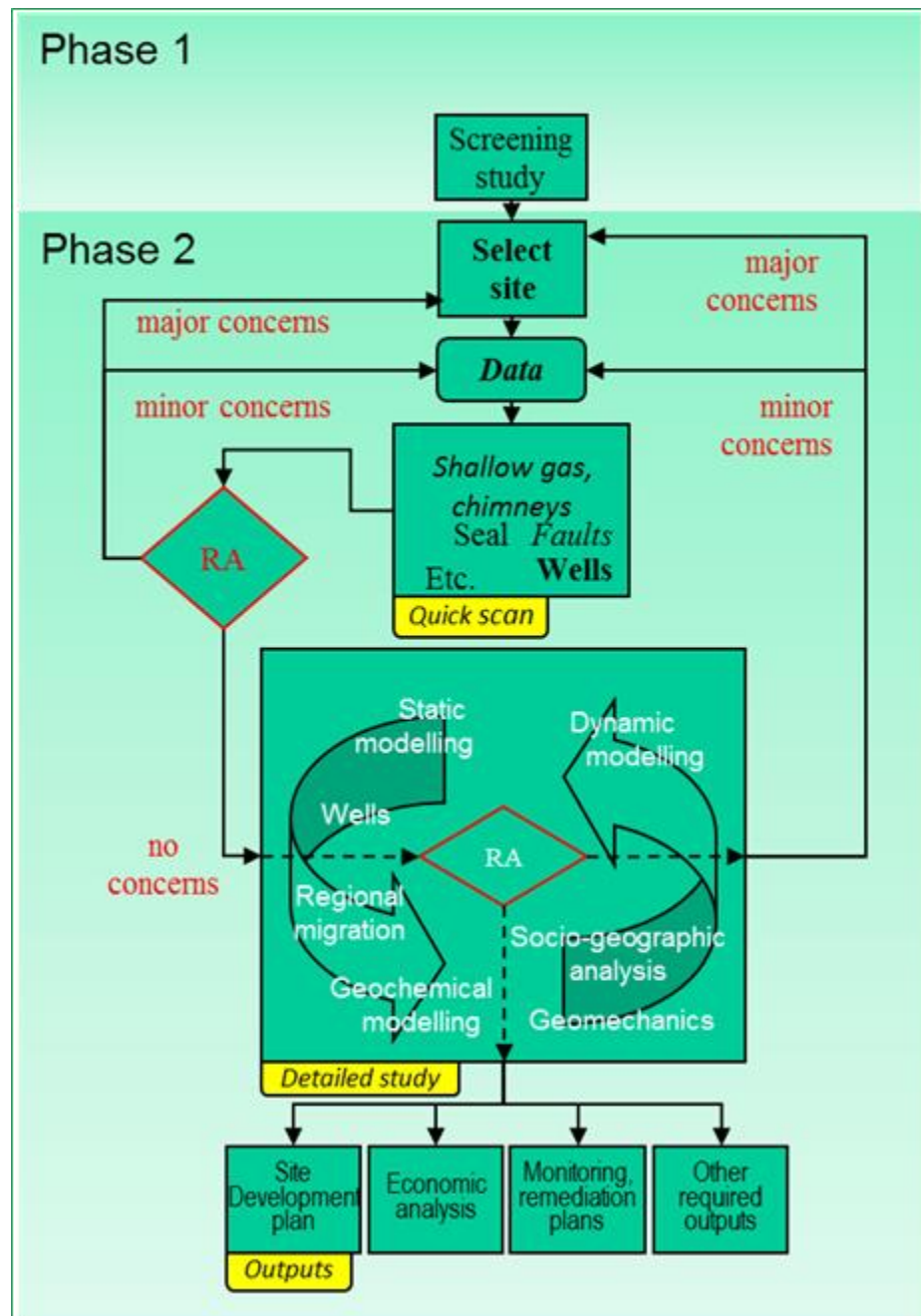


Figure 3-1 Workflow for site screening and characterization (Nepveu et al., 2015). RA is Risk Assessment

### 3.3 Risk assessment

The approach pursued in the risk assessment, e.g. the assignment of risk classes, is basically qualitative of nature and expert-based, although the underlying information used is often of a quantitative nature, e.g. output from model simulations or measurements of physical parameters like pressure.

The risk assessment consists of the following steps:

1. Identification of (a combination of) factors, which directly influence the containment of CO<sub>2</sub>
2. Detailed assessment of these (combined) factors and definition of potential risk reduction measures
3. Risk classification

Step 1 was performed in a workshop prior to the project in order to define the required assessment. Step 2, the detailed assessment of the risk factors and definition of potential risk reduction measures is reported in the present report in Sections 6 to 9; step 3 is described in Section 12.

Typically, the results of risk characterisation and classification are listed in a risk register (see Section 0) and summarized in accompanying risk matrices. For the classification of the risks, a risk matrix with classes of likelihood and consequences has been designed (see Figure 3-2), which is inspired by the work done by Van Eijs et al. (2011) and the risk assessment matrix included in the toolkit of the Energy Institute (2019) (website, version 15 Oct 2019). The definition of the classes of consequences has been linked to the concept and definition of the storage complex as described in the EU Storage Directive (EU, 2009).

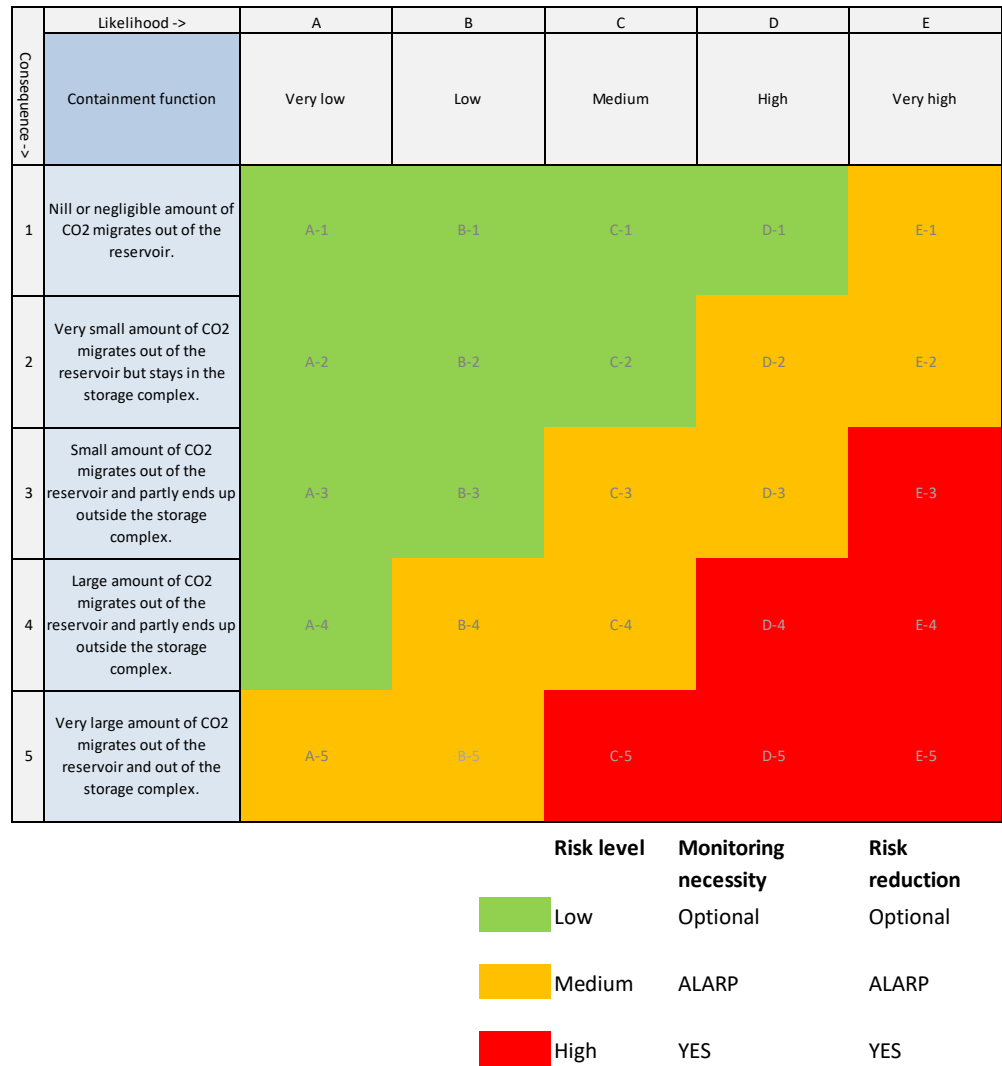


Figure 3-2 Proposed risk matrix nomenclature (modified after Van Eijs et al., 2011; Energy Institute, 2016).

Five classes of likelihood have been defined with the following definitions:

- Very low     Positive evidence for containment and large safety factor
- Low         No positive evidence and large safety factor
- Medium     Positive evidence and no large safety factor
- High        No positive evidence and no large safety factor
- Very high   No positive evidence and small or nil safety factor

The classes of consequence have been defined as follows:

- Negligible    Within natural variation and cannot be monitored
- Very small    Can be monitored and no impact on biosphere
- Small         Can be monitored and possible minor impact on biosphere
- Large         Can be monitored and possible impact on biosphere
- Very large    Can be monitored and possible adverse impact on biosphere

The resulting risk classes have been split in three categories (see Figure 3-2):

- Low risk      Strive for continuous improvement; monitoring and risk reduction are optional;

- Medium risk    Apply monitoring and risk reduction measures according to ALARP (As Low As Reasonably Practicable) principle;
- High risk       Risk reduction to acceptable levels and monitoring are obligatory.

## 4 P18-2 field overview

### 4.1 Introduction

The gas fields P18-2, P18-4, and P18-6, drilled from platform P18-A, are situated at approximately 3500 m depth below sea level and are located some 20 km NW from the port of Rotterdam (Figure 4-1). The reservoir rocks consist of sandstones which belong to the Triassic Main Buntsandstein Subgroup. The primary seal for the gas fields consists of unconformably overlying siltstones, claystones, evaporites and dolostones. The P18 gas fields are located in a heavily faulted area and consist mainly of fault bounded compartments, which are (at least on production time scales) hydraulically isolated from their surroundings. The bounding faults (which are well defined and clear to see on seismic) are sealing on a geological time scale due to juxtaposition of reservoir rock against impermeable rock.

High-calorific gas is being produced from these reservoirs since 1993. The gas is produced through the P18-A satellite platform and the P15-ACD processing and accommodations facilities in the adjacent P15 block, from where it is transported to the coast by a 40-km-long gas pipeline.

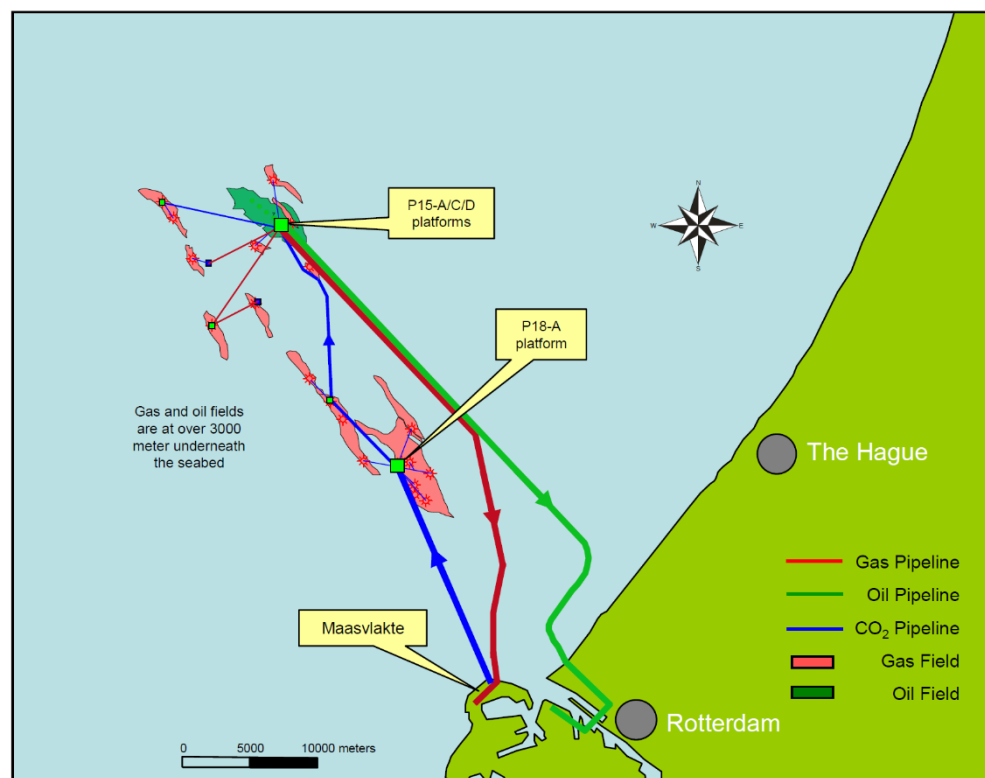


Figure 4-1: Overview of the locations of P15 and P18 fields (After TAQA, 2009)

### 4.2 Geological description

The P18 cluster consists of three fields, the P18-2, P18-4 and P18-6 fields (Figure 4-2). P18-2 was discovered in 1989 with the exploration well P18-02. It consists of three main compartments, 2-I, 2-II, and 2-III. This last compartment is now

considered to be consisting of two compartments (see Appendix B), and is therefore split into 2-III and 2-IV. Compartment 2-I came on stream first, in 1993. It contains three production wells: P18-02-A1, P18-02-A3ST2, P18-02-A5ST1, and the exploration well P18-02. Compartment 2-III contains one production well, P18-02-A6, and came on stream in 1997. Compartment 2-II came on stream in 2003, and also contains one production well, P18-02-A6ST1. For a while, this side track produced from Compartment 2-II only. After the whipstock had been perforated in 2005, well P18-02-A6 produced simultaneously from the 2-II and 2-III compartments. Field P18-4 was discovered in 1991, and production started from well P18-04-A2 in 1993. Field P18-6 was discovered in 2003, and production started from well P18-06-A7ST1 in 2003.

Peak production was reached in 1998, with a cumulative annual production of 2.2 bcm. At the end of June 2018, the total cumulative production of all P18 fields was 13.5 bcm. According to the updated Winningsplan from 2016, abandonment of the different fields is expected in 2024. Recovery factors by that time are expected to be 98% for P18-2 and P18-4, and 90% for P18-6.

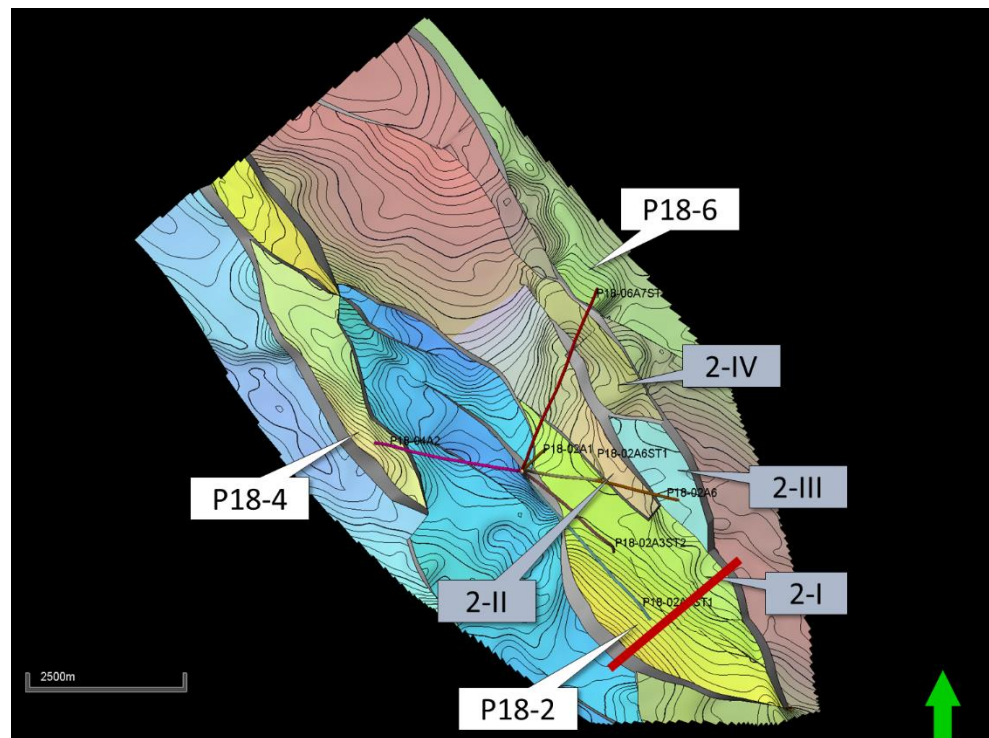


Figure 4-2: Overview of the three P18 fields (P18-2, P18-4, and P18-6), and the compartments of the P18-2 Field (2-I, 2-II, 2-III, and 2-IV). Red line indicates the position of the cross section shown in Figure 4-3.

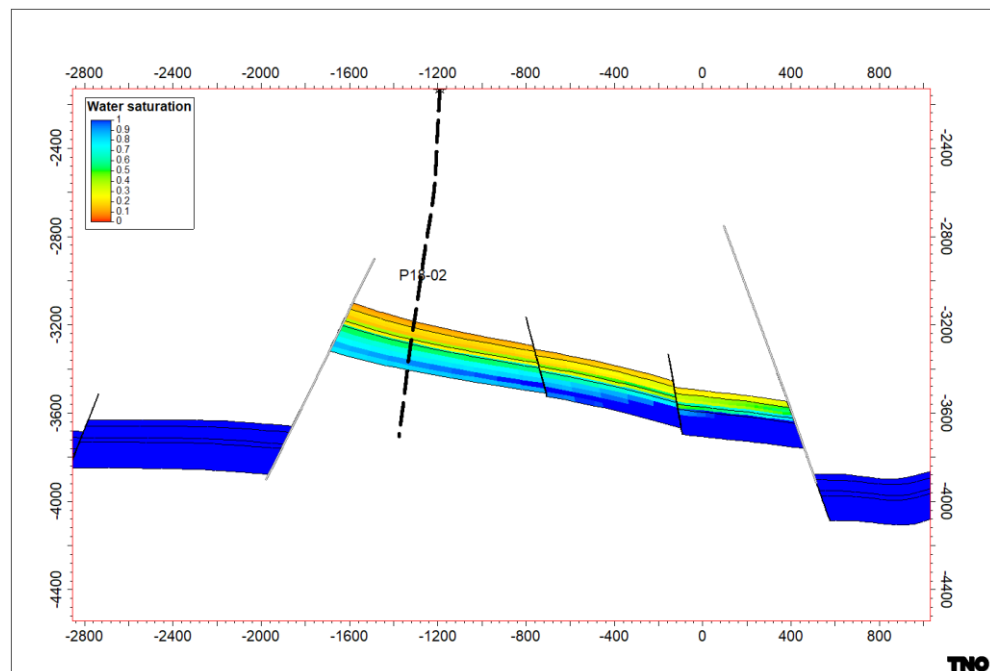


Figure 4-3: Cross section through the P18-2 field, showing compartment 2-I with initial water saturation. The location of the cross section is shown in Figure 4-2.

The structures that contain the reservoirs are bound by a system of NW-SE oriented faults in a horst and graben configuration, with a sinistral strike-slip component. The top of the reservoir compartments lies at a depth between 3175 m and 3455 m below sea level.

Compartment 2-I is the main compartment, and is bounded by two normal faults, F10 and F19/F20. A closer look at the offsets of these reservoir-bounding faults (Figure 4-3 and Figure 4-4) shows that they are sealing due to juxtaposition of reservoir zones against impermeable shales of the overlying Upper Triassic and Altona Groups (Figure 4-5).

Compartment 2-I is separated from compartment 2-II by fault F17, the offset of which is insufficient to be sealing by juxtaposition. Indeed, production data suggest that there is partial communication between the two compartments across this fault.

Compartment 2-III is separated from 2-II and 2-I by fault F19, which has enough offset to be sealing by juxtaposition, except for a small region at the northern end (Figure 4-4). However, no or very minor pressure communication was observed between the 2-I / 2-II compartments and the 2-III compartment, which suggests that fault F19 is sealing.

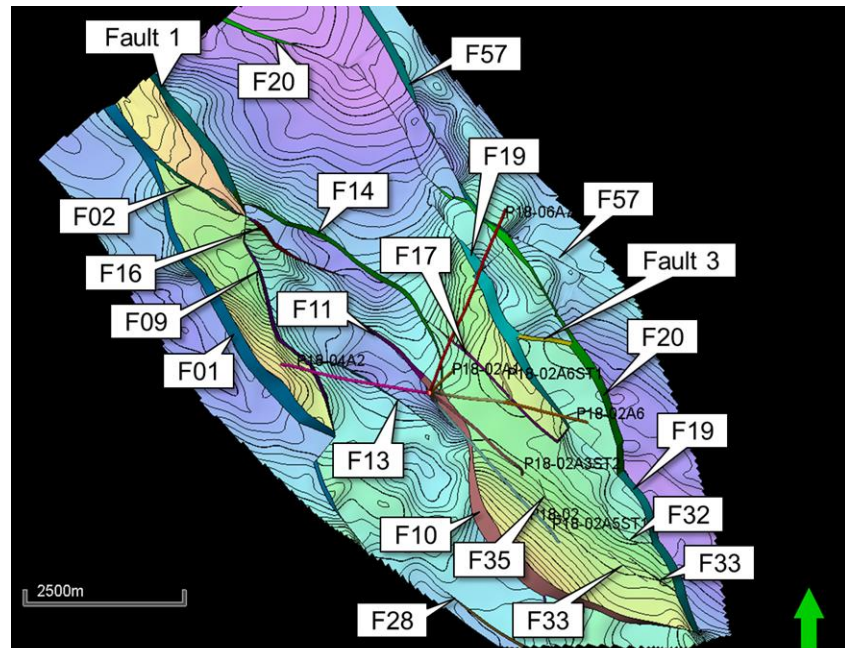


Figure 4-4: Map view of the Top Bunter in the P18 area with fault names used in this report.

The reservoir rocks of the P18 fields consist of four sandstone formations that belong to the Lower Germanic Trias Group, informally called Bunter. From top to base these are the Hardegsen, Upper Detfurth, Lower Detfurth and Volpriehausen Formations. (Figure 4-5). Each formation has highly variable porosity and permeability values. The Hardegsen Formation has in general the best reservoir properties.

Across a small zone at fault F14 low-permeable sandstones of the Volpriehausen and Lower Detfurth Formations in Compartment I are juxtaposed to permeable sandstones of the Hardegsen Formation (see Figure 4-4 for the location of fault F14). Figure 4-6 and Figure 4-7 show a cross section through fault F14 and an Allan diagram, respectively, with gas-filled formations juxtaposed against Hardegsen, Upper and Lower Detfurth and Volpriehausen. Communication – and flow of gas and CO<sub>2</sub> – across the fault cannot be established, as the impact of the volume of gas is too small to be visible on p/Z data. If this part of fault F14 is open to flow, the impact of CO<sub>2</sub> flow is negligible: potential communication applies only to the lower-quality reservoir formations which limits flow rate and the CO<sub>2</sub> would be remain structurally trapped against fault F14.

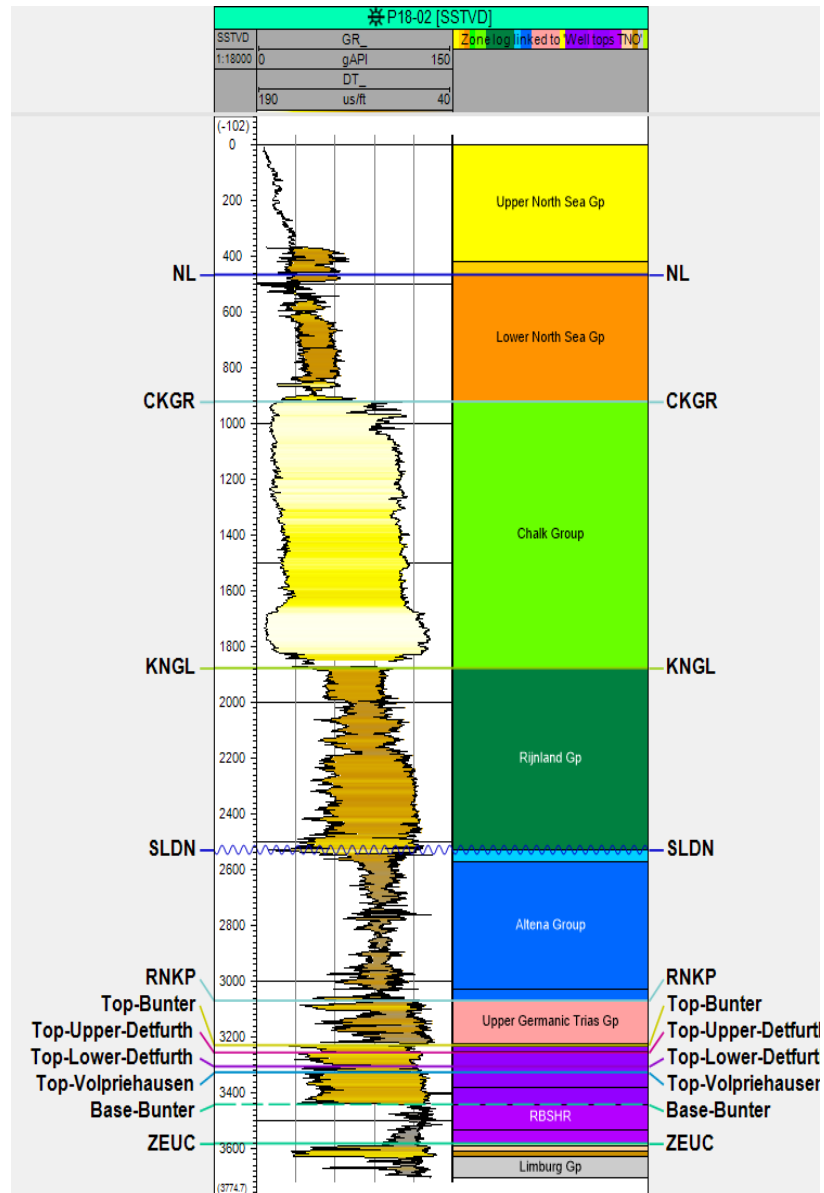


Figure 4-5: Stratigraphy and well logs of the reservoir interval and overburden of the P18 field

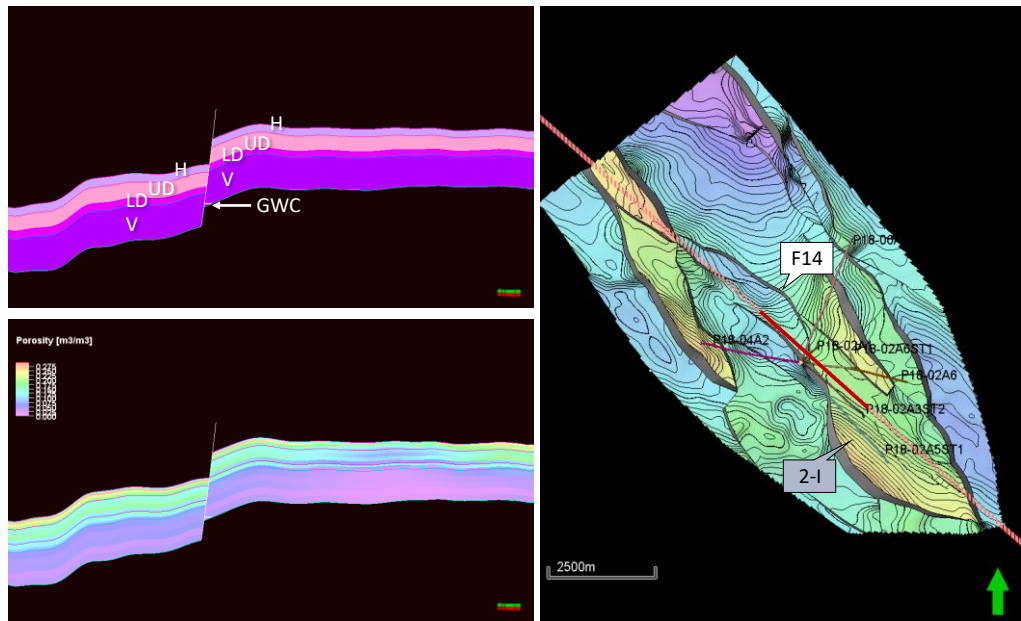


Figure 4-6: Cross section through fault F14, showing juxtaposition of gas-filled Upper Detfurth (UD), Lower Detfurth (LD), and Volpriehausen (V) against Hardegsen (H), Upper Detfurth, Lower Detfurth, and Volpriehausen. Upper left: Bunter formations, lower left: effective porosity, right: position of cross section (solid red line). GWC: gas water contact.

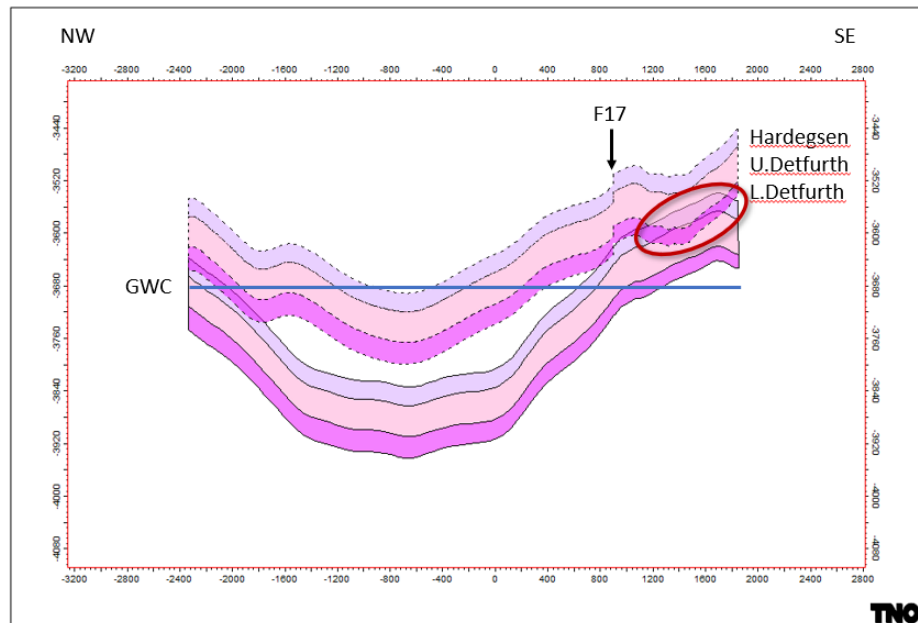


Figure 4-7: Fault juxtaposition diagram (Allan diagram) of fault F14. Blue line is the Gas Water Contact (GWC). Red ellipse indicates the area where the Hardegsen Fm is juxtaposed against Upper and Lower Detfurth.

### 4.3 Caprock

The seal to the P18 reservoirs is formed by the Upper Germanic Trias Group and the Jurassic Altona Group. The Upper Germanic Trias Group consists of siltstones, claystones, evaporites and dolostones. In well P18-02 it has a thickness of approx. 155 m. Directly above the Upper Germanic Trias Group lies the approx. 500 m thick

Altena Group (Figure 4-5), a thick succession of marine claystones, siltstones and marls of Early Jurassic age with excellent sealing quality. It includes the Posidonia Shale Formation that is easily recognized on seismic due to its excellent reflectivity.

The total thickness of the caprock of the P18 fields varies between 450 m and 750 m. The seal is excellent, as proven by the fact that it holds a gas column of nearly 600 m in the P18-2 compartment.

The rest of the overburden is formed by several geological formations, some of which can also be assumed to have good sealing properties. The Vlieland Claystone Formation (Figure 4-5) has proven itself as a good seal, as it forms the seal for the oil-bearing Lower Cretaceous sandstones in the West Netherlands Basin. It is considered here as the secondary caprock. Clayey sequences are also abundant in the North Sea Supergroup, especially in the lower part. These could very well act as secondary seals.

The nomenclature of the caprock as used in the present study is different from the one used in the CATO study of 2011. In the CATO study, the Upper Germanic Trias Group was designated the primary seal, and the Altena Group the secondary seal. In the present study the Altena Group and the Upper Germanic Trias Group are considered to form one seal, since there are no permeable formations in between the two. Therefore, the Upper Germanic Trias Group plus the Altena Group form the primary seal (Figure 4-8), and the Vlieland Claystone Formation the secondary seal.

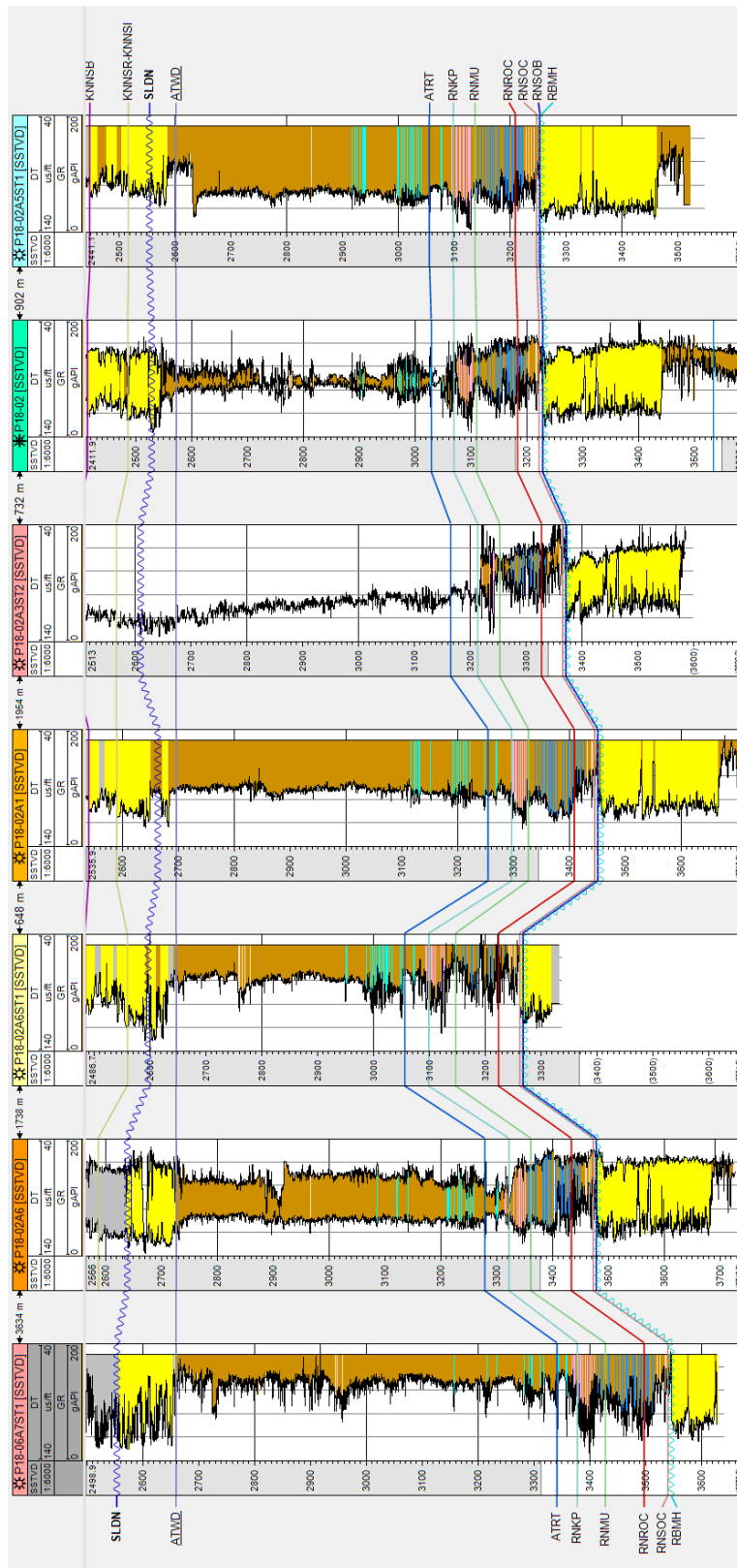


Figure 4-8: Well panel through the P18 wells of the immediate overburden of the Bunter formations showing that the Upper Germanic Trias Group plus the Alتنا Group form one continuous, primary seal over the entire storage complex.

#### 4.4 Naturally sealing formations

Recently the decommissioning of production platforms and infrastructure in the Southern North Sea has begun. A number of studies were initiated to investigate whether parts of the decommissioning process could be done more economically. One of these studies focused on well decommissioning, and specifically on the question whether naturally occurring ductile formations could be utilised to provide economic, self-healing and durable long-term sealing of wellbores. The outcome of the study, essentially based on existing literature, was that in the southern North Sea some formations are indeed suitable for creating effective annular barriers (Fischer et al., 2016; Geel, 2016). The idea is that if at the time of well abandonment it can be demonstrated that ductile clays or salts are hydraulically isolating the outer annulus and provide zonal isolation, no additional measures need to be taken at that point (as already accepted and practice in Norway and shown by Williams et al, 2009)). Of course, if this sealing behaviour can be demonstrated before CO<sub>2</sub> injection starts, it also reduces the risk of CO<sub>2</sub> leakage outside the well.

The shales from the Lower North Sea Group, The Vlieland Claystone Formation, and the Aalburg Shale were identified as having sufficiently ductile behaviour and swelling potential to create a sufficient seal around the casing (Figure 4-9). In addition, salts and possibly shales from the Upper Germanic Trias Group could have creeping or swelling behaviour.

The fact that all the above mentioned formations occur in the P18 area, it increases the probability that some or all will contribute to sealing the wells long term. This is further dealt with in Section 9.

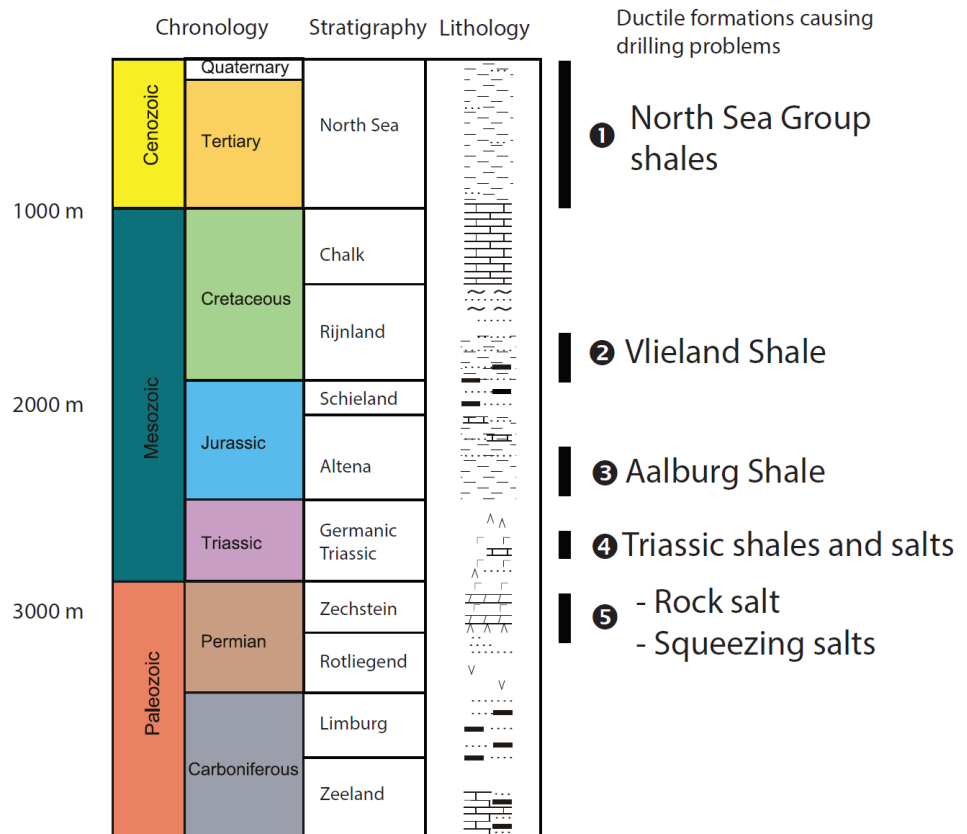


Figure 4-9 Typical stratigraphic column with potential self-sealing formations (Fischer et al, 2016).

#### 4.5 Overview of wells

Table 4-1 gives an overview of the wells that have been drilled in the P18-2 Field. Original holes of wells that were sidetracked (P18-02-A-03, P18-02-A-03ST1, and P18-02-A-05) have been omitted from the table. The trajectories of the proposed injectors are shown in Figure 4-10, and those of well tracks that have been plugged back are shown in Figure 4-11. Well P18-02A6ST1 is included here for the sake of completeness, but is advised in the current report to be plugged and abandoned (see Chapter 9).

Table 4-1: Overview of wells in the P18-2 compartment

NLOG name	Taqa name	Current well status	TDTotal Depth m MD (m)	Potential injectors	Remarks
P18-A-01	P18-02-A-01	Producing	3840	Yes	
P18-A-03S2	P18-02-A-03ST2	Producing	4302	Yes	
P18-A-05S1	P18-02-A-05ST1	Producing	5230	Yes	
P18-A-06	P18-02-A-06	Producing	4805	Yes	
P18-A-06S1	P18-02-A-06ST1	Producing	3954	No	
P18-02	P18-02	Suspended	3766	No	Discovery well

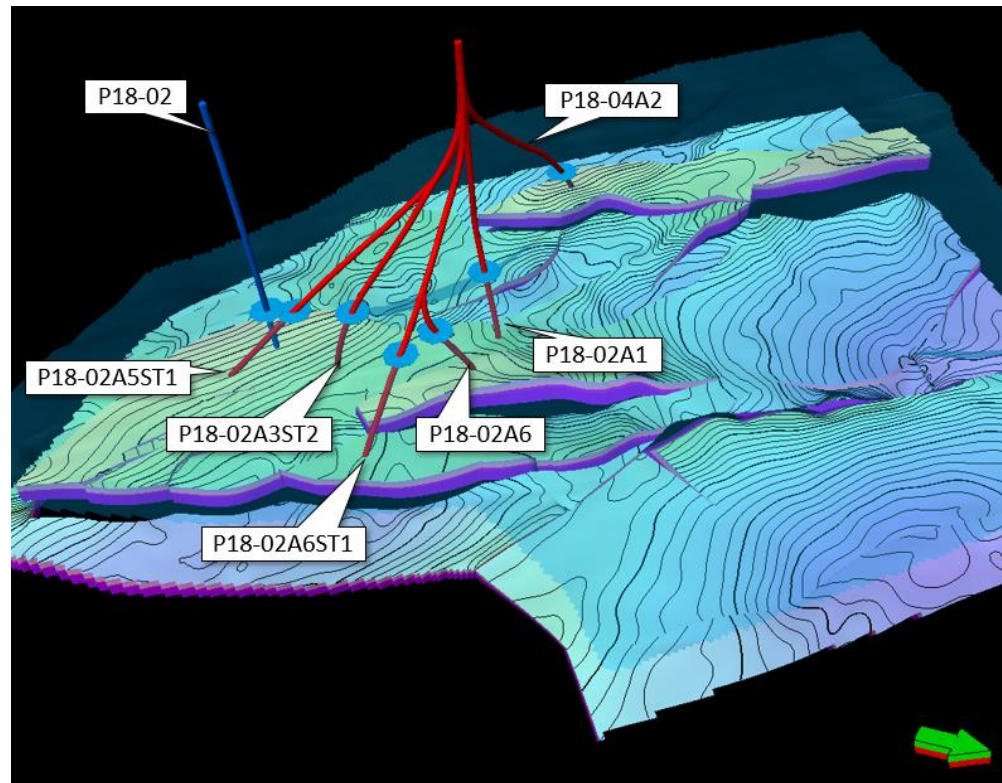


Figure 4-10: Overview of all envisaged injectors (in red) and suspended wells for P18-2. Light blue dishes denote entry points of wells into the caprock (=Base Schieland Gp). View to the southwest.

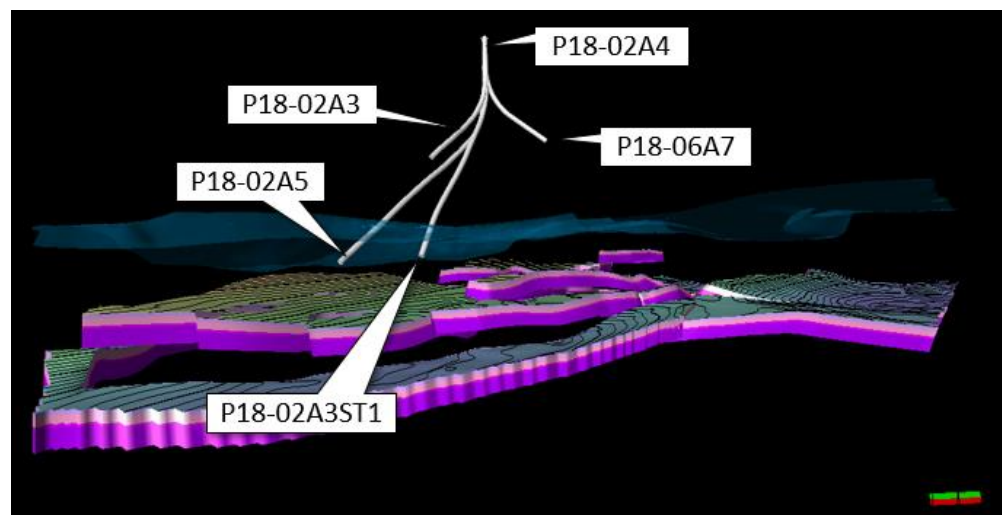


Figure 4-11: Overview of all plugged-back wells and sidetracks (in white) for P18-2. Light blue dishes denote entry points of wells into the caprock (=Base Schieland Gp). View to the west.

## 5 Injection scenario

### 5.1 Injection wells and well completion

Current plans for CO<sub>2</sub> storage in the P18-2, P18-4 and P18-6 fields are to use up to six injection wells. The P18-4 field has a single well, P18-04-A-02, which promises injection rates of the order of 1 Mt/yr (Vandeweijer et al., 2011). The P18-6 field also has a single well, P18-06-A-07, but the expected injection rates are significantly lower (Vandeweijer et al., 2011). Up to four injection wells are foreseen in the P18-2 field (see Table 4-1); in this study, well P18-02-A-06 is considered a back-up injection well and not included in the injection simulations.

The tubings in the existing wells can be replaced prior to injection, and the optimal tubing size needs to be based on dedicated well dynamics simulations (e.g., Belfroid, 2019). Such simulations need to be performed as part of a future study. For the purpose of the current study, for all wells considered for injection the tubing is assumed to have an external diameter of 4.5". This value follows from a trade-off between feasible injection rates at low and high reservoir pressure (Belfroid, 2019).

### 5.2 CO<sub>2</sub> supply scenarios

The future rate of CO<sub>2</sub> supply, to be delivered by emission sources in the Rotterdam harbour area, was uncertain at the time this study was undertaken. Based on the volumes of the CO<sub>2</sub> currently emitted in the harbour area and the volumes that could be captured at relatively low cost, a 'most likely' CO<sub>2</sub> supply profile was created (Figure 5-1).

Assuming that the P18-4 field will accommodate about 1 Mt/yr, or about 25% of the CO<sub>2</sub> supply, the supply profile to the P18-2 field is as given in Figure 5-2. The overall CO<sub>2</sub> supply reaches a plateau rate of 2.8 Mt/yr.

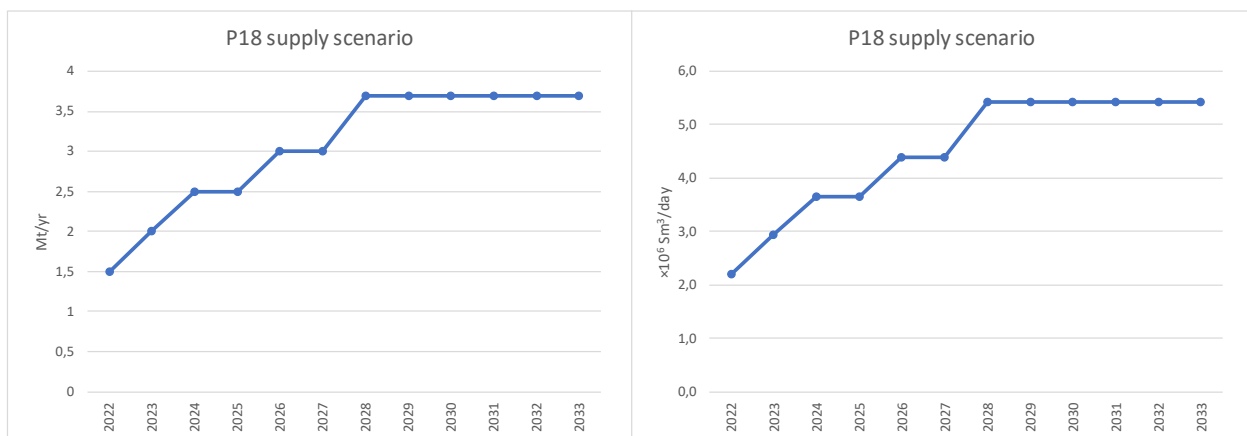


Figure 5-1 Potential future supply scenario for CO<sub>2</sub> from Rotterdam harbour sources. Flow rates increase from 1.5 Mt/yr by 2022 to 3.7 Mt/yr by about 2028 (about  $5.5 \cdot 10^6 \text{ Sm}^3/\text{day}$ ).

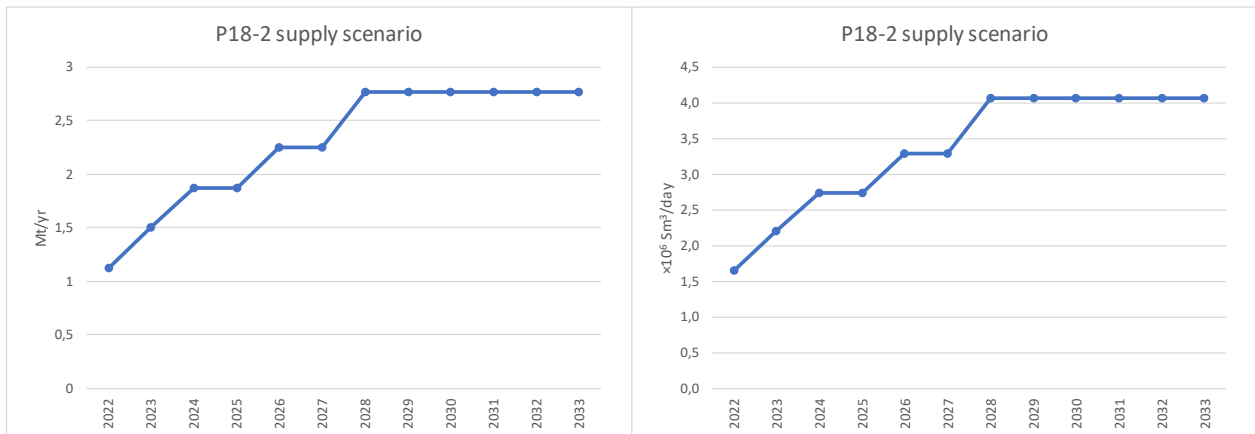


Figure 5-2 Potential future supply scenario for CO<sub>2</sub> to the P18-2 field: it is assumed that the three proposed P18-2 injection wells accommodate 75% of the total flow (Figure 5-1). Total flow rate to the P18-2 wells increases to 2.8 Mt/yr by 2028 (about  $4.1 \cdot 10^6$  Sm<sup>3</sup>/day).

### 5.3 CO<sub>2</sub> quality

At the time of the present study, no information was available about the potential sources of CO<sub>2</sub>. Recent work suggests that most available capture technologies can be expected to deliver CO<sub>2</sub> at a purity of 95% or higher (see, e.g., IEAGHG, 2016); sources in the Rotterdam harbour currently deliver CO<sub>2</sub> of more than 99% purity to the OCAP pipeline for use in greenhouses. While impurities alter the behaviour of CO<sub>2</sub> and may affect elements of the CCS chain, the results presented here were derived assuming pure CO<sub>2</sub>.

Figure 5-3 illustrates the effect of impurities on the phase behaviour of CO<sub>2</sub>. While pure CO<sub>2</sub> has a phase *line* that separates vapour conditions from those in which liquid CO<sub>2</sub> occurs (black curve in the figure), the presence of impurities in the CO<sub>2</sub> changes it into a *region* of pressure and temperature conditions in which the transition from liquid to gas phase occurs. Generally, two-phase flow is to be avoided in the handling of CO<sub>2</sub>, e.g. to prevent slugging. Two-phase flow is expected to occur in CO<sub>2</sub> injection wells without causing issues (Belfroid, 2019), but should be avoid in transport pipelines, risers and compressor. The conclusion that can be drawn from Figure 5-3 is that temperature and pressure should be chosen high enough to avoid the two-phase region of the CO<sub>2</sub> mixture being transported.

Impurities have an impact that extends beyond the phase envelope – for example, changes in density affect the operational window for injection as well as the storage capacity.

In the current study pure CO<sub>2</sub> was assumed in the simulations.

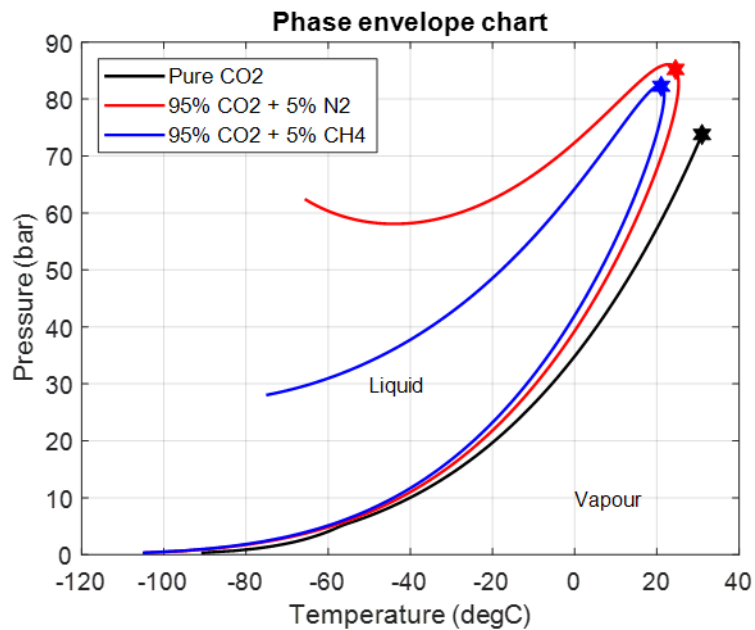


Figure 5-3 Effect of impurities (either 5 wt% N<sub>2</sub> or CH<sub>4</sub>, equal to 7.6 and 12.6 mol% respectively) on the location and shape of the CO<sub>2</sub> phase line. The data was generated using NIST REFPROP v10.

#### 5.4 Summary of injection conditions

To summarise, the injection of CO<sub>2</sub> into the P18-2 reservoir is subject to the following conditions.

- The CO<sub>2</sub> supply follows the profile as shown in Figure 5-2, with a plateau injection rate of 2.8 Mt/yr, distributed over three injection wells based on their injectivity. The three wells are P18-02-A-01, P18-02-A-03ST2 and P18-02-A-05ST1.
- The tubing in all injector wells will be recompleted (pers. comm. EBN, 2019). The external tubing diameter for all four injector wells is assumed to be 4.5". The actual well completion will be decided on at a later date, following a more detailed analysis of the operational window of the wells and the required flexibility in injection rates during the storage project.
- The CO<sub>2</sub> is assumed to contain no impurities. At the time of the present study, no quality/specification information was available about potential sources of CO<sub>2</sub>.

Additional assumptions apply to the conditions in the reservoir and to the downhole conditions of the CO<sub>2</sub>. These are explained in detail in Section 6.

- At the start of injection, the reservoir pressure is 20 bar; see Section 6.3.
- In the injection simulations, the average reservoir pressure will have a maximum that is equal to the initial reservoir pressure; see Section 6.3.
- The maximum downhole pressure is assumed to be equal to the initial pressure in the reservoir, 375 bar; see Section 6.3. This is the highest pressure for which faults and caprock have proven containment of natural gas.
- The minimum downhole temperature of the CO<sub>2</sub> was required to always be above 15 °C, to avoid CO<sub>2</sub> hydrate formation in the well and in the near-well area; see Section 6.4.

## 6 Evaluation of reservoir performance and integrity

### 6.1 Introduction

This section presents the results of an analysis of the process of injecting CO<sub>2</sub> into the P18-2 field. The analysis aims to:

- estimate of the storage capacity of the field (Section 6.3),
- establish the dispersion of CO<sub>2</sub> in the P18-2 field (Section 6.3),
- estimate the pressure and temperature levels in the injection wells and the fields during and after injection (Sections 6.3 and 6.4),
- assess the effects of interaction between CO<sub>2</sub> and the reservoir rock (Section 6.5).

The conclusions reached in this section are the following.

- The P18-2 field can store 32 Mt of CO<sub>2</sub>, assuming a final reservoir pressure of 351 bar (hydrostatic pressure, which is the pressure of the formations surrounding the storage reservoir). If the reservoir pressure is brought back to the initial pressure (375 bar at datum depth 3150 m), the storage capacity is 32.2 Mt of CO<sub>2</sub>.
- The injection wells together (P18-02-A-01, P18-02-A-03ST2 and P18-02-A-05ST1, together with the P18-4A2 well in the P18-4 field) can inject the target CO<sub>2</sub> supply rates given in Section 5.2, for a period of about 10 years from the start of injection. The last two to four years (2031 – 2035) of the target injection scenario would require another storage location.
- CO<sub>2</sub> fills the pore volume that was previously filled with natural gas and does not spill.
- The injection process must be managed to ensure that temperature and pressure in the well and in the near-well area remain outside the hydrate formation window.
- The injection of CO<sub>2</sub> will dry out the reservoir and may lead to salt deposition. The overall effect on permeability is expected to be negligible. Drying out of the reservoir reduces the probability of formation of hydrates.
- Chemical interaction between the CO<sub>2</sub> and the reservoir formation is insignificant.

The analysis presented in this section reveals no barriers to storage of CO<sub>2</sub> in the P18-2 field.

The results are a starting point for the assessment of fault stability (Section 7) and caprock integrity (Section 8).

### 6.2 Setup of injection simulations

Belfroid (2019) shows that the injection of CO<sub>2</sub> into a depleted field at low to very low pressure, such as the P18-2 field, can lead to low temperatures in the well, both at the wellhead and at bottomhole, due to the pressure difference between the high-pressure transport pipeline at the surface and the reservoir. Using a realistic setup for the Porthos compression and transport system and taking into account the phase behaviour of CO<sub>2</sub>, Belfroid (2019) presents injection scenarios for the P18-4 wells that lead to safe conditions at the wellhead and downhole, while meeting the

overall target rate shown in Figure 5-2. These downhole conditions show that CO<sub>2</sub> will be injected at temperatures well below the temperature of the reservoir.

The results show that the operational window for the P18-2 field is large: for a set of well characteristics a wide range of injection conditions is allowed, which do not lead to operational risks and result in feasible fluid velocities in the tubing. For the present study, the range of feasible injection rates is not a key issue; this study focuses on the response of the reservoir to CO<sub>2</sub> injection and on any restrictions for injection.

The simulation of injection of CO<sub>2</sub> into the P18-2 field was performed in two steps. In the first step, the injection and dispersion of CO<sub>2</sub> into the reservoir formations (see Section 4) is modelled using an isothermal simulator. While this ignores the temperature of the CO<sub>2</sub> upon injection, it provides a reliable estimate of the storage capacity of the field, as well as of the dispersion of the CO<sub>2</sub> during and after injection. The results from this first step are presented in Section 6.3.

The second step involves modelling the evolution of temperature within the reservoir formations. This approach takes into account the pressure and temperature of the CO<sub>2</sub>, but uses a less detailed representation of the storage reservoir. The results from this second step are presented in Section 6.4.

## 6.3 CO<sub>2</sub> storage capacity and CO<sub>2</sub> dispersion

### 6.3.1 *Setup of simulations*

This section evaluates the storage capacity of, and the dispersion of CO<sub>2</sub> in the P18-2 field. The injection wells are P18-02-A-01, P18-02-A-03ST2 and P18-02-A-05ST1, as listed in Table 4-1. Well P18-02-A-06 is also listed as injection well in Table 4-1, but is considered a back-up injection well and not included in the injection simulations presented below. The target injection profile is given in Figure 5-2.

### 6.3.2 *Simulation method*

A history matched dynamic model of P18-2 is used, see Section 17.7 for a description of the model. The following assumptions were made in the injection scenarios.

- The injection rate for each of the three injection wells depends on the local reservoir conditions and applied constraints and is calculated by the simulator.
- At the start of injection, the reservoir pressure is approximately 20 bar; the exact pressure distribution is based on the production history match and production forecast.
- The final average reservoir pressure (maximum allowable reservoir pressure) after CO<sub>2</sub> injection is assumed to be 375 bar (datum depth 3400m), which is equal to initial reservoir pressure. This is the highest pressure for which caprock, faults and reservoir have proven containment of natural gas.
- Injection simulations are run to a maximum average reservoir pressure that is equal to the initial gas pressure.
- The wells are constrained on group rate, therefore the total injection is equal to the most likely injection scenario for the P18-2 field (see Figure 5-2), but the distribution is based on the injectivity of the different injection wells.

- The wells are closed, when injection is no longer possible (i.e. when the maximum allowable reservoir pressure has been reached) or the injection rate is below  $5 \cdot 10^5$  Sm<sup>3</sup>/day (~0.03 Mt/yr). Since no leak-off test is available to set the value of maximum allowable reservoir pressure, this value is set equal to the initial pressure of the reservoir.
- It is assumed that the injectivity (used here to refer to the product of permeability and thickness) as derived from production data and information from logs can be used to simulate the CO<sub>2</sub> injection process.
- The maximum bottom hole pressure (BHP) of the injectors is set to 375 bar (equal to initial gas pressure).
- No changes occur in the well completion configuration.
- The saturation curves for gas-water systems are assumed to be the same for CO<sub>2</sub>-water systems.

Two injection scenarios were modelled: a base case and a high case. The base case scenario is the most probable injection scenario by filling up the reservoir up to 375 bar (initial reservoir pressure). In the second scenario, 'high case', injection is continued to an average reservoir pressure up to 450 bar to investigate the flow pattern of CO<sub>2</sub> at reservoir pressure higher than the initial pressure. Table 6-1 summarises the two scenarios.

Table 6-1: P18-2 injection scenarios

Injection Scenario	Target rate	BHP constraint (bar)	Avg reservoir pressure constraint (bar)	Minimum injection rate (Sm <sup>3</sup> /day)
Base case	- Figure 5-2. - Based on group constraint	375	375	$5 \cdot 10^5$
High case	- Figure 5-2. - Based on group constraint	450	450	$5 \cdot 10^5$

All simulations were performed with the Eclipse 300 reservoir simulator, a state-of-the-art compositional model that can handle the behaviour of CO<sub>2</sub> in the reservoir – including phase transitions – and the interactions between CO<sub>2</sub> and residual gas. See also Section 17.7.1.

Eclipse 300 cannot properly handle non-isothermal conditions, water evaporation or CO<sub>2</sub> dissolution. As a consequence the injected CO<sub>2</sub> has the temperature of the reservoir (126 °C), even though the temperature of the CO<sub>2</sub> is likely to be significantly lower (see Section 6.4).

The TOUGH2-ECOMG simulator was used to run non-isothermal injection scenarios (see also Section 6.4.2.1) to estimate the effect of cold CO<sub>2</sub> injection, CO<sub>2</sub> water interaction (water evaporation) and the related risk associated (cold front and dry out zone).

### 6.3.3 Simulation results

The total amount of CO<sub>2</sub> that can be stored in P18-2 is 32.2 Mt, assuming a reservoir pressure limit of 375 bar (initial pressure). Since the three injection wells are on group rate constraint the injection rate is distributed over the three wells based on injectivity (the product of permeability K and reservoir thickness H). An overview of the results of the injected volume and the distribution of injected volumes over the three injection wells is given in Table 6-2.

Table 6-2: P18-2 storage capacity for a final reservoir pressure of 375 bar, which is equal to the initial pressure (i.e., the pressure before production of the gas field).

P18-2 storage	Gas volumes (BCM) / relative contribution of each well (%)	CO <sub>2</sub> mass (Mt) / relative contribution of each well (%)
P18-02-A-01	1.56 / (9%)	2.92 / (9%)
P18-02-A-03ST2	1.31 / (8%)	2.45 / (8%)
P18-02-A-05ST1	14.3 / (83%)	26.8 / (83%)
<b>Total</b>	<b>17.2</b>	<b>32.2</b>

In Figure 6-1 and Figure 6-2 the injection profiles for the three wells are presented for the base case and high-case scenario.

The proposed injection wells together have an injectivity that is high enough to accommodate this target rate until 2033. The solid green curve in the graph labelled 'Field Gas Injection', represents the combined injection in the three wells and reproduces the supply curve in Figure 5-2.

It is observed that well P18-02-A-05ST1 injects more than 80% of the total injected volume; the other two injection wells contribute less than 10% each. This is due to the lower KH derived for the P18-02-A-01 and P18-02-A-03ST2 wells (see also Section 17.8.4.2).

The maximum injectivity is proportional to the pressure difference between the maximum allowable BHP (375 bar) and the reservoir pressure; this difference decreases over time. Until 2033, all CO<sub>2</sub> supplied by the emitters can be accommodated in the P18-2 field. After 2033 the injection becomes constrained by the BHP limit and the total injection rate starts to decline. Also the local reservoir pressure (9-point pressure) is set to 375 bar, which results in a long tail of CO<sub>2</sub> injection. A minimum injection rate was set of  $5 \cdot 10^5$  sm<sup>3</sup>/day. As a result, in 2040, injection ceases in all three injection wells as the reservoir reaches an average pressure of 375 bar (Figure 6-1 and Figure 6-2).

The sharp increase in injection rate that is observed in the profile of well P18-02-A01 around the year 2033 (Figure 6-1) is due to the group constraint set-up of the simulation; at this time the bottomhole limit of 375 bar is reached in well P18-02-A05ST2 and some of the flow is redirected to well P18-02-A01, for a short period until it reaches the bottomhole limit (Figure 6-2).

For completeness also the local reservoir pressure (9p pressure) and injection rate is shown for the two scenarios (base, high case), in Figure 6-3.

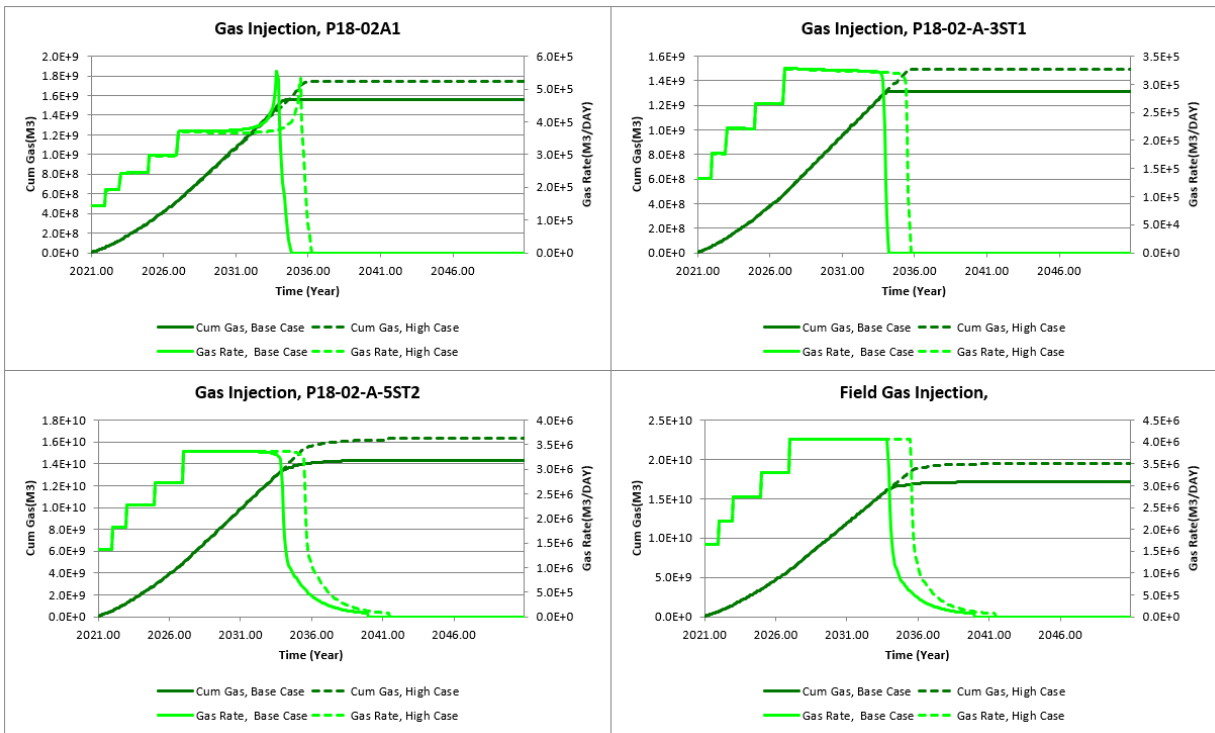


Figure 6-1: Injection rate and cumulative CO<sub>2</sub> mass injected for the three injection wells for a BHP constraint set to 375 (solid curves), representing the base case scenario, or 450 bar (dashed curves), representing the high-case scenario. See Table 6-1 for scenario parameters.

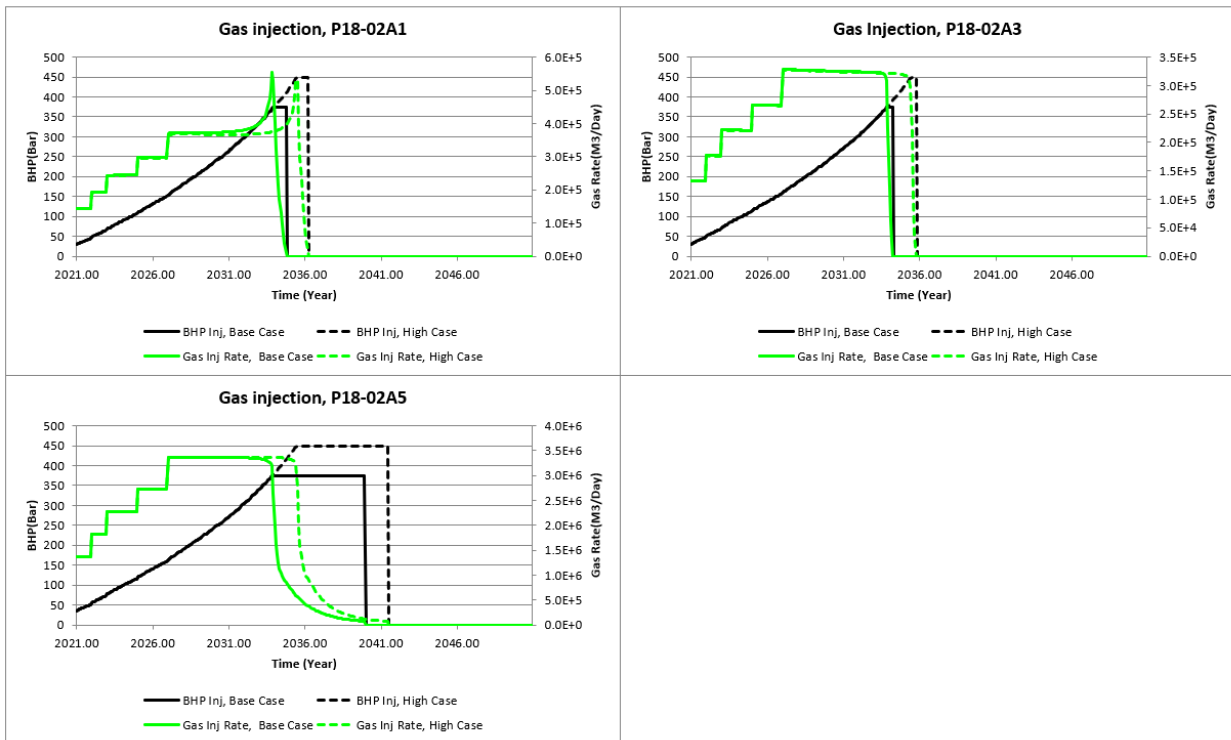


Figure 6-2: Injection rate and BHP for the three proposed injection wells for a BHP constraint set to 375 bar (solid curves), representing the base case scenario, or 450 bar (dashed curves), representing the high-case scenario. See Table 6-1 for scenario parameters.

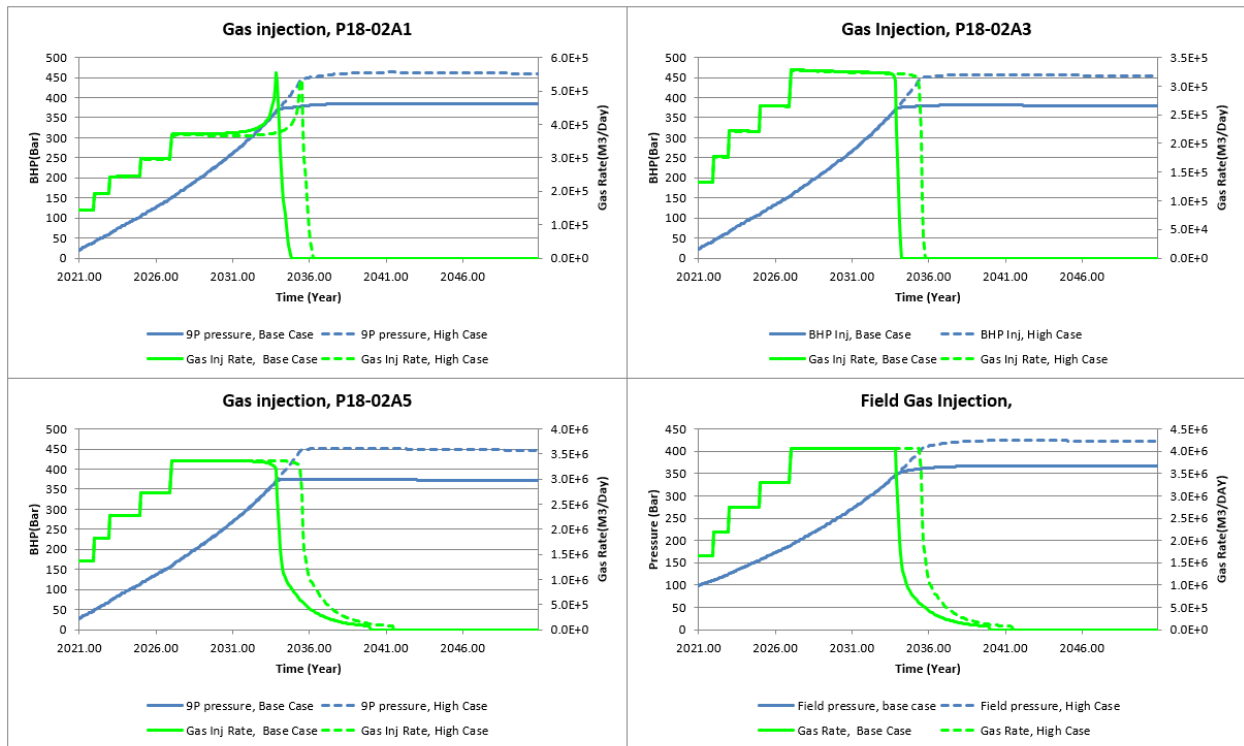


Figure 6-3: Injection rates vs well pressures (9-point pressures). In the right lower pane Injection rates vs field pressures for the three proposed injection wells for a BHP constraint set to 375 (solid curves), representing the base case scenario, or 450 bar (dashed curves), representing the high-case scenario. See Table 6-1 for scenario parameters.

From reservoir engineering perspective reservoir pressure can be brought back to initial pressure (375 bar). However, the results of well integrity analysis (Section 9.3) suggest reservoir pressure could be limited to hydrostatic pressure. Table 6-3 shows the storage capacity of the P18-2 reservoir when the average reservoir pressure after CO<sub>2</sub> injection is equal to hydrostatic pressure (351 bar).

Table 6-3: P18-2 storage capacity at hydrostatic pressure of 351 bar.

P18-2 storage	Gas volumes (BCM) / Relative contribution of each well (%)	CO <sub>2</sub> mass (Mt) / Relative contribution of each well (%)
P18-02-A-01	1.52 / (9%)	2.85 / (9%)
P18-02-A-03ST2	1.30 / (8%)	2.43 / (8%)
P18-02-A-05ST1	13.5 / (83%)	25.3 / (83%)
<b>Total</b>	<b>16.3</b>	<b>30.6</b>

6.3.4 Pressure, residual gas and CO<sub>2</sub> behaviour in the reservoir

For the base case scenario Figure 6-4, Figure 6-5 and Figure 6-6 shows maps of pressure, gas saturation and CO<sub>2</sub> molar density, respectively.

The pressure map (Figure 6-4) is similar at start of production and at the end of injection, which is expected. However there is one exception: at the end of injection compartment III is still at the depleted pressure level corresponding to the end of production (~50-60 bar), since no injection takes place in this particular

compartment and no communication exists with the other compartments (see Section 17.8).

In Figure 6-6, the CO<sub>2</sub> molar density is visible, at first as circular regions around the wells in compartment I (see saturation maps for the years 2021 and 2025). Later, the CO<sub>2</sub> progresses into compartment II. In the final stages of injection, it reaches compartment IV.

A comparison of the first panel in Figure 6-5 (this panel shows the initial GWC) with the panels in Figure 6-6 suggests that CO<sub>2</sub> migration occurs to beyond the initial gas-water contact (GWC) at the NW border of the reservoir. Also Figure 6-7 suggests CO<sub>2</sub> crossing the initial GWC, as well as CO<sub>2</sub> reaching the gas pocket. But, more importantly, the bottom panel of Figure 6-7 indicates that after injection, the CO<sub>2</sub> that crossed the GWC moves back towards the reservoir.

In conclusion the CO<sub>2</sub> might move beyond the GWC, however if so after the end of injection it will return to above the original GWC. The results also show that even though the CO<sub>2</sub> is moving below original GWC spilling is not occurring since the CO<sub>2</sub> is not flowing outside the storage complex, defined earlier.

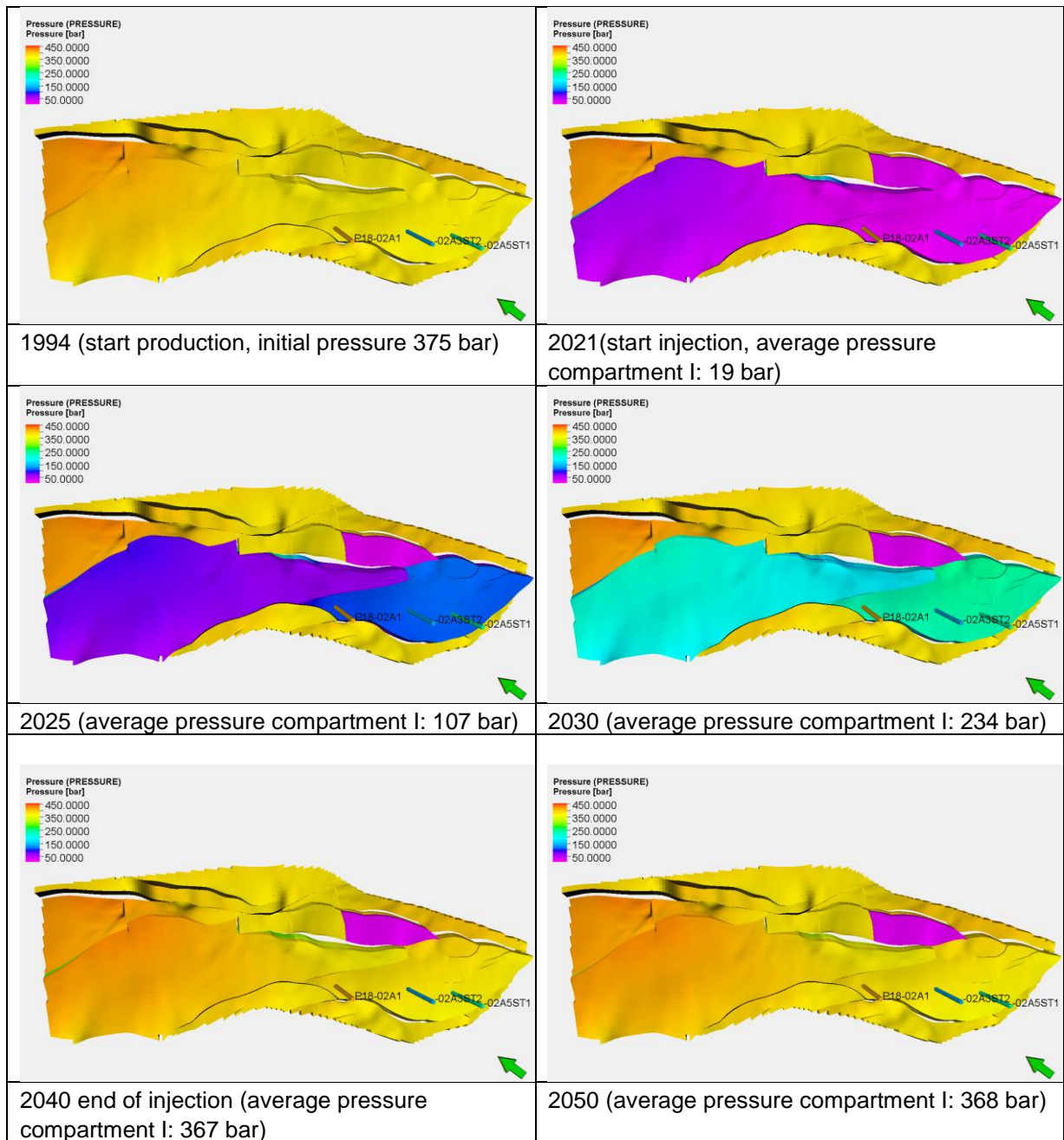


Figure 6-4: Pressure map at different stages of injection into P18-2. Average pressure in the hydrocarbon filled part of the field is about 375 bar in 1994 and in 2040. The map for 2050 shows equilibration in the ten years after injection was ceased. The pressures are HCPV weighted pressure in compartment 1.

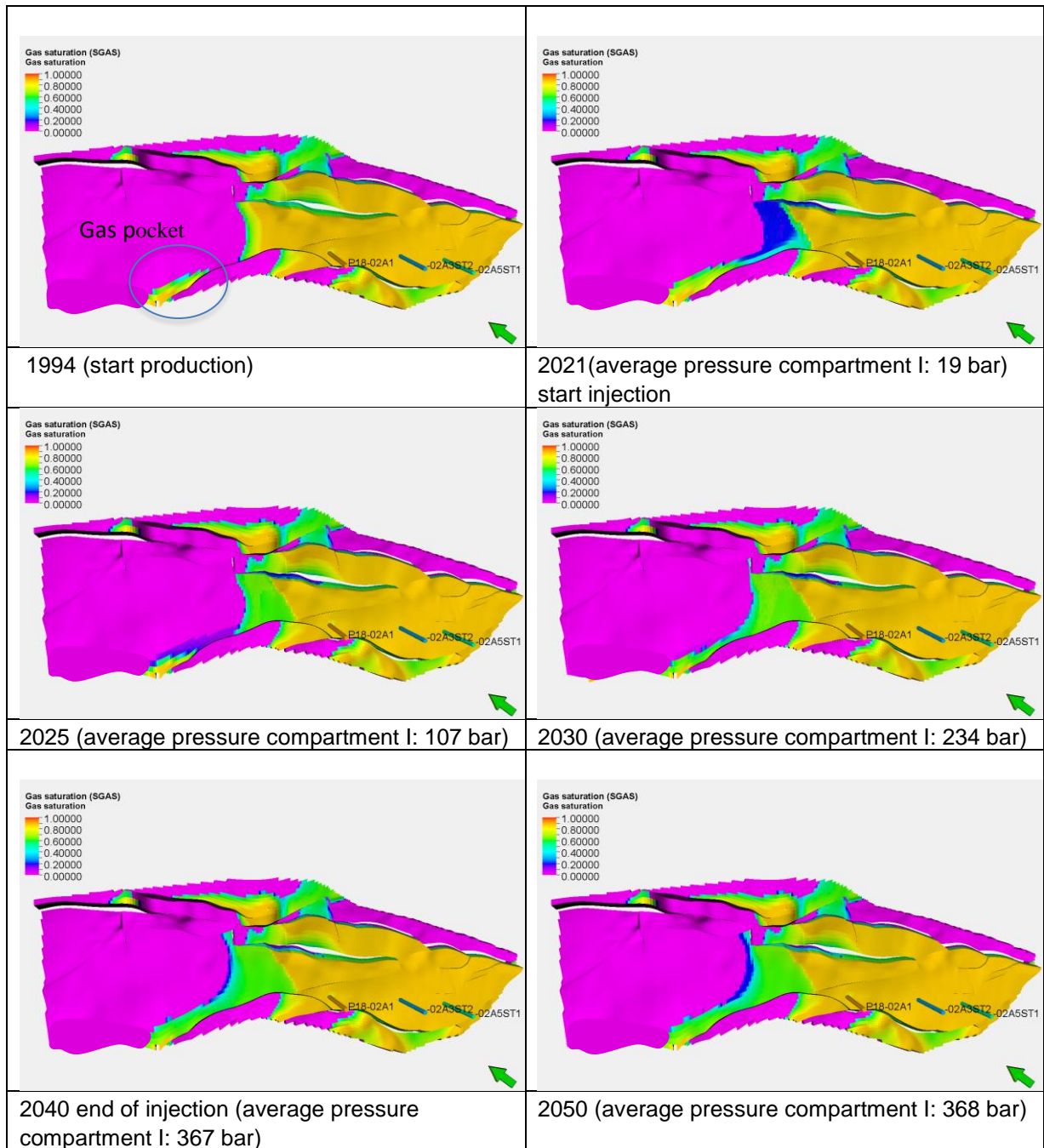


Figure 6-5: Gas saturation map at different stages of injection into P18-2. Gas in the 'gas pocket' near the NW border of the gas reservoir (see panel '1994 (start production)') is pulled towards the production wells; gas from the pocket contributes to the production. During injection, increasing reservoir pressure pushes residual gas back into the pocket.

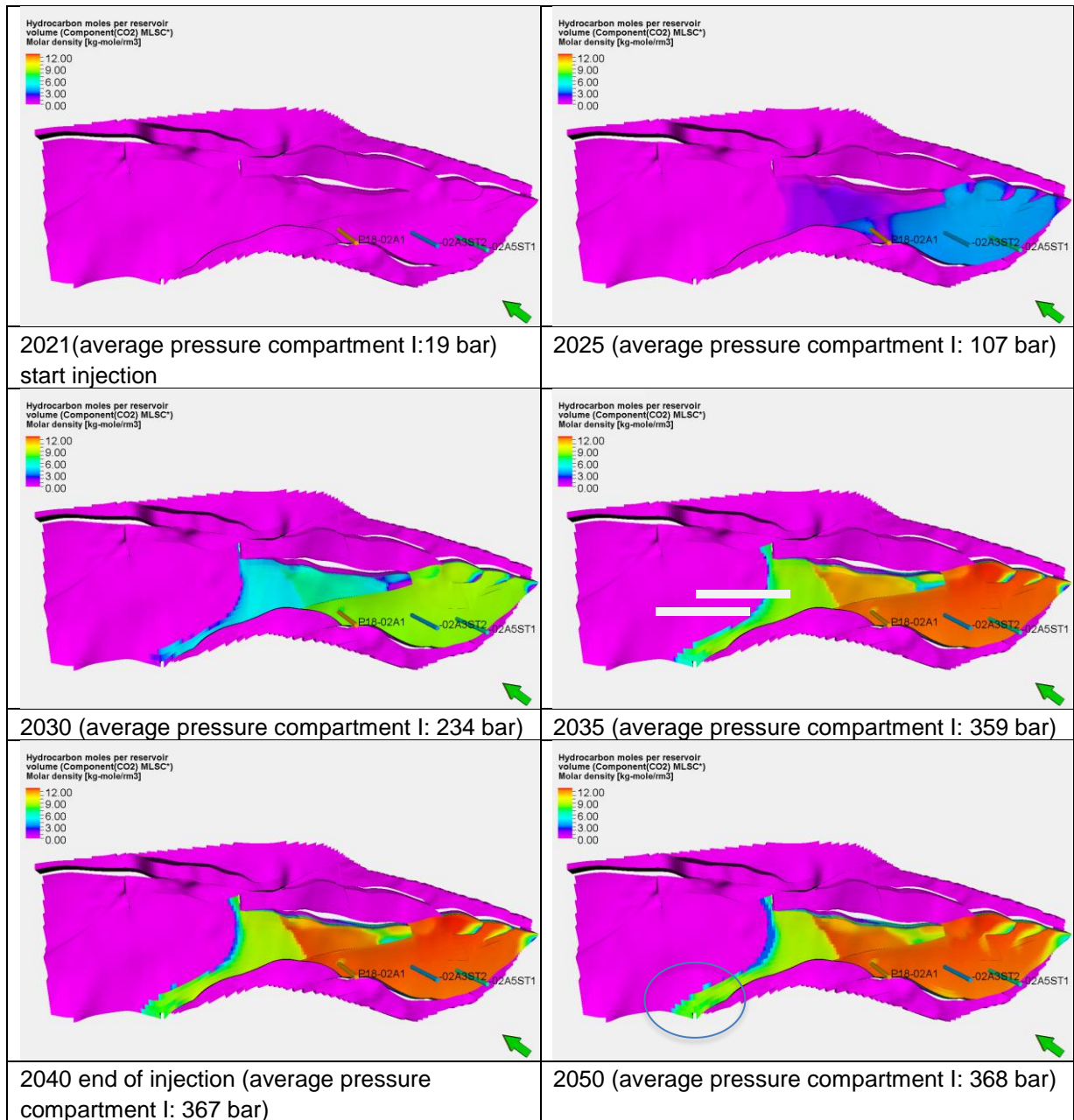


Figure 6-6:CO<sub>2</sub> molar density (kmol/m<sup>3</sup>; “kg-mole/m<sup>3</sup>” in the legend should be “kmol/m<sup>3</sup>”) map at different stages of injection into P18-2. CO<sub>2</sub> migrates beyond the original gas-water contact (compare panels in this figure with the first panel in Figure 6-5) and reaches the gas pocket (pocket indicated in the panel ‘2050’).

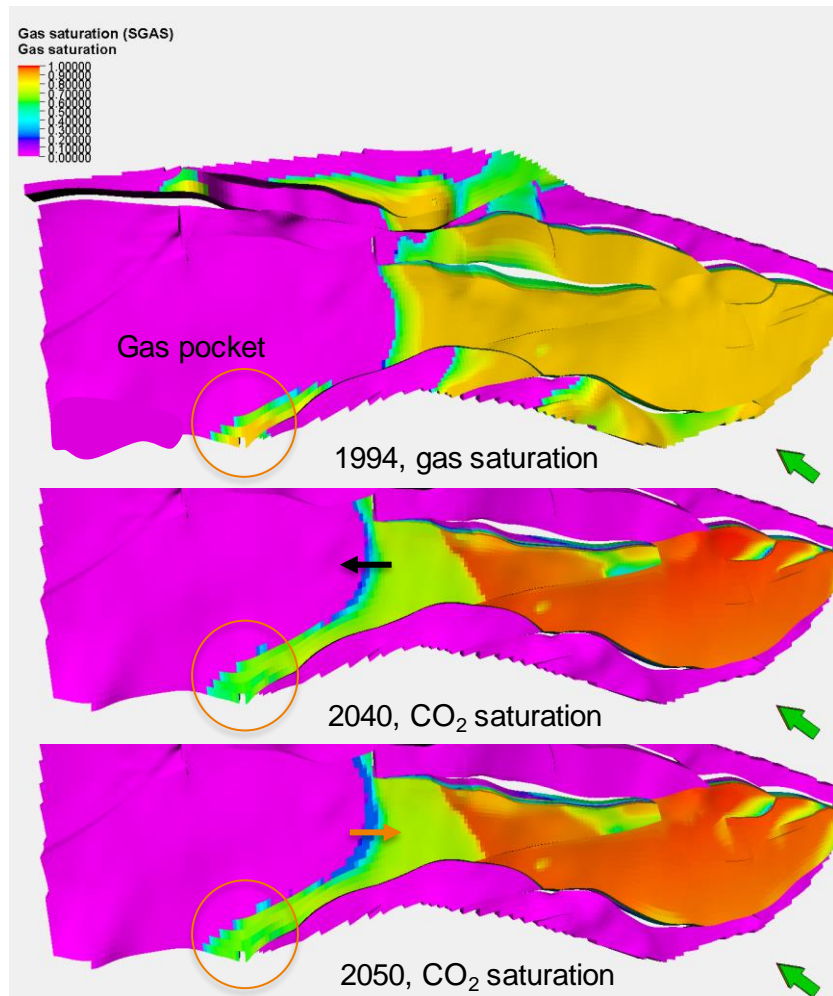


Figure 6-7: As Figure 6-6, now focusing on the period 2040 – 2050 and highlighting the behaviour of CO<sub>2</sub> in the NW corner of the reservoir. Top panel: initial gas saturation in 1994, prior to production, showing the gas-water contact (GWC). Middle panel: CO<sub>2</sub> saturation at the end of injection, in 2040. CO<sub>2</sub> has migrated beyond the initial GWC (black arrow), and has reached the gas pocket (in the circle). Bottom panel: CO<sub>2</sub> saturation in 2050, ten years after the end of injection. CO<sub>2</sub> has started migrating back into the reservoir (orange arrow); the CO<sub>2</sub> that has reached the gas pocket remains trapped. Colour coding indicates natural gas or CO<sub>2</sub> saturation: purple for zero saturation, red for full saturation.

### 6.3.5 Pressure communication with P18-6

Vandeweyer et al. (2011) state, on potential communication between P18-2 and P18-6: “Field P18-06 is located to the northeast of the main compartment. It is bounded by faults F13 and F57, of which only F13 has enough offset to be sealing by juxtaposition”. First of all, the numbering of the P18-2 faults from the Petrel project used in the current study (see e.g. Figure 4-4) is different from Vandeweyer et al. (2011). Fault F13 (a minor, transverse fault) is currently called F500, but F57 has retained its name.

Second, the seismic interpretation of the faults in this boundary area, especially F57, is different from Vandeweyer et al (2011)’s. Although F57’s throw is now much larger, it still suggests potential communication between P18-6 and Compartment II and IV of P18-2 which warrants further examination.

A closer look (Figure 6-8 and Figure 6-9) shows that P18-6 is disconnected from P18-2 by two faults, of which P18-6's boundary fault F57 is the most important one. In between the faults a small graben is filled by overlying caprock shale. The only contact is by Volpriehausen juxtaposition, which has a low permeability (lower than 1 mD). Furthermore, the faults in the graben are likely to have undergone severe cataclasis (Nieuwland, 2012), which reduces the across-fault permeability even further.

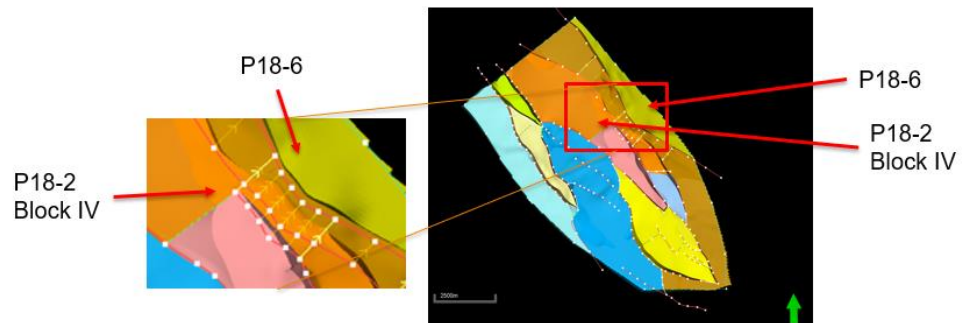


Figure 6-8: Overview fault between P18-2 and P18-6.

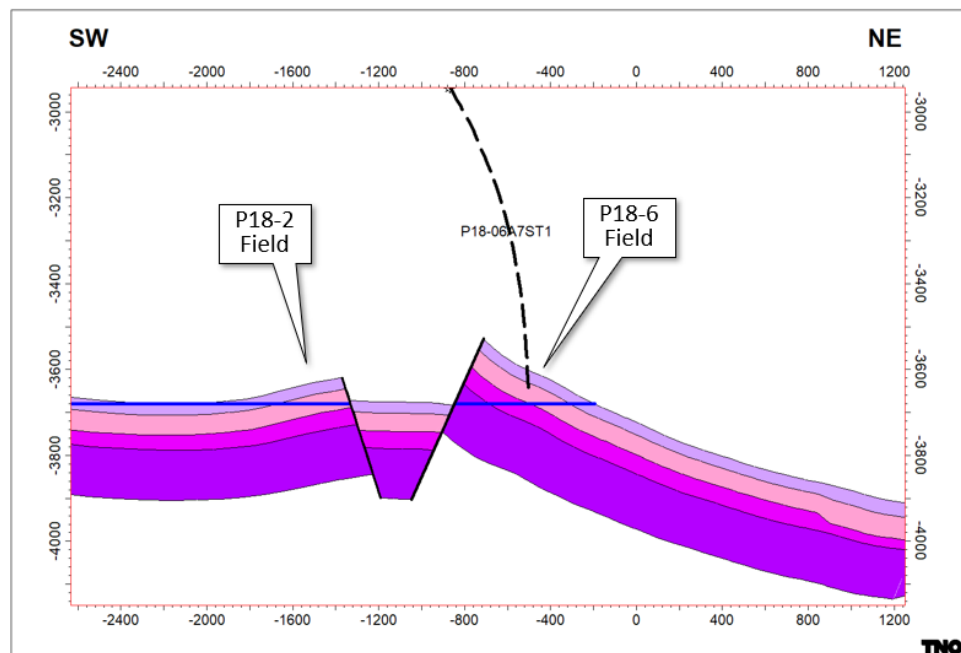


Figure 6-9: Cross section showing faults between P18-2 and P18-6.

The first pressure value from P18-6 was recorded in the end-of-well report (EOWR), available on nlog.nl; a pressure of 378 bar was inferred, in February 2003. A second pressure point is mentioned on nlog.nl: 305 bar, measured on 15-2-2004, after production of 0.074 bcm. Both data points are indicated by a star on the p/z plot in in Figure 6-10.

The data shown in Figure 6-10 suggest that measurements during periods of shut-in could have resulted in too low pressure values, due to relatively short shut-in times. For a poor quality reservoir such as P18-6 (~1 mD) pressure equilibration

requires long shut-in periods. Therefore we expect that in reality the p/z curve is a straight line and P18-6 is a depletion-driven reservoir.

The pressure data in Figure 6-11 show that after about 10 years of production from P18-2, the initial pressure found in the P18-6 reservoir was still about 275 bar higher than that in the P18-2 field. Therefore the conclusion can be drawn that these two compartments are not in pressure communication on a production timescale.

In addition, during the last years of production the pressure behaviour of the main compartment (Compartment I) of P18-2 is different from that of P18-6 (see Figure 6-11), which suggests that there is no pressure communication between the two reservoirs on production time scale.

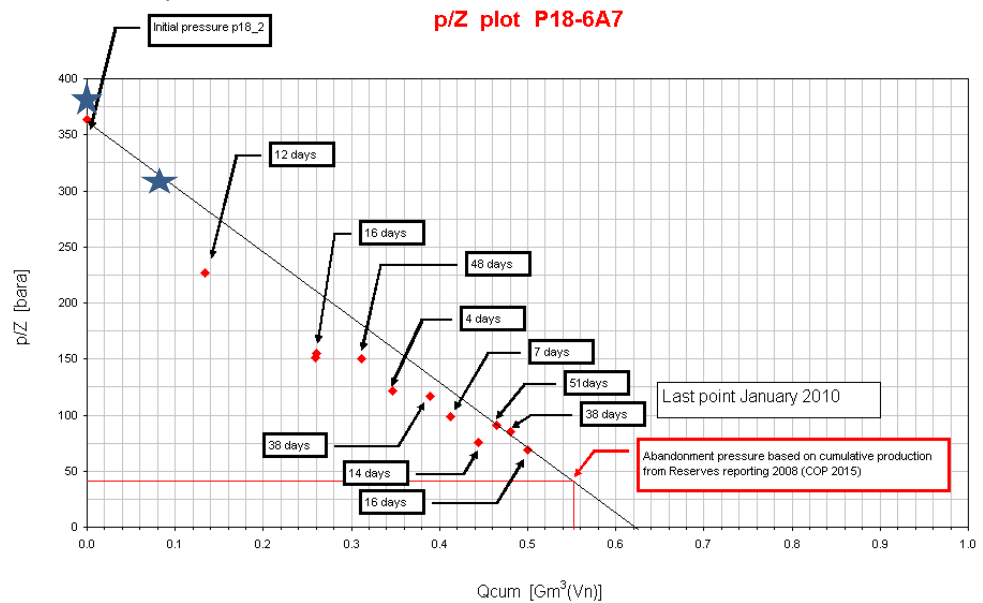


Figure 6-10: P/z plot for P18-6 with shut-in periods. Figure taken from Vandeweyer et al. (2011).). The two stars indicate pressure data reported on nlog.nl: 378 bar from the EOWR and 305 bar after production of 0.074 bcm. As also indicated, the initial pressure of the P18-2 field is added for comparison.

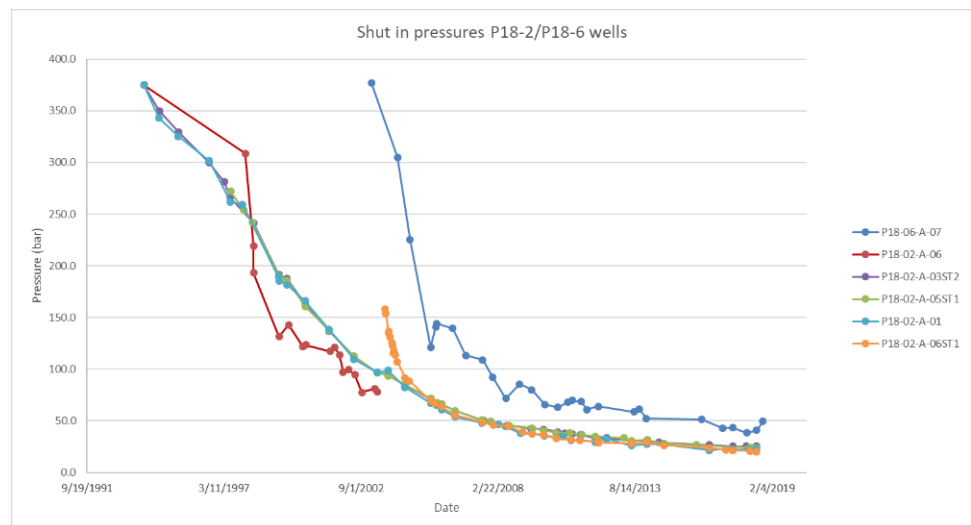


Figure 6-11: Pressure behaviour of P18-2 and P18-6 reservoirs.

### 6.3.6 Conclusions

The injection simulations lead to the following conclusions.

- Assuming a final reservoir pressure of 375 bar (initial reservoir pressure, datum depth 3400 m), the P18-2 field (using compartment I,II and IV) can store 32.2 Mt of CO<sub>2</sub>.
- Assuming hydrostatic reservoir pressure of 351 bar (datum depth 3400 m), the P18-2 field (using compartment I,II and IV) can store 30.6 Mt of CO<sub>2</sub>.
- From the point of view of the reservoir, the target CO<sub>2</sub> supply rates can be injected through the three proposed P18-2 injection wells together (P18-02-A-01, P18-02-A-03ST2 and P18-02-A-05ST1), for a period of about 10 years. The last two to four years (2034 – 2041) of the target injection scenario would require another storage location.
- About 83% of the stored CO<sub>2</sub> is injected through well P18-02-A-05ST1. The other two wells both contribute 8-9% to the total injection amount of CO<sub>2</sub>. It is to be noted that in the results presented here, any restrictions to flow from the tubing the wells is not included; such restrictions can result in a different distribution of flow over the wells.
- With the injection scenario used here, after the year 2033 combined injection capacity decreases to below the target level of about  $4.1 \cdot 10^6$  Sm<sup>3</sup>/day - although timing of the end of the injection plateau rate depends on the injection history and on the final pressure chosen for the reservoir.
- CO<sub>2</sub> fills the pore volume that was previously filled with natural gas. In compartment IV of the P18-2 field, the model employed suggests that CO<sub>2</sub> migrates some distance across the original gas-water contact into the connected aquifer, but does not spill.
- After the end of injection, the CO<sub>2</sub> is retained within the limits of the structures that make up the original P18-2 gas field. Post injection simulations shows gravitational segregation leads CO<sub>2</sub> to move back to the original GWC.

## 6.4 Temperature development in the reservoir

### 6.4.1 Introduction

As explained in Section 6.2, the simulations presented in the previous section do not take into account the temperature difference between the injected CO<sub>2</sub> and the reservoir. This section describes the evolution of the temperature effect in the P18-2 reservoir estimated by numerical simulations by the TOUGH simulator

Using the CO<sub>2</sub> supply scenario shown in Section 5.2 as the target, the conditions of the CO<sub>2</sub> at bottom hole, in the well, prior to inflow into the reservoir, were derived from a flow assurance study performed in parallel to the study presented here (Belfroid, 2019). The key results from the steady-state simulations, which are used for this study, are summarized below. For a full description of the study, including start-up and shut-in simulations, the reader is referred to Belfroid (2019).

The steady-state simulations were performed for a range of well characteristics: flow rates, CO<sub>2</sub> injection temperatures and reservoir pressure conditions. The compressor and transport pipeline to the P18-A platform were taken into account in deriving these results. The downhole temperature was required to always be above 15 °C, to avoid CO<sub>2</sub> hydrate formation in the well (which could happen when brine enters the well during shut-in periods) or in the near-well zone in the reservoir (due to the pressure drop between well and reservoir; see also Section 6.4.3).

Table 6-4 shows a feasible injection scenario over time, in which the mass flow rate is limited to 30 kg/s (about 1 Mt/yr) at the depletion pressure of 20 bar and increases to 60 kg/s (2 Mt/yr) once reservoir pressure increase to 60 bar or higher. At high reservoir pressure the injection rate decreases, due to a downhole pressure limit of 375 bar (see also Section 6.3.1). The downhole temperature (in this case, the temperature inside the wellbore) increases with increasing reservoir pressure. The lowest downhole temperature occurs during the first phase of injection, when the reservoir pressure is at its lowest. The additional pressure and temperature drop in the reservoir near the well is shown in Section 6.3.3.

It is to be noted that Table 6-4 shows results for a single well; Belfroid (2019) also provides injection scenarios with all (four) injector wells in P18-2 and P18-4 open. During injection, the CO<sub>2</sub> supplied to the platform will be distributed over the open wells; the wells will select the rate. The table provides an indication of the potential rates for a single well. Details of the simulations that led to the table are given by Belfroid (2019).

Table 6-4 CO<sub>2</sub> conditions at platform and downhole for several values of reservoir pressure, for a single well.

Reservoir pressure [bar]	Mass flow rate [kg/s]	P Platform [bar]	P Downhole [bar]	T Platform [°C]	T downhole [°C]
20	30	78	32	42	17
60	60	87	75	37	32
100	60	87	110	37	51
200	60	94	206	36	64
300	45	105	303	33	62

## 6.4.2 Setup of simulation

### 6.4.2.1 TOUGH2 simulator

The TOUGH2 simulator is used in combination with the ECO2MG module (Pruess, 2011; Loeve et al., 2014), which is designed to model the behaviour of CO<sub>2</sub> in the presence of brine in both gas reservoirs and aquifers. A key feature of the module is that it considers the transition from low pressure to high pressure across the CO<sub>2</sub> saturation line, which is an important process in the injection of CO<sub>2</sub> into depleted gas field. Also the dry-out zone around the well and salt precipitation is taken into account.

### 6.4.2.2 P18-2 model

A 20-layer radially symmetric model (Figure 6-12) that covers the different geological formations was created to analyse the temperature and pressure field of P18-2 field. The radial direction has 47 cells, which increase exponentially in size away from the well into the reservoir from 0.15 m to 137 m. The grid cell distribution is dense close to the well (left side of Figure 6-13) and also more dense on the interface with the Hardegsen and the caprock to allow a more detailed modelling around this interface. The average permeability of each formation is used in the model (Table 6-5).

Other parameters which are important for the temperature distribution and heat flow in the P18-2 reservoir are the heat conductivity of each formation (2.0 W/m/°C ) and the rock grain specific heat (1000 J/kg/°C for all formations).

Table 6-5: P18-2 properties used in radially symmetric model used to simulate the temperature development in the reservoir.

<i>Formation</i>	<i>Porosity</i>	<i>Permeability (mD)</i>	<i>H (m)</i>
Caprock	0.01	0.01	
Hardegsen	0.11	154	26
Upper Detfurth	0.09	38	49
Lower Detfurth	0.07	31	27
Volpriehausen	0.03	0.02	

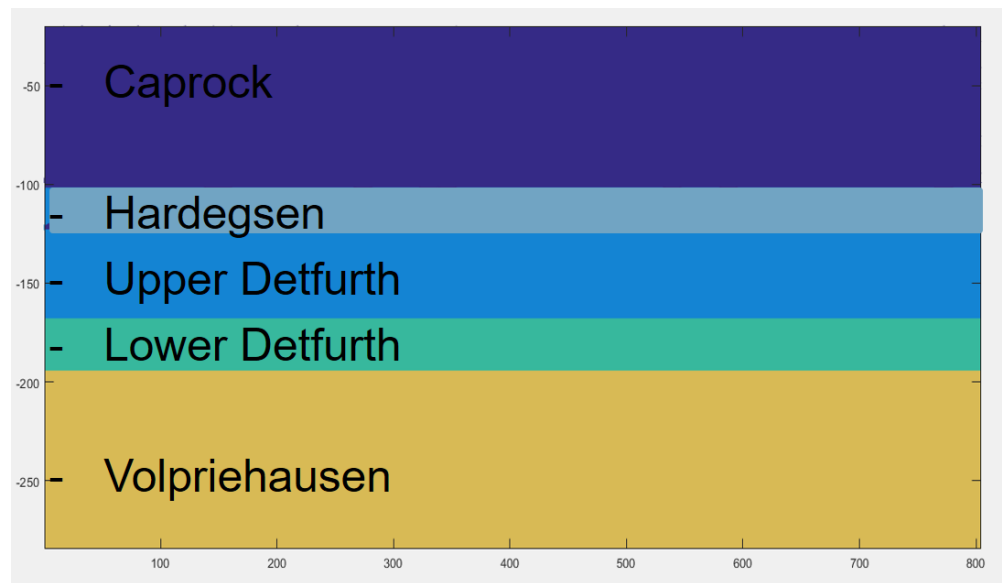


Figure 6-12: Radially symmetric model used for the modelling of the temperature field within the P18-2 reservoir.

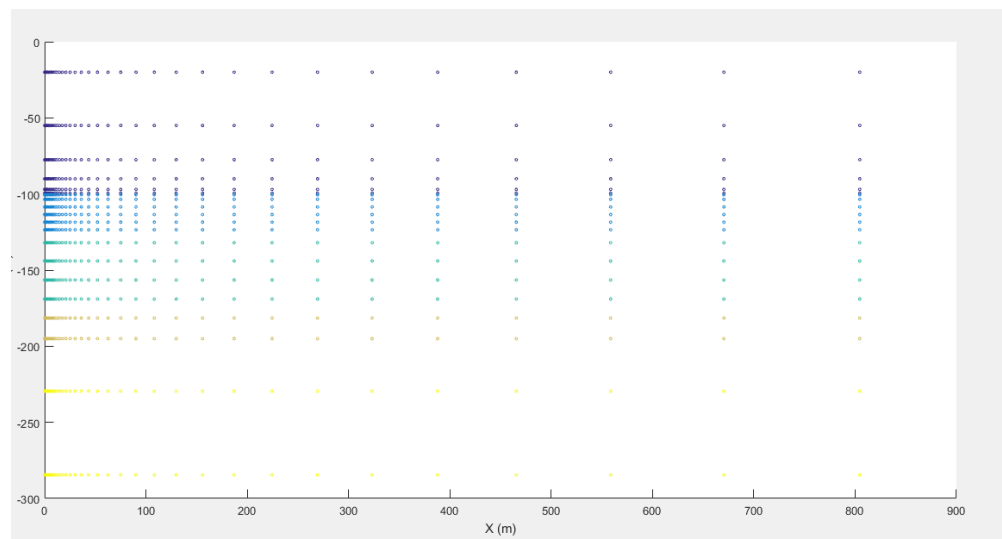


Figure 6-13: Grid cell distribution of the P18-2 radially symmetric model used for the modelling of the temperature field within the P18-2 reservoir; see also Figure 6-12.

### 6.4.2.3 Model settings

The initial reservoir conditions of P18-2 used are listed in Table 6-6.

Table 6-6: Initial conditions used for the modelling of the temperature field within the P18-2 reservoir.

Initial reservoir conditions	value
Reservoir pressure	20 bar
Reservoir temperature	100 °C;
Injection temperature	15 °C;
Injection duration	15 years
Injection rate	1.13 Mt/yr
Initial brine saturation	0.01

The reservoir pressure is set to 20 bar, which is assumed pressure after the production phase. The P8-2 reservoir temperature in reality is 126 °C, but the TOUHG2 simulator is limited to a maximum temperature of 103 °C; therefore the reservoir temperature in TOUGH2 model was set to 100 °C in the simulations. The results of all simulations miss the effect of the last 26 °C (e.g., faster heating of the cold CO<sub>2</sub>, larger effect on the stress changes).

The injection rate of 1.13 Mt/yr/well corresponds to a total injection of 4.5 Mt/yr into four proposed injection wells in the P18-2 and P18-4 reservoirs, which is the maximum injection scenario presented in Section 5.2.

Furthermore, there are two additional reasons why the modelled scenario is the most extreme injection scenario:

- The injection temperature is constant (15 °C) in the model, although the conditions described by Belfroid (2019) show that the temperature of the CO<sub>2</sub> remains close to 15 °C only during the initial phase of injection. In later stages the injection temperature is higher than 15 °C.
- The modelled duration of injection is 15 years with constant injection rate and no shut-in periods (e.g. due to maintenance). In this section, results for the first three years are considered.

The reservoir simulations showed that most of the CO<sub>2</sub> migrates into the Hardegsen Fm. upon injection and much less into the Upper and Lower Detfurth, the injection rates in the thermal simulations were distributed over the three formations accordingly: 60% into the Hardegsen, 28% into the Upper Detfurth and 12% into the Lower Detfurth.

### 6.4.3 Results

The temperature distribution and profiles from the modelling are presented in Figure 6-14 to Figure 6-17, for the injection rate of 1.13 Mt/yr/well. Even though the largest part of the CO<sub>2</sub> is injected in the Hardegsen Formation, the progression of the cold front is faster in the Detfurth Formations. The maximum extent of the cold zone is 400-500 m into the reservoir. The vertical extent of the cold plume into the caprock is less than 100 m), since no temperature effect is observed in Figure 6-15 (represents level '1' in Figure 6-14).

Just above the caprock / Hardegsen interface (10 m above the interface, level '2' in Figure 6-14) a cooling of 55 °C is observed (see Figure 6-16). In the reservoir itself, 60 m below the caprock / Hardegsen interface (level '3' in Figure 6-14) cooling due

to evaporation of brine combined with Joule Thomson effect of CO<sub>2</sub> is observed in the model, leading to temperatures below 10 °C around the injection well (see Figure 6-17).

A close analysis of the temperature effects in the near-well area (up to 50 m from the well) at low-pressure conditions (first 2-3 years at the injection rates used) shows that for the injection scenario the pressure and temperature conditions within the near-well zone are within the hydrate formation window (Figure 6-18).

(residual) pore water is available, hydrates could form and block the pore space, thereby decreasing the injectivity. The minimum temperature in the P18-2 model is 5.4 °C at 40 bar. Note that after 1.5 year of injection the minimum temperature observed in the model is 14 °C, which is outside the hydrate formation window.

However, Figure 6-19 shows that injection at the lower injection rate (0.56 Mt/a) the pressure and temperature conditions in the reservoir remain outside the hydrate forming conditions (Figure 7-1); the minimum simulated temperature is 10 °C at 30 bar.

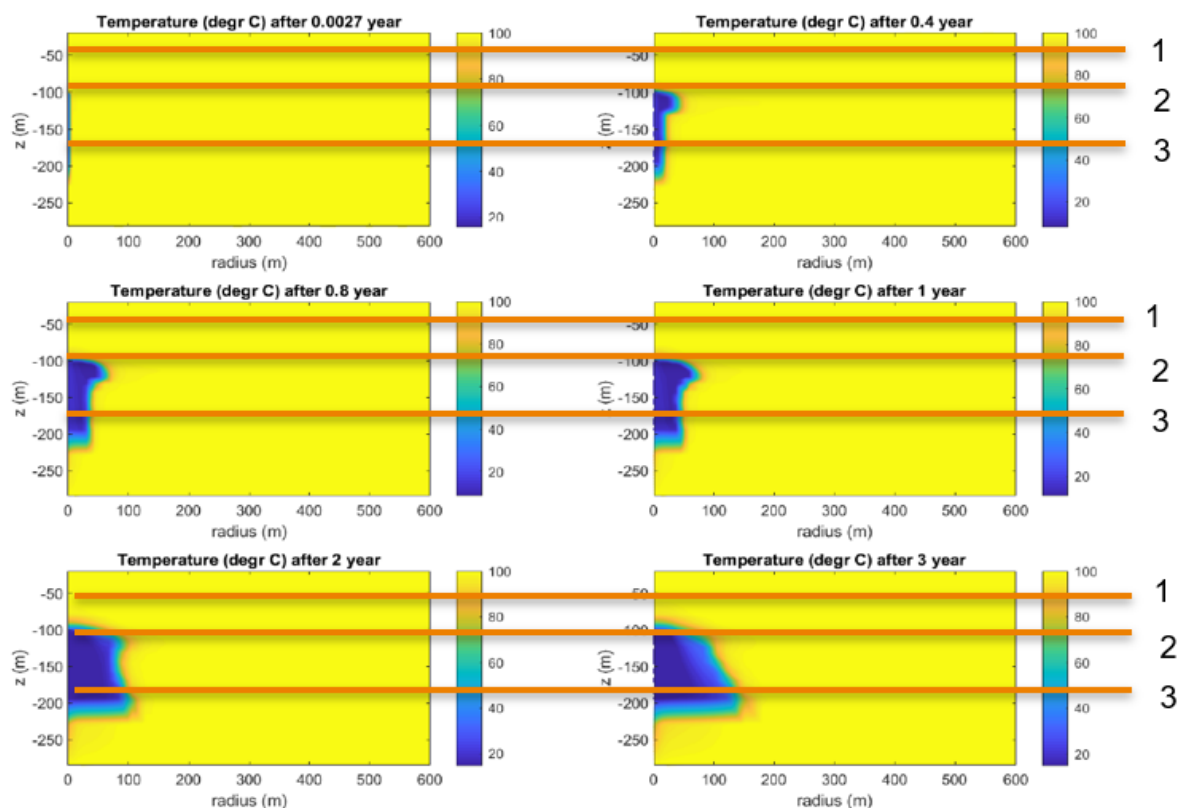


Figure 6-14: Temperature distribution in the P18-2 radially symmetric model for the maximum injection rate scenario 1.13 Mt/year/well. The numbers indicate three vertical levels in the model: level 1 is 100 m above caprock/Hardeggen interface, level 2 is 10 m above caprock / Hardeggen interface and level 3 is 60 m below caprock/Hardeggen interface; i.e., levels 1 and 2 are within the caprock, level 3 is within the reservoir. The injection well is located along the left vertical axis in each panel.

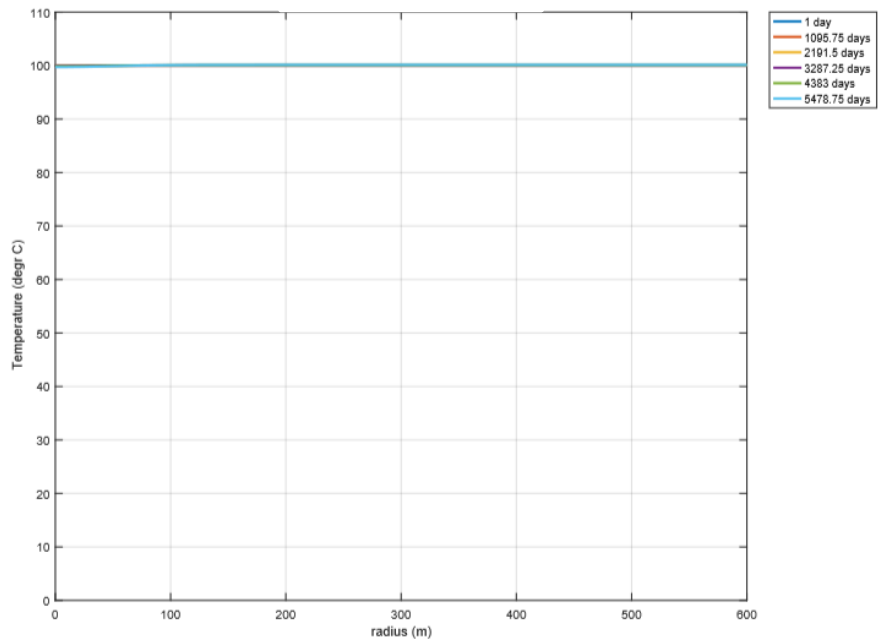


Figure 6-15: Temperature profile in the maximum injection rate scenario for level 1, which is 100 m above caprock / Hardegsen interface. The well is at zero radius.

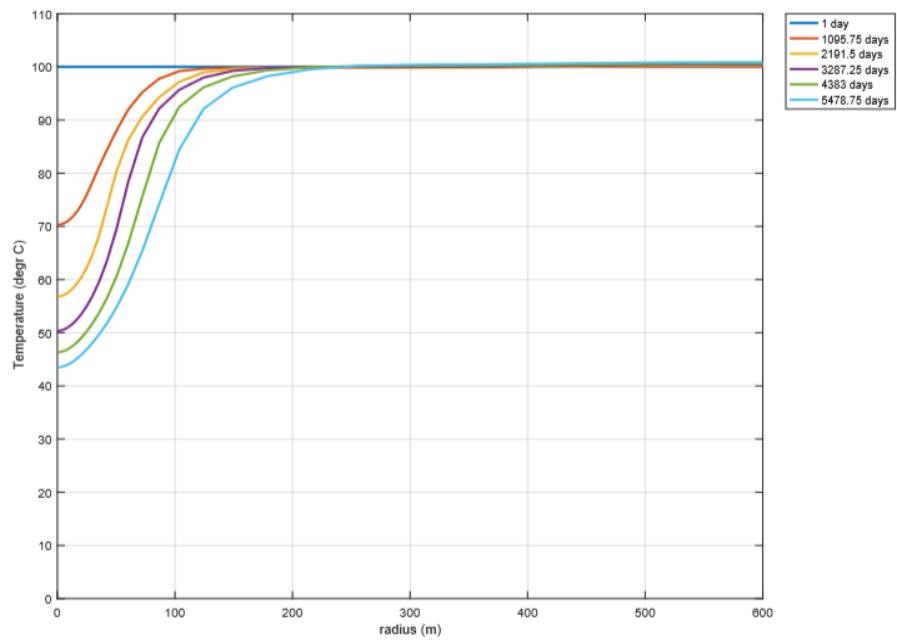


Figure 6-16: Temperature profile in the maximum injection rate scenario for level 2, which is 10 m above caprock / Hardegsen interface. The well is at zero radius.

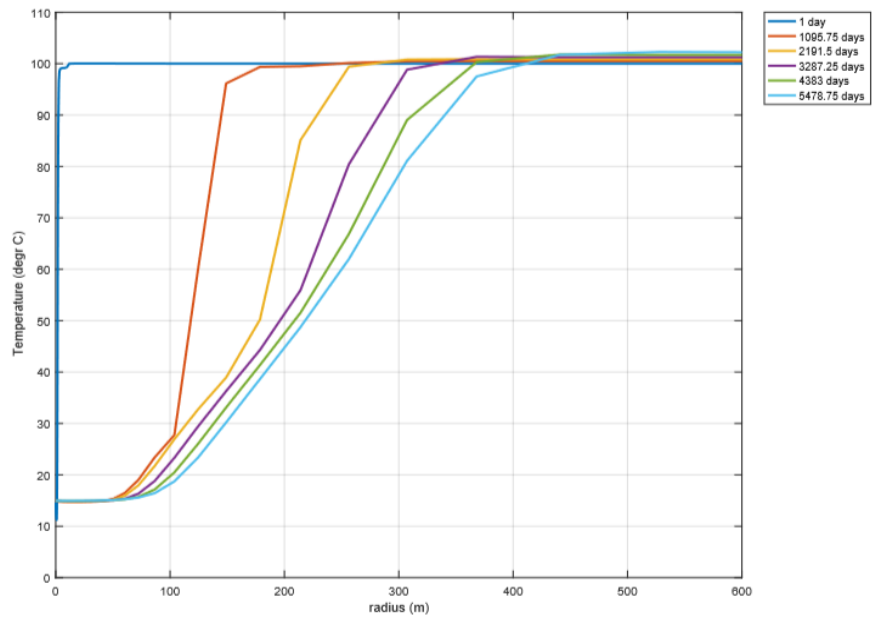


Figure 6-17: Temperature profile in the maximum injection rate scenario for level 3, which is 60 m below caprock / Hardegsen interface. The well is at zero radius.

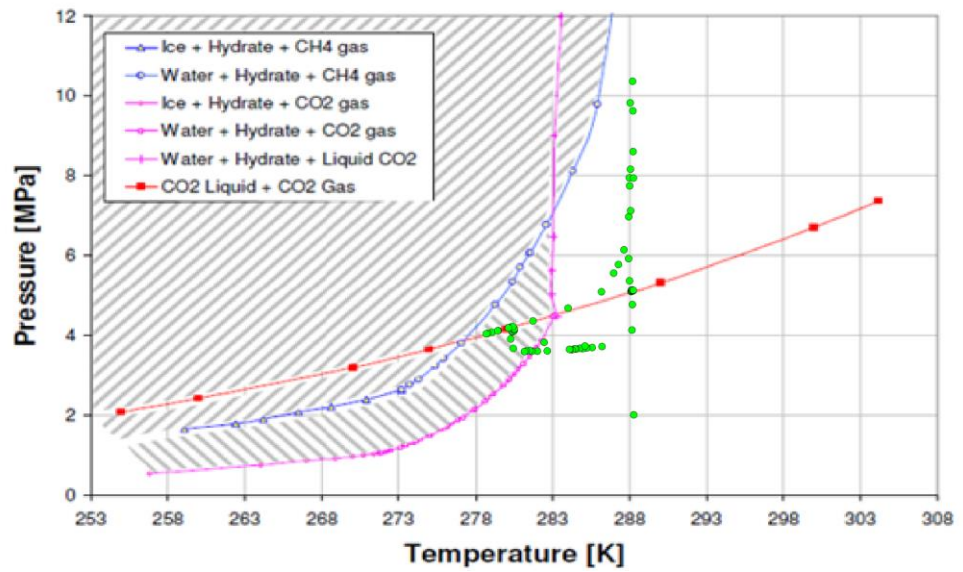


Figure 6-18: Hydrate formation window (hatched area), where hydrates can form, with overlain the temperature in the near-well zone (distance from the well smaller than 50 m): the green dots cover the ranges of temperature and pressure combinations as predicted by the P18-2 TOUGH2 model for the higher injection rate scenario.

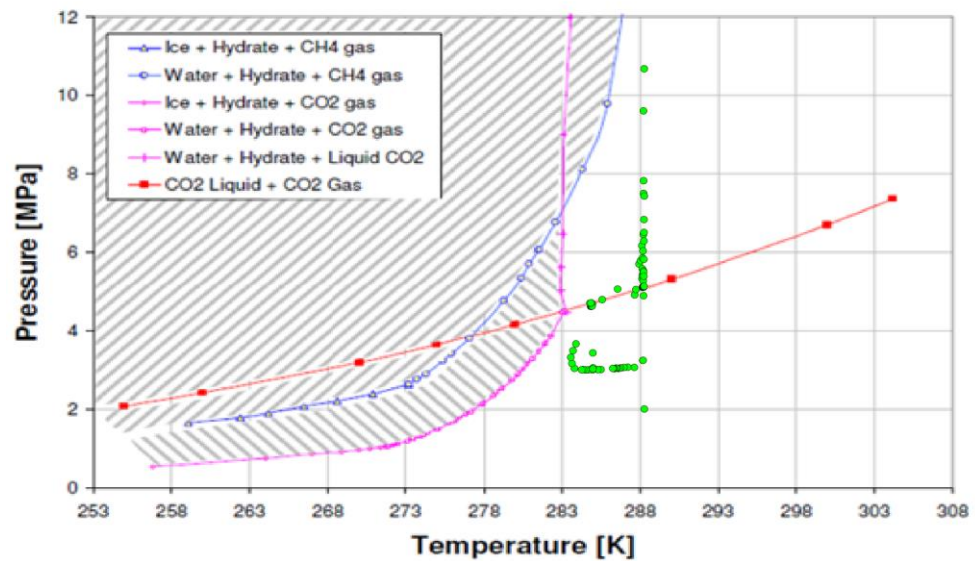


Figure 6-19: Hydrate formation window (hatched area), where hydrates start to occur, with overlain the temperature in the near-well zone (distance from the well smaller than 50 m): the green dots cover the ranges of temperature and pressure combinations as predicted by the P18-2 TOUGH2 model for the lower injection rate scenario.

#### 6.4.4 Risks

The injection scenarios used here were constructed to emphasise the development of a low-temperature zone around an injection well over time. The lowest temperatures of injected CO<sub>2</sub> are expected to occur when reservoir pressure is low (below about 50 bar), which corresponds with the first year at the rates used here. The interpretation should focus on the first few years of the results presented here.

The thermal modelling study identified two main risk factors: hydrate formation and low temperatures in the reservoir.

- When reservoir pressure is low, injection rates of the order of 1 Mt/yr/well and low injection temperature of 15 °C may lead to hydrate formation conditions in the near-well zone. Whether hydrates actually form under these conditions and affect injectivity remains a topic of further research. Hydrate formation does not affect safety or security of CO<sub>2</sub> storage. Hydrate formation due to injection can be avoided by managing injection temperatures and rates.
- The simulation shows a dry-out zone around the well, which results in additional cooling by the evaporation of the brine. In this dry-out zone, hydrates are unlikely to form since they need water. The interplay between drying out and conditions in the reservoir entering the hydrate formation window should be assessed.
- The progression of the cold front is initially fast but slows down with time due to increasing radius of the cold front. For the injection scenarios simulated, the cold front reaches about 100 m distance from the injection well after about two years of injecting low-temperature CO<sub>2</sub>.
- After about two years of injecting cold CO<sub>2</sub>, the cold front has not yet reached the fault that is nearest to an injection well. Well test data suggested that a fault is observed 128-148 m away from The P18-02-A-01 well; according to the static model this distance is 160 m. Section 7.3 investigates the geomechanical implications of a low-temperature front on fault stability.

A reliable modelling of the distribution of the cold plume requires the three-dimensional structure around the well (or wells) to be represented in the model, as well as the historical injection rate and injection temperature over time. Such work is to be done prior to injection, to define the safe injection window from the point of view of temperature development in the reservoir and near faults (see also Section 7.3)

#### 6.4.5 *Conclusions*

The TOUGH2 simulations using a simplified, radially symmetric model, demonstrated that the temperature effects of injecting cold CO<sub>2</sub> for worst case conditions result in:

- Near-well temperatures that could be in the hydrate formation zone. The formation of hydrates could temporarily deteriorate the injectivity. Hydrates, once formed, will disappear once the temperature has increased sufficiently for local conditions to no longer be inside the hydrate formation window. On the other hand the dry out zone around the injection well will prevent to form any hydrates at all by the injected (cold and dry) CO<sub>2</sub>.
- Progression of the cold front into the reservoir. The distance of the cold front depends on the duration and injection rate of injection of cold CO<sub>2</sub>. At high injection rates (over 1 Mt/yr/well) of cold CO<sub>2</sub>, the front is at about 100 m from the injection well in about 2 years. The impact of low temperatures on fault stability are investigated in Section 7.3).

More detailed reservoir simulations with a more advanced, non-isothermal reservoir simulator are needed to improve predictions of the temperature development near each of the three proposed P18-2 injection wells, taking into account the 3D structure of the reservoir.

## 6.5 Chemical interactions

### 6.5.1 *Introduction*

Within a storage reservoir, physical and chemical interactions between the CO<sub>2</sub>, the formation water and rock minerals will occur during and after CO<sub>2</sub> injection. On the short term, during the injection phase, the risk of porosity and permeability decrease and corresponding injection issues need to be evaluated. On the long term, during the post-abandonment phase, the CCS Directive (EU, 2009) requires evaluation of the fate of CO<sub>2</sub>, for which geochemical reactions play an important role. This section describes the short-term (injection phase) and long-term (post-abandonment phase) CO<sub>2</sub>-water-rock interactions and their impact on the feasibility of CO<sub>2</sub> injection and storage in the P18-2 reservoir, using recent literature. Most of the discussion is general and applicable to CO<sub>2</sub> storage in depleted gas fields. In addition results from previous modelling studies specifically for P18-2 are discussed.

### 6.5.2 *Injection phase: Effect of dry-out and salt precipitation on injectivity*

During injection of dry CO<sub>2</sub>, whether in an aquifer or a depleted hydrocarbon field, (residual) formation water will evaporate into the CO<sub>2</sub> in the near-well area. A dry-out zone will develop which can extend up to several tens of meters into the reservoir. As this will increase the relative permeability of CO<sub>2</sub>. On the other hand, as the mass of water decreases, the concentration of the aqueous species

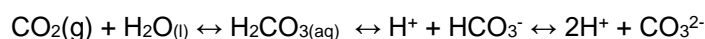
increases and minerals start to precipitate when the remaining water becomes saturated (Miri and Hellevang, 2016). The most common mineral to precipitate is halite salt (NaCl), since formation waters contain mostly Na<sup>+</sup> and Cl<sup>-</sup>, although other minerals such as sulphates or hydroxides can also form. Salt precipitation during CO<sub>2</sub> injection and corresponding permeability reduction and injectivity issues have been studied in the laboratory and by numerical simulations, primarily for the purpose of CO<sub>2</sub> storage in saline aquifers (e.g. Bacci et al., 2011, Kim et al., 2012, Roels et al., 2014). Field evidence of salt precipitation and injectivity impairment was obtained from the Ketzin injection pilot in Germany (Baumann et al., 2014) and the Snøhvit storage site in Norway (Grude et al., 2014). Based on those studies it can be concluded that the key parameter for salt precipitation to result in permeability and injectivity impairment is the availability of saline water for capillary backflow (migration of salt water towards the injection well) and hence continuous supply of salt. In the absence of capillary backflow of saline water, the maximum amount of salt precipitation is constrained by the volume of residual formation water and the concentration of aqueous species. The available species will then precipitate as thin coatings around the rock grains, in the space that was occupied by the residual brine, without significantly affecting the total permeability. This would be a more likely outcome for depleted pressure gas fields

In the P18-2 reservoir the water saturation at the beginning of CO<sub>2</sub> injection will be close to residual and hence it will be immobile. This is supported by the lack of (significant) water (brine) production during the production history of the field (see P18-2 production data at [www.nlog.nl](http://www.nlog.nl)). As a result, capillary backflow of brine during injection will not occur. Production data did not give any evidence for the presence of a strong aquifer support, implying that brine supply from below is also not expected to occur. Tambach et al. (2015a) reported on the modelling of CO<sub>2</sub> injection into a depleted gas reservoir (based on P18 characteristics) and the effect on salt precipitation. In the case of immobile brine the maximum amount of salt precipitation was 2.7% of the pore volume, with corresponding permeability decrease of 23%. Note that the degree of permeability decrease upon a reduction in porosity is highly uncertain, but much higher values than 23% are not to be expected. With permeability values as high as those of the P18-2 reservoir, injectivity impairment by this amount of salt precipitation is not expected to occur. The temperature decrease in the near well area related to the low temperature of injected CO<sub>2</sub> will not have major impact on the extent of salt precipitation.

Overall, the increased relative permeability due to decreased water saturation will have a more significant and positive impact on injectivity than the minor total permeability reduction related to salt precipitation when injecting CO<sub>2</sub> in a depleted gas field such as P18-2.

### 6.5.3 *Injection phase: CO<sub>2</sub>-water-rock interactions*

When CO<sub>2</sub> is injected into the reservoir, it will try to form a new physico-chemical balance with the (residual) formation water. The water starts to evaporate into the dry CO<sub>2</sub>, as described in the previous section, and CO<sub>2</sub> starts to dissolve into the formation water. In the near-well area, the dry-out will progress fast, not leaving any formation water for CO<sub>2</sub> to dissolve in. Beyond the progressing dry-out zone CO<sub>2</sub> dissolves into the formation water and further dissociates by the following reactions:



These reactions lead to an increased acidity of the formation water and a disequilibrium with the rock mineralogy. Both experimental and modelling studies show that on the short term the main reaction is the partial dissolution of carbonates, and potentially sulfides and sulphates, to buffer the pH. Of the carbonates, calcite dissolution is fastest, while the dissolution of other carbonates such as dolomite and ankerite is much slower. The mineralogy of the P18-2 reservoir, reported in the core analysis report for P18-A-01 (P/18-3 well), consists of mainly quartz, with lower amounts of K-feldspar, albite, plagioclase, dolomite, and clay minerals. Only occasionally anhydrite or calcite have been found, in small amounts.

Equilibrium batch reaction modelling with PHREEQC software, performed for the feasibility study of P18 in the CATO-2 project, predicted the dissolution of very small amounts of dolomite and pyrite, with negligible amounts of anhydrite and dawsonite precipitation (Vandeweyer et al., 2011). These reactions present a worst case scenario as the simulation was based on equilibrium modelling and did not consider kinetics. Also, these reactions would not occur in the near well zone where dry-out would occur. Since worst case conditions predict negligible impact of CO<sub>2</sub>-water-rock interactions on porosity, and hence on permeability, in the reservoir beyond the dry-out zone, it can be concluded that geochemical interactions will not negatively impact the injectivity.

#### 6.5.4 *Post-abandonment phase: CO<sub>2</sub>-water-rock interactions*

On the long-term, representative for the post-abandonment phase, the conditions in the reservoir will slowly move towards a chemical equilibrium. This implies that also silicate minerals have time to respond to the change in chemical equilibrium as a result of the high CO<sub>2</sub> partial pressure and partial CO<sub>2</sub> dissolution into the residual formation water beyond the dry-out zone. Since only residual, and thus immobile, formation water is present in the reservoir, a chemical equilibrium will only be obtained on the micro-scale; ions in the formation water can migrate by diffusion through the film of formation water as long as the film is connected. The scale on which formation water is connected is unknown and highly depends on the microstructural characteristics of the rock. Regardless of the scale of connection, diffusion of ions will be very slow, making it most likely to have chemical equilibrium on microscale only. The limited amount of water further slows down the reactions, as water acts as a facilitator for the dissolution-precipitation reactions.

Tambach et al. (2015b) performed simulations with TOUGHREACT to predict long-term mineral reactions and sequestration of CO<sub>2</sub> in carbonate minerals for the P18 reservoir. A key uncertainty in the simulations is whether or not to include dawsonite as a secondary mineral. Dawsonite is a controversial carbonate mineral which, if included in geochemical simulations, is predicted to sequester a large part of the CO<sub>2</sub> on the long term. Also the possibility of magnesite precipitation as a secondary mineral was questioned. In the chemical initialization of the reservoir formations by Tambach et al. (2015b), both dawsonite and magnesite were predicted to be present as initial minerals. Since they were both not measured in any of the P18 reservoir samples analysed, it can be questioned whether the chemical database contains correct chemical constants for these minerals.

In the same study by Tambach et al. (2015b) simulations for long-term CO<sub>2</sub>-water-rock interactions were performed with and without dawsonite and magnesite as secondary minerals. In both cases, long-term mineral reactions include the partial reaction of albite, K-feldspar and kaolinite to illite. In the scenario with dawsonite and magnesite as secondary minerals, the largest part of the CO<sub>2</sub> is predicted to be trapped in carbonate minerals within a few thousand years. In the simulation excluding dawsonite and magnesite as secondary minerals, leaving only calcite and dolomite as potential secondary carbonates, no CO<sub>2</sub> is predicted to be sequestered in carbonate minerals after equilibrium is reached within 10,000 years. Limited CO<sub>2</sub> partial pressure decrease from 365 bar after well closure to 300, 315 and 341 bar for the lower Detfurth, Upper Detfurth and Hardegsen Formation respectively is predicted after 10,000 years, related to a slight overall porosity increase due to dissolution-precipitation reactions. More than 95% of the CO<sub>2</sub> remains in the reservoir in the supercritical state. Hence the impact on Pressure and Temperature medium to long term is negligible

Studies on natural analogues only rarely report on the occurrence of dawsonite, and if present, only in very small amounts. Natural analogues are natural occurrences of CO<sub>2</sub>-rich gas reservoirs in which the CO<sub>2</sub> has had thousands to millions of years to reach chemical equilibrium with the reservoir formation water and mineralogy, and therefore present a unique opportunity to study the long term fate of CO<sub>2</sub> in a depleted hydrocarbon reservoir and validate geochemical models. The absence of large amounts of dawsonite in natural analogues suggests that dawsonite precipitation in geochemical simulators is not well defined.

Two major studies on natural analogues in the US and the UK show that in most cases negligible trapping in carbonate minerals occurred (Baines and Worden, 2004; Gilfillan et al., 2009), which is most likely due to the slow dissolution of silicate minerals which is a rate-limiting step (Baines and Worden, 2004). The study by Gilfillan et al. (2009) identified solubility trapping as the primary sink for the natural CO<sub>2</sub> fields analysed, but this is only possible in case of sufficient availability of formation water, which is not the case in depleted hydrocarbon fields without strong aquifer supports such as the P18-2 reservoir. Based on the insights obtained from natural analogues, the scenario by Tambach et al. (2015b) excluding dawsonite and magnesite as secondary minerals provides a more realistic prediction of the long term fate of CO<sub>2</sub>. We can conclude that almost all of the injected CO<sub>2</sub> will remain in the supercritical state for thousands of years.

## 6.6 Conclusions

### *CO<sub>2</sub> storage capacity, CO<sub>2</sub> injection rates*

The injection simulations lead to the following conclusions.

- Assuming a final reservoir pressure of 316 bar (90% of hydrostatic), the P18-2 field can store 26 Mt of CO<sub>2</sub>.
- From the point of view of the reservoir, the target CO<sub>2</sub> supply rates can be injected through the three proposed P18-2 injection wells together (P18-02-A-01, P18-02-A-03ST2 and P18-02-A-05ST1), for a period of about 10 years from the start of injection. The last two to four years (2031 – 2035) of the target injection scenario would require another storage location.

- About 83% of the stored CO<sub>2</sub> is injected through well P18-02-A-05ST1. The other two wells both contribute 8-9% to the total injection amount of CO<sub>2</sub>.
- With the injection scenario used here, after the year 2033 combined injection capacity decreases to below the target level of about  $4.1 \cdot 10^6$  Sm<sup>3</sup>/day - although timing of the end of the injection plateau rate depends on the injection history and on the final pressure chosen for the reservoir.
- CO<sub>2</sub> fills the pore volume that was previously filled with natural gas.
- CO<sub>2</sub> plume development far away from the injection well requires knowledge of fault transmissibility between Compartments I and II; using P18-02-A6ST1 as an observation well could provide relevant monitoring data.

#### *Near-well hydrate formation*

For a few days/weeks/months in each new injection well CO<sub>2</sub> is likely to be injected at conditions close to those allowing the formation of CO<sub>2</sub>-hydrates. A proper management of injection conditions is needed to ensure that temperature and pressure in the well and in the near-well area remain outside the hydrate formation window. However, dry-out of the near-well region by the CO<sub>2</sub> may prevent hydrate formation anyway. This is an aspect that requires further investigation. It should be noted that hydrate formation does not pose a risk to safe and secure storage of the CO<sub>2</sub>. It may just reduce injectivity temporarily.

#### *Near-well chemical clogging*

Injection of CO<sub>2</sub> into the reservoir will cause drying out of the reservoir. As a result the CO<sub>2</sub> relative permeability will increase. Total permeability decrease related to precipitation of salt will be negligible. Overall the injectivity of CO<sub>2</sub> is expected to increase. Near well clogging due to CO<sub>2</sub>-water-rock interactions in the area beyond the dry-out zone is expected to be insignificant.

#### *Temperature effects*

The injection of CO<sub>2</sub> at low temperature into the P18-2 gas field must be modelled and hence predicted in detail prior to the start of injection. . This is the most important base line conformance measure, and the most important set of lessons to be learned to assist the development of all future pressure depleted gas storage fields The cold CO<sub>2</sub> will affect bottomhole pressure during injection. The pressure in the reservoir will slowly increase as the CO<sub>2</sub> in the reservoir gradually reach initial reservoir temperature. A more detailed analysis is needed prior to the start of injection.

#### *Long-term reservoir integrity*

No significant chemical interactions between the CO<sub>2</sub> and the reservoir rock are expected. CO<sub>2</sub> is expected to remain in supercritical state in the reservoir for a period of the order of thousands of years.

## 7 Fault stability

### 7.1 Introduction

This section focuses on the evaluation of the potential of destabilization of intra-reservoir faults identified in the seismic cube and mapped in the static and dynamic models. The section addresses fault stability in relation to reservoir re-pressurisation (Section 7.2), to the low temperature of the injected CO<sub>2</sub> (Section 7.3) and to geochemical effects of CO<sub>2</sub> (Section 7.4).

The overall conclusion from the work presented in this section is that the risk of fault reactivation due to the injection of CO<sub>2</sub> is low.

The increasing reservoir pressure as a result of injecting CO<sub>2</sub> stabilizes the faults that bound the P18-2 field. CO<sub>2</sub>-related geochemical effects in fault zones are unlikely to lead to reactivation of the faults, or to CO<sub>2</sub> migration along faults.

If low-temperature CO<sub>2</sub> (the temperature can be about 100 °C cooler than the reservoir temperature) reaches a fault, the fault can be locally destabilized. This risk can be mitigated by monitoring and, if necessary, by reducing the injected amount of CO<sub>2</sub> through wells that are close to bounding faults. The well that is closest to a fault (well P18-02-A-01) has low injectivity which may already sufficiently mitigate this risk. Further analysis is needed to define the risk and mitigation requirements in more detail.

### 7.2 Fault stability: pressure effect

For the effects of pressure changes on inter-compartment fault reactivation we use MACRIS (Mechanical Analysis of Complex Reservoir for Induced Seismicity), a TNO-developed semi-analytical approach which allows us to evaluate both the poro-elastic effect and the direct pressure effect on stresses along the mapped faults.

Details of MACRIS are given in an Annex, Section 17.9. The required input for running MACRIS is the ECLIPSE reservoir grid with the flow simulations detailed in Section 6. Taking the ECLIPSE reservoir flow simulations as inputs MACRIS directly computes the stress induced by both the poro-elastic effect (i.e., the reservoir contraction/dilation due to depletion/injection of gas) and the direct pressure effect (i.e., the changes in effective normal stress due to the changes in pore pressure inside the faults). It is important to mention that MACRIS captures the effect of the differential compaction between two offset compartments. For the direct pressure effect, the average pore pressure between the two juxtaposed reservoir compartment at faults has been assumed.

It is not needed to rebuild a new geomechanical mesh with MACRIS; it directly works with the grid of the flow simulation (ECLIPSE). This way, MACRIS is extremely fast. Moreover, it allows the evaluation of stresses in 3D along all the mapped faults with high resolution.

For a simplified 3D single-fault tank reservoir model, the MACRIS stress solution has been compared with the solution given by the Diana FE (Finite Element) simulator. The results are presented in appendix 16.8 and clearly demonstrate the almost perfect match between MACRIS and the FE solution. It is important to keep in mind here that it would not be possible to use an FE approach for the 3D evaluation of the stresses along the multiple faults of the P18-2 field. Solely 2D cross-sections as it has been performed in the previous P18 study (Vandeweyer et al., 2011) could have been performed. Having access to the Coulomb stress distribution in 3D along the fault planes with MACRIS is extremely advantageous, since the along-strike variability is accessible and the area of excess Coulomb stress can be quantified. This area of excess Coulomb stress is key to evaluate the risk of fault reactivation.

All the input parameters used for MACRIS are reported in Table 7-1. One unique set of model parameters has been used in the present analysis; and thus the parameter sensitivity search has not been performed. The stress changes computed in MACRIS must be added to the initial stress tensor. In the West Netherlands Basin the minimum in situ stress is horizontal and the stress regime is extensional or normal-faulting (i.e. the largest principal stress is vertical). The largest vertical stress ( $S_v = S_{max}$ ) is calculated as the overburden weight, from seawater, rock, and pore fluid densities (see Table 7-1). The orientation of the minimum horizontal stress  $S_h$ , determined from borehole breakouts and the World Stress Map, is 55° (N55E). The magnitude of  $S_h$  is defined by applying the ratio of horizontal-to-vertical effective stress  $Ko' = S_h/S_v'$ ; a value of  $Ko' = 0.63$  is used for the analysis. Finally, the magnitude of the maximum horizontal stress  $S_H$  is defined by the ratio  $S_h/S_H = 0.9$ . It is important to note, that a single unique value of each of the parameters controlling the in-situ stress conditions (notably the orientation of  $S_h$ ,  $Ko'$  and  $S_h/S_H$ ) is used for the geomechanical analysis. In other words, a parameter sensitivity search has not been carried out. However, the input parameter values are aligned with the ones used in the geomechanical analysis of Vandeweyer et al. (2011).

Table 7-1 Input model parameters used for the MACRIS semi-analytical approach.

MACRIS model parameters	
<i>S<sub>h</sub> orientation</i>	N55E
$Ko' = S_h/S_v'$	0.63
<i>S<sub>h</sub>/S<sub>H</sub></i>	0.9
$\rho_{rock}$	2260 kg/m <sup>3</sup>
$\rho_{water}$	1150 kg/m <sup>3</sup>
$\rho_{gas}$	200 kg/m <sup>3</sup>
<i>E<sub>reservoir</sub> (Young's modulus)</i>	18GPa
<i>E<sub>overburden</sub> (Young's modulus)</i>	25GPa
<i>E<sub>underburden</sub> (Young's modulus)</i>	28GPa
<i>v (Poisson's ratio)</i>	0.2
$\mu$ (friction coefficient)	0.6
$\alpha$ (Biot's coefficient)	1.0

From the new full stress tensor, including the induced stress changes, one can derive the shear stress  $\tau$  and effective normal stress  $\sigma'$  for any fault orientations. In order to assess the potential reactivation of a fault, one needs to combine both stresses, the shear stress promoting slip whereas the normal is clamping the fault.

One convenient way is generally to calculate the Coulomb stresses  $C$  or the Fault Shear Capacity (FSC), respectively defined as:

$$C = \tau - \mu\sigma' \quad (8.1.1)$$

$$FSC = \frac{\tau}{\tau_{max}} = \frac{\tau}{\mu\sigma'} \quad (8.1.2)$$

where  $\mu = 0.6$  is the friction coefficient. When  $C$  starts to be positive or alternatively FSC reaches unit, a pre-existing fault can be reactivated since the shear stress is larger than the frictional strength defined as  $\mu\sigma'$ .

Figure 7-1 displays the initial negative Coulomb stresses (see equation 8.1.1 for the definition of the Coulomb stress) computed by MACRIS, that is before any pressure depletion. All the faults are coloured mostly in red, meaning that for all the faults and at any locations along these faults, the initial Coulomb stresses are mostly negative around minus 10-15 MPa. These negative Coulomb stresses represent the initial distance to failure, that is the required additional Coulomb stresses for the faults to be reactivated.

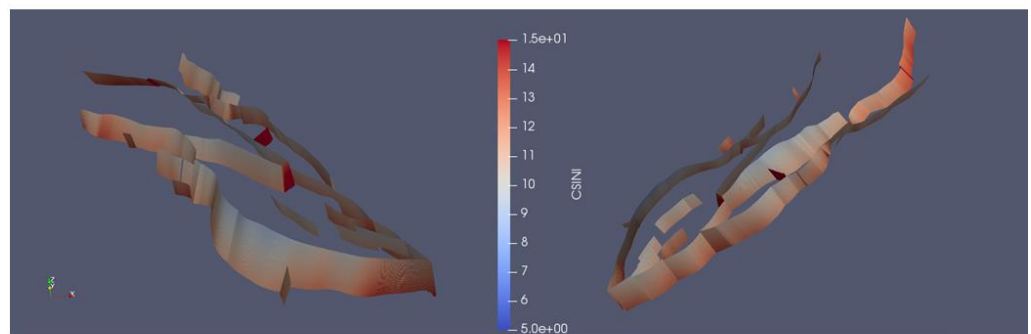


Figure 7-1: Initial distance to failure along the P18-2 faults. Colours indicate the negative Coulomb stress in units of MPa at the initialization of the MACRIS analysis, that is before any pressure depletion.

At the end of the depletion period, elongated areas of large Coulomb stress changes along the strike direction can be localized at the reservoir edges (see Figure 7-2). These areas of high Coulomb stress changes sometimes exceed the failure line (see Figure 7-3) meaning that potentially the concerned fault could be reactivated. However, as observed in Figure 7-3, most of the Coulomb stress peaks exceeding the failure line are expected to disappear during the injection period. The fault pillar displayed in Figure 7-3 is of particular interest, because it is at a close distance from a well. This aspect is further discussed in Section 7.3.

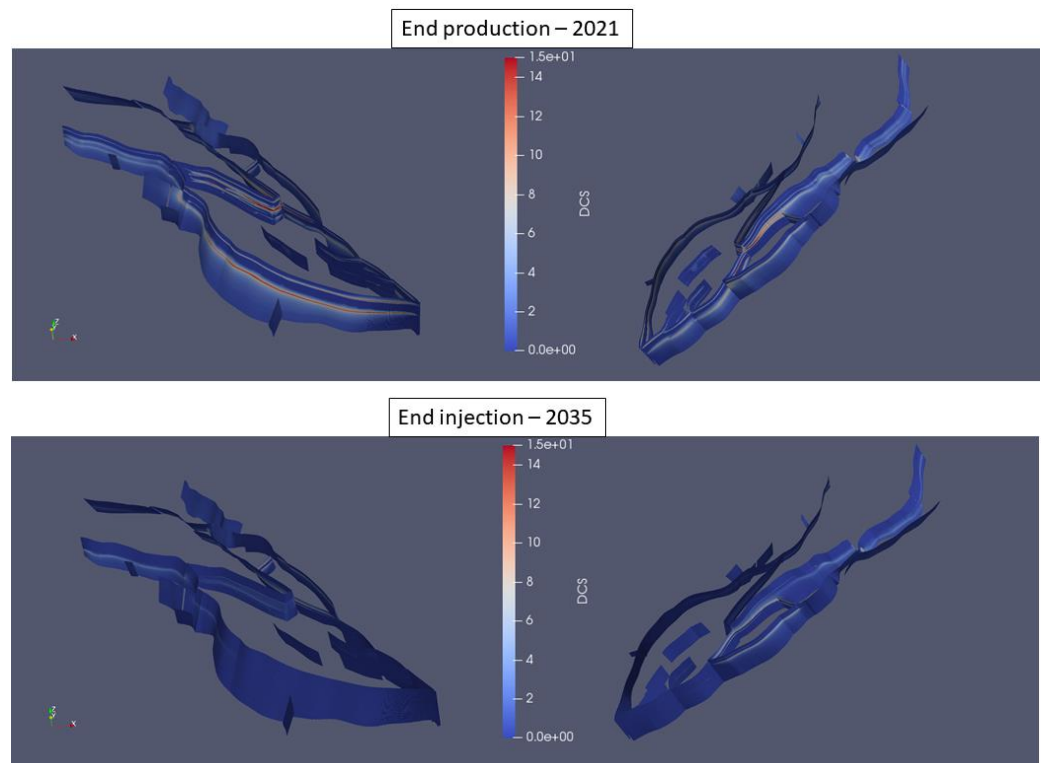


Figure 7-2 Changes in Coulomb stresses in units of MPa along the P18-2 faults inferred from MACRIS analysis.

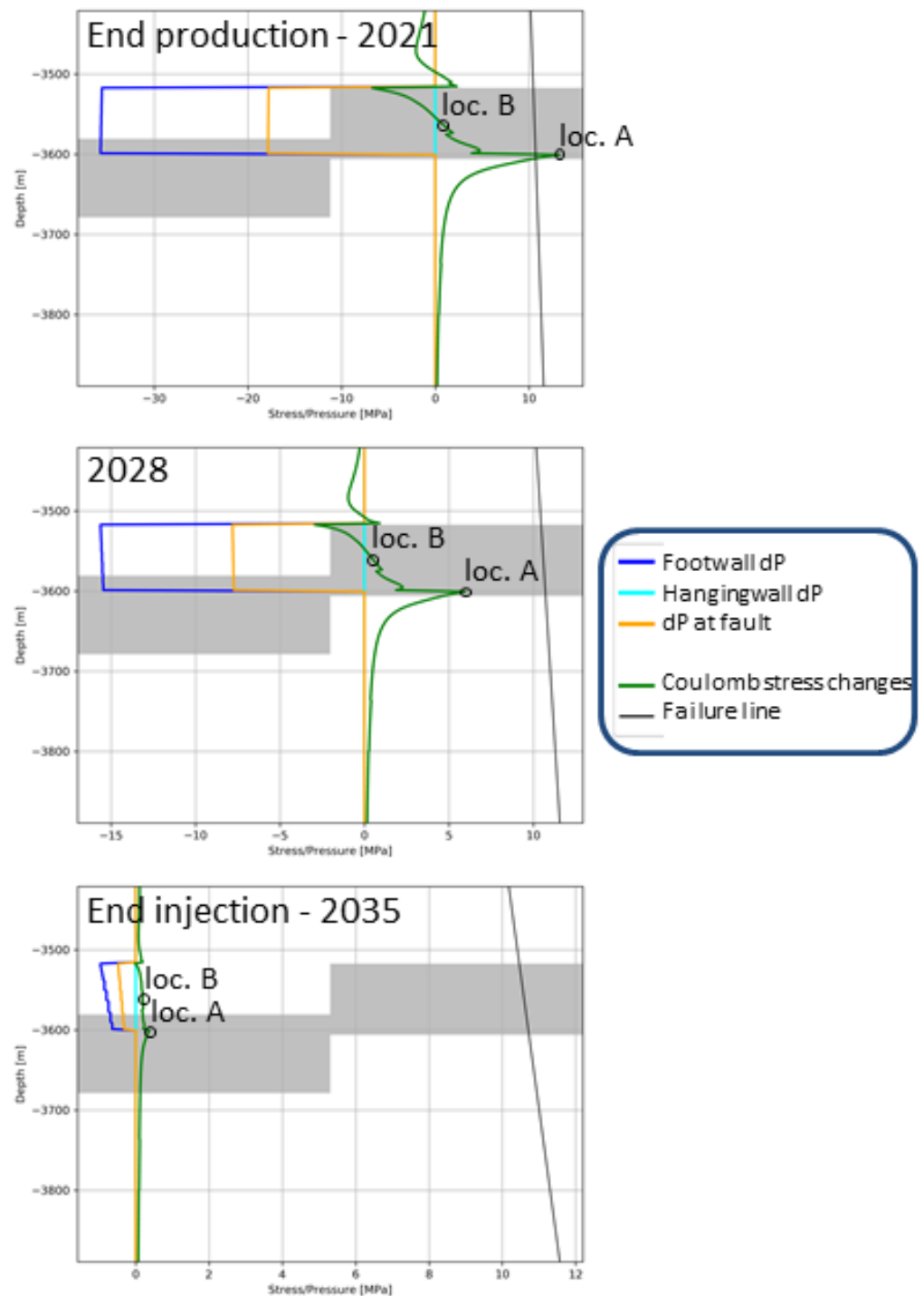


Figure 7-3 Changes in Coulomb stresses and pore pressures (inferred from MACRIS analysis) along representative fault pillars. “Footwall dP” and “Hangingwall dP” represent the changes in pore pressure in the reservoir grid blocks juxtaposed to the fault in the footwall compartment and in the hanging wall compartment, respectively. “dP at fault” corresponds to the pore pressure inside the fault, taken as the average pressure between “Footwall dP” and “Hangingwall dP”. The two grey rectangles delineate the two offset reservoir compartments. At the end of the production period, changes of Coulomb stresses exceed the failure locally at one reservoir edge. This Coulomb stress peak vanishes during the injection period. Stress state at locations A and B (loc. A and loc. B) are further detailed in Figure 7-4 and Figure 7-5. For the sake of visibility, the ranges of the x-axis have been separately adjusted for each graphs.

Figure 7-4 and Figure 7-5 give more detail on the changes of the stress state during the production and injection period illustrated by Mohr circles. At locations where the Mohr circle crosses the Coulomb failure envelope, fault instability is expected. Due to the differential compaction effect, even two nearby locations along the same fault pillar can experience a contrasted stress history. Location A, at the reservoir edge, is characterized by a stress path leading to fault reactivation. Instead, for location B, in the centre of the reservoir, the stress path remains parallel to the Coulomb failure envelope.

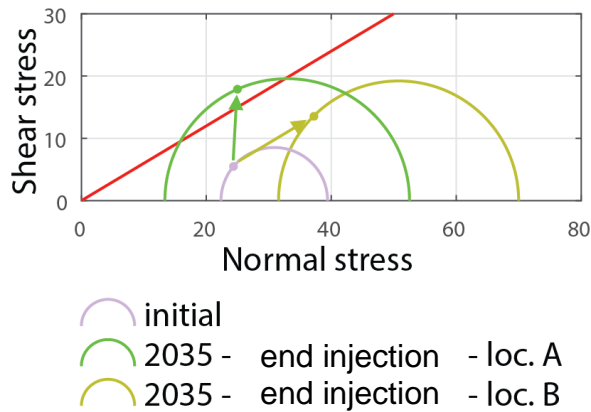


Figure 7-4 Heterogeneity of the stress field (in units of MPa) at the end of the injection period: Mohr-Coulomb analysis for two locations (loc. A and loc. B) along the same fault pillar displayed in Figure 7-3. The Coulomb failure envelope ( $\tau_{max} = \mu\sigma'$  with  $\mu = 0.6$ ) is displayed in red.

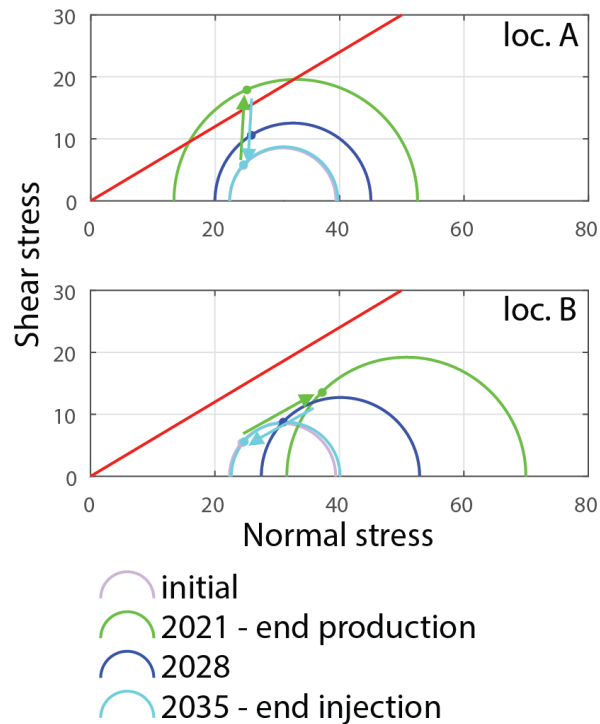


Figure 7-5 Contrast in stress path: Mohr-Coulomb analysis for two locations (loc. A and loc. B) along the same fault pillar displayed in Figure 7-3. The Coulomb failure envelope ( $\tau_{max} = \mu\sigma'$  with  $\mu = 0.6$ ) is displayed in red. In units of MPa.

Figure 7-6 is complementary to Figure 7-2, giving us access to the 3D along-strike variability of the fault reactivation likelihood. Figure 7-6 confirms that at the end of the injection period most (if not all) of the areas where the Fault Shear Capacity FSC (equation 8.1.2) is exceeded, present at the end of the depletion period, disappear. The faults are thus expected to be stable at the end of the injection period. This conclusion would only be disputed in the case of either (1) direct injection inside a reservoir fault or (2) direct flow communication between the well and a reservoir fault. Assuming we are not missing pre-existing faults in the structural reservoir model, one can already confirm that injection inside a reservoir fault is not occurring. The second scenario is also unlikely to happen since unidentified in the reservoir simulations.

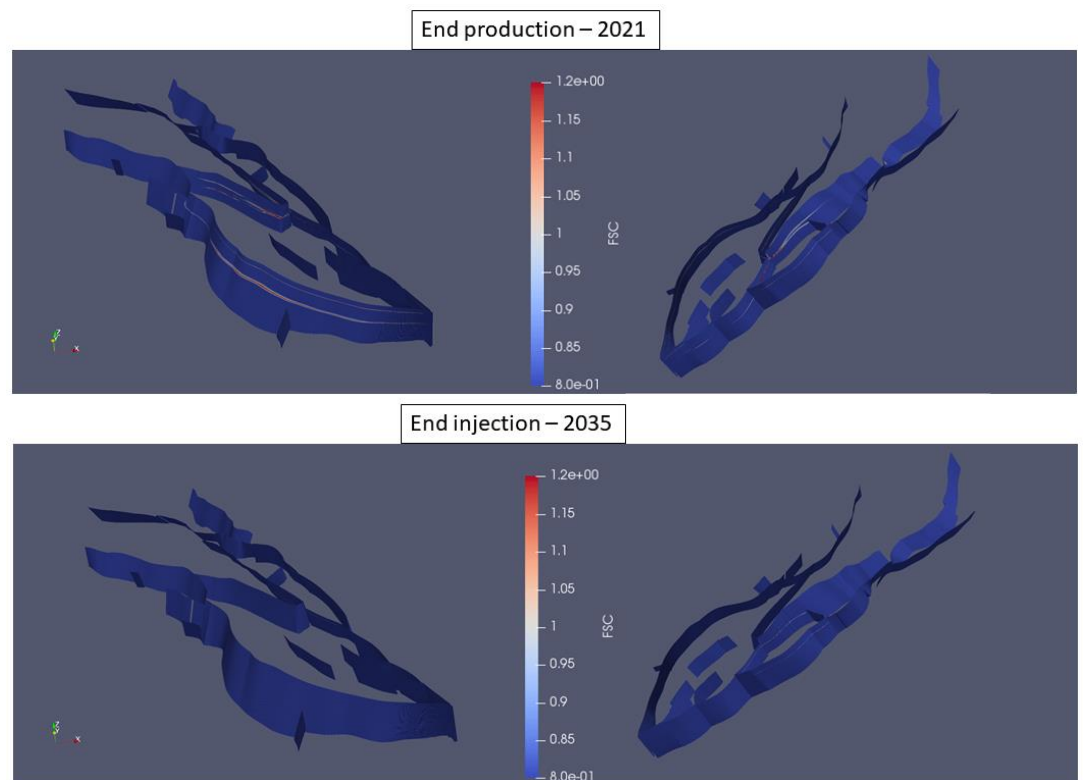


Figure 7-6 Fault Shear Capacity (FSC) along the P18-2 faults inferred from MACRIS analysis. At the end of the production period, only very locally (at the reservoir edges) the Fault Shear Capacity exceeds unity, meaning that the shear stress is larger than the frictional shear strength (“max shear stress”). During the injection period, these very local areas of exceedance of the frictional shear strength disappear.

### 7.3 Fault stability: temperature effect

Up to this point, results of the MACRIS analysis consider the pressure effect only. The temperature effect on the stability of the intra-reservoir faults is now addressed.

To answer this question, we used a TNO-developed geomechanical semi-analytical approach detailed in an Annex, Section 17.9.2. The required input for this approach is the radially symmetric temperature field resulting from the TOUGH2 flow simulation introduced in Section 6. The reader is referred to Table 7-2. for the input parameters required for this analysis. The TOUGH2 flow simulation and the

geomechanical semi-analytical approach should be seen as one-way coupled, and the temperature effect on the fluid viscosity is handled by the TOUGH2 simulator.

Table 7-2 Input model parameters used for the thermo-elastic semi-analytical approach.

Thermo-elastic model parameters	
$\Delta T$	-90°C
<i>Sh orientation</i>	N55E
$Ko' = Sh'/Sv'$	0.63
<i>Sh/SH</i>	0.9
$\rho_{rock}$	2260 kg/m <sup>3</sup>
$\rho_{water}$	1150 kg/m <sup>3</sup>
$\rho_{gas}$	200 kg/m <sup>3</sup>
<i>E (Young's modulus)</i>	18GPa
<i>v (Poisson's ratio)</i>	0.2
$\alpha_T$ ( <i>linear thermal expansion coefficient</i> )	10 <sup>-5</sup> K <sup>-1</sup>
$\mu$ ( <i>friction coefficient</i> )	0.6
$\alpha$ ( <i>Biot's coefficient</i> )	1.0

We take the temperature field after 5 years of injection as representative (see Figure 7-7). We will argue later that this is not a limitation, since the critical parameter for the risk assessment is the distance between the cooling front and a pre-existing fault.

The transient temperature field after 5 years of injection from TOUGH2 is first approximated as an homogenous cylindrical field at a temperature relative to that of the undisturbed reservoir of -90 °C, with a height equal to the reservoir height, and with a radius  $r=200m$  (see Figure 7-7). This approximation of sharp temperature front is often assumed for fast analytical approaches (Candela et al., 2018). The semi-analytical approach, detailed in Section 17.9.2, provides an estimate of the thermo-elastic stresses inside and around the cylindrical field which are induced by cooling.

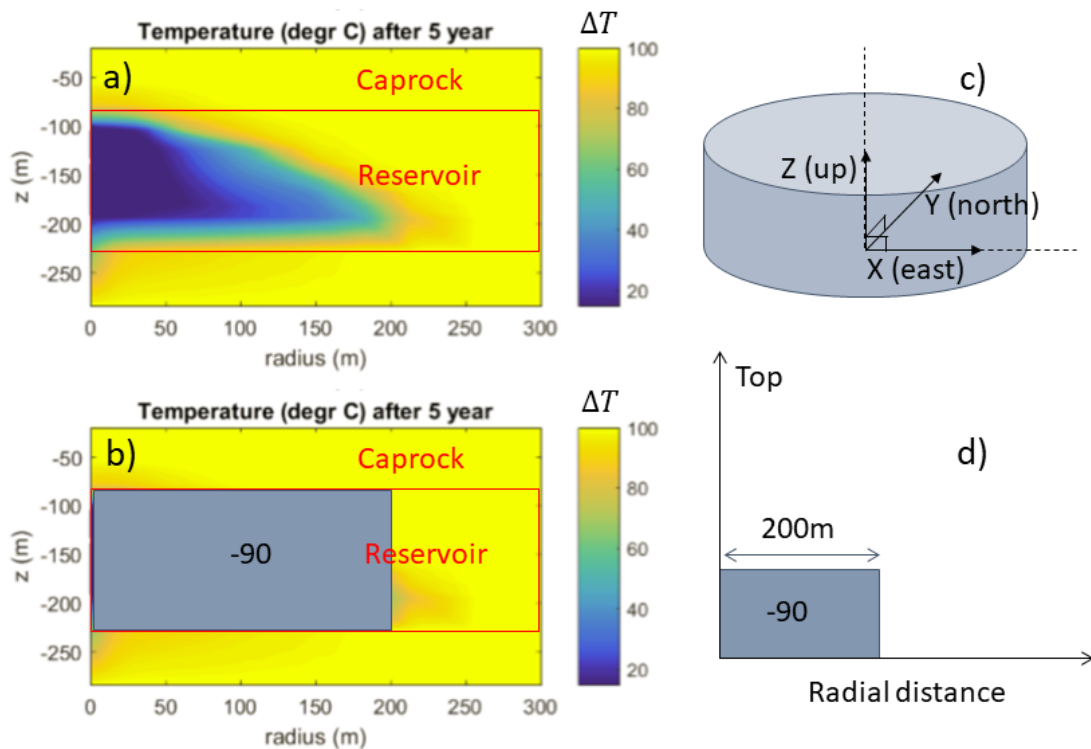


Figure 7-7 Temperature distribution and geometry of the geomechanical semi-analytical approach used to evaluate thermo-elastic stresses. a) Transient temperature field simulated by TOUGH2 (see Section 6.4.3). b) Cylindrical-shape approximation of the transient temperature field in a). The temperature change is homogeneously distributed and fixed at -90 °C. c) and d) Geometry of the geomechanical semi-analytical approach.

Following the semi-analytical approach, faults are not explicitly modelled (as it was the case in the MACRIS analysis for the pressure effect) but the changes in stress which are induced by the reservoir cooling can be calculated at any location inside the reservoir and caprock. From equation 8.1.1 the changes in Coulomb stress induced by the temperature effect at any reservoir fault can be calculated. As soon as the cooling front reaches a fault, Figure 7-8 and Figure 7-9 show that the change in Coulomb stress can reach value as high as 10MPa. This result holds for a range of fault planes orientations whom are relevant for the P18 field. Ahead of the cooling front, the thermally-induced Coulomb stresses rapidly decay; at 100 m from the cooling front the Coulomb stresses are around 2.5 MPa.

It is important to point out that even if the temperature field at the end of 15 years of injection was used as input, (instead of 5 years), the same results are expected in terms of magnitude of change of Coulomb stress inside the cooled reservoir and in terms of stress decay with distance ahead of the cooling front. The distance reached by the cooling front is then the determining parameter for the fault stability analysis. At the end of 15 years of injection, the TOUGH2 simulations (see Section 6.4) predict that the cooling front could extend as far as 300 m from the injection well after 15 years of injection. Given this constraint, only one injection well (P18-02-A-01) can be identified at a radial distance shorter than 300 m from a pre-existing identified fault cross-cutting both the reservoir and caprock (see Figure 7-3). Well P18-02-A-05ST1 is close to fault F35 (230 m), but has not been taken into account because it has a small throw (max 15 m), is an internal fault, and has

two tips. It will therefore form no baffle to flow, will not act as a pressure barrier, and will therefore not change its stress state.

However, in order to conclude about fault reactivation, if any, one needs to add to the changes in Coulomb stress the initial stress situation before injection of cold CO<sub>2</sub>. Figure 7-3 indicates this initial stress situation at the end of the production period and along the fault pillar closest to a well. As pointed before, the initial Coulomb stresses are spatially highly heterogeneous along the fault pillar; at the reservoir edge the Coulomb stresses are already reaching the failure line but some other locations are at more than 10 MPa from the failure line. Adding up the 10 MPa of thermally induced Coulomb stresses to the initial Coulomb stresses induced by the reservoir depletion, one can estimate that almost two-thirds of the fault pillar would overreach the failure line. One can thus conclude that for this particular fault close to a well, the likelihood of reactivation is high. This result will still hold even if the cooling front would reach this fault later during the injection period since the Coulomb stresses solely induced by pressure changes still remain at around 10 MPa from the failure line (see Figure 7-3). Finally it is important to repeat the limitations of TOUGH2 here; indeed, the highest temperature than TOUGH2 can model is 103 °C whereas the initial reservoir temperature was ~126 °C. One can thus expect the change in temperature to be more severe than the -90 °C used in our geomechanical semi-analytical approach; and it results that the modelled change of Coulomb stress could be even higher.

However, it is to be noted that the cooling front modelled here represents a worst-case scenario with a low probability of occurring: the cooling is due to prolonged injection of CO<sub>2</sub> at a temperature equal to the lower limit at bottom hole and at a rate corresponding to the maximum load scenario. Also, in reality one can expect a more gradual temperature front, and thus the area of excess of Coulomb stress relatively to the failure line, will be more limited in space. In other words, the potential of reactivating a pre-existing fault inside the reservoir would be confined to a small area beyond the cooling front. Finally, a solution here is to adjust the injection rate at this particular well located close to a reservoir fault. This way, the extent of the cooling front can be constrained to stay at a safe distance from the fault.

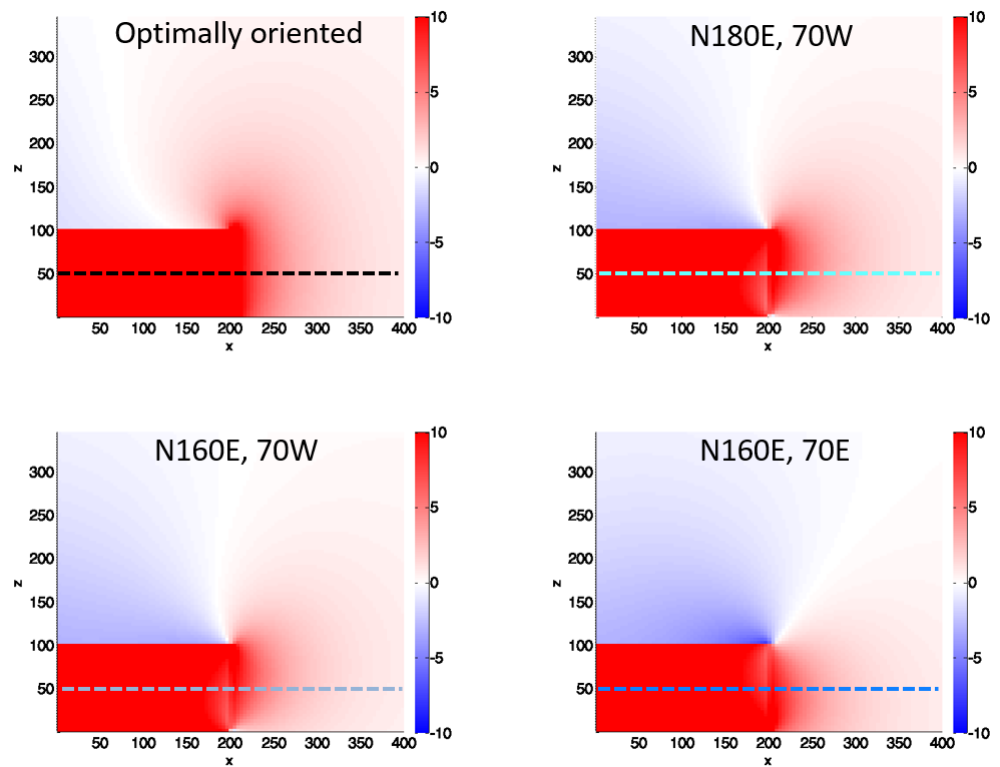


Figure 7-8 Thermo-elastically induced Coulomb stress changes in units of MPa for different fault orientation. Top left: fault planes with the highest Coulomb stress changes; Top right: fault planes with a North-South strike and dipping 70 degrees toward West; Bottom left: fault planes with a N160E strike and dipping 70 degrees toward West; Bottom right: fault planes with a N160E strike and dipping 70 degrees toward East. The model input used to generate these results is the homogenous temperature field presented in Figure 7-7. The horizontal dashed lines in the centre of the reservoir represent the stress profiles displayed in Figure 7-9.

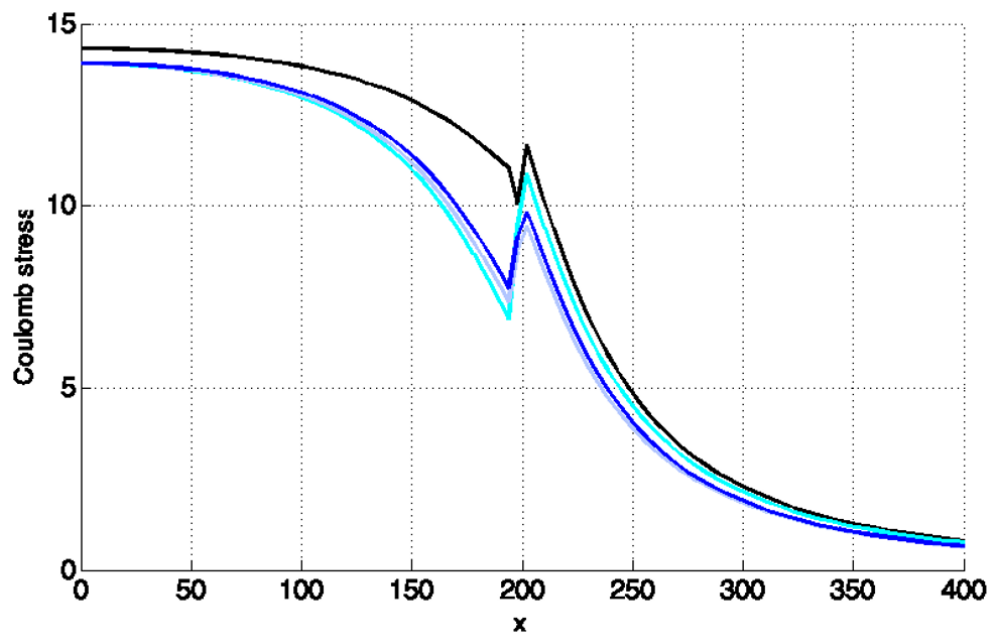


Figure 7-9 Profiles of thermo-elastically induced Coulomb stress changes in units of MPa. Each colour corresponds to each fault families presented Figure 7-8.

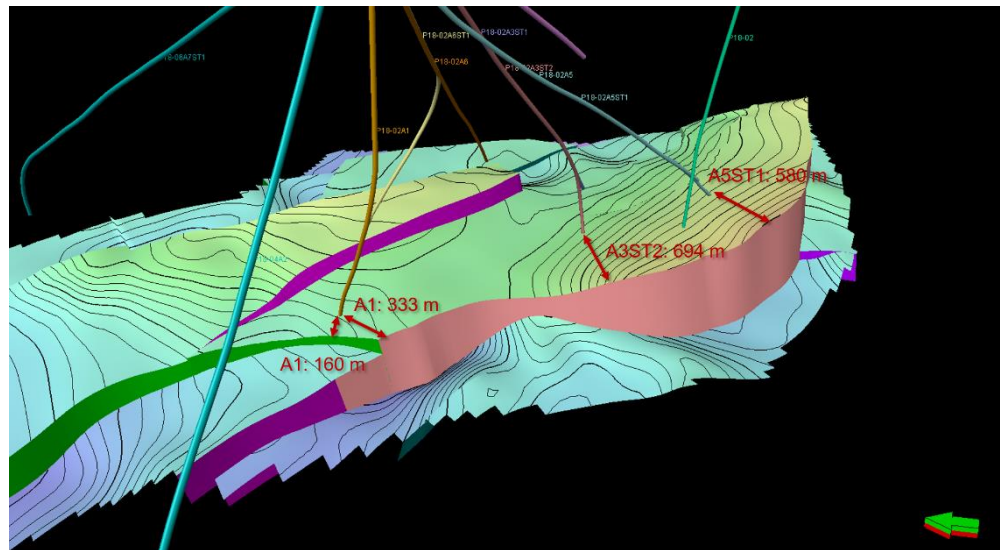


Figure 7-10 Distances faults – wells. Only in the vicinity of one well (P18-02-A-01), one fault is located at a distance smaller than 300 m.

After fault reactivation, a relevant question is about the magnitude of the induced earthquakes. To answer this question, we would need additional modelling results. However, we can shed light here on the expected end-members in terms of event magnitude. One first end-member is the case where a rupture will remain confined to the perturbed zone and thus the induced event would be small (magnitude < 1). The perturbed zone is the area of the fault already included in the cooled domain with the excess Coulomb stress. The second end-member is the case where the rupture will propagate all the way through the fault area extent. In this case, the magnitude of the event would be large (magnitude well above 1). Note here that we do not consider the case where the rupture could jump to another fault and extend even further. The reality is probably between the first and the second end-member. One dominant factor that controls the event propagation and thus its final size is the initial Coulomb stress level at the start of the fault reactivation. This initial Coulomb stress is the one at the end of the depletion period and given by the MACRIS analysis (see Figure 7-2 and Figure 7-3). Due to the differential compaction effect, this initial Coulomb stress level is spatially highly heterogeneous; with only some locations at the reservoir edge close to the failure line or already at the failure line. From this picture one can make the assumption that the propagation of an induced event will remain confined to the perturbed zone and will quickly die out outside because of the lack of high stresses to sustain its propagation. However it is important to point here again that to give a more definitive answer on the potential magnitudes of induced events, we will need to carry out new geomechanical models focusing on this particular matter.

## 7.4 Fault stability: geochemical effects

### 7.4.1 Introduction

The P18 reservoir compartments that have been assigned as potential storage reservoirs are fault bounded. These faults have effectively proven that they do not

allow across-fault fluid flow by the mere fact that they were able to support a large gas column over geologic time span. The compartments are hydraulically isolated from their surroundings due to juxtaposition of the reservoir against impermeable shales. Also several large faults intersect the compartments, such as those that subdivide the three main compartments of P18-2. Some of these faults are sealing, whereas some provide partial communication across the fault (see Section 4.2). Large-scale faults are generally surrounded by an area with a large number of smaller faults and fractures and matrix consisting of fault gouge. Instead of 'faults' we should refer to the 'fault (damage) zone' (Fisher, 2013). If porous rocks or sediments are faulted in early stages of consolidation, the damage zone generally has a lower permeability than the undeformed material (Fisher, 2013).

For storage integrity purposes, a difference should be made between sealing *across* and *along* the fault zone. Juxtaposition against a sealing formation can result in hydraulic isolation due to sealing across the fault. Yet, if the fault zone extends to above the caprock and the fault gouge is permeable, the risk of upward migration exists. In a previous analysis of migration scenarios for P18, shallow gas pockets in the overburden were found, but these most probably originated in the overlying Jurassic Posidonia shales (Vandeweyer et al., 2011). No evidence was found for gas leakage from the P18 reservoir, supporting a conclusion that the fault zones of each of the faults penetrating the caprock are sealing. The non-sealing faults might allow along fault fluid migration, but still not allow leakage towards the overburden if the fault ends within the caprock.

When CO<sub>2</sub> is injected in the reservoir, geochemical reactions between CO<sub>2</sub> and minerals within the fault might change the sealing capacity (in case of sealing faults) and/or cause reactivation. The geochemical effects of CO<sub>2</sub> on the faults, and the impact of these effects on its sealing integrity and reactivation potential need to be evaluated to assess the risk of leakage through the faults of the P18-2 reservoir and the potential of reactivation on the long term. These are described based on recent literature.

#### 7.4.2 *Geochemical effects of CO<sub>2</sub> on sealing capacity*

Where there is juxtaposition of the reservoir against impermeable shales, we can assume that the fault zone mineralogy of sealing faults is made up of crushed and mixed sandstone and shale components, whereas the non-sealing faults which did not juxtapose the reservoir against impermeable shales is made up of crushed reservoir material only. Although the Triassic sandstones have a relatively high clay content, the intra-compartment faults probably contain less clay than the compartment to shale faults. They will have comparable mineralogy, with variable mineral contents consisting of quartz, feldspars, clay minerals, carbonates, anhydrite and accessory minerals.

Similar to geochemical effects of CO<sub>2</sub> on caprock integrity, the only migration mechanism for CO<sub>2</sub> into sealing faults is by diffusion in dissolved form. Therefore, horizontal and vertical penetration of the geochemically affected zone is of the same order of magnitude as the vertical penetration into the caprock: several meters after 10,000 years. Changes in mineralogy will include partial dissolution of silicate minerals and precipitation of carbonate and clay minerals. Corresponding porosity changes will be too small to affect the sealing capacity.

A non-sealing fault zone might allow migration of supercritical CO<sub>2</sub>. Migration across the fault zones is not an issue if the compartment across the fault is also used as storage reservoir or is part of the storage complex. Migration of CO<sub>2</sub> into the fault zone could lead to enhanced chemical reactions. According to Fisher (2013), the most common type of fault gouge in Triassic reservoirs is cataclastic faults. For 19 Triassic fault gouges, gas permeability values ranged from 0.0007 to 1.8 mD (Fisher, 2013). A non-sealing fault will have a permeability at the high end of this range, but it is still a low permeability. Low flow rates will enhance self-sealing of the leak path by carbonate precipitation, especially in the presence of sufficient clay minerals which can provide the required cations for reaction with dissolved CO<sub>2</sub> to form carbonate minerals. However, the rate of self-sealing is not well known and will probably be highly dependent on many variables and fault characteristics.

#### 7.4.3 *Geochemical effects of CO<sub>2</sub> on reactivation potential*

Chemical interactions between the carbonized brine and fault zone mineralogy will result in slight mineralogical changes. These changes will only occur in the first few meters at the contact with the reservoir for sealing fault zones after thousands of years. In case of non-sealing faults, mineral reactions might have occurred across the fault zone. The chemical reactions on the long term are uncertain and will be affected by local differences in mineralogy. Overall, it is predicted that the carbonate content will increase because of the interaction with dissolved CO<sub>2</sub> with cations in the formation water, and on the long term with cations from silicate minerals. Few geomechanical studies have been done to investigate the effect of carbonate content on mechanical properties of faults. They concluded that with increasing carbonate content, fault gouge has an increased friction coefficient, indicating lower potential for fault reactivation (Samuelson et al., 2012; Adelinet et al., 2014; Bakker et al., 2016). In case fault reactivation *does* occur, higher carbonate contents increase the tendency for velocity weakening (which makes the fault weaker and sliding can continue, e.g. unstable slip) and can therefore increase the probability of microseismicity to occur (Samuelson et al., 2012). This is supported by an experimental study in which fault gouge from an outcrop which was very heavily altered by CO<sub>2</sub> interactions showed unstable slip at reservoir temperatures, whereas less heavily altered fault gouge resulted in stable slip (Bakker et al., 2016). The permeability of fault gouge material shows a tendency to decrease by orders of magnitude upon displacement during slip (Bakker et al., 2016), although it is not clear whether this occurs for both stable and unstable slip.

#### 7.4.4 *Evidence of leakage from field data*

In Arizona, USA, CO<sub>2</sub> leakage from a large natural CO<sub>2</sub> reservoir through faults was studied in order to quantify leakage rates (Miocic et al., 2019). In this specific area, faults extended from the reservoir up to the surface, and CO<sub>2</sub> rich fluids have been leaking for 420.000 years through fractures present in the damage zones around the faults. It was estimated that the average leakage rate through the faults is up to 36 kt/yr, which is less than 0.01% leakage per year for this reservoir.

In case of the P18-2 storage site, the faults do not reach the surface, but end in the Cretaceous aquifers. In a worst case, that the non-sealing faults turn out to be leakage paths, and self-sealing by carbonate precipitation does not occur, dense-phase or gaseous CO<sub>2</sub> would migrate up to the Cretaceous aquifers and dissolve into the formation water, but only if the reservoir CO<sub>2</sub> pressure is above hydrostatic

conditions (see also Section 9.3.4). From the Arizona study it was concluded that leakage along faults does not negatively impact the suitability of a reservoir from the point of view of CO<sub>2</sub> emission reductions (Miocic et al., 2019).

## 7.5 Conclusions

### *Pressure effect on fault stability*

The 4D distribution of Coulomb stresses has been computed along the mapped faults. Following the MACRIS approach, these Coulomb stresses combined (1) the poro-elastic effect, (2) the direct pressure effect at faults and (3) the effect of the fault offset. This analysis indicates that these Coulomb stresses only exceed the failure line very locally at the reservoir edge and at the end of the production phase. This outcome of our modelling workflow is supported by the fact that no tremors have been detected up to now. During the injection phase, the risk of fault reactivation due to pressure effect is even lower.

### *Temperature effect on fault stability*

In order to model the temperature effect on fault stability a TNO-developed geomechanical semi-analytical approach has been used. The distance reached by the cooling front is the determining parameter for the fault stability analysis. When the cooling front reaches a fault, the induced Coulomb stresses by the temperature effect can be such that locally, at this particular location, the fault can be reactivated. Given this distance criteria, only one single fault close to a well has been identified as potentially locally reactivated by the coupled temperature and pressure effect. Adjusting the injection rate at the particular well close to this fault can be a solution to maintain the distance of the cooling front at a safe distance from the fault. The injection simulations shown in 6.1 suggest that the injection rate in well P18-02-A-01, which is closest to faults, will be significantly lower than that of well P18-02-A-05ST: this may well satisfy this recommendation.

### *Geochemical effects on fault stability*

The impact of geochemical alterations in fault zones is unlikely to lead to CO<sub>2</sub> migration along faults. This, in turn limits the speed and depth of penetration of CO<sub>2</sub> into a fault zone, rendering the impact of chemical alterations insignificant.

## 8 Caprock integrity

### 8.1 Introduction

This section focuses on the potential reactivation of faults in the caprock due to pressure increase during CO<sub>2</sub> injection (Section 8.2), to temperature effects from the injection of low-temperature CO<sub>2</sub> (Section 8.3). Changes in pressure and temperature inside the reservoir can induce different stress changes between intra-reservoir section of the pre-existing faults and their caprock section. Section 8.4 discusses geochemical effects of interaction between CO<sub>2</sub> and the caprock.

The caprock overlying the P18-2 field has a thickness of more than 450 m. Only a few of the faults that exist in the field or that bound the field extend to above the caprock; most of the faults terminate in the caprock. While for the latter the consequences of fault reactivation are likely to be limited, the potential of fault reactivation needs to be quantified for the former.

The conclusion from the results presented below is that the risk of reactivation of faults in the caprock due to the injection of CO<sub>2</sub> is very low. The interaction between CO<sub>2</sub> and the caprock is expected to be insignificant.

### 8.2 Pressure effect on caprock integrity

This section considers the potential of destabilization of pre-existing faults inside the caprock due to the pressure effect. These faults are the ones present inside the reservoir flow model and that extend upward into the caprock. The pressure-induced Coulomb stress changes along the pre-existing fault planes are thus calculated following MACRIS analysis and is detailed in Section 7.2; implicitly it is thus also assumed that generating a new fault will require larger stress changes.

Figure 7-2, Figure 7-3 and Figure 7-6 show that the Coulomb stresses rapidly decay on top of the reservoir inside the caprock. The pressure effect is thus not expected to contribute to the risk of fault reactivation in the caprock.

### 8.3 Temperature effect on caprock integrity

A temperature decrease of reservoir rock due to the injection of relatively cold CO<sub>2</sub> induces contraction of the rock mass and a change in total stress, depending on the boundary conditions. The induced stress changes take place inside the reservoir, but also in the caprock on top of it. This section addresses the magnitude and distribution of temperature-related stress changes in the caprock. The main question addressed in this section is: what are the risks of reactivating a pre-existing fault in the caprock due to the temperature-induced stress changes?

To answer this question we used a TNO-proprietary geomechanical semi-analytical approach detailed in Section 17.9 and already introduced in the previous Section 7.3. We take as input the same temperature field after 5 years of injection as the one considered for intra-reservoir fault reactivation (see Figure 7-7).

According to the semi-analytical approach, and as mentioned previously, faults are not explicitly modelled but the changes in Coulomb stress which are induced by the reservoir cooling can be calculated for any fault orientation and at any location inside the caprock. The Coulomb stress changes are thus defined for any fault plane in the caprock; generating a new fracture will require larger shear stress than those for reactivating a fault plane. The fault planes should therefore be seen as “potential fault planes” since faults have not explicitly been identified in the seismic cube.

The results achieved (see Figure 8-1 and Figure 8-2) indicate that on top of the cooled part of the reservoir, the changes in Coulomb stress are negative. On these locations in the caprock, therefore, there is no risk of fault reactivation due to cooling of the reservoir below it. Only on top of the reservoir beyond the edge of the cooling front, the changes in Coulomb stress start to be positive (see Figure 8-1 and Figure 8-2). For our analysis we decided to pick the optimally oriented fault planes, that is for any location we picked the fault orientations where the Coulomb stress changes are maximum. Consequently, the current approach in terms of risk quantification can be seen as conservative, or worst case. However, Figure 7-8 shows that instead of considering the optimally oriented fault planes but the orientations of the P18 faults cross-cutting both the reservoir and caprock, it would have led to similar changes in Coulomb stress.

To summarize, the potential risk of reactivating a pre-existing fault in the caprock is very low.

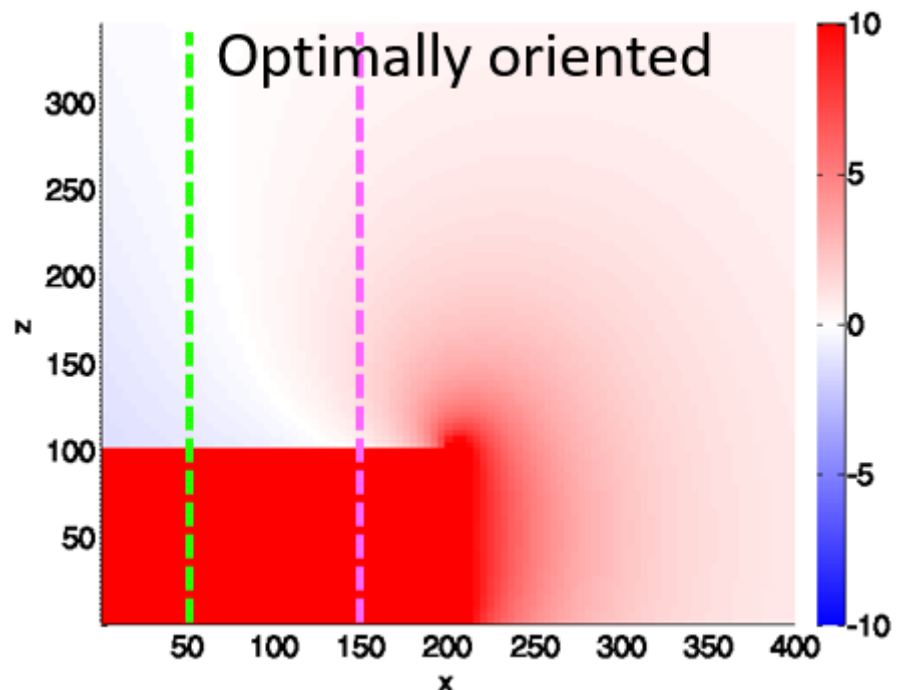


Figure 8-1 Thermo-elastically induced Coulomb stress changes in units of MPa along optimally oriented fault planes. The vertical dashed lines represent the stress profiles displayed in Figure 8-2.

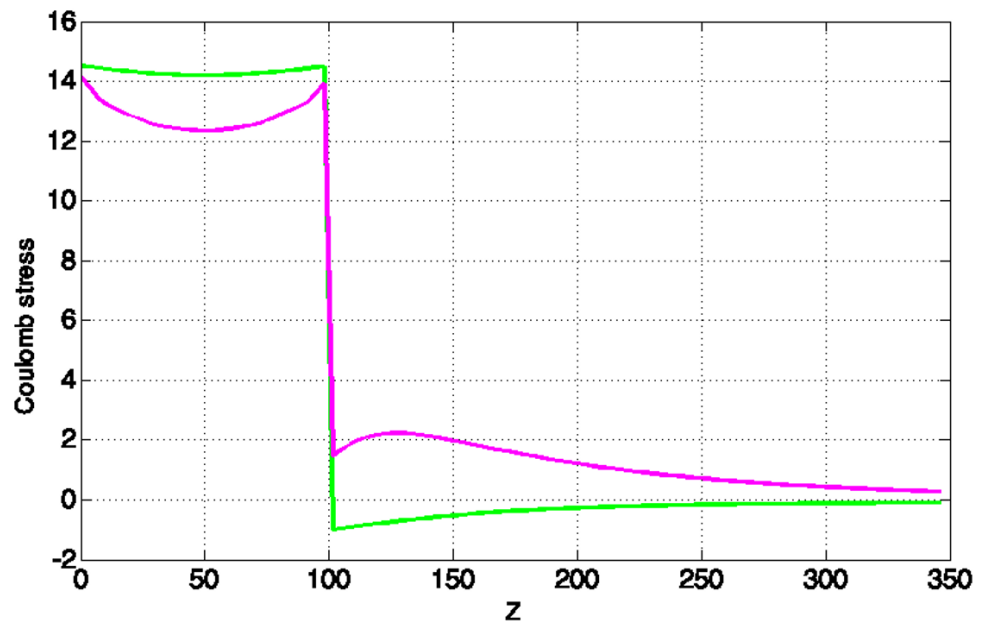


Figure 8-2 Profiles of thermo-elastically induced Coulomb stress changes in units of MPa. Each colour corresponds to different vertical cross-sections for the stress profiles as displayed in Figure 8-1.

## 8.4 Geochemical effects

### 8.4.1 Introduction

Geochemical reactions between CO<sub>2</sub> and caprock minerals can change the sealing capacity. The geochemical effects of CO<sub>2</sub> on the caprock, and the impact of these effects on its sealing integrity need to be evaluated to assess the risk of leakage through the thick caprock of the P18-2 reservoir on the long term. These are described based on recent literature.

### 8.4.2 Geochemical effects of CO<sub>2</sub> on caprock integrity

The caprock of the P18 reservoirs is made up of the Upper Germanic Trias Group and the Jurassic Altona Group. Caprock material of the P18 reservoirs has not been analysed. Caprock material of the nearby Q16 reservoir as analogue for P18 caprock was characterized by Peach et al. (2010). Eight caprock samples from the Solling and Röt Formations (both Formations belong to the Upper Germanic Trias Group) were measured for gas permeability and porosity. All permeability values were below 0.1 mD and porosity ranged between 0.02 and 5.3%. Four samples from the Röt Formation were analyzed by XRD and eight samples of Solling and Röt Formations were analysed by optical microscopy. The samples were carbonate-rich mudrocks with a mineralogy mainly made up of carbonates (ankerite or dolomite), phyllosilicates (mica and clay) and quartz (Peach et al., 2010).

The caprock of both the P18 and the Q16 gas fields has a proven sealing capacity for natural gas. Yet, CO<sub>2</sub> behaves differently than natural gas, both from physical and chemical perspective. The low permeability measured for the Q16 caprock samples justifies the assumption that penetration of CO<sub>2</sub> into the caprock will not occur, as long as the CO<sub>2</sub> pressure in the reservoir remains below the pre-production gas pressure. Specific numbers on safe CO<sub>2</sub> pressures cannot be given. However, as long as the capillary entry pressure of the caprock is not exceeded, the

only way for the CO<sub>2</sub> to migrate into the caprock is by upward diffusion in dissolved state. The diffusion is driven by increased concentration of dissolved CO<sub>2</sub> in the pore water of the reservoir and at the contact with the caprock. Tambach et al. (2012, 2015b) report on 1D reactive transport simulations that were performed with PHREEQC to assess the interaction of dissolved CO<sub>2</sub> during upward migration into the caprock. Due to the lack of detailed caprock mineralogical analysis, the mineralogy was based on samples from the adjacent P15 field, analysed and reported by Spain and Conrad (1997). The detailed analysis showed a much higher quartz content than the analyses by Peach et al. (2010). Dolomite, illite and anhydrite are present in moderate amounts, and small amounts of K-feldspar, albite, siderite and pyrite were identified. The simulation results showed that upward diffusion of dissolved CO<sub>2</sub> and the associated pH decrease is very slow. During the upward migration, mineral reactions occur to buffer the pH and convert the dissolved CO<sub>2</sub> into carbonate minerals. This further slows down the upward migration of the dissolved CO<sub>2</sub>. After 10,000 years some mineral reactions and a minor porosity increase was simulated only in the 5-10 metres above the reservoir-caprock contact (Figure 8-3). A sensitivity study on mineral types and reactive surface areas predicted a porosity increase in the bottom part of the caprock of no more than 0.7%. Only one simulation predicted a porosity decrease of 1.8% in the first metre and porosity increase up to 5 metres into the caprock (Tambach et al., 2012).

Gaus et al. (2005) found similar orders of magnitude for the extent and scale of geochemical reactions in shale caprock at the Sleipner injection site in Norway. These authors predicted either a porosity increase or decrease in the lowest few metres of the caprock, depending on the mineralogical composition of the rock, 3,000 years after injection. The predicted porosity increases are below 0.05%, porosity decreases are up to 2.6%. Depending on the type of plagioclase (albite versus anorthite; generally no distinction is made in mineralogical analyses), the migration of dissolved CO<sub>2</sub> reached either 1.5 or 10 meters into the caprock after 3000 years (Gaus et al., 2005). In the first scenario, the more reactive anorthite was able to sequester the CO<sub>2</sub> in carbonate minerals much faster, thereby retarding the upward migration of dissolved CO<sub>2</sub>. The study shows how sensitive geochemical effects are to the rock mineralogy. Generally, the exact composition of the minor minerals define the reactivity. Yet, even the more reactive compositions will not significantly affect the sealing integrity of caprocks.

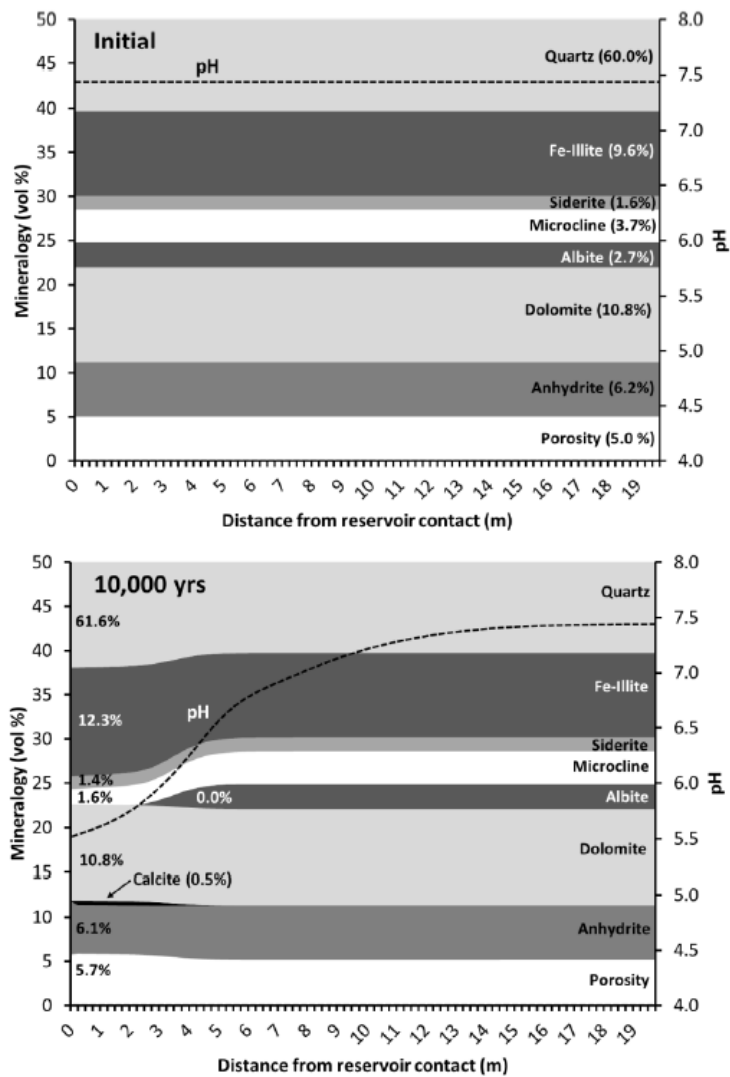


Figure 8-3: Initial mineralogy of the caprock and mineralogy after 10,000 years of simulation as a function of the distance from the reservoir contact. Up to 50 vol% is shown, the remaining part is made up of quartz. From Tambach et al. (2012).

In a more elaborate reactive transport simulation, assessing the impact of heterogeneities in shale caprock, local penetration of scCO<sub>2</sub> was predicted in areas of a caprock with lower sealing capacity (Tian et al., 2019). Local changes in porosity and permeability (both positive and negative) were predicted, related to variations in mineral compositions. Vertical migration of the scCO<sub>2</sub>, in those areas that penetration occurred, reached almost 50 m into the caprock after 500 years (Tian et al., 2019). Migration of small amounts of CO<sub>2</sub> out of the storage would take > 1,000 years (the total caprock thickness for the P18-2 reservoir is several hundreds of meters) Such a scenario represents a worst case condition, as exploration data for the P18-2 did not show any evidence for penetration of gas into the caprock, providing evidence for the overall sealing capacity of the P18-2 caprock.

## 8.5 Conclusions

*Pressure effect on caprock integrity*

Following the MACRIS approach, both induced Coulomb stresses along the intra-reservoir part of the faults and those along the intra-caprock part of the faults have been assessed. These Coulomb stresses rapidly vanish on top of the reservoir inside the caprock; the intra-caprock mapped faults are thus not expected to be reactivated by the pressure effect.

*Temperature effect on caprock integrity*

In order to model the temperature effect on pre-existing faults in the caprock, a TNO-proprietary geomechanical semi-analytical approach has been used. The geomechanical analysis shows that the risk of intra-caprock fault reactivation is very low.

*Geochemical effects on caprock integrity*

CO<sub>2</sub> is not expected to significantly interact with or migrate into the caprock.

## 9 Well integrity

### 9.1 Introduction

The wells relevant in the context of CO<sub>2</sub> injection into the P18-2 block have been evaluated regarding their current status and integrity risks. The wells considered are listed in Table 9-1, which repeats Table 4-1. The wells listed in the table are the wells that penetrate the cap rock (see Figure 4-10); wells that do not penetrate the caprock (shown in Figure 4-11) are not considered in this section.

Well integrity is considered at four levels:

- The integrity of the wells in their current state (Section 9.2);
- Mechanical effects of injecting cold CO<sub>2</sub> on the integrity of the well cement (Section 9.3);
- Geochemical processes acting on the cement (Section 9.3.4);
- Well abandonment (Section 9.4).

Table 9-1: Wells in the P18-2 compartment considered in well integrity analysis (repeats Table 4-1 in Section 4.5).

NLOG name	Taqa name	Current well status	Total Depth (m)	Potential injectors	Remarks
P18-A-01	P18-02-A-01	Producing	3840	Yes	
P18-A-03S2	P18-02-A-03ST2	Producing	4302	Yes	
P18-A-05S1	P18-02-A-05ST1	Producing	5230	Yes	
P18-A-06	P18-02-A-06	Producing	4805	Yes	
P18-A-06S1	P18-02-A-06ST1	Producing	3954	No	
P18-02	P18-02	Suspended	3766	No	Discovery well

The conclusions from the well integrity analysis are the following:

- *Well integrity.* All wells reviewed have the potential to be used safely as CO<sub>2</sub> injectors (with the exception of well P18-02, which is to be decommissioned). Appropriate mitigation measures are proposed to make them fit for storage operations.
- *Effects of injecting cold CO<sub>2</sub> on well integrity.* It is highly likely that de-bonding of cement interfaces will take place upon cold CO<sub>2</sub> injection, creating microannuli. The characteristics of the microannuli and pressure conditions determine whether upward CO<sub>2</sub> migration would actually take place. Keeping the CO<sub>2</sub> pressure in the reservoir below the hydrostatic pressure conditions will reduce the likelihood of leakage through microannuli.
- *Well abandonment.* Appropriate methods should be used for the abandonment of the wells. Given the likelihood of microannuli forming during the injection of cold CO<sub>2</sub>, abandonment methods that remove these potential leakage paths could be considered. As an example, full-bore pancake like plugs would provide formation-to-formation closure of the injection wells.

## 9.2 Status of the well barriers

### 9.2.1 *Well Integrity assessment approach*

Currently there are no specific industry standards for CO<sub>2</sub> injection wells. Therefore the approach followed in this well integrity assessment is to utilize existing oil and gas industry standards that address well integrity for injectors and complement any specific gaps for CO<sub>2</sub> injection wells if required.

The standards on which this well integrity assessment is based are:

1. NORSOK Standard D10, rev. 4 June 2013 - Well integrity in drilling and well operations (NORSOK, 2013);
2. ISO standard 16530-1:2017, March 2017 - Petroleum and natural gas industries - Well integrity, Part 1: Life cycle governance (ISO/TC 67/SC 4 Drilling and production equipment, 2017);
3. NOGEPa industry standard no. 45, 12 October 2016 - Well decommissioning (NOGEPa - OPCOM, 2016).

The reports related to well integrity and CO<sub>2</sub> storage and used for this assessment are:

4. MiReCOL report, February 2015 - D8.1 Description of leakage scenarios for consideration in the work in SP3 (Vrålstad, et al., 2015);
5. Dutch State Supervision of Mines (SSM/SodM), January 2019 – The integrity of onshore wells (SodM, 2019).

For the sake of completeness some relevant sections of the above mentioned standards and reports are presented.

1. The NORSOK D10 standard refers to well integrity by:
  - General principles: A two well barrier concept of primary barrier and secondary barrier for wells penetrating into hydrocarbon bearing formations and/or formations with the potential to flow to surface.
  - Structural integrity: the key components (conductor, guide base, risers) that provide structural integrity of the well during its service life shall be evaluated with respect to loads, wear and corrosion.
  - Injection / disposal wells: The well shall be constructed such that the injected media will be contained within the targeted formation zone (reservoir) without risk of out of zone injection.
  - WBS examples: Permanent well decommissioning (abandonment) is illustrated by a primary well barrier at caprock, secondary well barrier at intermediate section and an open hole to surface barrier.
2. The ISO well integrity standard refers to the NORSOK D10 standard and considers:
  - Structural integrity monitoring: The well operator should establish suitable systems to model or measure degradation in the structural well operating limits. The conductor, surface casing (and supporting formations) and wellhead assembly typically provide structural support for the well. Failure of these structural components can compromise well integrity and escalate to a loss of containment. For each well the well operator should assess the risk of failure of such structural components.

3. The NOGEPa no. 45 standard on well decommissioning has the following statements on well decommissioning.
  - Summarised mandatory requirements for Well Decommissioning:
    - o A permanent barrier shall extend across the full cross section of the well covering all annuli.
    - o The depth of the permanent barrier shall be selected to be adjacent to the caprock of adequate thickness with an estimated formation fracture pressure that exceeds the maximum anticipated pressure at depth.
    - o In case of cement, the permanent barrier length inside the inner wellbore shall be:
      - At least one hundred meters long (100 m), or
      - At least fifty meters (50 m) when placed on top of a tested mechanical support in cased hole.
4. The MiReCOL D8.1 report refers to Norsok D10 and includes the following information on well integrity:
  - The report considers well barrier breaches (CO<sub>2</sub> migration along the well bore) and includes the in-situ formation of the previous casing behind the liner lap as a barrier element to mitigate the risk of out of zone injection (which is conform NORSOK D10).
  - Aging issues with cement degradation, casing corrosion and wear, and thermal loads imposed on the well infrastructure are examples of the most likely causes for well leakages.
5. SodM (2019) categorizes CO<sub>2</sub> storage wells as gas wells from a well integrity perspective with the associated well failure model identifying potential leak paths, see Figure 9-1 (this is based on the ISO 16530 well failure model).

It should be noted that SodM defines the Surface tree (also known as the X-mas tree) as a secondary barrier element and the Surface Controlled SubSurface Safety Valve (SCSSSV) as primary barrier element, which is conform the NORSOK D10 standard. However, they do define failures of the tubing above the SCSSSV, the control line, tubing hanger and feedthroughs (blue items 3, 16 and 17 in Figure 9-1) as primary leakage elements, which is a variation on the NORSOK D10 standard. In this report NORSOK D10 is primarily followed, as a result all elements above the SCSSSV are considered to be secondary barrier elements (because they are isolated in the event of an SCSSSV closure).

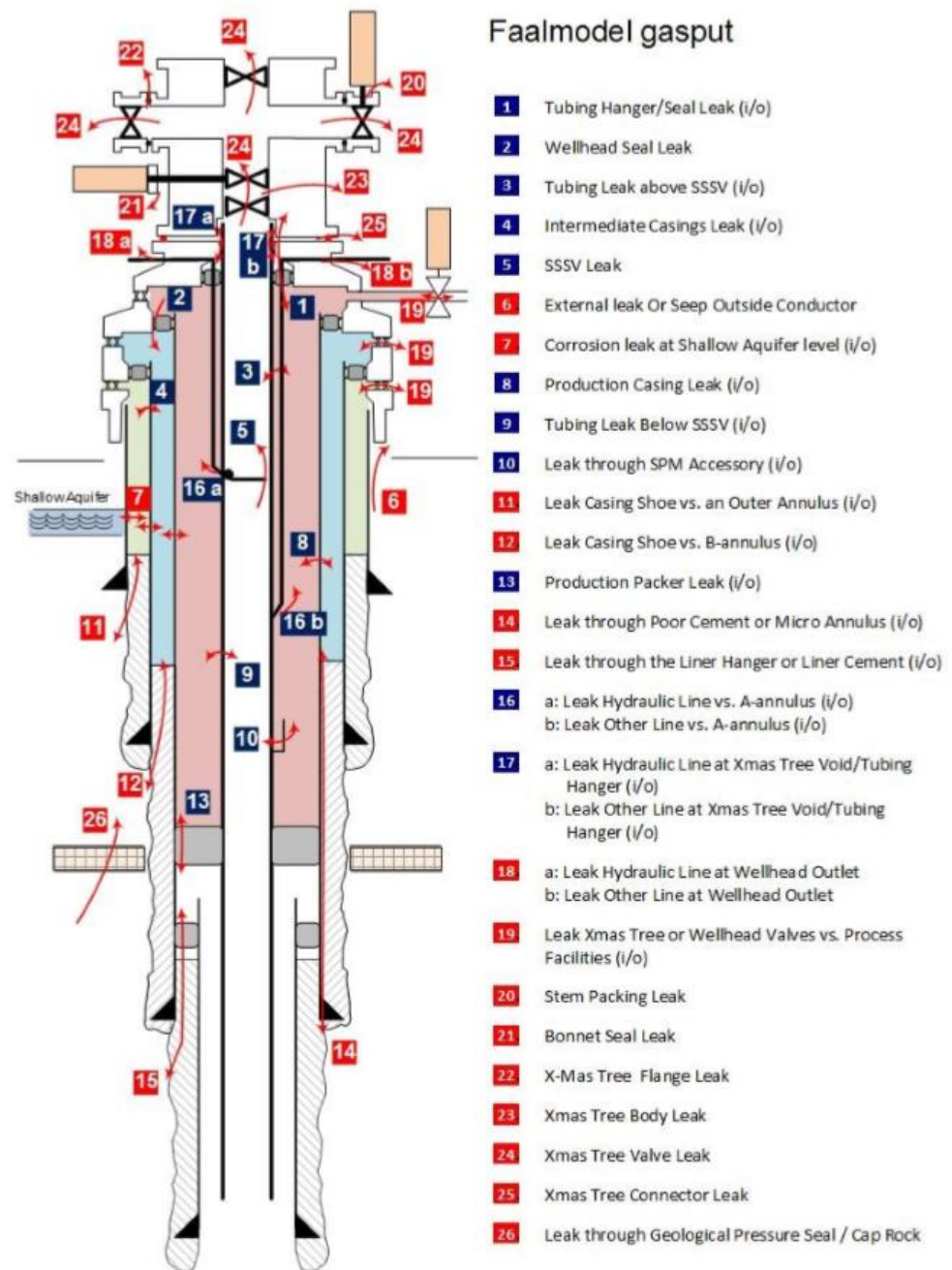


Figure 9-1 Well failure model for gas wells, including storage wells. (SodM, 2019). The blue numbers are primary barrier element failures and the red numbers are secondary barrier element failures.

#### 9.2.1.1 Well integrity assessment concept

Based on the reviewed standards and reports, the scope of the well integrity assessment in this report includes and reviews the following elements:

- a) The primary and secondary well barrier elements from reservoir caprock to surface, conform NORSOK D10.

- b) The risk of out of zone CO<sub>2</sub> injection due to a failure of a primary and/or a secondary barrier, with supporting in-situ formation of the previous casing below the liner lap.
- c) Structural integrity of the load bearing surface casing, conductor or riser.

The definition of the barrier elements for this assessment comes from NORSOK D10.

- Primary well barrier: first well barrier that prevents flow from a potential source of inflow.
- Secondary well barrier: second well barrier that prevents flow from a potential source of inflow.

The structural integrity assessment of the load bearing surface casing is for this assessment limited to a review of the “as built” status, identifying the potential well integrity risk.

It should be pointed out that the assessment of the influence of fatigue or corrosion on well integrity, with the structural load effects and associated thermal and pressure cycles, is not in the scope of the current work. This should be considered as the next fundamental step in assessing the structural well integrity lifecycle for the CO<sub>2</sub> injection program.

#### 9.2.2 *P18-2 well integrity analysis*

The P18 fields have been subjected to CO<sub>2</sub> storage assessment and well integrity evaluations in the CATO-2 R&D programme (Akemu, et al., 2011). The previous well integrity assessment focused on the P18-4 field and identified and evaluated barriers of wells relevant for the foreseen storage operation and identified gaps or uncertainties about barrier status in general. Based on this previous study it was not possible to decide on the suitability of the P18-2 wells for CO<sub>2</sub> injection and storage given the new operating envelope. The present assessment is based upon the previous work and addresses the gaps that were identified earlier. It considers new findings, as well as information that was not available at the time of the first studies.

The present study includes:

- An assessment of the wells penetrating the P18-2 reservoir;
- An assessment of earlier identified gaps, by detailed review of the end-of-well reports (EOWR), newly obtained records and quantification of the relevant barrier elements for the primary, secondary and structural barriers in place;
- Illustrations of well barrier envelope status in well barrier diagrams combined with potential risks for each barrier, with the aim to assist selecting suitable wells for injection of CO<sub>2</sub> in the P18-2 reservoir.

The wells relevant for the planned storage were re-evaluated. The scope of the assessment includes the following wells: P18-2A1, P18-2A3-ST1-2, P18-2A5-ST1, P18-2A6-ST1 and P18-2 (suspended well).

#### 9.2.3 *General well integrity P18-2 and well status issues*

The status of the wells penetrating the P18-2 reservoir that emerges from the review of previous work is as follows:

- a) The wells have not been assessed for the well completion load case for CO<sub>2</sub> injection with respect to temperature and pressure, except for the P18-4A2 well.

- Previous assessment (Akemu, et al., 2011) indicates that the type of retrievable production packers used in P18-2 wells will unseat when injecting cold CO<sub>2</sub>.
- b) The same type of retrievable production packers has been used in the other P18-2 wells identified for CO<sub>2</sub> injection, no well completion load case assessment has been done so far for these wells.
  - c) No assessment records were found on the lifecycle assessment of load bearing surface casing and conductor. External corrosion due to corrosive fluids and metocean induced fatigue of the load bearing casing could reduce its lifecycle load capacity. This is a fundamental requirement to assess the lifecycle of the well and the risk of loss of well integrity.
  - d) The bond logs for cement have been assessed previously (Akemu, et al., 2011); in the review the interpretation method has been verified and found to be correct.
  - e) The expected final CO<sub>2</sub> reservoir pressure for P18-2 is maximised at initial pressure (see Section 5.4); this has been considered in the assessment of individual barriers.
  - f) The surface tree material, trim and temperature classification must be validated against the operating envelope associated with injection of CO<sub>2</sub>.
  - g) The material specifications of the flow wetted barrier elements like surface tree, tubing hangers, completion accessories and seals / elastomers need to be validated against the CO<sub>2</sub> injection operating envelope.
  - h) Akemu et al. (2011) report that 5", 13Cr-L80 completions are installed. However, in this assessment it has been concluded that the completions are actually 5½", 13Cr-L80 for P18-2A1, P18-2A3 and P18-2A6, the P18-2A5 well is completed with a 7", 13Cr-L80 completion combined with a 5 ½", 13 Cr-L80 SCSSSV section.

The assessment of the individual wells is presented in sections 9.2.4 to 9.2.8.

#### 9.2.4 *Well P18-2-A1*

A well barrier diagram with well barrier envelopes and elements defined for well P18-2-A1 is provided in Figure 9-2, the evaluation of the elements can be found in Table 9-2. The evaluation of the well integrity barriers leads to the following observations.

##### Primary barrier

- The EOWR (End of Well Report) states that the 7" liner was run and installed for later production. The cement report in the EOWR of P18-3, that was later renamed to P18-2A1, shows a good cement job with a calculated top of cement reported to be at 3508 m MD. The well status diagram has recorded the TOC at 3477 m MD, this is a discrepancy in the reporting. For this assessment the depth reported in the cement report (3508 m MD) is taken because that represents the worst case scenario (cement report). The cement bond log (CBL) on the 7" liner cement, indicates poor bonding.
- No A-annulus pressures or pressure build-up has been reported, this has also been confirmed by the TAQA annular pressure history.
- The production packer is installed in a liner with a poor cement bond according to the bond log, this puts the packer with liner and liner cement as barrier elements at risk.

##### Secondary barrier

- The liner lap is positioned above the packer, the liner as barrier element is at risk, due to possible corrosion behind the carbon steel liner as a result of the poor cementation (bond log) and presence of CO<sub>2</sub> in the production life of the well and during future CO<sub>2</sub> injection.
- The liner lap was not tested upon installation. However, the liner lap is exposed to a hydrostatic overbalance of completion brine in the production annulus that confirms liner lap integrity. The current overbalance is estimated to be about 4060 psi (~280 bar) based on assumed annulus completion brine with a density of 1.10 s.g. and a reservoir pressure of 1230 psi (85 bar).
- The 9 5/8" casing shoe has a Formation Integrity Tests (FIT) reported that is above the final CO<sub>2</sub> storage reservoir pressure. The EOWR mentions for the cement job of the 9 5/8" casing a bump plug pressure of about 2000 psi (140 bars). There is no top of cement (TOC) reported in EOWR, the well status diagram shows the TOC at seafloor level.
- The 9 5/8" casing penetrates two formations with natural formation sealing potential (natural swelling clay); the Vlieland and Aalburg shales. These could improve the sealing performance over time (Fischer, et al., 2016).

#### Structural well integrity:

- The 13 3/8" casing is placed at 1963 m MD and had a successful FIT of 13.8 ppg, the casing is cemented to 175 m MD (calculated depth).
- The 20" casing is set at 404 m MD and is cemented to seafloor.
- The 30" conductor is piled to 131 m MD.

From a structural load bearing capacity point of view there appears to be adequate cement overlap to transfer the well loads. The 20" casing is cemented to seafloor this leaves the 20" casing inside the conductor exposed to potential risk of corrosion of the fluids in the conductor annulus from wellhead to seafloor, this needs to be verified.

#### Discrepancies:

- Akemu et al. (2011) reports a pressure test of 5000 psi (~345 bar) for the 9 5/8" casing and the 7" liner. The EOWR only reports a 9 5/8" pressure test to 5000 psi (~345 bar) prior to liner installation.
- Akemu et al. (2011) reports the production tubing to be 5", 13Cr-L80, in this study it was confirmed to be 5½", 13Cr-L80.
- The EOWR reports a calculated TOC for the 7" liner at 3508 m MD, the well status diagram shows the TOC at 3477 m MD.
- The EOWR has no report on top of cement (TOC) for 9 5/8" casing, the well status diagram shows the TOC at seafloor.

#### Summary

- The well currently appears to have no apparent leaks.
- From Table 9-2 can be seen that most barrier elements have been validated, except for the cement behind the 7" liner, there is a discrepancy on the TOC level in the 7" liner cement report and well status diagram of 31 m.
- The low quality of the 7" liner cementation at packer depth, combined with the fact that the 7" liner is made of carbon steel material, poses the risk of external degradation due to corrosion from potentially corrosive reservoir fluids. This would require mitigation, possibly by recompletion i.e. repositioning of the production packer into a liner / casing with a good cement bond.

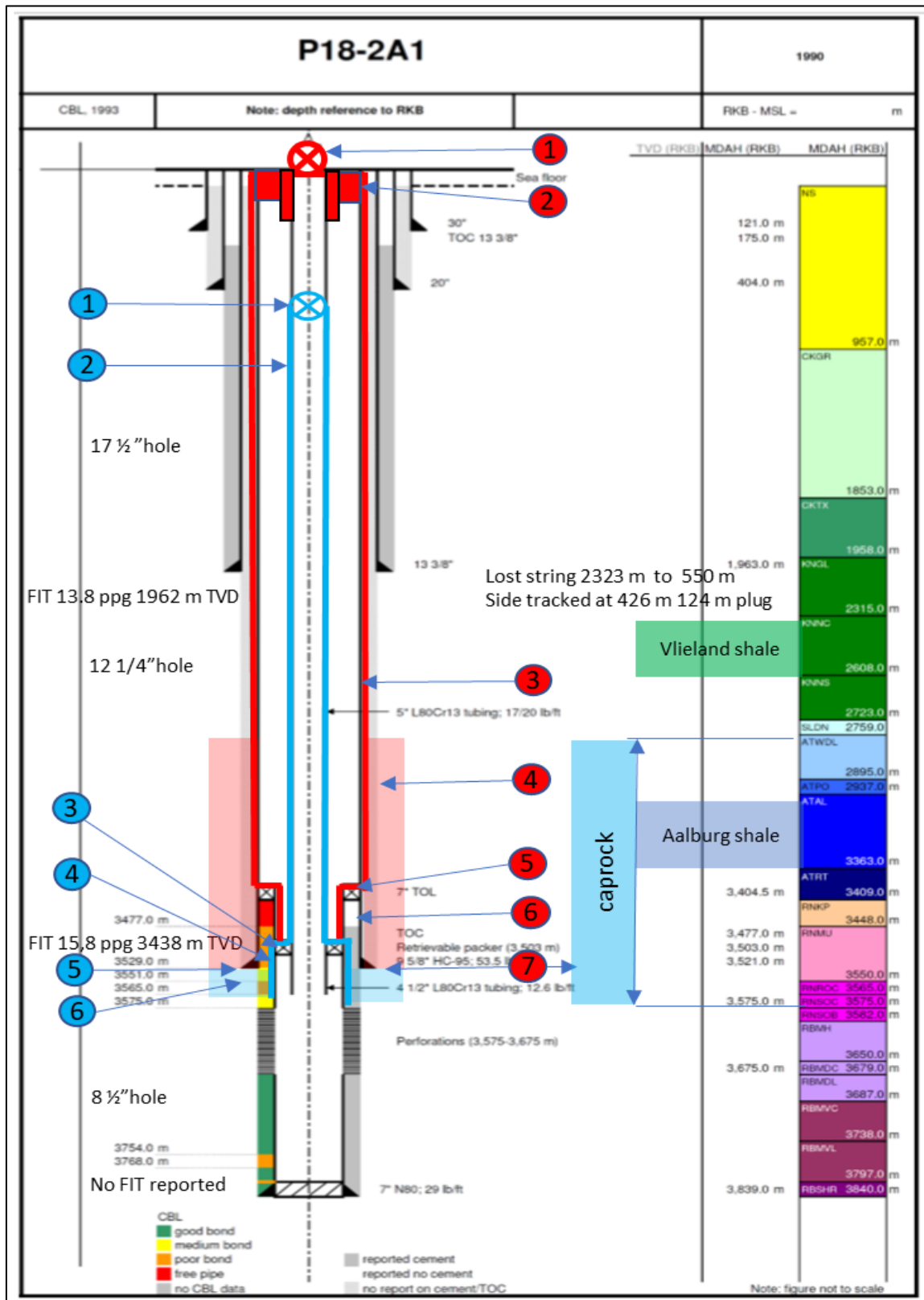


Figure 9-2 Well P18-2A1 barrier diagram with barrier elements defined. See Table 9-2 for a discussion of the barrier elements (indicated by the numbered circles).

Table 9-2 Well P18-2A1 barrier element assessment based on current data set. The numbers in the first column correspond with the numbers in coloured circles in Figure 9-2.

no	P18-2A1 Element	As built	Monitor	Barrier validated	Validation Criteria
<b>Primary well barrier</b>					
1	5 1/2" Scssv	Tested to 5000 psi	Maintained	Yes	Tested & maintained
2	5 1/2" Tubing	Tested to 5000 psi	Annular pressure records	Yes	Tested, no annular pressure build up reported
3	7" Production packer	Installed at 3503 m MD which is 26 m below the TOC in the 7" liner. Tested to 5000 psi	Annular pressure records	Yes	Tested, no annular pressure build up reported.
4	7" Liner	Liner report for P18-3 (previous name of P182A1) The liner covers 50 m of caprock	NA	Yes	The liner and production packer are under continuous high hydrostatic differential pressure of the A annulus. No annular pressure build up recorded
5	In-situ formation (Cap rock)	FIT of 15.8 ppg at 3488 m TVD	NA	Yes	FIT of 15.8 ppg at 3488 m TVD reported
6	7" Liner cement	Cement report of P18-3 (previous well name) reports the TOC at 3508 m MD. The well status diagram shows the TOC at 3477 m MD. The CBL indicates a poor bond	NA	No	The well status diagram shows the TOC 3477 m MD. The CBL indicates a poor bond. The TOL is set at 3404 m MD, this leaves 73 m of uncemented liner combined with poor bond.
<b>Secondary well barrier</b>					
1	Surface tree & tubing hanger	Tested to 5000 psi	Maintained	Yes	Tested & maintained
2	Well head & casing hanger	Tested to 5000 psi	Maintained	Yes	Tested & maintained
3	9 5/8" Casing	Tested to 5000 psi	Annular pressure records	Yes	Tested, no annular pressure build up reported
4	9 5/8" Casing cement	Cement report does not provide a TOC, the report quotes for the 9 5/8" cementation: minimal losses during circulation, cementation in 2 stages with 2000 psi bump plug pressure	Annular pressure records	Yes	Good cement report on placement of cement in caprock NFS potential - Vlieland shale & Aalburg shale
5	7" Liner + liner lap	The CATO-2 report (Akemu et al. 2011) quotes a 5000 psi test that is not mentioned in the end of well report.	Annular pressure records	Yes	The liner is tested by default; the differential pressure from annulus to reservoir by hydrostatic column is approximately 280 bar
6	7" Liner cement	The cement report of P18-3 (previous well name) reports the TOC at 3508 m MD. The well status diagram shows the TOC at 3477 m MD. The CBL indicates a poor bond	Annular pressure records	No	The well status diagram shows the TOC 3477 m MD. The CBL indicates a poor bond. There is 47 m of uncemented liner above the production packer
7	In-situ formation (Cap rock)	FIT of 15.8 ppg at 3438 m TVD	NA	Yes	FIT 15.8 of ppg at 3438 m TVD reported

### 9.2.5 Well P18-2A3-ST2

A well barrier diagram with well barrier envelopes and elements defined for well P18-2A3-ST2 is provided in Figure 9-3, the evaluation of the elements can be found in Table 9-3. The evaluation of the well integrity barriers leads to the following observations.

#### Primary barrier:

- The 7" liner is installed with the casing shoe in the caprock. According to the EOWR it shows a good cement job. The in-situ formation integrity test (FIT) of 15 ppg at 3269 m TVD and a 4000 psi (272 bar) casing test confirmed the integrity of these elements.
- There has been no pressure build-up reported for the A-annulus, this has been confirmed by the TAQA annular pressure history.
- The retrievable production packer has been installed in the 7" liner with a good cement bond at about 200 m below TOC / top of liner.
- The side track (ST-1) was drilled to 3718 m MD and plugged back from 3425 m MD due to a lost drilling assembly with a length of 4.65 m. The well was side tracked (ST-2) again from 3375 m MD, this leaves an 8 1/2" open borehole of ST-1 from 3718 m MD to 3425 m MD that penetrates 177m of caprock. The caprock is present from 3375 m MD to 4070 m MD, given the penetration of 343 m, this leaves 352 m of caprock in place. The production packer (primary barrier) is positioned at 3715 m MD. The ST-1 borehole extends 3 m below this

depth, therefore ST-1 appears to be well isolated and is not considered a risk from a well integrity perspective, mainly because of a good 7" liner cementation.

#### Secondary barrier:

- The 7" liner has a good cementation in accordance with the EOWR, cement was properly displaced and positively pressure tested, the risk of liner lap failure above the production packer is mitigated by the 7" integrity status.
- The 9 5/8" casing shoe has a FIT that is above the final CO<sub>2</sub> storage reservoir pressure. The EOWR reported a good cement job with TOC of 1806 m MD.
- Two formations with natural formation sealing potential are penetrated by the well, the Aalburg shale that covers the 7" liner and the Vlieland shale that covers the 9 5/8" casing shoe, and part of the 7" liner. These could improve the sealing performance over time.
- In the original hole before (ST-1), is a lost drill string positioned with top cemented and cased off. This provides a conduit from 2323 m to 550 m outside the existing wellbore, this conduit does not penetrate the caprock and is not considered as a risk.

#### Structural well integrity:

- The 13 3/8" casing is placed at 1806 m MD and had a successful FIT of 13 ppg, the casing is cemented to 151 m MD calculated.
- The 20" casing is set at 408 m MD and is cemented to seafloor.
- The 30" conductor is piled to 132 m MD.

From a structural load bearing capacity point of view there appears to be adequate cement overlap to transfer the well loads. The 20" casing is cemented to seafloor this leaves the 20" casing inside the conductor exposed to potential risk of corrosion of the fluids in the conductor annulus from wellhead to seafloor, this needs to be verified.

#### Discrepancies:

- Akemu et al. (2011) report the production tubing as 5", 13Cr-L80 but it was confirmed in this study to be 5½", 13Cr-L80.

#### Summary

- The well currently appears to have no apparent leaks.
- From Table 9-3 can be seen that all barrier elements have been validated.
- The CO<sub>2</sub> injection load case capacity and the material compatibility for the retrievable packer to be assessed and potentially to be mitigated to make this well a suitable CO<sub>2</sub> injector.

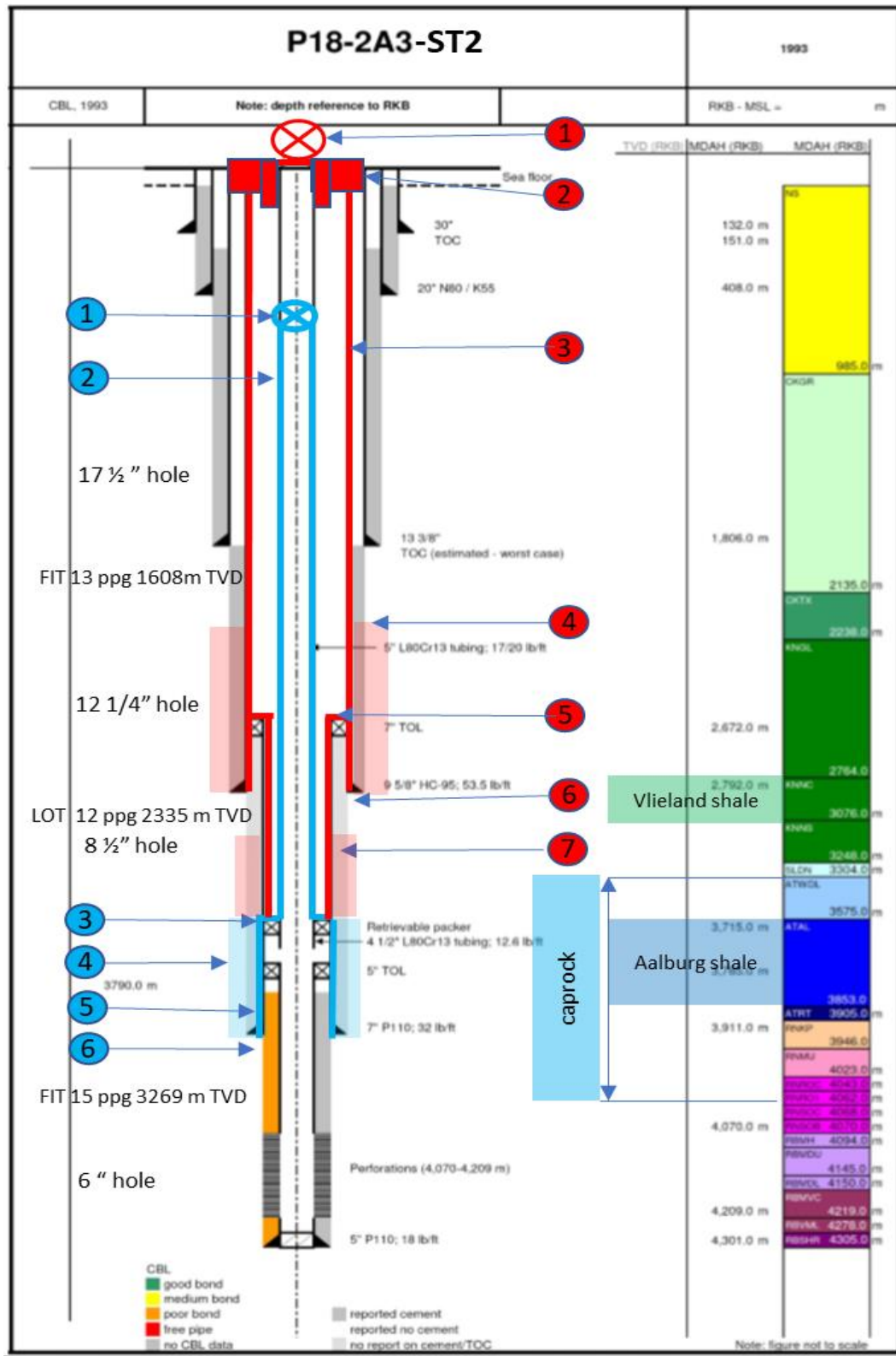


Figure 9-3 Well P18-2A3-ST2 barrier diagram with barrier elements defined. See Table 9-3 for a discussion of the barrier elements (indicated by the numbered circles).

Table 9-3 Well P18-2A3-ST2 barrier element assessment based on current data set. The numbers in the first column correspond with the numbers in coloured circles in Figure 9-3.

no	P18-2A3-ST2 Element	As built	Monitor	Barrier validated	Validation Criteria
<b>Primary well barrier</b>					
1	5 1/2" Scsssv	Tested to 5000 psi	Maintained	Yes	Tested & maintained
2	5 1/2" Tubing	Tested to 5000 psi	Annular pressure records	Yes	Tested & no annular pressure build up reported
3	7" Production packer	Retrievable packer that is tested	Annular pressure records	Yes	Tested & no annular pressure build up reported
4	7" Liner cement	Cement was fully displaced	Annular pressure records	Yes	Good cement report Identified NFS potential - Aalburg shale
5	7" Liner	Tested to 4000 psi	Annular pressure records	Yes	Tested & no pressure in annulus reported
6	In-situ formation (Caprock)	FIT of 15 ppg at 3269 m TVD	NA	Yes	FIT of 15 ppg at 3269 m TVD reported The plugged back side track 1 did not fully penetrate the caprock, there is 468 m of undisturbed caprock in place
<b>Secondary well barrier</b>					
1	Surface tree & tubing hanger	Tested to 4000 psi	Maintained	Yes	Tested & maintained
2	Wellhead & casing hanger	Tested to 4000 psi	Maintained	Yes	Tested & maintained
3	9 5/8" Casing	Tested to 4000 psi	Annular pressure records	Yes	Tested to 4000 psi, no annular pressure build up reported
4	9 5/8" Casing Cement	The TOC is estimated to be at 1806 m MD. A top up job of 13 3/8" by 9 5/8" annulus has been reported	Annular pressure records	Yes	Cement was displaced and tested
5	7" Liner + liner lap	Tested to 4000 psi	Annular pressure records	Yes	Tested to 4000 psi, no annular pressure build up reported
6	In-situ formation	LOT of 12 ppg at 2335 m TVD	NA	Yes	LOT of 12 ppg at 2335 m TVD reported Identified NFS potential - Vlieland shale
7	7" Liner cement	The TOC is calculated to be at the top of liner at 2672 m MD. The plug is bumped with 800 psi pressure, the reported over-displacement pressure was 2400 psi	Annular pressure records	Yes	Good cement report Identified NFS potential - Aalburg shale

### 9.2.6 Well P18-2A5-ST1

A well barrier diagram with well barrier envelopes and elements defined for well P18-2A5-ST1 is provided in Figure 9-4, the evaluation of the elements can be found in Table 9-4. The evaluation of the well integrity barriers leads to the following observations.

#### Primary barrier

- The 7" liner is placed almost entirely in the caprock. The liner has a good cement report and CBL assessment. The TOC was calculated to be at 3805 m MD and this has been confirmed by a log, the liner was tested to 5000 psi (~345 bar).
- The Aalburg shale, a potential naturally sealing formation, covers the 7" liner and potentially provides additional support for the good cement.

#### Secondary barrier

- There is a sustained casing pressure reported up to 610 psi (42 bar), that is bled down to 100 psi (7 bar). In the annular pressure history has been found that this pressure has been up to 98 bar, which is within the Maximum Allowable Annular Surface Pressure (MAASP) of 1650 psi (114 bar). The source of the annular pressure build-up is assumed to be from the casing side as the hydrostatic pressure in the production casing exceeds the tubing pressure at packer depth. Mainly fluid returns were found when bleeding off the pressure. No further investigation has been undertaken to date.

- The 9 5/8" casing has a good cement job with the TOC reported at 2338 m MD.
- The 9 5/8" casing shoe has a FIT that is above the final CO<sub>2</sub> storage reservoir pressure.
- The potential natural sealing formation Vlieland shale covers part of the 9 5/8" casing.

It should be pointed out that the original bore hole has a lost drilling assembly that is plugged back with cement and is positioned with the top of fish at 3900 m to 4404 m MD, this penetrates the caprock to 4404 m. The bottom of the caprock is at 4800 m MD, this leaves 400 m of undisturbed caprock in place and is not considered a risk.

#### Structural well integrity:

- The 13 3/8" casing is placed at 2488 m MD and had a successful FIT of 12.3 ppg, the casing is cemented to 991 m MD calculated, an ECP is set at 942 m MD.
- The 20" casing is set at 991 m MD and is cemented to main sea level according to well status diagram, the EOWR does not contain a cement report on the 20" casing.
- The 30" conductor is piled to 131 m MD.

From a structural load bearing capacity point of view there appears to be adequate cement overlap to transfer the well loads, the 20" casing is cemented to main sea level this leaves the 20" inside the conductor exposed to potential risk of corrosion of the fluids in the conductor annulus from wellhead to mean sea level, this needs to be verified.

#### Discrepancies:

- Akemu et al. (2011) reports the production tubing to be 5", 13Cr-L80, but it was confirmed in this study to be a 7", 13Cr-L80 completion, with a 5 1/2", 13Cr-L80 SCSSSV and a 5 1/2", 13Cr-L80 tubing to surface.

#### Summary

- From Table 9-4 it can be seen that most barrier elements have been validated, with the exception of the secondary barrier 9 5/8" casing due to the sustained casing pressure.
- The sustained A-annulus pressure, is managed within the Maximum Operating Pressure (MOP) for the current natural gas production situation. The risk associated with multi barrier failure and out of zone injection of CO<sub>2</sub> may require mitigations to the current well status, i.e. the A-annulus pressure needs investigation / recompletion.

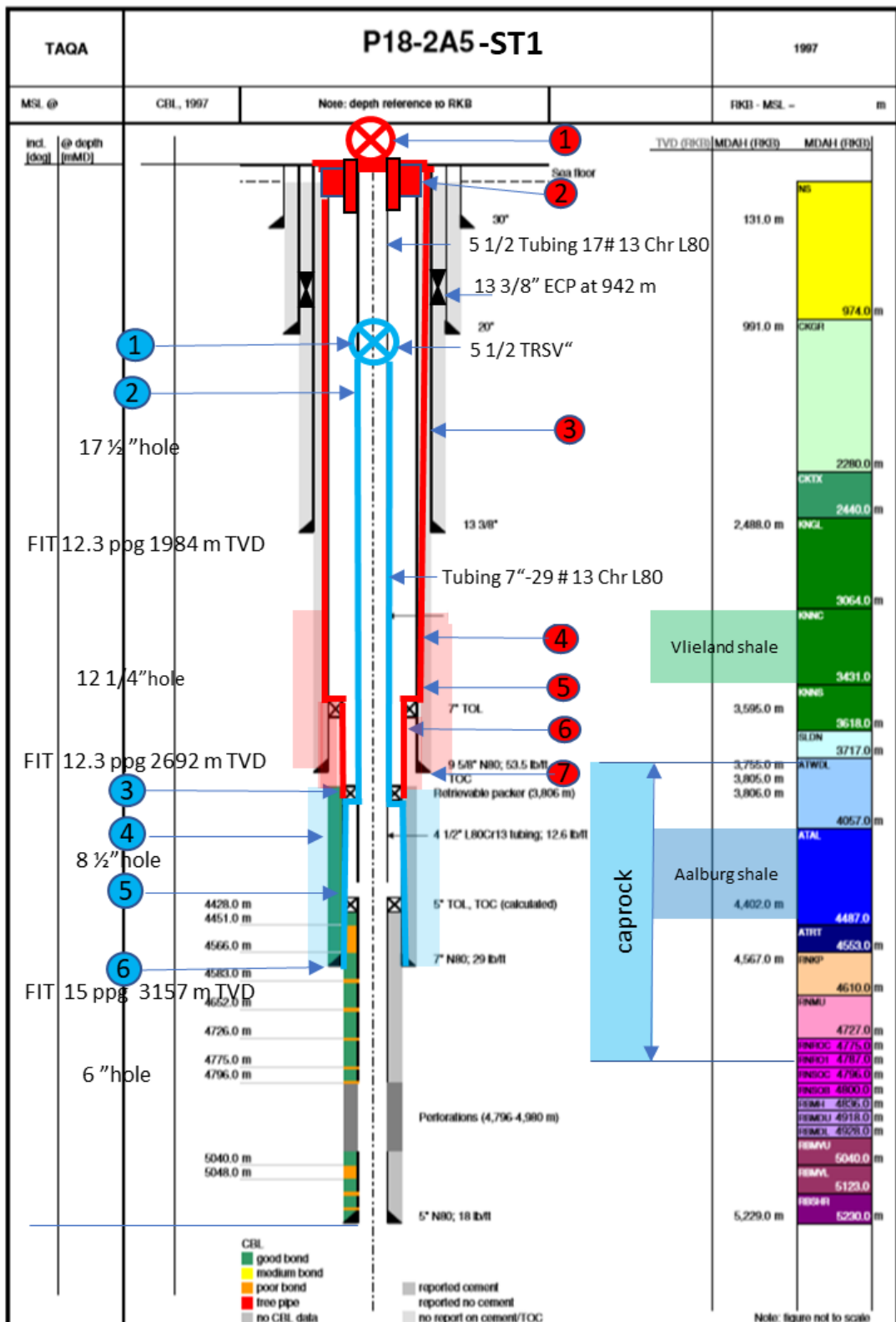


Figure 9-4 Well P18-2A5-ST1 barrier diagram with barrier elements defined. See Table 9-4 for a discussion of the barrier elements (indicated by the numbered circles).

Table 9-4 Well P18-2A5-ST1 barrier element assessment based on current data set. The numbers in the first column correspond with the numbers in coloured circles in Figure 9-4.

no	P18-2A5-ST1 Element	As built	Monitor	Barrier validated	Validation Criteria
<b>Primary well barrier</b>					
1	5 1/2" Scssv	Tested	Maintained	Yes	Tested & maintained
2	7" Tubing	Tested	Annular pressures recorded	Yes	Tested, some annular pressure reported but no gas bled off
3	7" Production packer	Tested, the retrievable packer is installed at 3806 m MD, the TOC is reported to be at 3805 m MD	The sustained annular pressure in the A annulus is within MOP	Yes	The A annulus has a sustained pressure of 40 bar on average, there was only liquid bled off. The source is not from producing reservoir because pressure is too low to be able to leak into the hydrostatic fluid column in the annulus. A possible source of pressure is the formation behind the casing or liner lap, this is not certain
4	7" Liner cement	The TOC is at 3805 m MD, no detailed cement report available. The cement is fully displaced to 43 m MD above the 7" shoe. Good cement bond log	Annular pressures recorded	Yes	Tested and fully displaced cement job Good cement bond log
5	7" Liner	Test reported with no value	Annular pressures recorded	Yes	Liner is tested and exposed to hydrostatic overbalance of annulus
6	In-situ formation (Caprock)	FIT of 15 ppg at 3157 m TVD The original borehole penetrates the top of the caprock for 28 m with a stuck drilling assembly, it is plugged back leaving 960 m of undisturbed caprock in place	NA	Yes	FIT of 15 ppg at 3157 m TVD reported Identified NFS potential - Aalborg shale
<b>Secondary well barrier</b>					
1	Surface tree & tubing hanger	Tested at 5000 psi	Maintained	Yes	Tested & maintained
2	Wellhead & casing hanger	Tested at 5000 psi	Maintained	Yes	Tested & maintained
3	9 5/8" Casing	Tested at 5000 psi	The sustained annular pressure in the A annulus is within MOP	No	The A annulus has a sustained pressure of 40 bar on average, there was only liquid bled off. The source is not from producing reservoir because pressure is too low to be able to leak into the hydrostatic fluid column in the annulus. A possible source of pressure is the formation behind the casing or liner lap, this is not certain
4	9 5/8" Casing cement	The TOC is calculated to be at 2338 m MD, the cement is fully displaced to 104 m above the shoe	Annular pressures recorded	Yes	A cement top up job is reported for the 13 3/8" by 9 5/8" annulus. Identified NFS potential - Vlieland shale
5	7" Liner + liner lap	A test is reported without pressure value	Annular pressures recorded	Yes	The liner lap is exposed to annular pressure and hydrostatic brine column
6	7" Liner cement	The TOC is at 3805 m MD, no detailed cement report is available. The cement is fully displaced to 43 m above the 7" line shoe. The CBL indicates a good cement bond	Annular pressures recorded	Yes	Tested and fully displaced cement job Good cement bond log
7	In-situ formation	FIT of 12.3 ppg at 2692 TVD	NA	Yes	FIT of 12.3 ppg at 2692 TVD reported

### 9.2.7 Well P18-2A6 + ST

Well barrier diagrams with well barrier envelopes and elements defined for well P18-2A6 MB (mother bore) and P18-2A6-ST are provided in Figure 9-5 and Figure 9-6, whereas the evaluation of the elements can be found in Table 9-5. The evaluation of the well integrity barriers leads to the following observations.

#### Primary barrier

- The 9 5/8" retrievable production packer is installed at 2145 m MD and tested. This is above the 9 5/8" tieback at 2223 m MD that is tested.
- The 9 5/8" tie-back casing is cemented and tested, the EOWR mentions a good cement job. The TOC is reported to be at 1631 m MD, there is a cement report from Halliburton that states that the cement slurry is placed to 2022 m MD, this cement report has been taken as TOC in this assessment (worst case scenario).

- The tubing and SCSSSV are tested, no annular pressures have been observed or reported.
- This defines the primary barrier above the production packer as validated.
- The side track window is uncemented which has implications for the well integrity:
  - The EOWR reported the TOC to be at top of liner (TOL). The cement across the 7" side track liner was logged from the 7" liner shoe at 3711 m MD to 2180 m MD (approximately 308 m above the 9 5/8" casing. The bond log of the 7" side track liner across the 9 5/8" side track exit window at 2495 m MD shows "ratty" cement across the window down to 2753 m MD. The cement bond is poor from 2753 m MD to an approximate depth of 3158 m MD. From 3158 m MD to the 7" liner shoe (at 3709 m MD) the cement bond quality appears to be very good.
  - The 7" side track liner is perforated at the depth of the hollow whip-stock, this connects both the mother bore and the side track reservoirs through the uncemented side track window and the surrounding open borehole formation at the casing window.
  - The 9 5/8" casing is uncemented from 3000 m MD (TOC) to 2284 m MD (the 13 3/8" casing shoe). The 7" side track liner has "ratty" cement (no bond) from 2753 m MD to 2284 m MD (the 13 3/8" casing shoe). This results in a section of +/- 1185 m of uncemented formation; 716 m of 12 1/4" hole and 469 m of 8 1/2" side track.
  - The in-situ formation has been tested at 1961 m MD TVD to 12 ppg (pounds per gallon), equivalent to 4060 psi (280 bar) pressure.
  - The above compromises the integrity of the primary barrier in mother bore and side track below the production packer.

#### Secondary barrier:

- The secondary barrier consists out of the 9 5/8" tieback casing that is tied back to below production packer and is tested.
- The top of the 9 5/8" casing cement inside the tieback annulus is reported in the EOWR to be at 1613 m MD. The well status diagram has two depths for TOC: the 9 5/8" tie-back packer TOC is calculated to be at 2022 m MD and the TOC of the 9 5/8" casing at 1631 m MD. The TOC reported in the EOWR (at 2022 m MD) has been taken in this assessment (worst-case scenario).
- The annular pressure is monitored and recorded, no sustained annular pressures are reported confirming integrity.

#### Structural well integrity:

- The 13 3/8" casing is placed at 2284 m MD and had a successful FIT of 12 ppg at 1961 m TVD, the casing is cemented to 200 m MD estimated with a multistage packer at 932 m.
- The 20" casing is set at 987 m MD and is cemented with cement returns to surface.
- The 30" conductor is piled to 131 m MD.

From a structural load bearing capacity point of view there appears to be adequate cement overlap to transfer the well loads, the 20" casing is cemented to surface and partly washed out, this leaves a small top portion of the 20" inside the conductor exposed to potential risk of corrosion of the fluids in the conductor annulus, this needs to be verified.

#### Discrepancies

- Akemu et al. (2011) reports the production tubing as 5" 13Cr-L80, it has been confirmed to be 5 1/2", 13 Cr-L80 .
- The EOWR repeatedly reports for the 9 5/8" a top of cement at 1631 m MD, the cement report and final well status diagram show 2022 m MD.
- The EOWR reports on the 7" side track liner a top of cement at top of liner, the bond log shows no or "ratty" cement from top of 7" side track liner to 2753 m MD.

#### Summary

- The well primary barrier is limited to the production packer set above the tieback packer and the side track window.
- The producing reservoir formations from the side track and the mother bore connect at the side track window that is not isolated. Although this imposes a risk of out of zone injection below the primary and secondary barrier envelop; about 1185 m of uncemented borehole (open formation) is exposed.
- For this well to be used as CO<sub>2</sub> injector the primary well integrity barrier has to be restored to the caprock of the mother bore reservoir and the integrity of the window has to be restored. This has most likely to be done by plug and abandonment (P&A) of the side track and installing a cemented scab or tie back liner to restore the mother bore integrity.
- The mother bore original primary and secondary barrier can be restored, it has a good cementation and in-situ formation at caprock level.
- The 13 3/8" casing has 25% casing wear and therefor the burst rating has been reduced from 3860 to 2500 psi (262-170 bar). A 9 5/8" tieback has been installed to mitigate the risk of exceeding the reduced burst rating for drilling the next section.



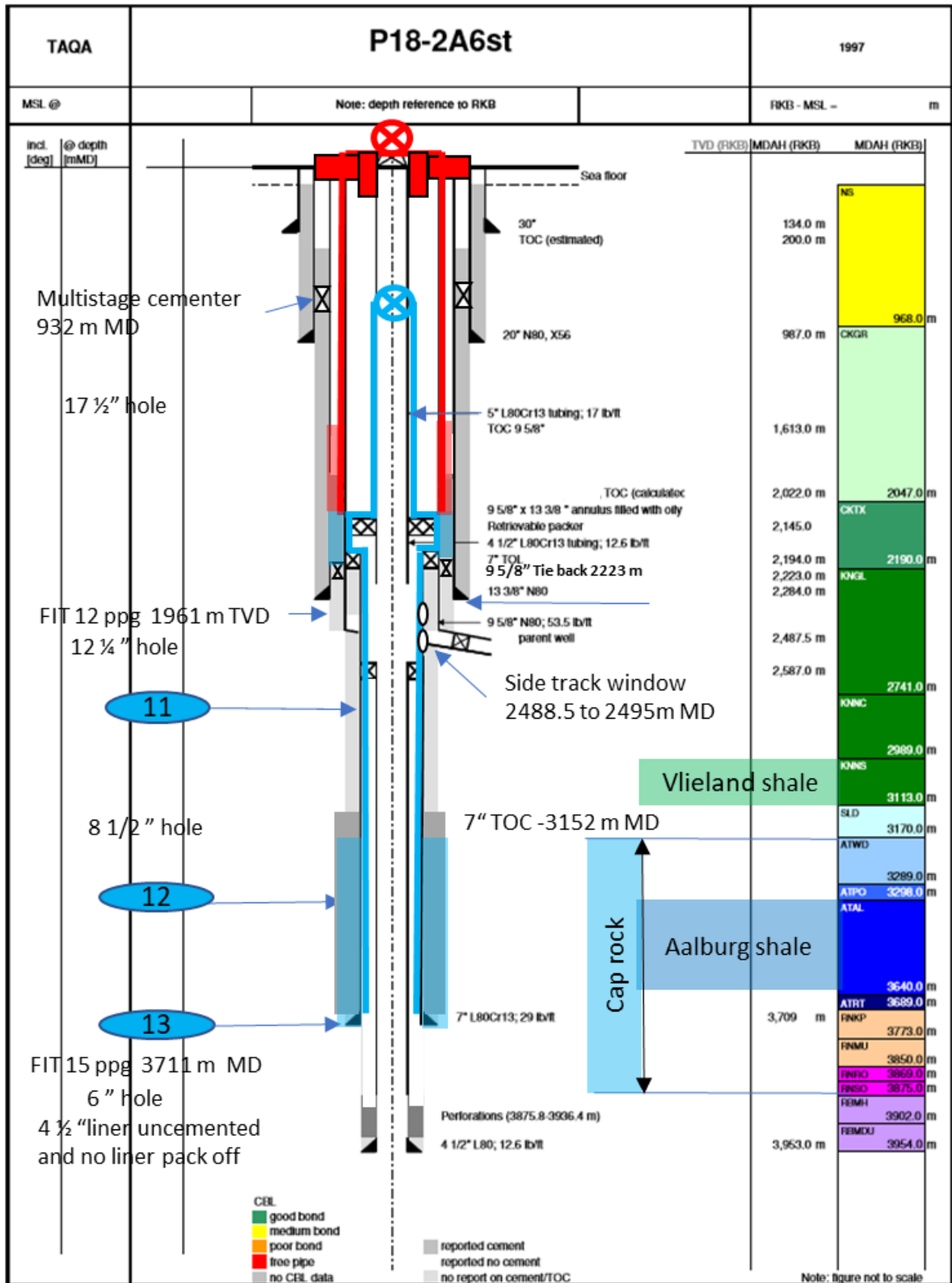


Figure 9-6 Well P18-2A6-ST1 barrier diagram with barrier elements defined. See Table 9-5 for a discussion of the barrier elements (indicated by the numbered circles).

Table 9-5 Wells P18-2A6 and P18-2S6-ST1 barrier element assessment based on current data set. The numbers in the first column correspond with the numbers in coloured circles in Figure 9-5 and Figure 9-6.

no	P18-2A 6-ST1 Element	As built	Monitor	Barrier validated	Validation Criteria
<b>Primary well barrier</b>					
1	5 1/2" Scssv	Tested at 5000 psi	Maintained	Yes	Tested & maintained
2	5 1/2" Tubing	Tested at 5000 psi	Annular pressures recorded	Yes	Tested, no annular pressure build up reported
3	9 5/8" Retrievable production packer	Set at 2144 m MD and tested	Annular pressures recorded	Yes	Tested, no annular pressure build up reported
4	9 5/8" Tie-back casing cement	The 9 5/8" casing cement is part of the tieback packer that is set at 2233 m MD. The top of the production packer is at 2145 m MD, the total length of the primary seal is 78 m.	Annular pressures recorded	Yes	There is a good cement report on the 9 5/8" tie-back casing. The TOC is reported in the EOWR to be at 1613 m MD. The Halliburton cement report indicates the TOC to be at 2022 m MD, this is a conflict in the reports. In this report 2022 m MD has been used as this is the worst case scenario with total length of the primary seal of 78 m
5	9 5/8" Tie-back casing	Tested, this is the 9 5/8" contingency tieback for the risk of casing wear risk of the 13 3/8" casing	Annular pressures recorded	Yes	Tested, no annular pressure build up reported
6	9 5/8" Tie-back packer	Tested to 5000 psi together with the 7" liner before the side track	NA	Yes	Tested
7	In-situ formation	FIT of 12 ppg at 1961 m TVD	NA	Yes	FIT of 12 ppg at 1961 m TVD reported
8	9 5/8" Casing	Tested before side track window is created to 5000 psi	NA	No	Integrity compromised by uncemented side track window Identified NFS potential - Vlieland and Aalborg shales
9	9 5/8" Casing cement	Cement report indicates good cement to 3000 m MD	NA	No	The integrity is compromised by the uncemented side track window
10	In-situ formation (caprock motherbore)	FIT of 12 ppg at 3447 m TVD	NA	Yes	FIT of 12 ppg at 3447 m TVD reported Note: The FIT is affected by the uncemented window and the reported FIT is at 12 ppg at 1961 m TVD
11	7" Side track liner	The liner is perforated at the side track window to facilitate commingled flow	NA	No	The integrity is compromised by the uncemented side track window
12	7" Side track liner cement	The EOWR states cement to the top of liner. The CBL reports the TOC at 3152 m MD, this is about 660 m MD below the sidetrack window	NA	No	The Integrity is compromised by the uncemented side track window and perforated section at the side track window Identified NFS potential - Vlieland and Aalborg shales
13	In-situ formation (caprock side track)	FIT of 15 ppg at 3711 m TVD	NA	No	The FIT is compromised by the uncemented window and the FIT of 12 ppg at 1961 m TVD
<b>Secondary well barrier</b>					
1	Surface tree & tubing hanger	Tested to 5000 psi	Maintained	Yes	Tested & maintained
2	Wellhead & casing hanger	Tested to 5000 psi	Maintained	Yes	Tested & maintained
3	9 5/8" Tie back casing	Tested to 5000 psi	Annular pressures recorded	Yes	Tested, no annular pressure build up reported
4	9 5/8" Casing cement	Tieback string is mitigating the risk of wear of the 13 3/8" casing The EOWR calculated the TOC at 1613 m MD and at 2022 m MD	Annular pressures recorded	Yes	There is a good cement report on the 9 5/8" tie-back casing. The TOC is reported in the EOWR to be at 1613 m MD. The Halliburton cement report indicates the TOC to be at 2022 m MD, this is a conflict in the reports. In this report 2022 m MD has been used as this is the worst case scenario with total length of the primary seal of 78 m

### 9.2.8 Well P18-02

The P18-02 well is suspended and left with a mud line suspension in place to allow potential re-entry. The well is plugged at various depths with a total of 4 plugs. The well was re-assessed in view of CO<sub>2</sub> storage with following results (see also Figure 9-7 and Table 9-6).

The assessment is done based on current standards in place; Norsok D10 section 9.6.5.1 (permanent abandonment open hole) and NOGEP A 45. The NOGEP A 45 standard is currently under review with reference to decommissioning requirements for CO<sub>2</sub> storage wells, this implies that this assessment has to be reviewed when the updated NOGEP A 45 standard is available.

#### Primary barrier

- The 7" liner EZSV (trademark of a drillable plug) is installed above top perforations at 3300 m MD with a 1.5 m cement plug from 3300 m to 3298.5 m. This is below the caprock bottom which is located at 3275 m MD. Therefore the plug is not considered to be a primary barrier element as it is located below the cap rock (see section 9.2.1.1 point a).
- The second 7" mechanical plug is installed in the 7" liner at 3006 m MD and tested to 2000 psi (~140 bar). The cement plug is placed from 3006 m MD to above the top of the 7" liner with a TOC of 2956 m MD in the 9 5/8" casing. Resulting in 50 m cement.
- The 7" liner is cemented to 3005 m MD TOC, this is 49 m below the top of the liner at 2956 m MD, this implies that, at the depth of the cement plug, there is no cement behind the 7" liner. Therefore there is no cement across all annuli at this depth.
- The cement plug covers the 9 5/8" over a length of 60 m, from the top of liner at 2896 m MD to the TOC of the plug at 2956 m MD. The 9 5/8" cementation is reported to be good in the cement report, but the CBL indicates poor bonding.
- The in-situ formation (Caprock) was tested by a FIT to 14.8 ppg at 3711 m TVD.

#### Secondary barrier

- The mechanical plug is set in the 9 5/8" casing at 1915m MD and tested to 2000 psi. The cement plug is placed from 1915 m MD to 1846 m MD with a total length of 59 meter.
- The 9 5/8" cementation was done in 2 stages with the multistage cement packer at 1893 m MD and with the TOC of the first stage cementation at 1932 m MD. This implies that there is no cement in the 9 5/8" by 13 3/8" annulus from 1932 m MD to 1893 m MD.
- The EOWR reports a premature landing of the shut of plug ahead of the cement that resulted in a failed placement of the first stage cement job. The bond log shows no cement at plug depth, the second stage cementation is from 385 m MD to 69 m MD TOC.

#### Open hole barrier

- There are no specific requirements for the open hole barrier, it has been assessed based on the NORSOK D10 9.6.5.1 barrier diagram example for permanent abandonment for open hole wells.
- The open hole barrier has a 65 m cement plug placed on a mechanical plug from 154 m MD to 85 m MD. There is no cement in the 9 5/8" by 13 3/8" annulus at this depth, the 13 3/8" by 20" annulus is cemented.

#### Structural integrity

All wellheads are removed and the 9 5/8", 13 3/8" and 20" casings were backed out and removed at the mudline hanger. A casing stick up protector has been placed at seabed.

#### Discrepancies

- The well status diagram shows that the 13 3/8" casing is cemented with the TOC at 1627 m MD, while the final well report indicates there is no cement placed at the first stage cementation.
- Akemu, et al., (2011) did not address the discrepancy of the uncemented 13 3/8" casing at cement plug depth.

### Summary

- From Table 9-6 it can be seen that multiple barrier elements for this suspended well could not be validated, the well needs to be planned for re-assessment and decommissioning conform the updated NOGEP A 45 standard for CO<sub>2</sub> storage decommissioning when these are available.

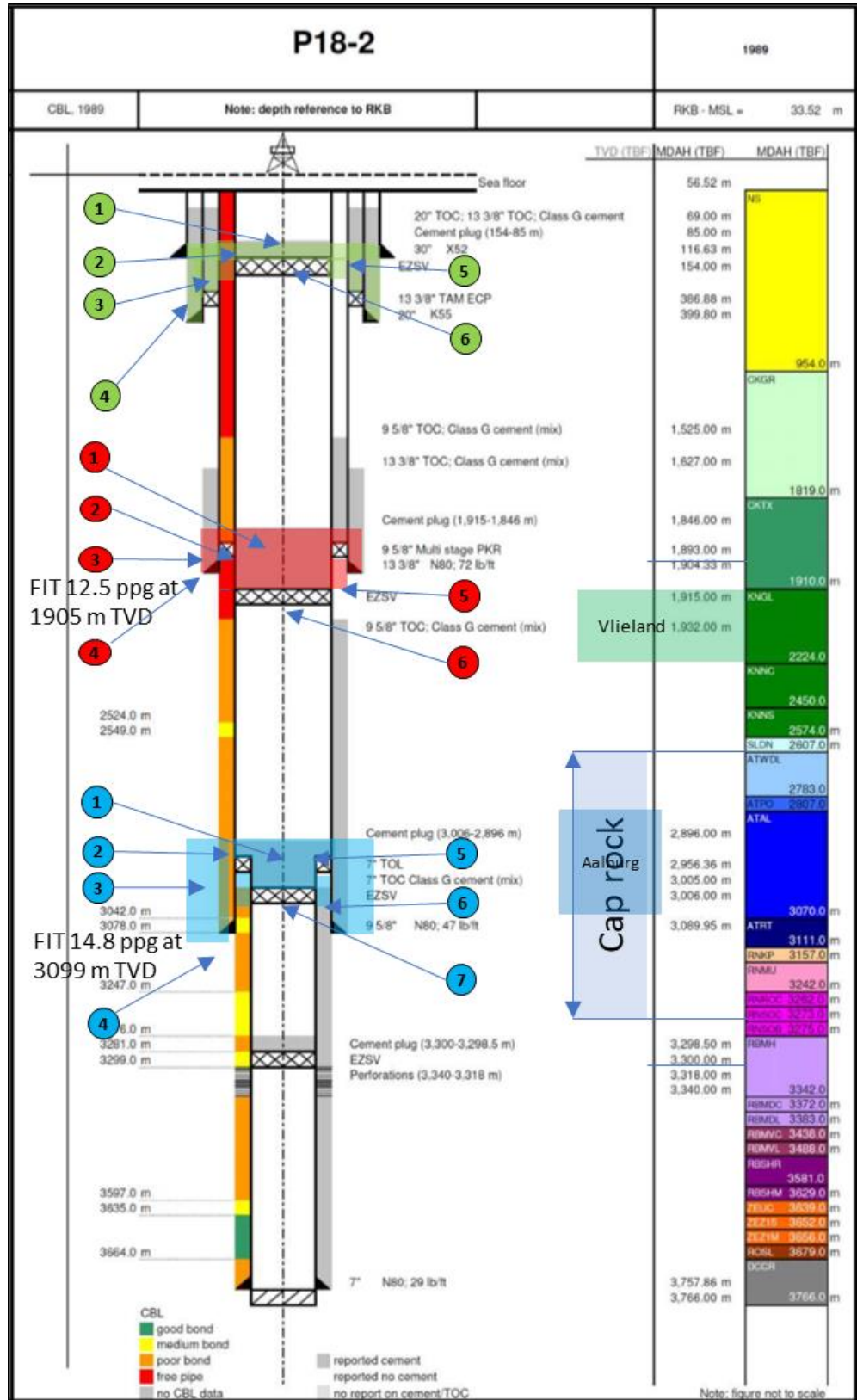


Figure 9-7 Well P18-2 barrier diagram with barrier elements defined. See Table 9-6 for a discussion of the barrier elements (indicated by the numbered circles).

Table 9-6: Wells P18-02 barrier element assessment based on current data set. The numbers in the first column correspond with the numbers in coloured circles in Figure 9-7.

no	P18-2A1 Element	As built	Monitor	Barrier validated	Validation Criteria
<b>Primary well barrier</b>					
1	5 1/2" Scssv	Tested to 5000 psi	Maintained	Yes	Tested & maintained
2	5 1/2" Tubing	Tested to 5000 psi	Annular pressure records	Yes	Tested, no annular pressure build up reported
3	7" Production packer	Installed at 3503 m MD which is 26 m below the TOC in the 7" liner. Tested to 5000 psi	Annular pressure records	Yes	Tested, no annular pressure build up reported.
4	7" Liner	Liner report for P18-3 (previous name of P182A1) The liner covers 50 m of caprock	NA	Yes	The liner and production packer are under continuous high hydrostatic differential pressure of the A annulus. No annular pressure build up recorded
5	In-situ formation (Cap rock)	FIT of 15.8 ppg at 3488 m TVD	NA	Yes	FIT of 15.8 ppg at 3488 m TVD reported
6	7" Liner cement	Cement report of P18-3 (previous well name) reports the TOC at 3508 m MD. The well status diagram shows the TOC at 3477 m MD. The CBL indicates a poor bond	NA	No	The well status diagram shows the TOC 3477 m MD. The CBL indicates a poor bond. The TOL is set at 3404 m MD, this leaves 73 m of uncemented liner combined with poor bond.
<b>Secondary well barrier</b>					
1	Surface tree & tubing hanger	Tested to 5000 psi	Maintained	Yes	Tested & maintained
2	Well head & casing hanger	Tested to 5000 psi	Maintained	Yes	Tested & maintained
3	9 5/8" Casing	Tested to 5000 psi	Annular pressure records	Yes	Tested, no annular pressure build up reported
4	9 5/8" Casing cement	Cement report does not provide a TOC, the report quotes for the 9 5/8" cementation: minimal losses during circulation, cementation in 2 stages with 2000 psi bump plug pressure	Annular pressure records	Yes	Good cement report on placement of cement in caprock NFS potential - Vlieland shale & Aalburg shale
5	7" Liner + liner lap	The CATO-2 report (Akemu et al. 2011) quotes a 5000 psi test that is not mentioned in the end of well report.	Annular pressure records	Yes	The liner is tested by default; the differential pressure from annulus to reservoir by hydrostatic column is approximately 280 bar
6	7" Liner cement	The cement report of P18-3 (previous well name) reports the TOC at 3508 m MD. The well status diagram shows the TOC at 3477 m MD. The CBL indicates a poor bond	Annular pressure records	No	The well status diagram shows the TOC 3477 m MD. The CBL indicates a poor bond. There is 47 m of uncemented liner above the production packer
7	In-situ formation (Cap rock)	FIT of 15.8 ppg at 3438 m TVD	NA	Yes	FIT 15.8 of ppg at 3438 m TVD reported

### 9.2.9 Conclusion on current well status

The selected wells relevant in the context of CO<sub>2</sub> injection into the P18-2 field have been evaluated regarding their current status and well integrity risks. All wells reviewed have the potential to be used safely as CO<sub>2</sub> injectors. Appropriate mitigations can make them fit for storage operations as given below.

#### 9.2.9.1 Generic well integrity issues of the wells

- The currently installed production packers are retrievable and need to be replaced based on the expected CO<sub>2</sub> injection load case. The workover would include the change or refurbishment of the surface tree and associated sealing components, which should be suitable for the CO<sub>2</sub> injection operating envelope, i.e. pressure, temperature, CO<sub>2</sub> composition and flow rate.
- The operating temperatures for equipment are specified in the API standards with specific requirement for extreme (cold) conditions, all materials should be checked for suitability for the expected low temperatures.
- Seals and pack-offs that have been reported as leaking could be restored with appropriate sealing arrangements; this holds for the non-flow-wetted operational envelope.

- The well load cases must be assessed for CO<sub>2</sub> injection and evaluated against the status of the load bearing surface casing and completion design, considering sudden load changes during start-up / shut-down of CO<sub>2</sub> injection.
- Where flow-wetted components have been exposed to production fluids, like casing or liners, these may need to be assessed for corrosion of wet CO<sub>2</sub> (presence of water / brine).
- The condition of these liners may require recompletion below the current packer depths or above the liner laps depending on the identified risks to mitigate the risk of potential failure of the liner due to wear or corrosion.

#### 9.2.9.2 Summary

All wells reviewed P18-2A1 / 2A3-ST2 / 2A5-ST1 / 2A6 + ST could be re-used safely for CO<sub>2</sub> injection if the risks identified are mitigated properly; see overview in Table 9-7.

Table 9-7 Overview of P18-2 CO<sub>2</sub> injector wells selection.

Well	Status	Integrity for CO <sub>2</sub> injector	Remarks
P18-2A1	Producer	Yes	Needs recompletion and repositioning of production packer in liner / casing with good cement bond
P18-2A3-ST2	Producer	Yes	Retrievable packer CO <sub>2</sub> injection load case and material compatibility are the components to be mitigated to make this well a suitable CO <sub>2</sub> injector
P18-2A5-ST1	Producer	Yes	'A'-annulus pressure needs investigation / recompletion for CO <sub>2</sub> injection
P18-2A6 + ST	Producer	Yes	Needs restoration of the side track window in order to be able to use it for CO <sub>2</sub> injection.
P18-2	Suspended	No	Requires to be re-assessed against new CO <sub>2</sub> storage abandonment requirements (Nogepa / SodM) and decommissioned in accordance to this standard.

### 9.3 Influence of cooling on well cement

Injection of CO<sub>2</sub> at a lower temperature than the temperature of the surrounding rock can cause thermal contraction of the materials and associated stress reduction of the surrounding rock in the near-well area that may affect the structural integrity of the well barriers. The operating envelope of P18 CO<sub>2</sub> injection wells needs to consider cooling effects, which are not part of the current operating envelope designed for natural gas production.

In this section we provide an estimate of the effects of cooling due to cold CO<sub>2</sub> injection on the structural integrity of the injection well, focussing on the integrity of annular cement behind the casing, and discuss the risk of leakage along the outside of the well. Potential failure modes of the sealant (cement sheath) that can create potential continuous leakage pathways up the well across the caprock are of primary interest (Figure 9-8). The most likely leakage mechanism is related to the flow of fluids along a microannulus formed by de-bonding of the cement-casing interface or the cement-formation interface.

Note that, in order for CO<sub>2</sub> to migrate and eventually leak to the overburden through a microannulus, several events have to take place and several constraints with regard to subsurface conditions have to be met. The likelihood of cement-casing or cement-rock debonding to take place during injection of cold CO<sub>2</sub> in a P18-2 well is investigated using a numerical model based on the DIANA finite elements<sup>6</sup>. Subsequently, the likelihood that a continuous microannulus forms along the entire caprock level towards the overburden, and the conditions that need to be met for CO<sub>2</sub> to migrate through a microannulus into the overburden are discussed. For a worst-case scenario where all events occur and all conditions are met, an estimate of the leakage rate will be given and this will be discussed in the context of the total storage capacity in P18-2.

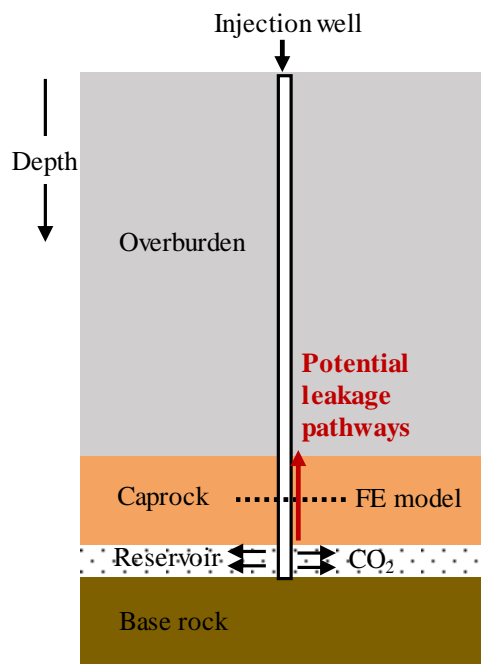


Figure 9-8: Sketch of an injection well showing the location of a finite element (FE) model for well integrity analysis at the caprock level. The model represents a cross-section of the near-wellbore area normal to the well axis at the analysis depth (see ).

### 9.3.1 *Pressure and temperature in the CO<sub>2</sub> injection well*

The initial flow assurance study for the Porthos consortium by Belfroid (Belfroid, 2019) presents several scenarios and sensitivities that can be used to estimate the possible variation of pressure and temperature conditions in CO<sub>2</sub> injection wells for different reservoir and injection conditions. This flow assurance work will be repeated and refined throughout well and project design and regularly throughout the injection years. Here we focus on CO<sub>2</sub> injection in a single well and present pressure and temperature (P&T) profiles obtained using the OLGA simulator. The OLGA model includes the entire pipeline and considers the reservoir conditions relevant for the P18-2 CO<sub>2</sub> injection (Table 9-8). Well geometry is based on an idealized well (P18-4A2) and is considered to be representative for other planned injection wells.

<sup>6</sup> See [dianafea.com](http://dianafea.com).

Steady-state simulations were performed for six scenarios (or cases in (Table 9-8) with an injection rate of 30 kg/s (~1 Mt/yr).

Table 9-8: Overview of steady-state cases of well flow simulations.

Case name	Mass flow rate (kg/s)	Reservoir pressure (bar)	Pipeline pressure control (bar)	Compressor outlet temperature (°C)
Case_b1	30	20	85	80
Case_b2	30	60	85	40
Case_b3	30	80	85	40
Case_b4	30	100	85	40
Case_b5	30	200	85	40
Case_b6	30	20	30	80

Simulated pressure profiles in the well for steady-state injection conditions are plotted in Figure 9-9. For a very low reservoir pressure of 20 bar and two-phase flow in the well, the wellhead pressure is higher than the bottom hole pressure (cases P\_b1 and P\_b2 in Figure 9-9). In other cases with a higher reservoir pressure the flow is mostly or fully single-phase and the bottom hole pressure exceeds the well head pressure due to the weight of the column of supercritical CO<sub>2</sub> in the well.

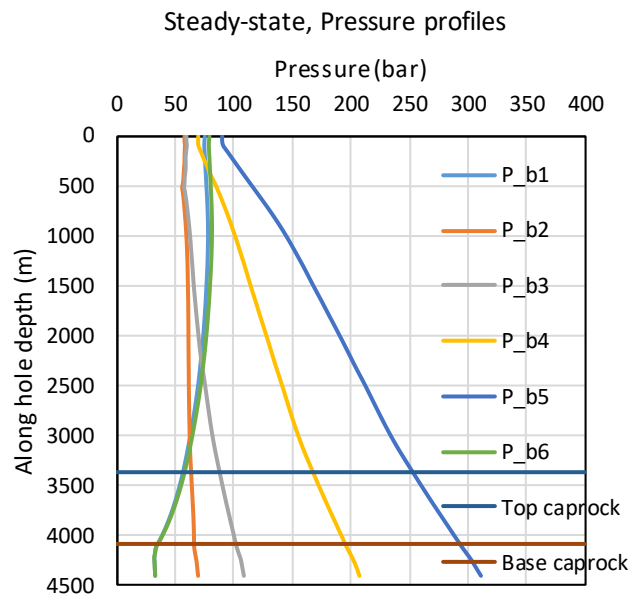


Figure 9-9: Pressure profiles in the well as a function of the along hole depth for the cases of steady-state CO<sub>2</sub> injection from Table 9-8.

The corresponding simulated temperature profiles for steady-state injection conditions are plotted in Figure 9-10. In the upper part of the well, at the depth range of 500 to 1500 m, temperature of injected CO<sub>2</sub> is higher than that of the surrounding rock. The temperature of the tubing, casing, annular cement and surrounding rock formation will increase, i.e. heating. At larger depths, below 500 to 1500 m, the temperature of the tubing, casing, annular cement and surrounding rock formation will decrease, i.e. cooling. For steady-state conditions, cooling is

most severe in the case of a low reservoir pressure of 20 bar and occurs at the level of the caprock (cases T\_b1 and T\_b6 in Figure 9-10). The CO<sub>2</sub> inside the well at the caprock level is 70°C to 100°C colder than the surrounding formation. For higher reservoir pressure, the degree of cooling decreases to 30°C to 40°C.

Figure 9-10 shows temperature profiles for steady-state conditions; the temperature in the well during a non-steady-state operation (such as a shut-in procedure) may lead to lower temperatures of the CO<sub>2</sub> in the well, but the heat capacity of the well system (such as liner and annulus fluid) prevents those short-lived low-temperature events from significantly changing the temperature of the cement and casing in the deeper parts of the well<sup>7</sup>. The profiles shown in Figure 9-10 can be used as a reliable estimate of the conditions in the well.

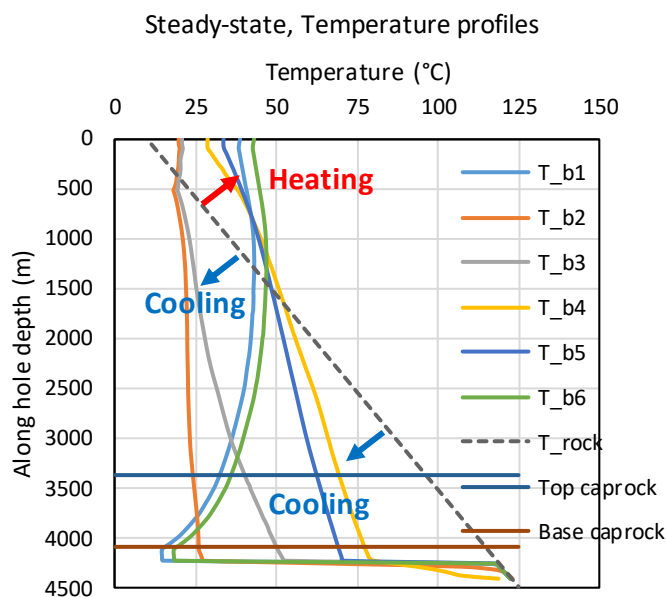


Figure 9-10: Temperature profiles as a function of the along hole depth for the cases of steady-state CO<sub>2</sub> injection from Table 9-8. Dashed black line denotes the formation temperature (T<sub>rock</sub>).

### 9.3.2

#### *Numerical modelling of the effects of cold CO<sub>2</sub> injection on well cement integrity*

A numerical model was developed to investigate the impact of thermal effects on well integrity, in particular on the integrity of annular cement behind the casing. Thermo-mechanical non-linear finite element analyses considered a section of a CO<sub>2</sub> injection well across the caprock (Figure 9-11), to evaluate whether failure of the well barriers could result in debonding of the annular cement with the casing and/or rock interfaces at caprock level, thereby creating a microannulus. In a worst case scenario, when such a microannulus is continuous from reservoir to above the caprock, a leakage path is formed.

<sup>7</sup> S. Belfroid, personal communication, 2019.

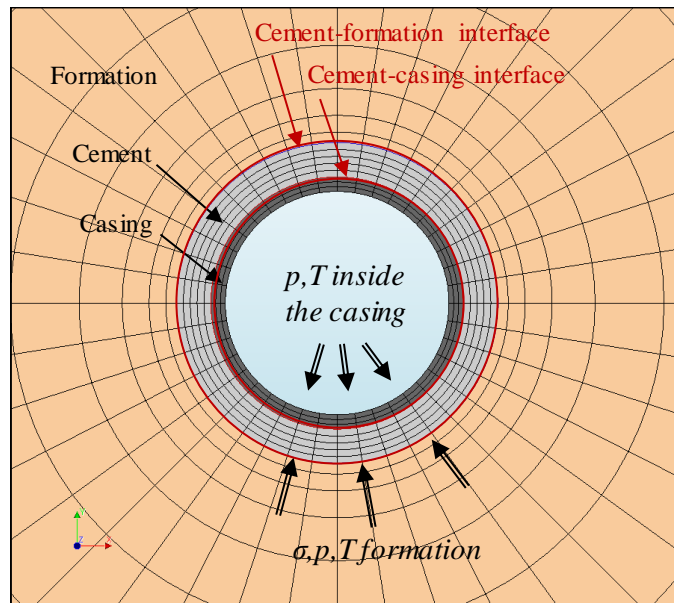


Figure 9-11: Mesh for a 2D finite element model of a cross-section of the near-well area.

The non-linear finite element simulator DIANA was used to generate meshes for 2D numerical models of the well system and run simulations. The workflow for well integrity analysis is automated through a dedicated user interface called the DIANA SEALEC application. Based on the user input in DIANA SEALEC, meshes of the well system can be generated automatically and well integrity analyses mimicking the entire lifetime of a well can be conveniently defined and executed.

The numerical model of the near-well area was developed on a cross-sectional area normal to the well axis. The model comprises well casing(s), cement sheath(s) and the surrounding rock formation. Two models with different well completion geometries were developed: completion with a single casing (Figure 9-12a) and completion with a double casing (or a liner lap; (Figure 9-12b). Chosen sizes and characteristics of casings in the models are representative of the P18-2 wells. The possible injection wells are completed over the caprock depth interval with a 9 5/8" casing and a 7" liner, and in some cases with a 5" liner.

Complete plane strain elements are used for bulk materials and zero-thickness interface elements are used for the casing-cement and the cement-formation interfaces. All materials in the model are assumed to be elastic and the well material interfaces are assumed to be rigid. The model input parameters are given in Table 9-9.

Table 9-9: Model input parameters.

Parameter	Unit	Caprock	Cement	Casing	Interface
E Young modulus	GPa	26	8.3	200	rigid
$\nu$ Poisson coefficient	-	0.3	0.1	0.3	-
Thermal expansion coeff.	$K^{-1}$	$1 \cdot 10^{-5}$	$1 \cdot 10^{-5}$	$1.3 \cdot 10^{-5}$	-
Volumetric specific heat	$Jm^{-3} K^{-1}$	$2.24 \cdot 10^6$	$4 \cdot 10^6$	$4 \cdot 10^6$	-
Thermal conductivity	$Wm^{-1} K^{-1}$	2.3	0.87	15	-

The effects of cooling were assessed by applying a temperature load of  $-1^{\circ}\text{K}$  ( $-1^{\circ}\text{C}$ ) on the inner side of the casing instantly at the start of the analysis. As all the well materials in the model were assumed elastic, the magnitude of induced thermo-mechanical stresses ( $\sigma_{\Delta T}$ ) scales linearly with the degree of cooling ( $\Delta T$ ), i.e. the stress magnitude due to cooling by  $\Delta T < -1^{\circ}\text{K}$  is obtained simply by multiplying  $\Delta T$  with the stress magnitude predicted by the model ( $\sigma_{\Delta T = -1\text{K}}$ ). A staggered heat flow and mechanical analysis is then performed. First a transient temperature field is calculated for a change in temperature of  $-1^{\circ}\text{K}$  ( $-1^{\circ}\text{C}$ ) and then the related thermo-mechanical stresses caused by this temperature change.

Note that the model is initially stress-free, i.e. the initial stress state in the cement sheath is set to zero as our aim is to estimate the net thermo-mechanical stress induced by cooling. Estimating the initial, i.e. present day (compressive) stress in annular cement of gas producing wells is difficult: direct in-situ measurement of stress in cement at downhole conditions is not possible; stress estimates can only be obtained by modelling the entire well history, taking into account the different phases in the lifetime of a well, cement material properties, quality of executed cement job, interactions with the surrounding rock formation, etc.. Modelling well histories is beyond the scope of this task, which focusses on the thermo-mechanical effects of cooling on well cement integrity.

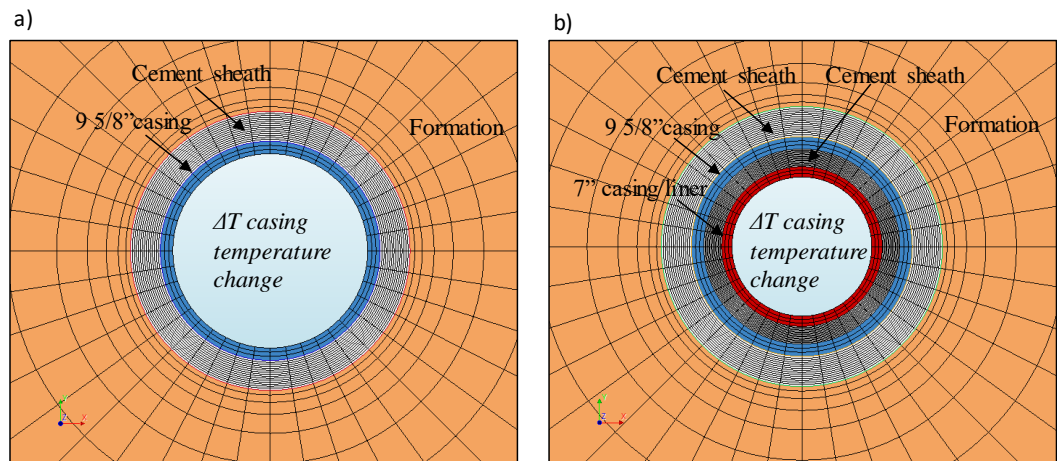


Figure 9-12: Meshes for 2D finite element models of the near-well area at the level of caprock for well sections completed with (a) a single casing and (b) a double casing (liner lap).

Simulation results show gradual extension of the cooled area radially into the surrounding rock (Figure 9-13 and Figure 9-14). After 1 year of injection, the radial extent of cooled area is about 10 m and has reached the edge of the model. The largest drop in temperature occurs within a radius of 1-3 m from the injection well (Figure 9-14).

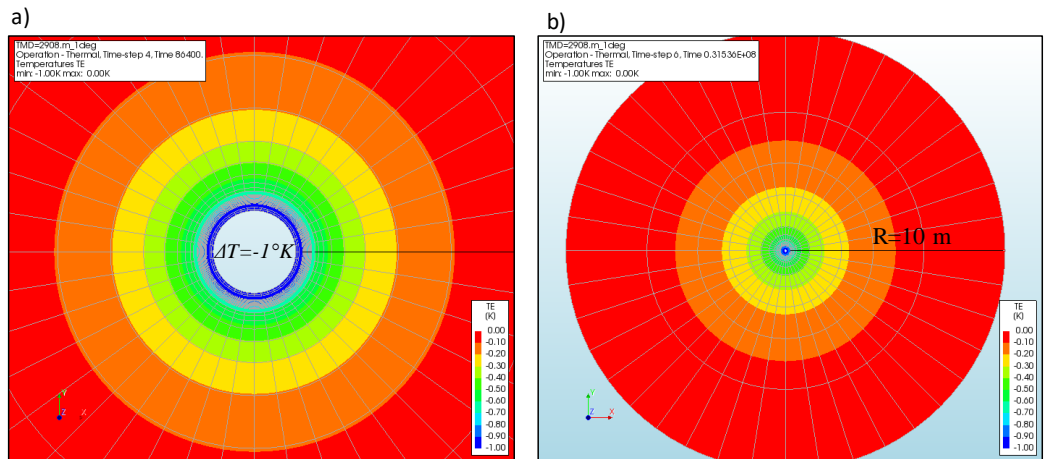


Figure 9-13: Contours of temperature change in the near-well area due to a casing temperature change of  $-1^{\circ}\text{K}$  (or  $-1^{\circ}\text{C}$ ) after (a) 1 day and (b) 1 year. The contour interval is  $0.1^{\circ}\text{K}$ .

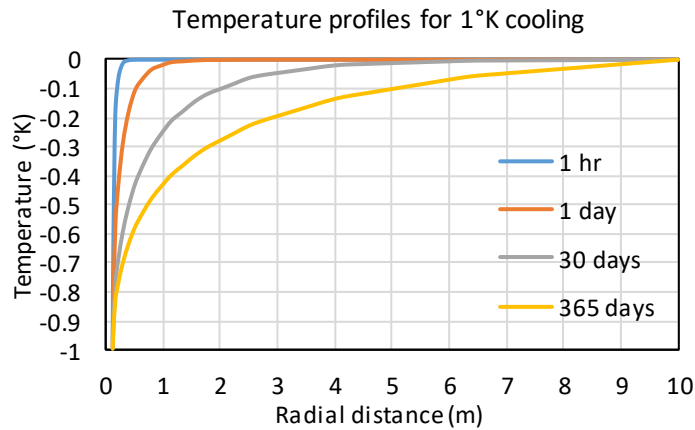


Figure 9-14: Profiles of temperature change as a function of radial distance from the well due to a casing temperature change of  $-1^{\circ}\text{K}$  (or  $-1^{\circ}\text{C}$ ) for different times.

Cooling induces thermal contraction which in turn induces thermo-mechanical tensile stresses in the radial direction. As expected, the magnitude of tensile stress increases with time, as the cooling front propagates deeper into the surrounding formation, and decreases with the radial distance from the well casing.

For a single casing well model, the magnitude of tensile stresses is larger at the casing-cement interface, which is closer to the inner side of the casing than at the cement-formation interface (blue bar and orange bar, respectively in Figure 9-15). The magnitudes of tensile stresses range between  $0.1$  and  $0.17 \text{ MPa}/1^{\circ}\text{C}$ . For a decrease of casing temperature by  $100^{\circ}\text{C}$ , tensile stresses at the interfaces will be thus 100 times higher and can reach 10 to 17 MPa. If the initial stress in cement is less than these values, de-bonding of the interfaces will occur.

In a double casing well model there are four well interfaces and the evolution of tensile stresses at the interfaces with time is more complex (Figure 9-16). Initially, just after the start of cooling, the magnitude of tensile stresses at the interfaces decreases with the distance from the inner casing (Figure 9-16, 1hr). This pattern was also observed in the single casing well model. However, for longer cooling

times, from 1 day onwards, the largest magnitude of tensile stresses occurs at a more distant interface between the 9 5/8" casing and cement (grey bar in Figure 9-16). These magnitudes of  $\sim 0.19$  MPa per  $1^\circ\text{C}$  cooling are larger than in the case of a single casing well model (grey bar for 365 days in Figure 9-16). Overall, the magnitude of thermal stresses is dependent on the values of elastic and thermal properties for the well materials (casing, cement and rock) and their interfaces.

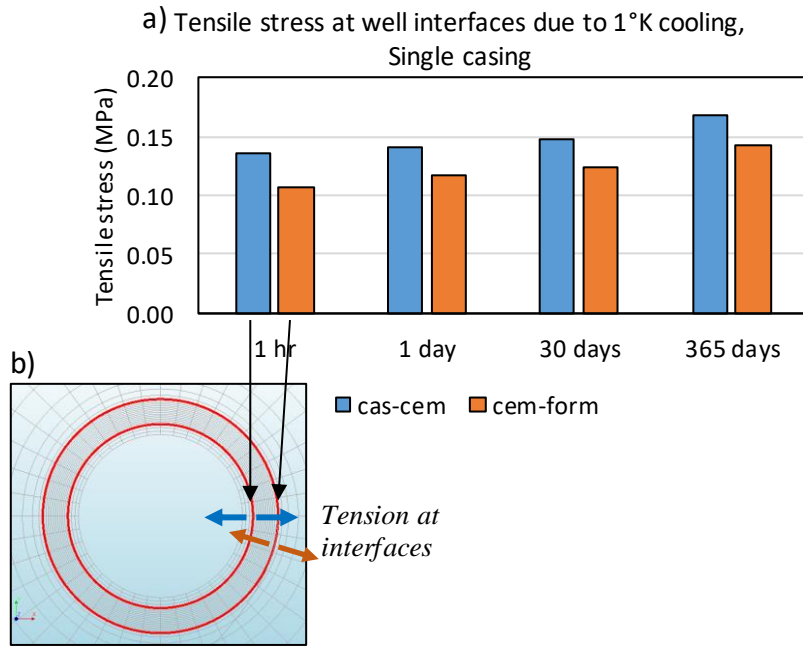


Figure 9-15: (a) Tensile stresses at the well interfaces due to a casing temperature change of  $-1^\circ\text{K}$  (or  $-1^\circ\text{C}$ ) after 1 hour, 1 day, 30 days and 365 days. (b) Sketch showing locations of the monitoring points at the two interfaces in a single casing well model.

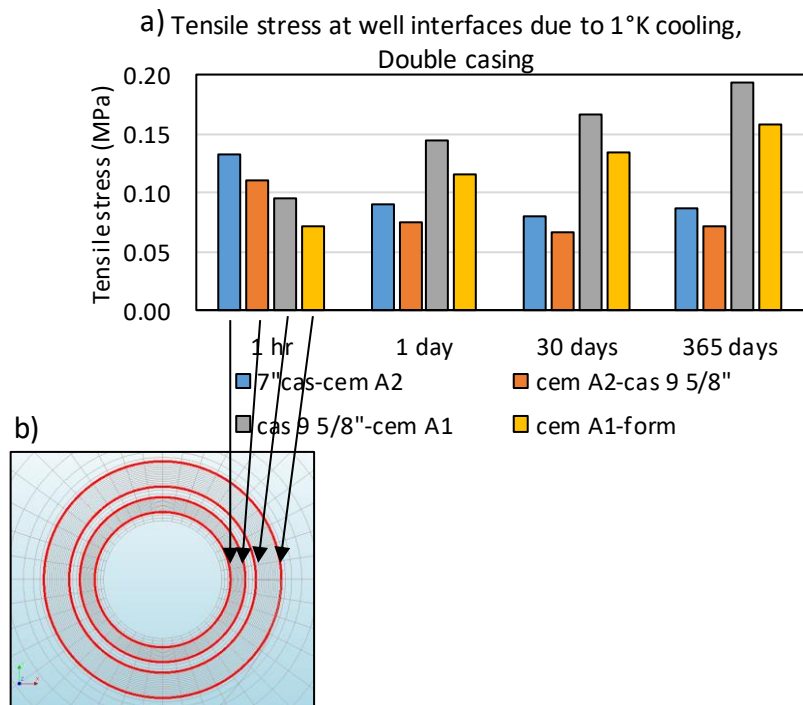


Figure 9-16: (a) Tensile stresses at the well interfaces due to a casing temperature change of  $-1^{\circ}\text{K}$  (or  $-1^{\circ}\text{C}$ ) after 1 hour, 1 day, 30 days and 365 days. (b) Sketch showing locations of the monitoring points at the four interfaces in a double casing well model.

### 9.3.3 *Implications of debonding on formation of potential leakage pathway*

Annular cement across the caprock in the P18-2 wells consists of sections with good cement and sections with poor/absent cement. Sections with poor cement are not considered to be sealing. Sections with good cement, which are in many cases a few tens of meters long, are most sensitive to debonding. For creation of a leakage pathway from reservoir to overburden, across the entire caprock thickness, de-bonding needs to occur along all sections with good cement, in order to connect sections with poor cement. Debonding of good cement is likely to occur at the level of caprock due to cooling by  $60\text{-}100^{\circ}\text{C}$  because of:

- large induced thermo-mechanical tensile stresses, which tend to cause de-bonding ( $\sim 10\text{-}20\text{ MPa}$ );
- very low tensile strength of the well cement interfaces (that counteracts the tensile stress) of  $0.1\text{-}3\text{ MPa}$  for a good cement bond and  $\sim 0\text{ MPa}$  for a poor cement bond;
- possibly low, largely uncertain magnitudes of the radial compressive stress in the annular cement (that counteracts the tensile stress).

The actual permeability and therefore also the flow rate is stress-dependent. The microannulus may be open and act as a conduit or closed and act as a seal. The permeability of circumferential microannulus created by debonding depends on the effective normal stress acting on that fracture ( $\sigma_n'$ ) and the fluid pressure inside the microannulus ( $p$ ); when  $p > \sigma_n'$ , the microannulus is open and acts as a conduit, when  $p < \sigma_n'$  the microannulus is closed and acts as a seal.

The effective normal stress  $\sigma_n'$  is either:

- The radial stress in annular cement ( $\sigma_n'\text{-cem}$ ) acting on the casing-cement interface. The  $\sigma_n'\text{-cem}$  is largely uncertain and could be low especially in the case of cement sheath located in-between two casings. The  $\sigma_n'\text{-cem}$  could possibly be lower than the hydrostatic stress ( $< 0.10\text{-}0.11\text{ bar/m}$ ). This implies that the hydrostatic fluid pressure inside the microannulus could keep the leakage path at the casing-cement interface open. Although a microannulus at the casing-cement interface can be kept open under a pressure lower than the hydrostatic pressure, the hydrostatic pressure conditions will still exist at the tip of a microannulus transecting the caprock. Keeping the  $\text{CO}_2$  pressure in the reservoir below the hydrostatic pressure conditions will prevent the  $\text{CO}_2$  from displacing the brine in the micro-annulus, as discussed in more detail in the next section.
- The radial stress in the rock formation ( $\sigma_n'\text{-rock}$ ) acting on the cement-rock interface. The  $\sigma_n'\text{-rock}$  could be:
  - (i) lower than the minimum in-situ horizontal stress  $Sh_{min}$  ( $0.17\text{-}0.18\text{ bar/m}$ ), but likely larger than the hydrostatic pressure ( $\sim 0.10\text{ to }0.11\text{ m/bar}$ ), if a plastic zone was formed in the (brittle) rock formation surrounding the wellbore;
  - (ii) close to the  $Sh_{min}$  ( $0.17\text{-}0.18\text{ bar/m}$ ) if the wellbore is surrounded by naturally sealing formations, which are either ductile (Aalburg Shales) or viscous (Röt salt, halitic parts). Potential advantage of naturally sealing formations is that they can improve annular sealing around non-cemented or poorly cemented parts of casing strings simply by moving or creeping onto the casing strings. Additional advantage is an increase in the compressive stresses in the near-well area, which could become equal to the far-field stresses in

these naturally sealing formations (0.17-0.18 bar/m in shales and 0.21 bar/m in halite). This implies that the hydrostatic fluid pressure inside the microannulus cannot keep the leakage path at the cement-formation interface open. The microannulus is closed and acts as a seal. Several shale layers and potentially salt layers in the caprock of the P18-2 reservoir have been identified as natural sealing formations. Local sealing of a microannulus could make the leakage path discontinuous and therefore prevent leakage.

Leakage risk and the effect of chemistry

#### 9.3.4 *Leakage risk and the effect of chemistry*

The well integrity simulations demonstrated that de-bonding of the well interfaces is likely to occur at the good cement sections of the P18-2 wells due to the mechanical stress related to cooling on the well materials and interfaces. In a worst case scenario, de-bonding could result in the formation of a leakage path (a microannulus), connecting the storage reservoir with the overburden, as discussed in the previous section.

Figure 9-17 gives a schematic representation of the pressure evolution in the reservoir and overburden in the various stages of the reservoir from initial (pre-production) to post-CO<sub>2</sub> injection. The initial reservoir conditions at the start of the gas production phase show the equilibrium of the water and gas pressure as developed during the geologic time of its existence. The hydrocarbon buoyancy pressure anywhere in the reservoir above the water-gas contact, equal to the average capillary pressure, is higher than the water pressure. Because of the capillary entry pressure of the caprock, which is higher than the prevailing buoyancy pressure if leakage does not occur, the gas remains in the reservoir.

In the gas production phase, both the water and the gas pressure in the reservoir decrease to low and sometimes very low levels. In case of a 'tank reservoir' where (strong) aquifer support is absent, the pressure remains low after production has ceased.

At the reservoir-caprock interface, a sharp water pressure transition exists because the water in the caprock is practically immobile on the time scale of hydrocarbon production and CO<sub>2</sub> injection. During CO<sub>2</sub> injection, both the water and gas pressure in the reservoir increase. As long as the gas pressure remains below the hydrostatic conditions at the base of the caprock, the gas will not be able to displace the water column in the overburden and leakage will not occur, even if a leakage path such as a microannulus exists. Over time, the reservoir conditions will move towards an equilibrium state due to water influx from the over- and underburden into the reservoir, implying re-pressurisation of the reservoir. In case of a tank reservoir, this influx is very small and it will take thousands of years before the gas pressure in the reservoir will become higher than the overlying hydrostatic column. This implies, that even if a leakage path such as a microannulus exists, a CO<sub>2</sub> leakage mechanism is absent.

In the unfortunate event that the gas pressure does increase to above the hydrostatic pressure, it is still uncertain whether CO<sub>2</sub> would migrate through a microannulus. Microannuli with small apertures will have a capillary entry pressure, similar to caprocks. The gas pressure has to be higher than the sum of the hydrostatic pressure at the base of the caprock and the entry pressure.

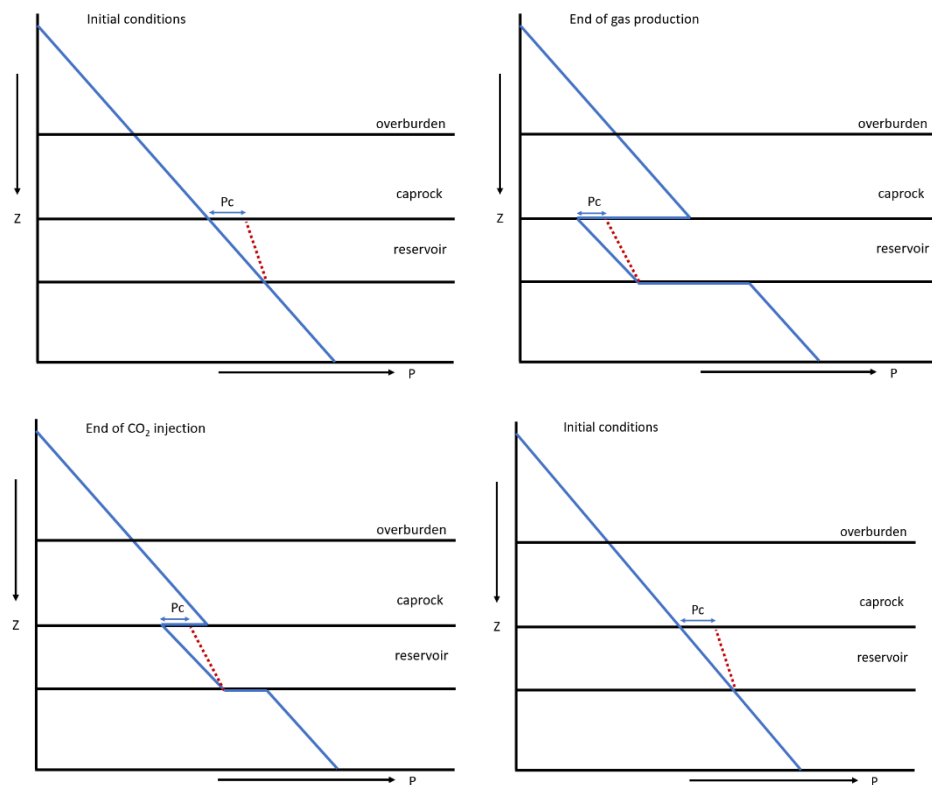


Figure 9-17: Pressure conditions in the various stages of the reservoir.

If CO<sub>2</sub> could displace the water column within the microannulus and starts migrating upwards, chemical interaction will take place with the cement. Assuming that the cement is of good quality, horizontal migration of CO<sub>2</sub> into the cement will take place by diffusion in dissolved state. Cement, which has a very high pH, is susceptible to interaction with carbonized water as cement minerals can quickly dissolve when the pH of the pore water decreases. The complex chemical interaction between cement minerals and carbonized brine is described in many publications (e.g., Kutcho et al., 2007; Rimmelé et al., 2008; Duguid et al., 2010). The most important reactions involve the dissolution of portlandite (CaOH<sub>2</sub>), the decalcification of Ca-silicate hydrate (CSH) and the precipitation of calcite (CaCO<sub>3</sub>) (Figure 9-18). Depending on the location of calcite deposition, complete pore clogging of the cement can occur, preventing further diffusion of carbonized brine and thereby further degradation of the cement. The upward flow of CO<sub>2</sub> through the microannulus adds another complicated component to the process, and has been described in Koenen and Wasch (2018). Instead of calcite precipitation in the pore spaces of cement, the calcite can accumulate within the microannulus and block the leakage path. The potential presence of sulfate in the caprock formation water can result in anhydrite precipitation in the microannulus, supporting the microannulus clogging by calcite (Koenen and Wasch, 2018). Whether clogging occurs depends on the upward flow rate of the CO<sub>2</sub> and the width of the microannulus. A low flow rate and/or small microannulus will allow calcite (and anhydrite) deposit to grow and block the leakage path. A high flow rate and/or large microannulus will not allow calcite growth, and instead, the leakage path will get worse in time due to cement mineral dissolution. This is illustrated in Figure 9-19. The worst case conditions for a microannulus of 100 micron and a CO<sub>2</sub> pressure 10 bar above hydrostatic conditions give a migration rate of CO<sub>2</sub> towards the overburden in the order of 10<sup>-6</sup>

kg/s, adding up to slightly more than 30 kg per year (Koenen and Wasch 2018). Compared to storage volumes in the order of megatonnes, this amount of leakage can be considered as negligible.

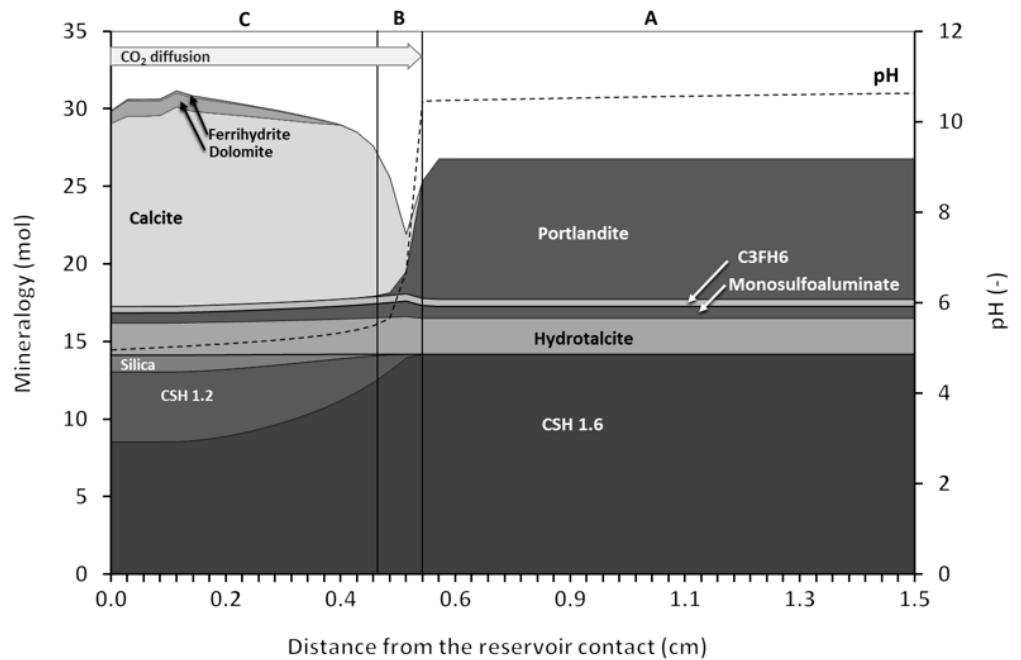


Figure 9-18: Simulated cement mineralogy with distance from the reservoir (or brine) contact after 300 days of inward diffusion of dissolved CO<sub>2</sub> and kinetic mineral reactions (PHREEQC software). Three zones develop: A: original cement, B: dissolution front, C: carbonated zone. The porosity of the cement decreases in the carbonated zone. From Koenen et al. (2014).

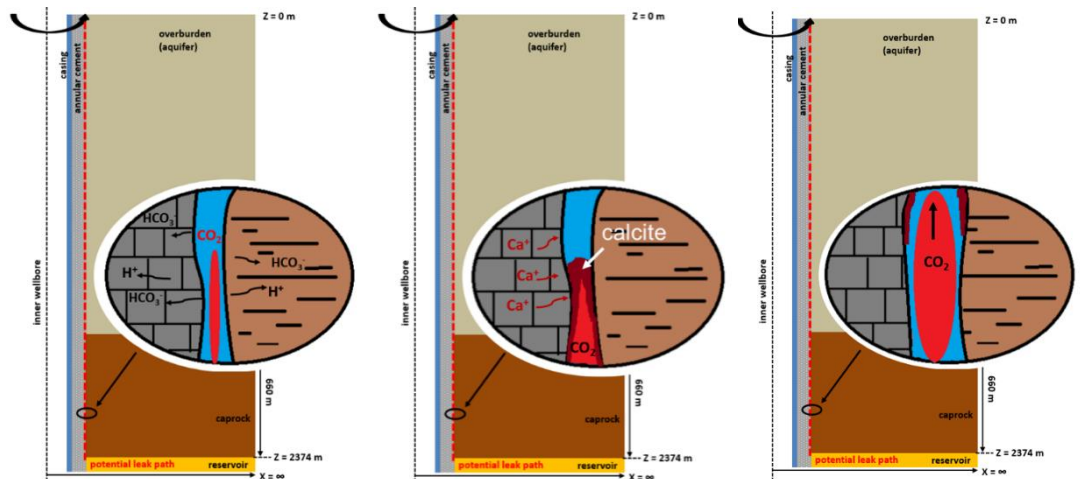


Figure 9-19: Schematic overview of CO<sub>2</sub> migration through a microannulus (red dotted line in between the annular cement and the surrounding rock). Left: initial state of microannulus and CO<sub>2</sub> migration. Middle: at low flow rate and/or small microannulus dissolved calcium migrates to the microannulus and is deposited as calcite, thereby blocking the leakage path. Right: at high flow rate and/or large microannulus the leakage path is enhanced as fast cement dissolution and CO<sub>2</sub> flow prevent calcite deposition. From Koenen & Wasch (2018).

### 9.3.5 Conclusions

Well dynamics simulations provided input on the temperature evolution along the wellbore with time. They showed that the CO<sub>2</sub> inside the injection well is 30 °C to 100 °C colder than the surrounding caprock formation, with largest temperature differences occurring in the initial phase of injection when the reservoir pressure is low (~20 bar) and the temperature of CO<sub>2</sub> at bottom hole is ~17 °C.

Based on performed simulations, debonding of well interfaces in P18-2 CO<sub>2</sub> injection wells is likely to occur due to cold fluid injection, thermal contraction and associated stress reduction in the near-well area. Debonding can, in principle, occur over lengths of tens of meters of caprock sections with good CBL. However, for migration of CO<sub>2</sub> with eventually leakage to occur, a continuous microannulus along the well cemented sections need to connect poorly cemented sections towards the overburden before we can speak of a leakage path. The presence of shale and potentially salt layers in the P18-2 caprock, identified as natural sealing formations could locally interrupt the leakage path. Even if a continuous leakage path would exist, it depends on the microannulus characteristics and pressure conditions whether upward CO<sub>2</sub> migration would actually take place. If the pressure conditions in the reservoir are high enough to overcome the capillary pressure within the microannulus, and migration does take place, the chemical interaction between CO<sub>2</sub> and cement can either prevent or enhance leakage towards aquifers overlying the caprock or towards the surface, also depending on the microannulus characteristics and pressure conditions. Keeping the CO<sub>2</sub> pressure in the reservoir below or at the hydrostatic pressure conditions will prevent the CO<sub>2</sub> from displacing the brine in the microannulus. In that case adequate monitoring during injection operations is required. The decommissioning method and procedures should result in well plugging from formation-to-formation (pancake plug or similar) in case microannulus formation is likely and poorly bonded annulus cement is not accepted as a leakage barrier. Based on performed simulations, debonding of well interfaces in P18-2 CO<sub>2</sub> injection wells is likely to occur due to cold fluid injection, thermal contraction and associated stress reduction in the near-well area. Debonding can, in principle, occur over lengths of tens of meters of caprock sections with good CBL. However, for migration of CO<sub>2</sub> with eventually leakage to occur, a continuous microannulus along the well cemented sections need to connect poorly cemented sections towards the overburden before we can speak of a leakage path. The presence of shale and potentially salt layers in the P18-2 caprock, identified as natural sealing formations could locally interrupt the leakage path. Even if a continuous leakage path would exist, it depends on the microannulus characteristics and pressure conditions whether upward CO<sub>2</sub> migration would actually take place. If the pressure conditions in the reservoir are high enough to overcome the capillary pressure within the microannulus, and migration does take place, the chemical interaction between CO<sub>2</sub> and cement can either prevent or enhance leakage towards aquifers overlying the caprock or towards the surface, also depending on the microannulus characteristics and pressure conditions. Keeping the CO<sub>2</sub> pressure in the reservoir below or at the hydrostatic pressure conditions will prevent the CO<sub>2</sub> from displacing the brine in the microannulus. In that case adequate monitoring during injection operations is required. The decommissioning method and procedures should result in well plugging from formation-to-formation (pancake plug or similar) in case microannulus formation is likely and poorly bonded annulus cement is not accepted as a leakage barrier.

Based on performed simulations, debonding of well interfaces in P18-2 CO<sub>2</sub> injection wells is likely to occur due to cold fluid injection, thermal contraction and

associated stress reduction in the near-well area. Debonding can, in principle, occur over lengths of tens of meters of caprock sections with good CBL. However, for migration of CO<sub>2</sub> with eventually leakage to occur, a continuous microannulus along the well cemented sections need to connect poorly cemented sections towards the overburden before we can speak of a leakage path. The presence of shale and potentially salt layers in the P18-2 caprock, identified as natural sealing formations could locally interrupt the leakage path. Even if a continuous leakage path would exist, it depends on the microannulus characteristics and pressure conditions whether upward CO<sub>2</sub> migration would actually take place. If the pressure conditions in the reservoir are high enough to overcome the capillary pressure within the microannulus, and migration does take place, the chemical interaction between CO<sub>2</sub> and cement can either prevent or enhance leakage towards aquifers overlying the caprock or towards the surface, also depending on the microannulus characteristics and pressure conditions. Keeping the CO<sub>2</sub> pressure in the reservoir below or at the hydrostatic pressure conditions will prevent the CO<sub>2</sub> from displacing the brine in the microannulus. In that case adequate monitoring during injection operations is required. The decommissioning method and procedures should result in well plugging from formation-to-formation (pancake plug or similar) in case microannulus formation is likely and poorly bonded annulus cement is not accepted as a leakage barrier.

Overall, the likelihood of CO<sub>2</sub> leakage through microannuli is small. De-bonding of cement-casing and cement-rock interface is very likely, but a leakage path requires a continuous microannulus from reservoir to overburden which is less likely. The presence of that natural sealing formations in the caprock could locally seal a microannulus, disconnecting the reservoir from the overburden. If a leakage pathway does exist, the CO<sub>2</sub> pressure in the reservoir should be high enough to displace the water in the microannulus. For a pressure below or at hydrostatic conditions, as is the plan for CO<sub>2</sub> storage in P18-2, this would not happen. In case the CO<sub>2</sub> pressure would be high enough to migrate through the microannulus, chemical interaction between the CO<sub>2</sub> and the cement would stimulate self-sealing of the leakage path by calcite precipitation. In a worst case scenario that self-sealing would not occur, leakage rates would be very low; e.g. <0.00001% of the total amount of CO<sub>2</sub> injected per year in the P18-2 storage plan.

## 9.4 Well abandonment

### 9.4.1 *Abandonment prior to start of injection*

Abandoning non-essential and non-injection wells before the start of CO<sub>2</sub> injection is considered a good practice with known reservoir conditions. This would reduce uncertainties with respect to well control during the well interventions for abandonment, compared to intervention after or during CO<sub>2</sub> injection. There is a strong case to decommission off-platform wells early, P18-02 for example, and sidetracks in platform wells that need isolating before injection begins. However, early decommissioning of platform wells removes them as candidates for monitoring activities.

The wells P18-02 and P18-2A6-ST need to be reworked or abandoned in accordance with P&A standards applicable for CO<sub>2</sub> storage wells (these standards are currently under development).

- The P18-02 well is suspended with P&A plugs, the mud line suspension for tie back strings is still installed. Some deficiencies have been identified for the P&A plugs; these should be managed in accordance with applicable P&A standards.
- For the P18-2A6-ST well some deficiencies have been identified at the side track window. From a reservoir storage aspect the side track should be P&A'd in accordance with applicable P&A standards and the P18-2A6 wellbore integrity has to be restored.

#### 9.4.2 *Abandonment after end of injection*

After completing the CO<sub>2</sub> injection through the P18-2 injection wells, these wells need to be abandoned in a way that conforms to good practice and meets required standards for a CO<sub>2</sub> storage site. After abandonment, the wells should ensure permanent and safe containment of the CO<sub>2</sub> in the reservoir.

Currently cement is the material of choice for annular seals and decommissioning of oil and gas wells. The abandonment plug has to extend across the full cross section of the well (“rock-to-rock”), whilst covering all annuli. If the cement behind the casing(s) is good, this can be achieved by placing a cement plug in the casing. If the quality of the annular seal is not sufficient or cannot be confirmed, pancake plugs have to be installed. This is achieved by removing the casing(s) and potentially cement and thereby creating a so called ‘window’. These are standard O&G practices, clearly described in the decommissioning standards.

Reaction of CO<sub>2</sub> with wellbore cement is a slow process if good construction practices and proper cement materials were used (IEAGHG, 2018). Degradation rates have been found to be proportional to temperature, pressure and the square root of time (Shell, 2015). According to literature the degradation of Portland cements could be up to about 12 m in 10.000 years. It is also reported that the permeability that can be created by the degradation is such that it still is within API criteria for cement (EPA, 2012).

Previous work (Vandeweyer et al., 2011) recommended placing pancake-type abandonment plugs. This approach to the P&A of CO<sub>2</sub> wells was also proposed in the permit application for the P18-4 reservoir. Whether pancake-type plugs will be the method of choice for abandonment of the P18-2 injection wells, and which materials to be used for the plug, depends on future developments until time of abandonment.

## 9.5 **Conclusions**

### *Well integrity*

The wells relevant in the context of CO<sub>2</sub> injection into the P18-2 field have been evaluated regarding their current status and integrity risks. All wells reviewed have the potential to be used safely as CO<sub>2</sub> injectors. Appropriate mitigation measures have been proposed to make them fit for storage operations.

### *Effects of injecting cold CO<sub>2</sub> on well integrity*

It is highly likely that de-bonding of cement interfaces will take place upon cold CO<sub>2</sub> injection, creating microannuli. In the unlikely case that the microannulus forms a continuous leakage path from reservoir to overburden, the characteristics of the

microannuli and pressure conditions determine whether upward CO<sub>2</sub> migration would actually take place. Keeping the CO<sub>2</sub> pressure in the reservoir below or at hydrostatic pressure conditions will prevent the CO<sub>2</sub> from migrating through the microannulus. This justifies the choice of keeping the reservoir pressure below or at hydrostatic conditions (Section 1.1). However, if for some reason the reservoir pressure would be high enough to displace the water column in the microannulus, the chemical interaction between CO<sub>2</sub> and cement can either prevent or enhance leakage, also depending on the microannulus characteristics and pressure conditions. For worst-case conditions, if CO<sub>2</sub> would migrate from the reservoir to the overburden through a microannulus, leakage rates would still be very low; i.e. <0.00001% on an annual basis. Overall, the likelihood and effect of leakage through microannuli is very low and can be considered insignificant.

#### *Well abandonment*

Appropriate methods should be used for the abandonment of the wells. Given the likelihood of microannuli forming during the injection of cold CO<sub>2</sub>, abandonment methods that remove these potential leakage paths would be preferred. As an example, full-bore pancake like plugs would provide formation-to-formation closure of the injection wells. However the choice of employing these techniques should be weighed up against 1) the guarantee that pressure in the reservoir stays below the surrounding pressure, preventing flow out of the reservoir through microannuli 2) even if flow occurred through microannuli the chemical reaction between CO<sub>2</sub> and cement would cause a permanent flow barrier 3) the expansion and elasticity of layers above the reservoir, including the caprock will eventually close around the wellbores squeezing shut any microannuli and guaranteeing permanent storage of the CO<sub>2</sub>. The use of pancake plugs is unlikely to be more successful than any of these effects individually.

## 10 P18-2 storage site and storage complex

### 10.1 Introduction

The assessment of leakage risks for CO<sub>2</sub> storage in the P18-2 field relies on a proper definition of the storage site and storage complex. In this Section we discuss these, based on definitions in the EU Storage Directive and insights from the detailed reservoir, fault, caprock and well evaluations in Sections 6 to 9.

### 10.2 Definitions in the Netherlands Mining Law and the EU Storage Directive

The EU Storage Directive (EU, 2009) introduced the concept of the storage complex in defining rules for environmentally sound and safe geological storage of CO<sub>2</sub>. This is to be accomplished by the characterization and assessment of the storage complex.

The following definition is given of the storage complex, *op. cit.*:

‘storage complex’ means the storage site and surrounding geological domain which can have an effect on overall storage integrity and security; that is, secondary containment formation

According to the Netherlands Mining Law (Mijnbouwwet, 10 April 2019):

“CO<sub>2</sub>-opslagcomplex: opslagvoorkomen voor CO<sub>2</sub> en de omringende geologische gebieden die een weerslag kunnen hebben op de algehele integriteit van de opslag en de veiligheid ervan”.

The definition of “storage complex” in the Netherlands Mining Law does not explicitly refer to “secondary containment formation” like in the EU Storage Directive. For the definition of “storage site” the Netherlands Mining Law uses the term “opslagvoorkomen van CO<sub>2</sub>”. Although it seems that this term can be linked to “storage site” in the EU Directive it is not clear if this will include “the associated surface and injection facilities” as well, like is defined in the EU Storage Directive (see below). For this report we assume that these facilities are part of the storage site. “Opslagvoorkomen” is: een voorkomen dat gebruikt wordt voor opslag”

The storage site according to the EU Directive is defined as, *op. cit.*:

‘storage site’ means a defined volume area within a geological formation used for the geological storage of CO<sub>2</sub> and associated surface and injection facilities  
Leakage then means “*any release of CO<sub>2</sub> from the storage complex*” and migration stands for “*the movement of CO<sub>2</sub> within the storage complex*” according to the EU Directive.

The Storage Directive (EU, 2009: Article 4, para 4) also says:

4. A geological formation shall only be selected as a storage site, if under the proposed conditions of use there is no significant risk of leakage, and if no significant environmental or health risks exist..

We consider the hydraulically connected pore space bordered by flow barriers together representing a physical trap, and we predict by dynamic modelling the dispersion of CO<sub>2</sub> inside the physical trap. Our predictions will be confirmed by operational monitoring (EU, 2009: Article 13).

This implies that monitoring activity should be focused particularly on providing the evidence for the effectiveness of the geological and engineering barriers that prevent significant risk of leakage (migration out of the storage complex).

Note that Guidance document no 2 (EU, 2011) suggests to allow for changes in the specific boundaries of the storage complex during the storage permit review and updating process.

CO<sub>2</sub> movement out of the storage site but remaining in the storage complex is called migration (in the Storage Directive). Movement of CO<sub>2</sub> out of the storage complex is called leakage under the Storage Directive, and if the CO<sub>2</sub> then reaches the atmosphere it is called emission under the implementing regulation of the ETS Directive (ETS directive, 2009; EU, 2018) and emission allowances need to be returned by the storage permit holder to the state. Leaks cannot be measured, they can only be estimated. From the monitoring plan and plan for corrective measures it needs to be defined how to recognise such movement of CO<sub>2</sub> and what actions or corrective measures to take.

### 10.3 Definition of the storage site

The storage site is what contains the CO<sub>2</sub> – the reservoir – and the injecting or not yet decommissioned wells and associated surface installations (wellheads) and injection facilities (tubing in wells). More specifically, the P18-2 storage site comprises the following:

- P18-2 Triassic reservoir rocks of the Volpriehausen Sandstone, Lower and Upper Detfurth Sandstones and the Hardeggen Formation. The lower 3 units are vertically hydraulically disconnected by the presence of low permeable zones in between (baffles). Strongly restricted flow is possible between the Upper Detfurth sandstone and the Hardeggen Formation (see Figure 17-14 and Figure 17-15)The reservoir consists of 4 partly hydraulically connected main compartments and is bounded by faults on all sides except for the northern boundary, which is downdip of the original the GWC. Near faults F14 and Fault1, the northern boundary is in a spill point just to the north of the reservoir (see Figure 10-1; more details are in Section 12.1).
- Wells penetrating the storage complex up to the wellheads;
- Related wellheads measurement equipment and christmas trees.

### 10.4 Definition of the storage complex

In addition to the components of the storage site mentioned in 10.3, the storage complex also includes the formations that seal off CO<sub>2</sub> in the reservoir and any surrounding formation that could contain CO<sub>2</sub>.

The Porthos P18-2 storage complex is proposed to include the following spatial compartments in addition to the storage site components:

- Massive caprock on top of the reservoir consisting of impermeable Upper Germanic Triassic Group and Altena Group with a thickness of 450 to 750 m;
- The formations below the storage reservoir consisting of the Triassic Rogenstein and Main Claystone Members.

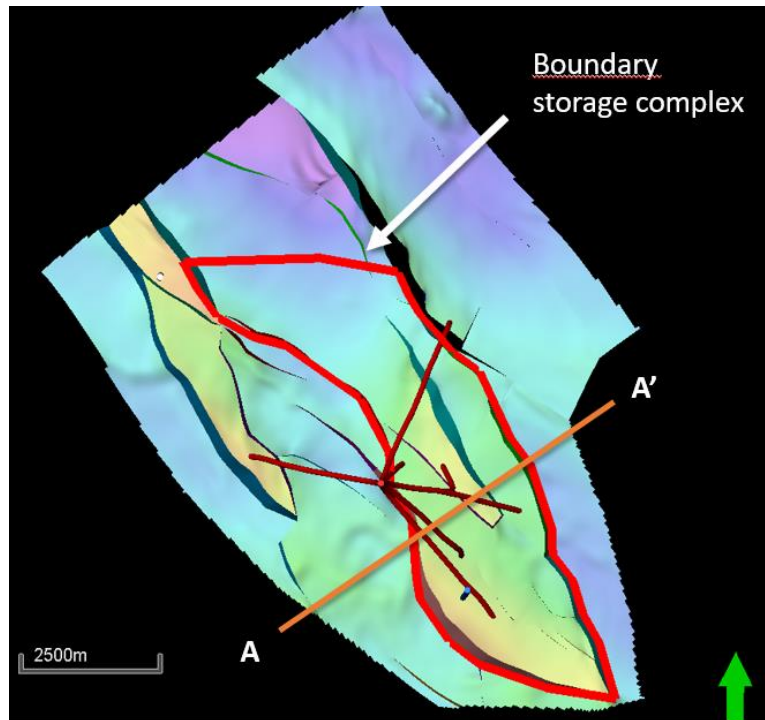


Figure 10-1 Depth map of the top of the reservoir with the proposed boundary of the storage complex at top reservoir level (red line) delimited by the bounding faults and an open boundary downdip of the GWC to the north; line segment A-A' represents the location of the geological cross section shown in Figure 10-2.

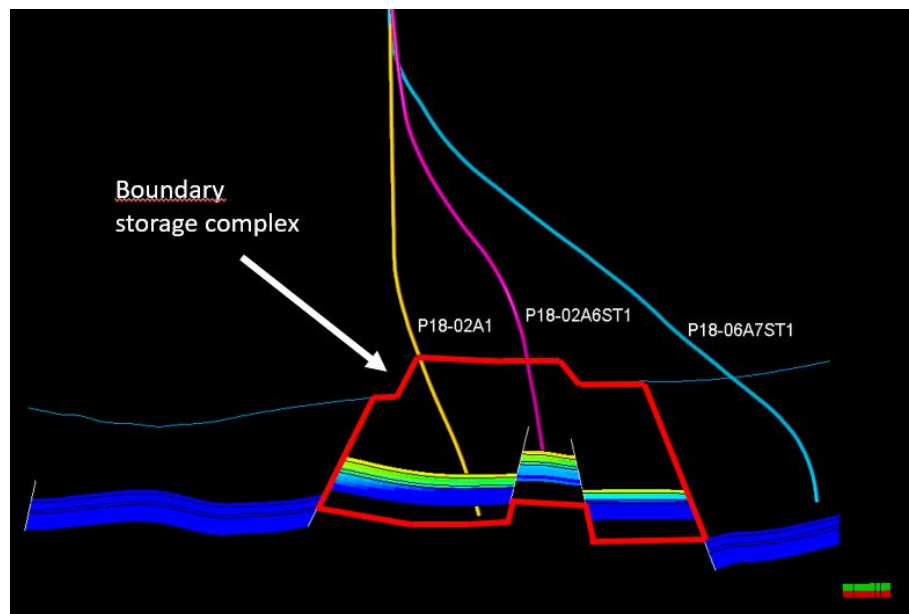


Figure 10-2 Geological cross section of the reservoir and the overburden with indication of the vertical extension of the storage complex (in red); location of cross section is shown in Figure 10-1. Blue line is top caprock (=Base Schieland Gp).

## 10.5 Differences with the P18-4 storage complex definition

In contrast to P18-2, the P18-4 storage complex includes the Lower Cretaceous aquifers and seals as a secondary containment system. The proposal for P18-2 relies on the containment by the massive seal of Triassic and Jurassic formations, which has a very low likelihood of CO<sub>2</sub> leaking out of this caprock sequence and thus complies with the Storage Directive requirement that no significant leakage risk exists or will develop. In addition, the storage reservoir pressure will be kept at or below the initial pressure. For these reasons it is not necessary to add an additional spatial compartment on top of the Triassic and Jurassic caprock sequence to warrant CO<sub>2</sub> containment.

Over a small section reservoir rocks of Compartment 2-IV in P18-2 and the adjacent P18-6 reservoir are juxtaposed. The huge pressure difference between the P18-6 reservoir (378 bar) and the P18-2 reservoir (100 bar) after 9 years of production from the P18-2 reservoir indicates that these reservoirs behave as two separate hydraulic units. Furthermore, Compartment 2-IV very likely is a separate hydraulic unit; CO<sub>2</sub> injected in Compartment 2-I will thus not reach Compartment 2-IV and the adjacent P18-6 reservoir. For these reasons it is concluded that the P18-6 reservoir can be excluded from the P18-2 storage complex (see also Section 6.3.5). In the case of the juxtaposed P18-4 and P15-9 reservoirs this evidence was not available as they were produced simultaneously and a large differential pressure was not built up. For that reason the P15-9 reservoir was included in the P18-4 storage complex.

In contrast to P18-4, P18-2 has two more potential structural spill points, one to the North and one to the Southwest of the P18-2 reservoir. Their acting as true spill points depends among other things on the degree of filling of the reservoir and the lateral hydraulic connectivity near the potential spill zones.

Reservoir simulations with highly exaggerated reservoir pressures up to 450 bar indicate that the CO<sub>2</sub> does not migrate beyond the northern limit of the storage site (see also Section 6.3.4 for more background information).

In a small section to the NW of Compartment I across Fault F14, low permeable Volpriehausen Sands (< 1 mD) are juxtaposed to the Hardeggen Formation. The low permeability makes it highly unlikely that significant amounts of CO<sub>2</sub> migrate across the fault (see also Section 12.1).

## 10.6 Barriers

### 10.6.1 Barriers in the storage complex

The storage complex includes the principle barriers for the permanently stored CO<sub>2</sub> in the P18-2 depleted gas reservoir.

The *geological barrier system* consists of:

- Massive caprock, consisting of Triassic and Jurassic shales, directly located above the reservoir rocks (see also Section 4.3);
- Sealing, reservoir-bounding faults;
- Structural relief trapping of CO<sub>2</sub>, e.g. at the northern boundary of the reservoir.

The *well engineering barrier system* consists of the two barriers, as described in Section 9.

#### 10.6.2 *Evaluating barrier integrity*

The various barriers have been evaluated in detail to further qualify the P18-2 reservoir for permanent CO<sub>2</sub> storage:

- The initial condition of the caprock and the faults is characterized in Section 4 and Appendix B (Section 17).
- The risk of lateral migration (spilling) from the reservoir compartment to the North was assessed in more detail in Section 6.
- The stability of the fault zone under the influence of chemical, mechanical and thermal processes were investigated (see Section 7).
- The possible effects of fracturing and chemical degradation on the integrity of the caprock have been evaluated with semi-analytic thermomechanical modelling and following a literature study, respectively (see Section 8).
- The integrity of all wells penetrating the reservoir have been evaluated and recommendations for qualifying the well for CO<sub>2</sub> storage have been defined (see Section 9).

The results of these investigations have been used to characterize the risks for loss of containment and to propose measures to lower the risk level if necessary (see Section 12). Section 13 describes the monitoring plan, which enables the early identification and intervention of potential issues for CO<sub>2</sub> containment.

# 11 Migration paths

## 11.1 Introduction

The EU storage directive requires an analysis of potential leakage pathways (EU, 2009, Annex I). The results presented in sections 6 through 9 support the conclusion that leakage of CO<sub>2</sub> (i.e., CO<sub>2</sub> moving out of the storage complex) along wells, faults or through the caprock is highly unlikely, if the injection process is conducted within safe limits (see Sections 12 and 14, below). Overfilling the reservoir (i.e., spilling of the CO<sub>2</sub> across a spill point) does not occur, as long as the average reservoir pressure is kept below initial gas pressure.

Nevertheless, with this starting point, an analysis was made of pathways that CO<sub>2</sub> would take in case of a hypothetical leak out of the reservoir, along one of the wells, or through the caprock. The analysis includes the identification of possible secondary containment at the level of the reservoir formations, or in the overburden.

A static overburden model was assembled, based on both 2D and 3D seismic surveys and well information. On the basis of the overburden model and the selected migration pathways, an evaluation of possible migration scenarios was developed.

The conclusions are that in case of overfilling of the reservoir, migration through the Buntsandstein (reservoir formations level), the CO<sub>2</sub> remains trapped and finally will migrate towards the adjacent gas reservoirs. In case of migration of CO<sub>2</sub> into the aquifers of the overburden, caused by a shortcut along the wellbore, it will remain trapped within these aquifers. However, migration of CO<sub>2</sub> along faults in the overburden (above the Altena Group) to a shallower aquifer level cannot to be excluded.

Overall, given the results presented in the previous sections, the conclusion from the analysis presented in this section is that the only potential pathway to the surface of CO<sub>2</sub> stored in the P18-2 field is via leaking wells, leaking directly into the atmosphere and not indirectly via pathways originating in deeper parts of the overburden.

## 11.2 Available data and workflow

A geological model was constructed with Petrel modelling software (Schlumberger). The model comprises an area with a 14 km minimum radius surrounding the P18 gas field.

In vertical direction the model spans the total overburden of the reservoir.

The workflow for building the model is described in *CATO-2-WP3.1-Geological report P18 (December 2010)*: seismic interpretation of the overburden was performed, and subsequently the model was built on the basis of a fault model with a grid cell size of 250m x 250m. The model was converted from time to depth, and tied to the wells.

Figure 11-1 shows the location of the P18 fields, with neighbouring fields and wells.

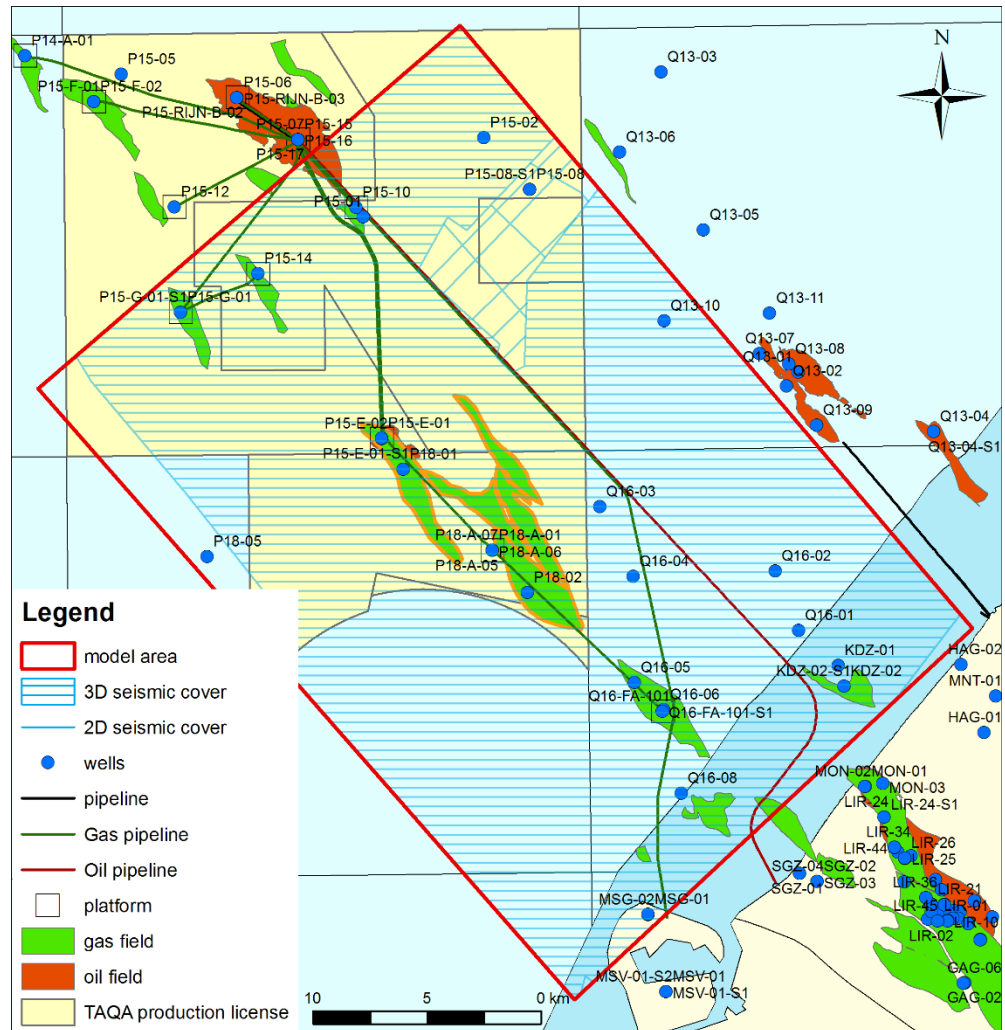


Figure 11-1: Location map of P18 model area. Target P18 gas fields are indicated with an orange boundary.

## 11.3 Geological model of the overburden

### 11.3.1 Overburden

The primary seal, made up by the Upper Germanic Trias and Altona Group is successively overlain by (see also Figure 11-2):

- The Schieland Group, which consists of shales and (stacked) channel sands of the Nieuwerkerk Fm. (Delft sandstone equivalent). The lateral continuity of the individual sandbodies (thickness 2-5m) is probably very limited.
- Lower Cretaceous Rijnland Group, which consist of marine sandstones, shales and marls. At the base of the Rijnland Group, the Rijn / Rijswijk Fm. is present. This sandstone is widely distributed in the P18 area. It is also known for its oil (P15) and gas (onshore) accumulations within the West Netherlands Basin. The sandstones are interpreted as transgressive sheet sands, with good lateral continuity. In the upper part of the Rijnland succession, the Holland Greensand Member is present. It consists of argillaceous sands and silts. The distribution is limited to the southern margin of the West Netherlands Basin. Although the Holland Greensand has good lateral continuity, permeability is general low.

- Upper Cretaceous Chalk Group, which consist at the base of the formation of sands and marls and a thick layer (900 m) of limestones (Chalk). The distribution of the basal Texel Greensand is limited to the southern basin margin.
- The North Sea Group, which consists of siliciclastic sediments. Two major aquifers can be distinguished; the Dongen sand, a basal transgressive sandstone, and the marine Brussels Sand Member.

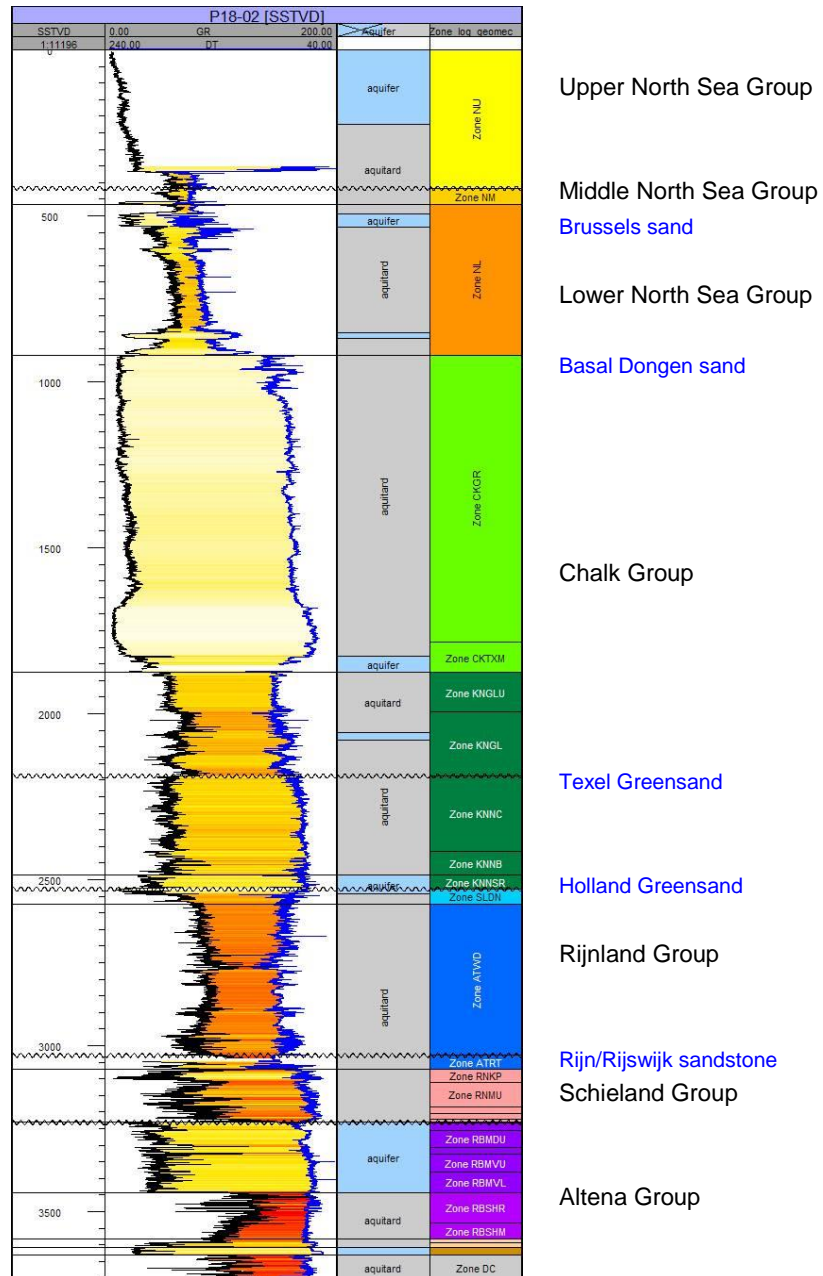


Figure 11-2: Composite well log (GR, DT) of P18-02 with main stratigraphic units and aquifer intervals

### 11.3.2 Faults

Faults present at reservoir level (Buntsandstein) in general continue till the Schieland group (white line) or base Rijnland Group (dark green line in Figure 11-3). Late Cretaceous inversion caused faulting of the sediments above the Base

Cretaceous Unconformity (base Rijnland) These faults (dashed lines Figure 11-3) have limited displacement, but continue to the Upper North Sea Group.

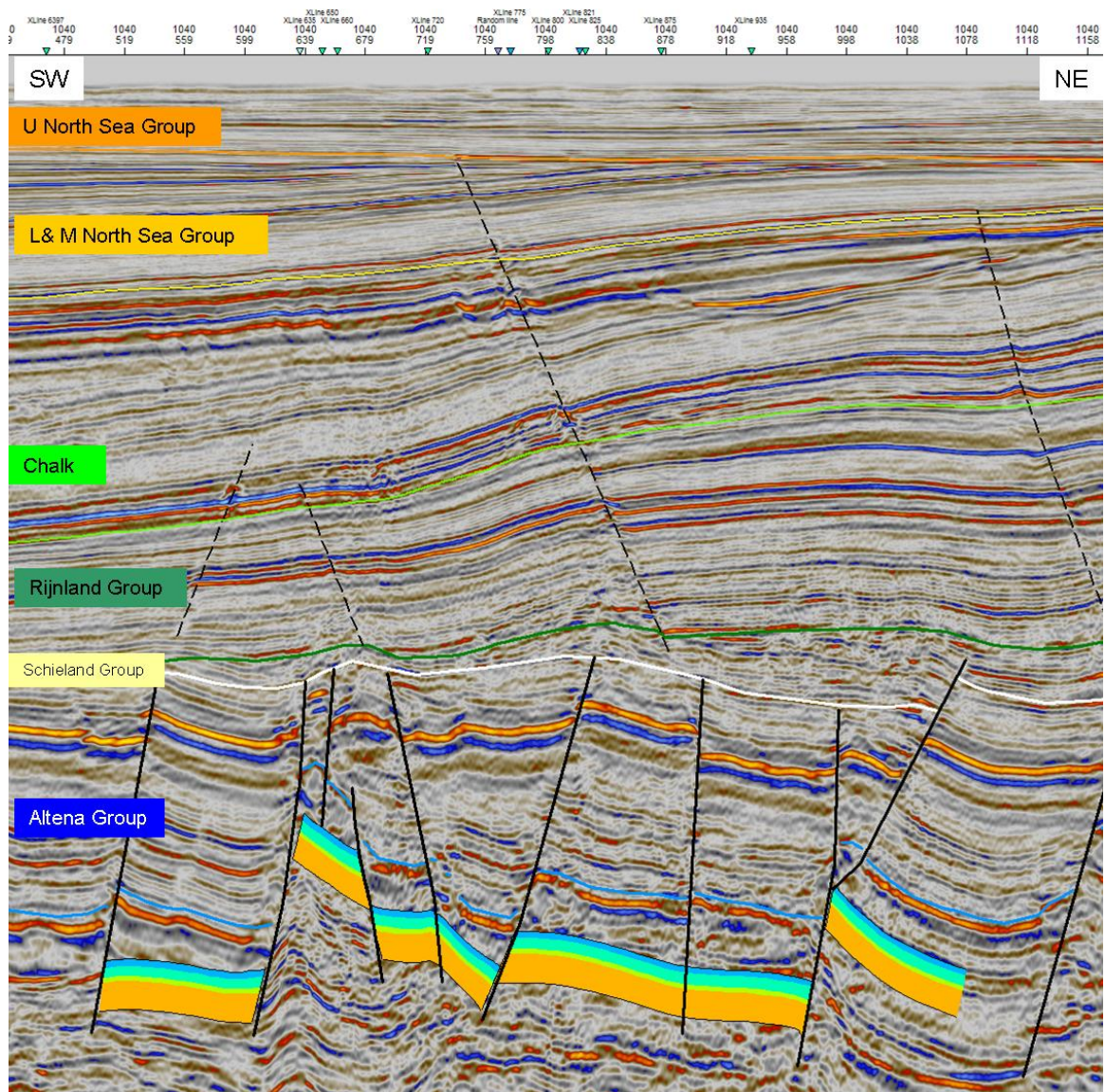


Figure 11-3: Seismic cross-section (inline 1040 of P15P18 seismic cube) through the P18 field, displaying the reservoir interval (coloured layering), the main bounding faults to the reservoirs (bold lines), the main stratigraphic units in the overburden and the faults in the overburden (dashed)

## 11.4 Migration scenarios

For the qualitative analysis three migration scenarios were considered.

- Spilling out of the gas reservoir, due to overfilling. This leads to migration within the Bundsandstein formations beyond the boundaries of the storage complex (hence, this would be classified as leakage). See Section 11.6.1.
- Leakage through the caprock due to fracture formation. This leads to CO<sub>2</sub> entering the Rijn/Rijswijk Sandstone (Section 11.6.2).
- A wellbore shortcut, opening pathways for CO<sub>2</sub> into formations overlying the caprock.

- Migration into Rijn/Rijswijk Sandstone (Section 11.6.2);
- Migration into Holland Greensand (Section 11.6.311.6.3);
- Migration into Texel Greensand (Section 11.6.4);
- Migration into Dongen & Brussel Sandstone (Section 11.6.5).

The sections below investigate the consequences of these scenarios occurring, in spite of their low to very low probability, given the results presented in Sections 6 (spilling out of the reservoir), 8 (caprock integrity) and 9 (well integrity).

## 11.5 Methods

Possible CO<sub>2</sub> migrations pathways were analyzed using the rapid trapping assessment tool PetroCharge Express of IES. With this tool a rapid analysis of the migration pathways based on the layer geometry is performed. The layer geometry was provided by the exported horizons from Petrel (regional scale model). The program uses the input top layer as bounding elements assuming these layers to be impermeable. Although in reality the layers are not completely impermeable the goal is to create a concept model from which migration routes within the layer can be deducted.

It should be noted that PetroCharge only looks at the geometry and does not describe various other aspects of flow. It was therefore decided to “inject” large amounts of CO<sub>2</sub> in the considered leakage scenarios and to focus on the migration paths and final accumulation structures.

## 11.6 Results

### 11.6.1 Migration scenario: Buntsandstein

In case of “overfilling” the gas reservoir with CO<sub>2</sub> (see also the comments in the introduction to this section) it might be possible that the CO<sub>2</sub> will pass by the original closure defined by the initial gas water contact (GWC).

- Overfilling the P18-2 main compartment could lead to migration towards the Q16-4 structure (Figure 11-4, arrow 1) and the P16-FA field (Figure 11-4, arrow 3)
- Overfilling the P18-4 compartment in combination with migration along faults could lead to migration towards the P15-E and P15-14 field (Figure 11-4, arrow 2).

It must be mentioned that the structure drilled by the (dry) exploration wells Q16-04 and Q16-03, only minor amounts of gas were encountered. If the containment were to fail by a mechanism describes above, the most probable failure would be of an absence of sideseal in combination with reservoir juxtaposition with Jurassic sandstones from for instance the Nieuwerkerk Formation.

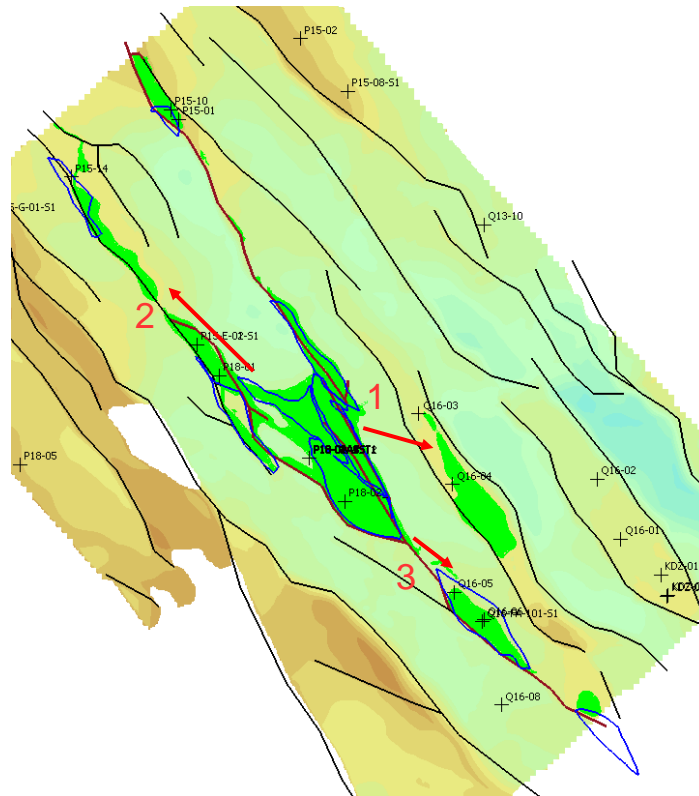


Figure 11-4 Structure map of Top Buntsandstein. Black lines indicate faults. Also shown are boundaries of gas accumulations and location of wells.

#### 11.6.2 Migration scenario: Rijn/Rijswijk sandstone

In case of fault reactivation or shortcut via a wellbore, CO<sub>2</sub> can hypothetically migrate into the Rijn/Rijswijk sandstone aquifer.

- CO<sub>2</sub> leaking along wells P18-02-A-01, P18-02-A-06 or P18-02-A-06-S1 will migrate towards Q16-03 & Q16-04 structure (Figure 11-5, arrow 1).
- Spill originating from wells P18-02, P18-02-A-03, P18-02-A-05 will migrate towards Q16-FA structure (Figure 11-5, arrow 2).

#### 11.6.3 Migration scenario: Holland Greensand

In case of a shortcut via a wellbore, CO<sub>2</sub> can hypothetically also migrate into the Holland Greensand aquifer

- Spill originating from wells P18-02-A-01, P18-02-A-03, P18-02-A-06, P18-02-A-06-S1, P18-06-A-07 will migrate towards Q16-03, Q16-04 structure (Figure 11-6, arrow 1)
- Spill originating from wells P18-02, P18-02-A-05 will migrate towards Q16-FA structure (Figure 11-6, arrow 2)
- Spill originating from P18-A-02 well will migrate towards P15-9 (E) structure (Figure 11-6, arrow 3)



- Spill from the P18-02 well will migrate towards Q16-FA structure and finally Q16-01 (Figure 11-7, arrow 2).

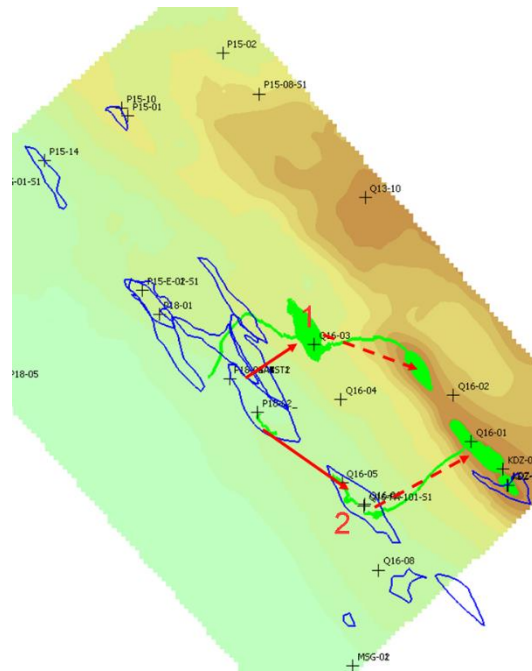


Figure 11-7: Structure map base Chalk Group.

#### 11.6.5 Migration scenario: Dongen sand & Brussel sandstone

In case of shortcut via a wellbore, CO<sub>2</sub> can hypothetically migrate into the North Sea Group aquifer

- Spill originating from P18-A production wells will migrate towards Q13-10 structure (Figure 11-8, arrow 2).
- Spill from the P18-02 well will migrate towards Q16-02 structure (Figure 11-8, arrow 2)

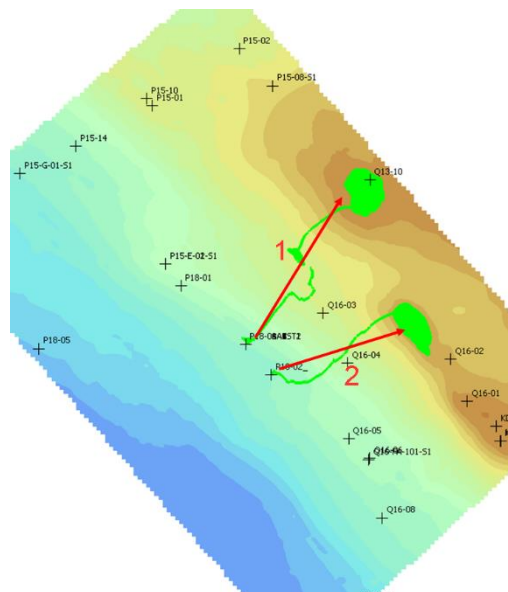


Figure 11-8: Structure map base North Sea Group.

### 11.7 Present day hydrocarbon migration

Inspection of the overburden revealed the possible existence of shallow gas pockets (*CATO-2-WP3.1-D01-Geological report P18 (December 2010)*). The gas most probably is sourced from Jurassic Posidonia shales (van Balen, 2000). The Posidonia shales are situated stratigraphically above the Bunter reservoir and seal, so this hydrocarbon migration is no proof of seal failure/leakage of the P18 Bunter reservoir.

Figure 11-9 shows a seismic section of the overburden, to illustrate hydrocarbon migration, and to illustrate a possible migration pathway for CO<sub>2</sub>. Gas is sourced from the Posidonia shale (strong reflector at the base of the lowest arrow), and migrates via a fault into the sands of the North Sea Group. The red ellipses indicate bright spots, which suggest the presence of gas. Migration is also possible within the Brussels sand, indicated by the arrows in Figure 11-9. At the location where the Brussels sand toplaps against the Upper North Sea Group (Mid Miocene Unconformity, orange line), an increase of amplitudes is observed, which suggest migration from the Brussels sand into the Upper North Sea Group.

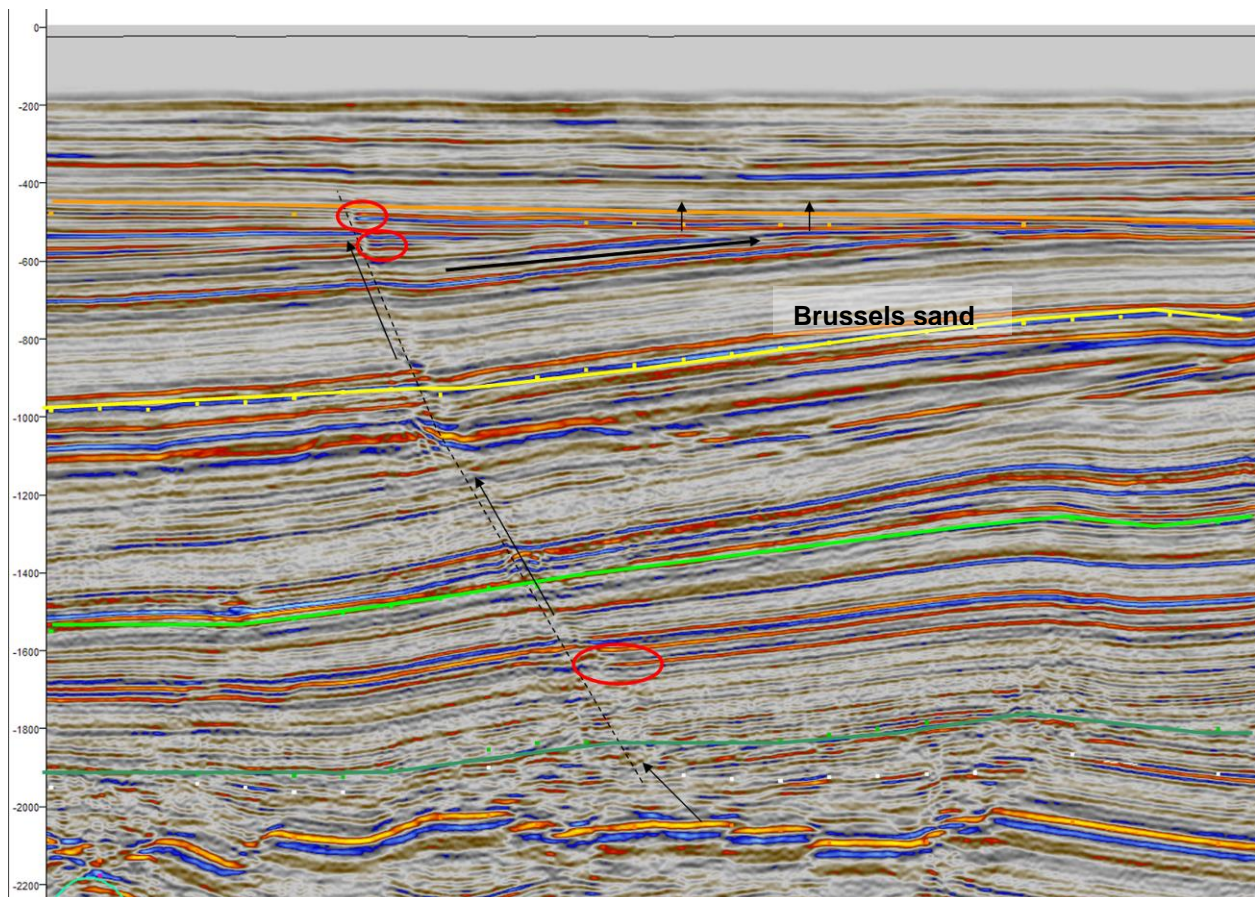


Figure 11-9: Seismic section of the P18 overburden. Arrows indicate hydrocarbon migration along a fault (dashed line). Red ellipses mark bright spots on the right side of the fault. Dark

green line: base Rijnland (BCU), bright green line: base Chalk, yellow line: base North Sea, orange line: base Upper North Sea (MMU).

## 11.8 Conclusions

A Petrel model of the overburden has been constructed, using on publicly available data and data provided by TAQA. Based on the geological model and selected hypothetical migration scenarios, a qualitative evaluation of the possible pathways was developed.

Starting from the results presented in sections 6 through 9, which support the conclusion that leakage of CO<sub>2</sub> (i.e., CO<sub>2</sub> moving out of the storage complex) along wells or faults is highly unlikely if the injection process is conducted within safe limits (see Sections 12 and 14, below), the conclusions are that in case of overfilling of the reservoir, migration through the Buntsandstein (reservoir formations level), the CO<sub>2</sub> remains trapped and finally will migrate towards the adjacent gas reservoirs. Also, in case of migration of CO<sub>2</sub> into the aquifers of the overburden, caused by a shortcut along the wellbore, it will remain trapped within these aquifers. However, migration of CO<sub>2</sub> along faults in the overburden (above the Altena Group) to a shallower aquifer level cannot to be excluded.

Overall, given the results presented in the previous sections, the conclusion from the analysis presented in this section is that the only potential pathway to the surface of CO<sub>2</sub> stored in the P18-2 field is via leaking wells, leaking directly into the atmosphere and not indirectly via pathways originating in deeper parts of the overburden.

## 12 Risk assessment and preventative measures

The current study on the feasibility of CO<sub>2</sub> storage in the P18-2 reservoir made optimal use of earlier work done on the P18 reservoirs, a large part of which was carried out as part of the national CATO2 programme until 2011. The main outcomes of the risk assessment work carried out at that time were presented and discussed during a workshop with representatives from Taqa, EBN, Royal HaskoningDHV and TNO on 12 November 2018. The results were used to verify the completeness of the initial scope of the present feasibility study and if necessary to expand it. This established the basis for the studies (in addition to those already carried out in 2011) presented in Chapters 6 through 9. The central question is where the CO<sub>2</sub> is at any given point in time and whether it could (partially) migrate out of the storage complex. In Section 10 the delimitations of the storage site and the storage complex including the intended storage reservoir have been presented.

After the identification and evaluation of the risks, measures were defined to diminish the risk level. The present chapter provides an extensive summary of this risk management exercise. The risk evaluations are presented for the individual spatial compartments, e.g. reservoir, caprock, fault zones and wells, which together make up the storage complex and leakage barriers. A summary of the risks and their evaluation is provided in the risk register (see Section 0).

The assessment presented here is based on a number of technical conditions (the list below repeats Section 5.4).

- The CO<sub>2</sub> supply profile is shown in Section 5.2; the profile has a plateau injection rate of 2.8 Mt/yr.
- Three wells are available for injection: P18-02-A-01, P18-02-A-03ST2 and P18-02-A-05ST1.
- The tubing in all injection wells will be recompleted (pers. comm. EBN, 2019). The external tubing diameter for all four injector wells is assumed to be 4.5" (Section 5.1).
- Additional conditions apply to the reservoir and the downhole conditions of the CO<sub>2</sub>.
  - At the start of injection, the reservoir pressure is 20 bar.
  - Downhole temperature is required to always be above 15 °C, to avoid CO<sub>2</sub> hydrate formation in the well and in the near-well area (Section 6.4).
- The maximum average reservoir pressure is equal to the initial reservoir pressure.
- The CO<sub>2</sub> is assumed to contain no impurities. At the time of the present study, no quality/specification information was available about potential sources of CO<sub>2</sub>.

The assessment is focused on the functioning of the P18-2 reservoir as a suitable 'container' for the storage of CO<sub>2</sub> to prevent significant leakage from the storage complex as required under the EU Storage Directive (EU, 2009). The permanent containment of CO<sub>2</sub> is provided by a number of geological and technical barriers. It is of great importance that any risk to this containment function is small, can be managed and is acceptable.

The risks of loss of containment relate to possible existing or future defects in the reservoir (pressure evolution and fluid flow leading to lateral flow or spilling of CO<sub>2</sub>), in the caprock (migration pathways, e.g. fractures), bounding faults (re-activation and increased likelihood for CO<sub>2</sub> migration) or the wells (migration pathways as a result of defects in well cement or casing).

The results from the risk assessment together represent a main building block for the Environmental Impact Assessment which is required for the storage permit application.

## 12.1 Reservoir

The P18-2 reservoir is bounded by sealing faults on all sides except for the north-western boundary of Compartment IV of the gas reservoir, which is in direct contact with the water saturated part of the Triassic reservoir rocks more downdip (see Figure 4-2). Along faults F14 and Fault 1 (Figure 4-4) the reservoir has an elongated extension. This extension might be prone to lateral flow or spilling of CO<sub>2</sub> further to the NW. At two other locations near bounding faults CO<sub>2</sub> might spill as in these zones reservoir rocks are juxtaposed to water or gas saturated rocks outside the reservoir.

In summary, three locations with potential hydraulic connections to permeable rocks outside the reservoir have been evaluated in more detail:

- NW margin of Compartment II represented by the outer boundary of the GWC, in particular near Fault 1;
- Small section to the NW of Compartment I across Fault F14;
- Small section along fault F57 between reservoirs P18-2 and P18-6.

### 12.1.1 *Evaluation of spilling at the NW margin of Compartment II*

Results from the reservoir flow simulations show that CO<sub>2</sub> that is injected in Compartment I will start dispersing into the NW elongated extension of the reservoir 9 years after the start of injection (see Section 6.1).

Reservoir simulations with overexaggerated reservoir pressures up to 450 bar show that the CO<sub>2</sub> does not migrate beyond the northern limit of the storage site (see also Chapter 6).

On the basis of the additional simulation work (e.g., Section 0) and proposed risk reduction measures the risk of spilling can be further reduced to a very low likelihood that a negligible amount of CO<sub>2</sub> migrates out of the reservoir and will not flow out of the storage site at all (risk classification A-1; see also Appendix C and Figure 12-1).

### 12.1.2 *Evaluation of spilling at the NW edge of Compartment I*

A small potential spill zone is identified at the NW edge of Compartment I across bounding fault F14 of the reservoir (Figure 4-6). Low-permeable sandstones of the Volpriehausen Formation (< 1 mD) are juxtaposed to permeable sandstones of the Hardegsen Formation across a small zone at fault F14 (Section 4.2).

The potential spill point is very likely not leading to migration of CO<sub>2</sub> out of the reservoir as the very low-permeable Volpriehausen (< 1 mD) and Hardeggen Formations are juxtaposed, hampering the flow of CO<sub>2</sub>.

Proper zonal isolation of wells and prevention of the re-activation of faults which may be present in the area of spilled CO<sub>2</sub> from the reservoir, will avoid vertical migration (see also Fault zone compartment).

The low permeability of the Volpriehausen Sandstone on the other side of Fault 14 juxtaposed to the P18-02 reservoir strongly restrains the lateral migration of CO<sub>2</sub> out of the P18-02 reservoir. This implies that there is a very low likelihood that any CO<sub>2</sub> can migrate out of the reservoir (risk class A-3; see Figure 12-1).

#### 12.1.3 *Evaluation of CO<sub>2</sub> flow between reservoirs P18-2 and P18-6*

Both the static model used during the CATO2 work and the new model for the current feasibility study indicate that there is a small section across the fault zone with juxtaposition of the low-permeable Volpriehausen Sandstone (see Section 6.3.5). The P18-6 reservoir is located directly to the NE of Compartment 2-IV of the P18-2 reservoir. Geological reservoir modelling and pressure history observations indicate that this compartment represents a separate hydraulic unit from the P18-2 reservoir, which implies that no CO<sub>2</sub> will migrate in this part of the reservoir and thus will not end up in the P18-6 reservoir.

The pressure in P18-06 was at the initial level of 377 bar whereas at the same time pressure has dropped to about 100 bar in the producing P18-2 reservoir (June 2003). Apparently, this pressure difference could exist, which indicates absence of flow and no pressure equilibration between the two reservoirs on production time scales. Any pressure communication would only be expressed on geological time scales in the order of 10<sup>3</sup> to 10<sup>6</sup> years.

A fault analysis of the P18 faults revealed that the faults between P18-02 and P18-6 have a high (to very high) probability of being sealing due to the high probability of impermeable fault gouge formation or cataclasis (Nieuwland, 2012).

The pressure difference of about 277 bar between the two reservoirs and the very low permeability of the Volpriehausen Sandstone show that there is a very low likelihood that even a negligible amount of CO<sub>2</sub> will migrate from P18-2 to P18-6 or no CO<sub>2</sub> is flowing out of P18-2 to P18-6 at all (risk class A-1; see Figure 12-1).

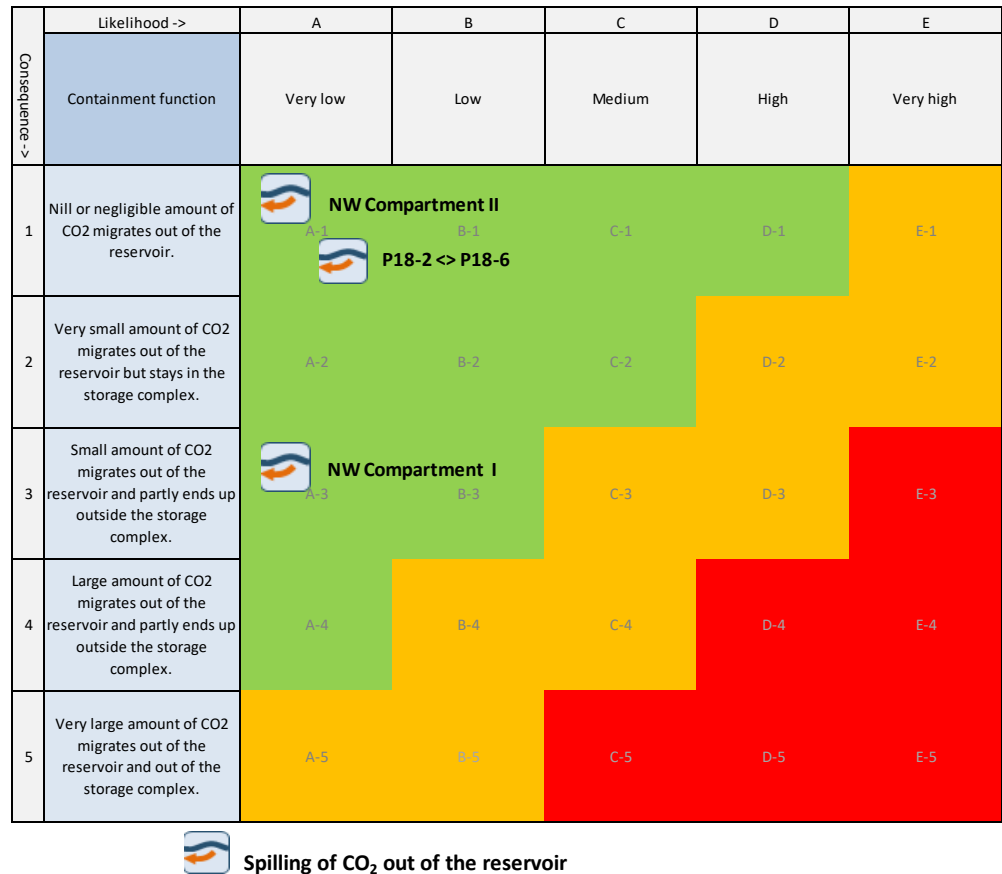


Figure 12-1 Geological risk matrix for the reservoir compartment with inclusion of proposed risk reduction measures.

## 12.2 Caprock

Impermeable shales of the Upper Triassic and Altona Groups overlie the P18-02 reservoir, which represent a good seal for the natural gas reservoir. The sealing capacity is evidenced by the presence of gas in reservoir below the seal with a thickness of 450 m to 750 m and a gas column of about 600 m. The average reservoir pressure after CO<sub>2</sub> injection will be lower than the initial pressure.

### 12.2.1 Initial condition

As the evidence for the initial sealing capacity of the caprock is very strong, it is a good seal for CO<sub>2</sub> storage as well and consequently the risk of CO<sub>2</sub> migration out of the reservoir is low to even negligible (see Figure 12-2).

### 12.2.2 Fracturing

Fractures in the seal may be caused by local stress variations due to initial gas production and subsequent CO<sub>2</sub> injection, and associated pressure and temperature changes. Fractures represent a potential conduit for CO<sub>2</sub> loaded fluids depending on their connectivity and continuity (see also Fault zone).

Semi-analytic modelling (Section 8) has shown that Coulomb stresses as a consequence of pressure build-up due to injection quickly decay inside the caprock. The pressure effect is thus not expected to contribute to the risk of fault reactivation

in the caprock. New fractures or faults will not be generated as they would require even higher Coulomb stresses. This is confirmed by earlier mechanical analysis of seal and fault based on P18-2; no critical factors identified (Vandeweyer et al., 2011: ch6, par 6.7, p108).

Although semi-analytic thermo-mechanical modelling shows that temperature-induced positive Coulomb stresses occur in the caprock near the edges of the cooling front (Section 8.3), they are not sufficiently large to re-activate faults in the caprock, nor will they result in new fractures in the caprock. The likelihood of thermomechanically re-activating a pre-existing fault in the caprock is thus very low.

If fracturing due to pressure increase and/or temperature drop would occur, this will only result in local effects. Considering the huge thickness of the caprock, the likelihood of fracturing the complete caprock is nil and consequently the risk is low to even negligible (Figure 12-2).

### 12.2.3 *Chemical degradation*

CO<sub>2</sub> if dissolved may react with minerals in the caprock near the interface with the CO<sub>2</sub> reservoir. Since the caprock has proven to be a seal for gas, the only way of upward migration is by diffusion of dissolved CO<sub>2</sub>, which is a very slow process. Chemical interaction between dissolved CO<sub>2</sub> and caprock minerals is very slow and has minor effects on porosity and permeability. Hence, no migration path is expected to be formed. The affected zone of migration of dissolved CO<sub>2</sub> and chemical interaction is in the order of several meters in thousands of years (Gaus et al., 2005; Tambach et al., 2012); see also Section 8.4.

Chemical degradation will only marginally influence the sealing properties of the caprock and thus will the overall integrity of the caprock stay intact. The likelihood of degrading the caprock is very low and its consequence will be nil or negligible (Figure 12-2).

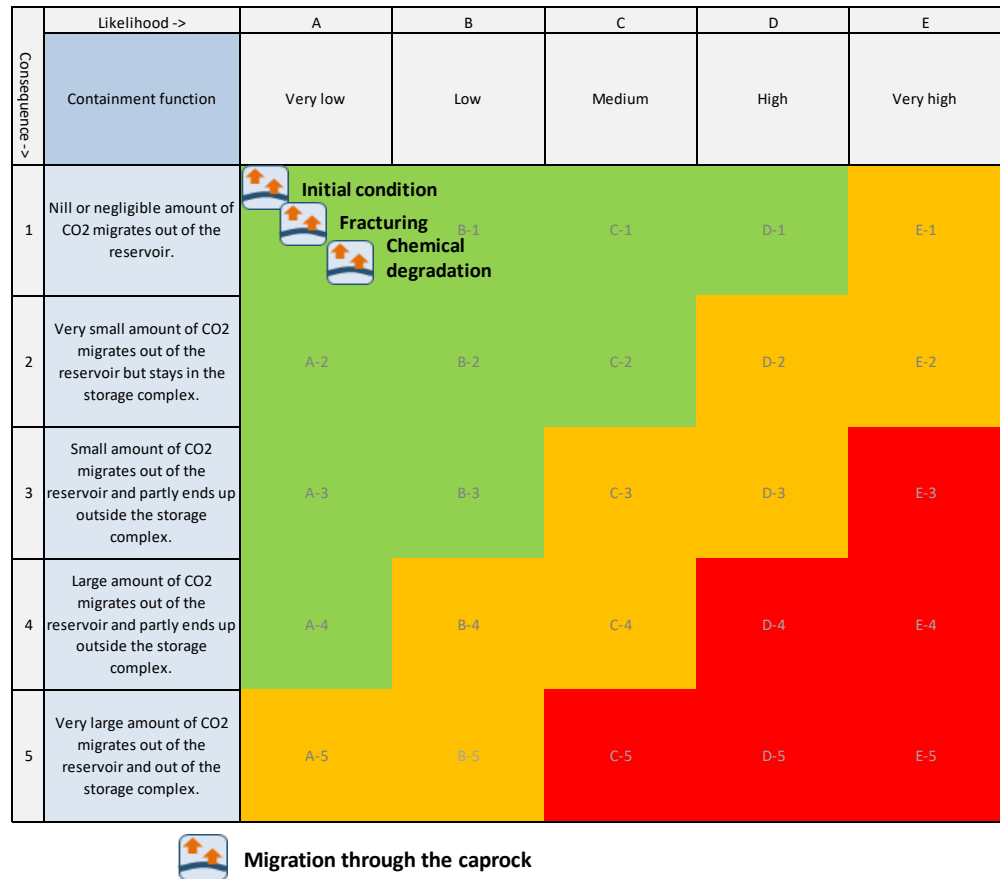


Figure 12-2 Geological risk matrix for the caprock compartment with inclusion of proposed risk reduction measures

### 12.3 Fault zones

#### 12.3.1 Initial condition

The sealing capacity of reservoir boundary faults is high as evidenced by the presence of gas on the reservoir side of the bounding faults and the permeability contrast of juxtaposed claystone and sandstone rocks on both sides of the bounding faults (see Section 4.2).

Bounding faults F19/F20 and F10 (Section 4.2) are effective seals as evidenced by presence of juxtaposed reservoir rock and sealing rock. In two cases reservoir rocks can be juxtaposed over a very small section on both sides of faults but in these cases reservoir rock with very low permeability (< 1 mD) is present on either one or both sides of the fault (see also discussion on reservoir spilling in Section 12.1).

As reservoir rocks next to bounding faults are sealed off by very low permeable rocks on the other side of the fault zone, there is a very low likelihood that a negligible amount of CO<sub>2</sub> will migrate across or along the fault and sealing rock (see Figure 12-3).

### 12.3.2 *Chemical degradation*

Chemical alteration of the fault zone may enhance migration of CO<sub>2</sub> along the fault. Currently, there is no evidence for gas migration from the P18-2 reservoir along the faults to overlying formations. In general, the geochemical reactions between CO<sub>2</sub>, formation water and fault gouge mineralogy will result in precipitation of carbonate minerals. On the longer term, silicate minerals might react, providing additional cations for carbonate precipitation. Porosity and hence permeability effects are predicted to be negligible. Increase of carbonate content in the fault gouge is known to increase the friction coefficient and to decrease potential for fault re-activation (Samuelson et al., 2012; Adelinet et al., 2014; Bakker et al., 2016). That is why it is highly unlikely that chemical degradation in itself leads to the migration of CO<sub>2</sub> across the fault zone (see Figure 12-3). See also Section 7.4.

### 12.3.3 *Fault stability: effects of re-pressurising P18-2*

Due to pressure changes during production and/or injection faults may be re-activated (Vandeweyer et al., 2011: par 6.7, p109) and potentially act as conduits for CO<sub>2</sub>.

No seismic activity during production was observed, based on the KNMI database (Vandeweyer et al., 2011). Semi-analytic modelling has shown that at the end of the injection period most (if not all) of the areas where positive Coulomb stresses which are present at the end of depletion, have disappeared (Section 7.2). The faults are thus expected to be stable at the end of the injection period. Injection of CO<sub>2</sub> is thus a mitigation measure in itself as it reduces the underpressure in the reservoir and consequently the risk of fault re-activation.

Based on the results from the semi-analytic modelling it appears to be highly unlikely that faults will be re-activated due to the increased pressure by CO<sub>2</sub> injection and consequently will not lead to migration of CO<sub>2</sub> along the fault (Figure 12-3).

### 12.3.4 *Fault stability: effects of injecting low-temperature CO<sub>2</sub>*

Injection of a cold CO<sub>2</sub> stream could re-activate a nearby fault and change its fluid transport properties. TOUGH2 simulations have shown that the cooling front could extend to 300 m from the injector after 15 years of injection (Section 7.3). Semi-analytic thermomechanical modelling indicates that the Coulomb stresses rapidly decay to around 2.5 MPa at a distance of 100 m from the cooling front. Thus injection wells at less than 300 to 400 m from a fault may thermomechanically influence its stability, if the cold front reaches the fault.

The above simulations do overestimate the effect as in reality the continuous pressure build-up in the reservoir will have a stabilizing effect on the faults. Secondly, the well P18-2-A1 which is close to a fault, has the worst injectivity and consequently a less pronounced cooling effect.

Lowering the injection rates of wells which are close to faults will reduce the advancement of the cold front and thus diminish the risk of fault re-activation and migration along the fault.

With inclusion of proper management of the injection rates in wells nearby faults the likelihood of thermomechanical fault re-activation leading to the migration of a very small amount of CO<sub>2</sub> out of the reservoir, will be low (Figure 12-3).

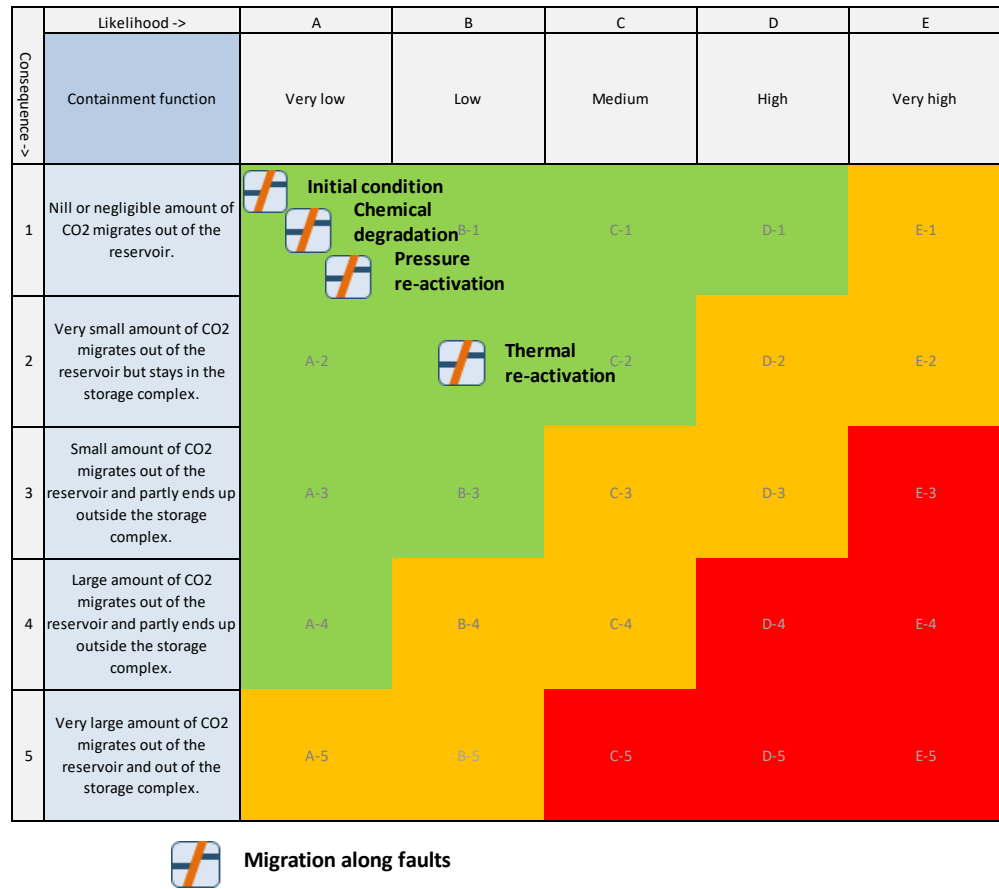


Figure 12-3 Geological risk matrix for the fault zones with inclusion of proposed risk reduction measures.

## 12.4 Wells

The following wells penetrating the P18-2 reservoir, were evaluated in detail:

- P18-02 (exploration well)
- P18-2A-01 (Compartment I)
- P18-2A-03/-S1/-S2 (Compartment I)
- P18-2A-05/-S1 (Compartment I)
- P18-2A-06/-S1 (Compartment III/Compartment II)

### 12.4.1 Surface casing of all injector wells

The condition of the outer casing inside the conductor may be reduced due to external corrosion or to fatigue by the cyclic nature of metoceanic movement. As a consequence the load bearing capacity of the casing and conductor could be reduced and seriously hamper the integrity of the well barriers. All potential injectors have adequate cement overlap in the surface part of the wells in order to transfer the loads.

As no assessment records were found on the load bearing capacity of the surface casing and conductor, it is recommended to perform for example, an external

surface casing corrosion log to confirm the remaining load capacity of the surface casing (see also Section 9.2).

After proper assessment and if needed workover of the injector wells, the likelihood that a negligible amount of CO<sub>2</sub> will migrate out of the reservoir; is characterized as low (see Figure 12-4).

#### 12.4.2 *P18-02 (exploration well)*

P18-02 well is suspended and left with a mud line suspension in place to allow potential re-entry. The well is plugged at various depths with a total of 4 plugs. Several barrier elements for this suspended well could not be validated. That's why the well needs to be planned for re-assessment and decommissioning conform the updated NOGEPa 45 standard for CO<sub>2</sub> storage decommissioning provided that these are available in time.

The current well layout seems to be inadequate for long-term containment of a near original reservoir pressurized CO<sub>2</sub> storage, as it may result in CO<sub>2</sub> migration pathways from the reservoir to shallower levels, bypassing the caprock (see also Section 9.2.8). The likelihood that deficiencies in the cement bond and the quality of the plug will lead to migration out of the reservoir and partly will leak out of the storage complex has been evaluated as medium. After the proposed re-assessment and workover activities, the likelihood that a negligible amount of CO<sub>2</sub> will migrate out of the reservoir is expected to become low (Figure 12-4).

#### 12.4.3 *P18-2A-01 (Compartment I)*

The low quality of the 7" liner cementation at packer depth, combined with the fact that the 7" liner is made of carbon steel material, poses the risk of external degradation due to corrosion by potentially corrosive reservoir fluids and consequently an inadequate hydraulic isolation over parts of the caprock. The production packer is installed across a zone with poor cement bonding. This results in a low likelihood that CO<sub>2</sub> migrates along the well and partly ends up outside the storage complex (see also Section 9.2.4).

By recompletion and repositioning the production packer in a casing or liner section with good cement bond, leakage from the well will be effectively prevented. With the implementation of the proposed measures the likelihood will become low that a negligible amount of CO<sub>2</sub> will migrate out of the reservoir (Figure 12-4).

After definite cessation of injection the well should be plugged according to CO<sub>2</sub> storage abandonment requirements (under development).

#### 12.4.4 *P18-2A-03/-S1/-S2 (Compartment I)*

All primary and secondary barrier elements have been validated and thus pose no significant risk for CO<sub>2</sub> leaking out of the well. The mother borehole and side-track S1 do not end in reservoir and thus do not increase the likelihood of CO<sub>2</sub> migration out of the reservoir.

The CO<sub>2</sub> injection load case capacity and the material compatibility for the retrievable packer are to be assessed and potentially to be mitigated to make this well a suitable CO<sub>2</sub> injector. With the implementation of the proposed measures leakage from the well should be prevented; the likelihood is low that a negligible amount of CO<sub>2</sub> will migrate out of the reservoir (Figure 12-4).

After definite cessation of injection the well should be plugged according to CO<sub>2</sub> storage abandonment requirements (under development).

#### 12.4.5 *P18-2A-05/-S1 (Compartment I)*

The mother bore was drilled to about 200 m TVD above the reservoir. Then the drill pipe parted and 500 m of drill pipe/BHA (Bottom Hole Assembly) was left in the mother bore hole (circulation was possible before the drill pipe parted) with a cement plug on top, after which the well was side tracked. As the mother borehole does not end in reservoir, this does not increase the likelihood of CO<sub>2</sub> migration out of the reservoir.

Sustained casing pressure was measured in the 9 5/8 " production casing, which is being managed by keeping the pressure below the Maximum Operating Pressure (MOP) for the current natural gas production. The current condition of this well indicates that there is a medium likelihood that a small amount of CO<sub>2</sub> migrates along the well and ends up outside the storage complex (see also Section 9.2.6).

The source of sustained pressure in the production casing needs to be investigated and if required being repaired. As a result, the likelihood that a negligible amount of CO<sub>2</sub> will migrate out of the reservoir should be low after the repair (Figure 12-4).

After definite cessation of injection the well should be plugged according to CO<sub>2</sub> storage abandonment requirements (under development).

#### 12.4.6 *P18-2-A-06/-S1 (Compartment II/Compartment III)*

The well connects P18-2 Compartments II and III. The producing reservoir formations from the side track and the mother bore connect at the side track window, which is not isolated.

For this well to be used as CO<sub>2</sub> injector the well barrier of the mother bore and the integrity of the side-track window have to be restored. This has most likely to be done by plug and abandonment (P&A) of the side track and installing a cemented scab or tie back liner to restore the mother bore integrity. The original primary and secondary barriers of the mother bore can be restored; it has a good cementation and in-situ formation at caprock level.

The current condition of this well indicates that there is a medium likelihood that a small amount of CO<sub>2</sub> migrates along the well and ends up outside the storage complex (see also Section 9.2.7). With the proposed measures the double barrier could be re-instated such that it sufficiently reduces the risk of leakage. As a result, the likelihood that a negligible amount of CO<sub>2</sub> will migrate out of the reservoir should be mitigated to low (Figure 12-4).

After definite cessation of injection the well will be plugged according to CO<sub>2</sub> storage abandonment requirements (under development).

#### 12.4.7 *Cooling of P18 injector wells*

Injection of cold CO<sub>2</sub> leads to thermal contraction of the wells. The induced tensile stresses can exceed the bonding strength and thus lead to debonding at the well-cement interface. The resulting micronannuli represent a potential pathway for CO<sub>2</sub>

migration which could be further enhanced by chemical interaction of CO<sub>2</sub> and the cement around the microannuli (see Sections 9.3 and 9.3.4).

Although the creation of microannuli is considered to be highly likely, the migration of CO<sub>2</sub> is prevented by the pressure of CO<sub>2</sub> which is to be maximised at the hydrostatic pressure. At the end of the injection phase an appropriate formation-to-formation plug is recommended.

A small to negligible amount of CO<sub>2</sub> may migrate through the thermally induced microannuli of the P18 injector wells and partly end up outside the storage complex (risk class C-3; see Figure 12-4). After appropriate abandonment of the injector wells the risk will be reduced to a low likelihood that a small amount of CO<sub>2</sub> migrates out of the reservoir (risk class B-1).

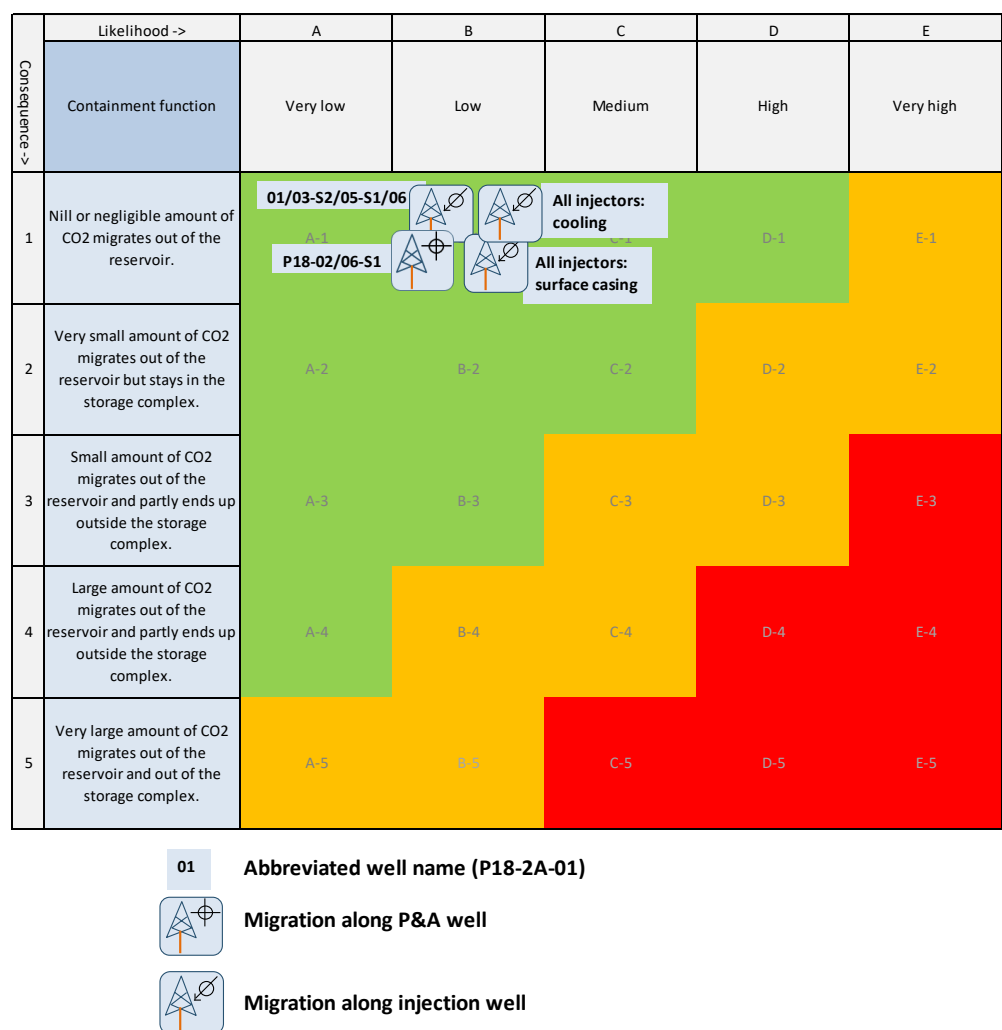


Figure 12-4 Well risk matrix after implementation of risk reduction measures; most well names are abbreviated: for example “01” stands for “P18-2A-01”.

## 12.5 Conclusion

*All risks can be reduced to acceptable, low levels*

All geological and subsurface well engineering risks in the P18-2 field can be reduced to acceptable, low levels, with no significant environmental impacts if the store is properly designed, managed and abandoned. The conclusion is that there are no prohibitive risks to storing CO<sub>2</sub> in the P18-2 field. All risks can be managed so that their risk level is low and acceptable.

#### *Well workovers required*

All selected wells will need workover activities to some degree to qualify them for CO<sub>2</sub> injection and storage. Proper management of injection rate and temperature is necessary to prevent undesired effects of cooling on faults nearby wells and re-heating of the near well area on the pressure evolution in the reservoir in the post-injection phase. For that purpose pressure, temperature and flow rate of injected CO<sub>2</sub> should be monitored (see Section 13).

#### *Reservoir pressure after injection*

As mentioned above, all risks identified here can be reduced to acceptable, low levels, provided the storage site is properly designed, managed and eventually closed. Part of this is the design of safe injection scenarios and management of pressure and temperature in the wells and reservoir. It should be noted that the simulation of the injection of CO<sub>2</sub> into the reservoir, the integrity of the caprock and the stability of faults pose no limits to the average reservoir pressure at the end of injection (apart from the maximum given by the initial pressure, which represents the maximum pressure at which the reservoir, caprock and faults have proven containment). Safe and secure storage is possible for reservoir pressure up to initial pressure (i.e., the pressure that existed in the field prior to production).

However, the study did identify a risk that requires reservoir pressure to be maximised at hydrostatic pressure. The potential migration of CO<sub>2</sub> through microannuli formed between casing (liner) and cement due to the low temperature of the injected CO<sub>2</sub> becomes small to negligible when reservoir pressure is kept below hydrostatic pressure.

## 13 Monitoring and corrective measures plan

### 13.1 Introduction

A thorough risk based approach to monitoring is adopted. This means that the elaboration of the plan depends on the results of the location-specific risk assessment, which is laid out in the previous sections.

A risk-based monitoring plan:

- Aims to ensure the safety and integrity of the storage complex;
- Reveals the necessary information for transfer of responsibility to government after the end of injection;
- Can supply and incorporate additional learning with respect to large-scale CCS;
- Should be able to prove the effectiveness of corrective measures;
- Provide a balance between efficiency and costs.

New techniques and equipment will be included whenever judged appropriate, provided that these techniques do not add to the complexity associated with operating an offshore unmanned installation.

The monitoring and corrective measures plans are part of a set of related plans that are part of the storage permit. The location specific risk assessment (Section 10) is the main input for the corrective measures and closure plans. The development of the monitoring plan is also based on a location specific risk analysis and has strong links with the corrective measures plan. Figure 13-1 illustrates the links and the consistency between the plans.

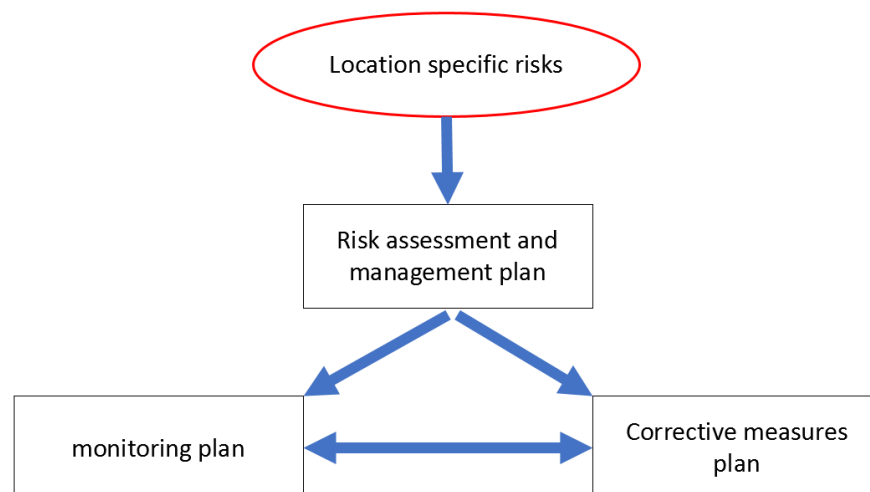


Figure 13-1. Consistency between risk management, monitoring and corrective measures plans.

Monitoring requirements of the CCS Directive 2009/31/EC and OSPAR are framed around enabling the operator to understand and to demonstrate understanding of

ongoing site processes, to predict future site behavior and to identify any leakage. Further requirements of the monitoring include early identification of deviations from predicted site behavior, provision of information needed to carry out remediate actions and the ability to progressively reduce uncertainty.

#### 13.1.1 *Reading Guide*

The foundation of the plan is given first. This refers to the legislation, regulations and other preconditions that have been taken into account. Then the philosophy of the monitoring plan is explained. Finally, the elaboration of the operational monitoring plan is explained, while the detailed monitoring plan is documented in Section 19. The cross-references to the corrective measures plan are explicitly indicated.

The plan described here represents the draft monitoring plan, to be updated and detailed prior to the start of injection.

### 13.2 **Foundation of the monitoring and corrective measures plan**

For the P18-2 storage project the monitoring plan needs to comply with the following regulations and requirements:

- Provisions of two key regulatory treaties governing CO<sub>2</sub> storage in the European offshore area, which are the OSPAR Guidelines (OSPAR, 2007) and the European Storage Directive (EU, 2009) and its implementation in the Dutch Mining Law.
- Requirements of the EU Emissions Trading System (ETS), as defined under the EU Monitoring and reporting Guidelines (EU, 2017), which deals with the accounting of leaked emissions from storage sites.
- Specific requirements to the P18-2 storage project as a first of a kind project for The Netherlands.

The starting point for developing the monitoring and corrective measures plan is an adequate characterization and risk assessment.

The general requirements for both site characterization and risk assessment are given in the Dutch mining law, the EC Storage Directive and its Annexes. Clarifying details are provided in the EU guidance documents (EU, 2011).

The detailed site characterization benefited from the fact that the storage reservoir is part of a larger natural gas field which has been produced for more than two decades. This has led to an abundance of information on the site.

The monitoring plan must relate to preventative and corrective measures. In the adopted template in this report, potential risks, monitoring techniques and mitigation measures are linked together.

With respect to the phases of a storage operation, the plan describes a 'workflow' for monitoring activities during the pre-injection (site qualification), injection (operation), post-injection (closure and post-closure) phases and after transfer of responsibility (long-term stewardship). However, monitoring in the different stages of a project is not fundamentally different. The philosophy of the monitoring plan is that it must be complete, transparent, consistent, and verifiable.

An additional requirement for the P18-2 storage project is that the monitoring plan may also serve the first of a kind character of the project, in combination with CO<sub>2</sub> injection in the P18-4 field and, potentially, the P18-6 field. This could mean gathering more data for a deeper understanding of the storage process, learning of findings.

#### 13.2.1 *General requirements from Directive 2009/31/EC*

A monitoring plan should meet the requirements according to the EU CCS Directive (EU, 2009; Annex II), as listed below.

##### **Initial plan**

The monitoring plan shall provide details of the monitoring to be deployed during the main stages of the project, including baseline, operational and post-closure monitoring.

The following shall be specified for each phase:

- 1 Parameters monitored;
- 2 Monitoring technology employed and justification for technology choice;
- 3 Monitoring locations and spatial sampling rationale;
- 4 Frequency of application and temporal sampling rationale.

For the purpose of:

- Comparing actual and modelled behaviour of CO<sub>2</sub> and brine
- Detecting significant irregularities
- Detecting CO<sub>2</sub> migration
- Detecting CO<sub>2</sub> leakage
- Detecting significant negative effects for environment, drinking water, nearby residents, the biosphere
- Evaluating the effectiveness of corrective measures taken in case of leakage
- Proving safety and integrity of the storage complex, including the assessment of complete and permanent storage.

The parameters to be monitored are identified so as to fulfil the purposes of monitoring. However, the plan shall in any case include continuous or intermittent monitoring of the following items:

- Fugitive emissions of CO<sub>2</sub> at the injection facility;
- CO<sub>2</sub> volumetric flow at injection wellheads;
- CO<sub>2</sub> pressure and temperature at injection wellheads (to determine mass flow);
- Chemical analysis of the injected material;
- Reservoir temperature and pressure (to determine CO<sub>2</sub> phase behavior and state).

The choice of monitoring technology shall be based on best practice available at the time of design. The following options shall be considered and used as appropriate:

- Technologies that can detect the presence, location and migration paths of CO<sub>2</sub> in the subsurface and at surface;
- Technologies that provide information about pressure-volume behaviour and areal/vertical saturation distribution of CO<sub>2</sub> to refine numerical 3-D-simulation

to the 3-D-geological models of the storage formation established pursuant to Article 4 and Annex I of the Storage Directive (EU, 2009);

- Technologies that can provide a wide areal spread in order to capture information on any previously undetected potential leakage pathways across the areal dimensions of the complete storage complex and beyond, in the event of significant irregularities or migration of CO<sub>2</sub> out of the storage complex.

### Updated plan

The monitoring system initially installed and related procedures need to be updated on the basis of the evaluation and modelling activity, or the verification results. Monitoring plans must be updated, at least every five years, to take into account changes to assessed risk of leakage, changes to assessed risks to environment and human health, new scientific knowledge, and improvements in the best available technology. National authorities may set a more stringent frequency.

According to Annex II of the Storage Directive one has the following updating requirements:

- a. The data collected from the monitoring shall be collated and interpreted. The observed results shall be compared with the behaviour predicted in dynamic simulation of the 3-D-pressure-volume and saturation behaviour undertaken in the context of the security characterization.
- b. Where there is a significant deviation between the observed and the predicted behaviour, the 3-D-model shall be recalibrated to reflect the observed behaviour. The recalibration shall be based on the data observations from the monitoring plan, and where necessary to provide confidence in the recalibration assumptions, additional data shall be obtained.
- c. Steps 2 and 3 of Annex I of the Storage Directive shall be repeated using the recalibrated 3-D model(s) so as to generate new hazard scenarios and flux rates and to revise and update the risk assessment.
- d. Where new CO<sub>2</sub> sources, pathways and flux rates or observed significant deviations from previous assessments are identified as a result of history matching and model recalibration, the monitoring plan shall be updated accordingly.

Post-closure monitoring shall be based on the information collected and modelled as in a) through d). The plan must now also provide information needed for the transfer of responsibilities to the competent authority (long-term stewardship). Especially the site's permanent containment must be indicated, based on all available evidence.

### 13.2.2 Emissions accounting for ETS

The Monitoring and Reporting Guidelines for CCS under the ETS describe the method for quantifying potential CO<sub>2</sub> emissions from a storage project.

Potential sources for CO<sub>2</sub> emissions from the geological storage of CO<sub>2</sub> include:

- Fuel use at booster stations and other combustion activities such as on-site power plants;
- Venting at injection or at enhanced hydrocarbon recovery operations;
- Fugitive emissions at injection;
- Breakthrough CO<sub>2</sub> from enhanced hydrocarbon recovery operations;

- Leakage from the storage complex.

Quantitative monitoring for ETS will only be required if there is an indication of leakage. There is no requirement for emissions accounting as long as there is no evidence that the site leaks. However, in case irregularities are observed for example in the downhole pressure and temperature measurements, the need for additional monitoring to detect migration pathways out of the storage complex becomes stringent.

The key question for quantitative monitoring is of course to what extent the state-of-the-art technology allows for an accurate quantification. In that perspective NSBTF (2009) suggests choosing a combination of a model-driven approach in combination with a monitoring strategy to best estimate the leakage for ETS purposes.

In the unlikely event that there is evidence for CO<sub>2</sub> flow out of the storage complex, or that irregularities occur that give rise to the need to check for anomalies outside of the storage reservoir, a strategy would be to detect leakage to the surface by geophysical methods like seismic data (detection of gas chimneys) or sea-bottom sonar techniques (detection of pockmarks) and then carry out in situ gas measurements and/or sample these leakage areas for direct CO<sub>2</sub> detection. Based on these observations an estimate can be made of leakage rates for the area. However, it should be noted that in the case of CO<sub>2</sub> storage in depleted gas fields, seismic methods have limited value. Most currently operational CO<sub>2</sub> storage projects use saline aquifers, such as Sleipner and Snøhvit in Norway, in which case seismic methods provide an efficient way to monitor the development of the CO<sub>2</sub> plume in the storage reservoir and verify containment by the caprock (e.g., Furre et al., 2017). Seismic methods cannot be used to monitor the distribution of CO<sub>2</sub> in a depleted gas field, as seismic waves cannot discriminate between CO<sub>2</sub> and residual natural gas in the reservoir. In addition, gas fields offer high certainty that CO<sub>2</sub> will be contained in the depleted reservoir (as shown here in Sections 4 through 8), effectively removing the need to check for anomalies above the caprock. Only in case of evidence of unforeseen circumstances or non-conformance would seismic methods be considered as monitoring tool for CO<sub>2</sub> in depleted gas fields.

### 13.2.3 *Specific requirements for the P18-2 storage project*

CO<sub>2</sub> storage is the main objective of the P18-2 storage project. For the project, and the storage permit in particular, the monitoring plan serves to make supported statements about the following:

- Safety and integrity, regarding possible damage to the environment or the soil. Monitoring will have to support that the CO<sub>2</sub> remains stored in the reservoir and does not end up in the biosphere. The lasting quality of the structure of the reservoir and the sealing layer must also be clear. Monitoring offers the opportunity to take action if anomalies occur.
- Demonstration character of the project, learning of findings, some situations can be better understood through measurements.
- Commercially, regarding the ETS and the amounts stored. Monitoring must show that the captured CO<sub>2</sub> is in fact permanently out of circulation and no emission rights for this CO<sub>2</sub> need to be surrendered.
- Legally, regarding the delineation of the storage location. Monitoring must show that the CO<sub>2</sub> does not enter other reservoirs for which no storage permit has been issued.

- Offer a foundation to support the transfer of responsibility after injection is concluded.

### 13.3 Philosophy of the monitoring plan

Besides meeting all legal requirements, the monitoring plan should be based on a balance between efficiency and costs.

#### 13.3.1 *Regular measurements*

A significant part of the monitoring program is measuring primary operational parameters and verifying the underlying model of the subsurface.

A plan has been devised that includes regular measurements, such as flow, pressure and temperature. These parameters will be used to test whether the injection program is proceeding according to plan and the extent to which anomalies occur with respect to the modelled behavior.

#### **Traffic light model**

The measurement program uses the so-called traffic light model. This means that for the measurements, the expected values are indicated in ranges: green, yellow and red. Quantification of these monitoring value ranges is a key element of the monitoring plan update prior to the start of injection.

In the traffic light model, a green zone is given for each operational parameter; the value of the parameter falls within this range, when the operation is proceeding as expected. Outside of this range, threshold 1 (see Table 19-1), a yellow zone exists, indicative of a deviation from the predicted behaviour, without a direct need for corrective measures. When values fall within this range, it is important that insight is gained into the cause of the anomalous results. For that reason, additional measurements should be taken (extra measurements and/or the use of other measuring techniques, depending on the circumstances). Finally, there is a red zone, threshold 2 (see Table 19-1), indicating measurements that are so far outside of the expected range that corrective measures are probably necessary. If such an unexpected event occurs, undesired effects may develop. In order to limit such consequences as much as possible, corrective measures may be deployed. The monitoring program serves to indicate the effectiveness of these corrective measures.

#### **Business as usual**

When the injection proceeds as predicted, with measured values consistent with predicted values (green zone), the frequency of measurements could gradually be decreased.

#### **Scale-up**

If the measurements deviate from the expected values (yellow zone), this will lead to a higher frequency of measurements, or the introduction of other types of measurements. If this does not provide sufficient illumination of the situation, the monitoring program will be expanded further.

#### **Adjusting the model**

Monitoring data can also provide (new) information and insights about the subsurface; this information should be used to adjust and calibrate any models used. The adjusted models can be used to predict future behavior with higher reliability, so that the behavior of the CO<sub>2</sub>, the well, the reservoir and the sealing layer can be predicted more accurately as the injection process proceeds.

### 13.3.2 *Special measurements*

Pre- injection, injection and post-injection monitoring do not differ in intent. Risks may be deemed higher in (parts of) the injection phase, notably the beginning of the injection activities. The monitoring plan reflects higher degrees of risk through more frequent and / or different monitoring techniques. Besides the measurements for the verification of predicted behavior during injection, there are a number of special measurements included in the monitoring program. These concern baseline measurements, measurements before closure and transfer, as well as measurements under special circumstances during the injection process.

#### **Baseline measurements**

In the pre-injection phase there will be a period of monitoring in order to determine the current status of the storage site. During this period baseline data will be gathered. It is of key importance to identify all possible baseline data that might be needed later in the injection and post-injection phases both for required monitoring and for contingency monitoring.

The baseline data will serve as a reference for monitoring during and after the injection process.

Baseline and repeat measurement acquisition, processing and interpretation are part of the monitoring plan (Table 19-1), where the relation with risk assessment and preventive/corrective measures is also described.

#### **Measurements before closure and transfer**

Measurements should be made before the closure of the reservoir and before the transfer to the competent authority. Their purpose is:

- Measurements to determine whether the behaviour of the CO<sub>2</sub> stored in the reservoir is such that the well can be abandoned.
- Measurements necessary after the conclusion of injection to establish whether the CO<sub>2</sub> stored is in or moving towards a stable situation so that it is possible to transfer responsibility to the government.

#### **Measurements under special circumstances**

During CO<sub>2</sub> injection, the pressure in the reservoir increases; the temperature, pressure and flow rate through each well are chosen such that injection can take place safely. During the injection process, the injection rates of CO<sub>2</sub> will vary, with occasional interruptions. Part of the monitoring program is to measure the conditions that arise during such transient operations.

The period required for monitoring after abandonment of the wells and prior to decommissioning of the platform is not defined yet, neither is the period between decommissioning of the platform and transfer of liability to the state authorities. The required lengths of these periods need to be established in agreement with State Supervision of the Mines (SodM).

### 13.3.3 *Direct and indirect determination of possible leakage*

Two ways can be distinguished to enable verification of the points above. On the one hand, there are direct detection methods that can be used to demonstrate the presence of CO<sub>2</sub> migration from the reservoir. An example of this can be CO<sub>2</sub> measurements at wells.

On the other hand, there are also indirect detection methods available, which can be used to verify that the CO<sub>2</sub> injected is behaving as predicted. The predictions are derived from static and dynamic models created beforehand, but also from updates to these models based on available monitoring data (such as pressure measurements in the reservoir). For this reason, important parameters have been included in the monitoring plan for the purpose of indirect monitoring. These include:

- pressure and temperature measurement in the wells;
- annular pressures of the wells;
- volume of injected CO<sub>2</sub>;
- composition of the injected gas;
- well integrity measurements ;
- measurements of irregularities at the seabed.

### 13.3.4 *Different stages*

Different stages can be distinguished throughout the lifetime of the CO<sub>2</sub> storage project. This leads to different monitoring requirements through the lifetime of the project. The different stages are listed below.

- Pre-injection

Prior to actual injection, the monitoring focuses on recording the starting situation (baseline monitoring).

- Injection

In the operational phase CO<sub>2</sub> is injected until the reservoir is filled to an extent that further injection is not desired or allowed, or until no more CO<sub>2</sub> is delivered and a decision is made to conclude CO<sub>2</sub> injection.

- Post-injection

After CO<sub>2</sub> injection has stopped, there is a period of observation. During this period, it will be decided whether a stable end situation will be reached. If this is the case, the well will be closed with a plug. If the plug is shown to be of an acceptable quality, the wells will be sealed.

- Post-injection — abandonment

If the seal is shown to be of acceptable quality, the wells will be permanently abandoned. Later, responsibility can be transferred to the government.

- Post-injection — transfer of liability

Once a stable situation is achieved, the responsibility of the filled reservoir may be transferred to the competent authority. After the transfer, the developments in the reservoir will be followed periodically. The competent authority is responsible for a monitoring period of 30 years from the moment of transfer.

For each stage, the monitoring plan (Table 19-1) indicates the parameters to be measured, the frequency, the technology used and the location for each activity. The expected duration of each monitoring period is also indicated.

### 13.3.5 *Report monitoring results*

Prior to the start of injection activities, a baseline report will be compiled, describing the starting state of the wells and the storage site. This is the basis that will be used to map any changes.

An annual report of the monitoring results will be presented to the competent authority. The report should hold operational information, possible anomalous situations and information towards closure and transfer.

Prior to both site closure and site transfer a report is compiled, recording the state of both the well and the subsurface.

### 13.3.6 *Conclusion*

#### **Deviations from expectations**

Deviations from any expected behaviour of the storage complex may indicate migration or leakage of the injected CO<sub>2</sub>. In the P18-2 case the main activities in determining such deviations from the expected behaviour consist of monitoring the CO<sub>2</sub> pressure and temperature.

A thorough and reliable history match has been established. Deviations from the expected pressure development (p/Z curve) throughout and after the operational phase, could be an indicator of migration of CO<sub>2</sub> from the reservoir or leakage from the storage complex. To this end the pressures at the top of the wells are measured in any case (in the wellhead) as well as the pressures at the bottom of the wells (downhole).

Should unexpected deviations be measured and migration of CO<sub>2</sub> from the reservoir be suspected, measures need to be taken. Taking into account the comments about the application of seismic methods in the case of CO<sub>2</sub> storage in depleted gas fields given in Section 13.2.2, these may include time-lapse seismic monitoring, which allows possible migration paths or shallow CO<sub>2</sub> accumulations to be detected with an expected observation threshold of several tens of kilotons. The detection limit and measurement precision will be specified with the submission of the revised monitoring plan prior to injection and after detailed engineering.

The shallower the gas accumulation occurs, the better the chance that it can be detected. Baseline monitoring prior to injection will be used to make an inventory of pockmarks already present. This will allow the change with respect to the initial situation to be determined in case of a possible migration or leakage.

#### **Well integrity**

Various techniques are used to monitor the integrity of the (injection) wells. These include:

- Logging across the depth of the well;
- Measurement of the pressures in the annuli;
- Periodic analysis of the liquids in the annuli, in order to test for the presence of CO<sub>2</sub>.

Prior to the commencement of CO<sub>2</sub> injection, each injection well will be worked over and its state will be recorded as the baseline for later determinations of the integrity

of the well. After injection, the well will be safely sealed and permanently abandoned. However, before the well is entirely abandoned, there will first be a period in which the integrity of the plug (FFP) is measured at seal level. These measurements consist of tests monitoring the annular pressures, logs and taking samples of the liquids from the well above the seal in order to analyse for the presence of CO<sub>2</sub>.

#### **Monitoring of the seabed**

Finally, there is monitoring of the seabed. This is mainly in order to show that there are no changes and therefore there is no migration of CO<sub>2</sub> to the seabed. Various acoustic technologies (multibeam echo sounding, side scanning sonar, etc.) can be used to identify changes in and at the seabed as a result of changes in the deep underground (often in the shape of pockmarks) and possible CO<sub>2</sub> bubble streams in the water column. In addition, seabed samples (via coring) can be used to establish the presence or absence of leaking CO<sub>2</sub>.

### **13.4 Interpretation**

Abovementioned aspects have led to the monitoring plan presented here. The following aspects will be monitored:

- Injection process
- Well integrity
- Reservoir integrity
- Environmental monitoring (for leakage of CO<sub>2</sub> from the storage complex)

#### *13.4.1 Categories*

Monitoring of CO<sub>2</sub> storage can be achieved either by measuring the absence of any leakage through direct detection methods, or by verifying indirectly that the CO<sub>2</sub> is behaving as expected in the reservoir based on static and dynamic modelling and updating thereof corroborated by monitoring data. The main challenge for measuring absence of any leakage consists of spatial and temporal coverage of the monitoring method, i.e. "Where and when do we need to monitor in order to be sure that no leakage occurs". The strategy should therefore be based on identified risks.

For the indirect model-based monitoring the emphasis is more on scenario confirmation. As long as monitoring data demonstrates that the storage system is behaving according to the predictive models, the understanding of both the processes occurring and the behaviour of the storage complex can be considered sufficient. In case of significant deviations, one should find the causes of the deviations and where necessary recalibrate the models and perform new predictive simulations. If however the deviations fall well beyond the uncertainty ranges of the predictive models, then additional monitoring and possibly contingency measures need to be taken.

In practice often a combination of approaches is applied required and the optimum monitoring plan will be guided by the risk assessment and the site characterization.

Following the NSBTF (2009) and the draft EU guidance documents (EU, 2011), the following categories for monitoring are identified:

1. Mandatory monitoring: in any case for all sites. A number of parameters to be monitored is mandatory based on the EU storage directive (EU, 2009).

2. Required monitoring: site specific. This monitoring group is directed to gathering evidence for containment in the reservoir and to demonstrate integrity of seal, fault and wells in case of regular development.
3. Contingency monitoring. The third group refers to a contingency monitoring system which will only be installed if irregularities show up. In the CCS Directive a “significant irregularity” is defined as ‘...any irregularity in the injection or storage operations or in the condition of the storage complex itself, which implies the risk of a leakage or risk to the environment or human health’.

It is to be noted that these three categories as such have not been implemented in Dutch legislation, therefore the term *mandatory* should be read as “mandatory following the CCS Directive”. Similar for the term *required*, which is not as such defined in legislation. Required in the context of this report means a preliminary proposal of essentially risk-based monitoring with the current state of knowledge.

The quantification of a leakage at the sea bottom for ETS purposes is considered as part of the contingency monitoring. Quantitative monitoring for ETS will only be required, if there is an indication of leakage. For the North Sea the strategy suggested by NSBTF (2009) would be to detect leakage to the surface by geophysical methods like seismic data (detection of gas chimneys) or sea-bottom echo-sounding (detection of pockmarks) and then sample these leakage areas for direct CO<sub>2</sub> detection repeatedly. Based on the sampling profiles an estimate can be made of leakage rates over time for the area. In case of wellbore leakages an additional monitoring program in and around the well is suggested.

In the operational execution, the following categories are distinguished, and for each category the measurements performed for general testing are indicated, as well as the measurements that relate to gaining insight into deviations and to conclusion and transfer.

### 13.5 The monitoring plan

Following NSBTF (2009) and the draft EU guidance documents (EU, 2011), Table 13-1 lists the categories for monitoring that have been identified, as well as the aspects to be monitored. Table 13-2 gives a summary of the monitoring plan describing the equipment or method that can be used to measure certain processes.

The complete monitoring plan for P18-2, in the form of a table, is given in Table 19-1. Below is a description of the parameters mentioned in the table. These parameters follow both from the mandatory monitoring obligations as stipulated by the storage directive and the risk assessment.

#### Column 1

The first column describes the parameters to be monitored. These parameters follow both from the mandatory monitoring obligations as stipulated by the storage directive and from the risk assessment.

Table 13-1. Summarized monitoring classification table.

	<b>Mandatory (Mandatory monitoring according to Annex II of the EU directive)</b>	<b>Required (Preliminary estimation of required monitoring)</b>	<b>Contingency monitoring</b>
<b>Injection process</b>	Flow, pressure, temperature and composition of injected CO <sub>2</sub>		
<b>Well integrity</b>	Various Integrity measurements, well head pressure & temperature	Various baseline measurements, plug integrity measurements	
<b>Reservoir integrity</b>	Flowing pressure and temperature measurements	Stabilized pressure and temperature measurements	Seismic survey in case of irregularities
<b>Environmental monitoring</b>		Various baseline measurements, Microseismic monitoring	Various surveys in case of irregularities

**Column 2**

The second column indicates the proposed technique adopted to measure the parameter. A more detailed description of the technique is provided outside the table.

**Column 3**

The third column indicates the category of monitoring (mandatory according to the EU directive, required, contingency).

**Column 4 and 5**

The fourth and fifth columns give a description of both the temporal frequencies (column 4) and spatial coverage (column 5) of the data acquisition foreseen in the different phases of the project (pre-injection, injection and post-injection including long-term stewardship after transfer of responsibility). The rationale behind the monitoring strategy related to the identified risks is described in the following section.

**Column 6**

Column six provides a description of the expected values that indicate normal behavior and of the expected accuracy of the monitoring method. Expected values and therefore this column is colored green.

**Column 7**

The seventh column indicates threshold values, where normal behavior as anticipated stops and where irregularities start. As long as the measured values remain below these threshold values, no actions are required (green column). In case threshold values exceeded, the seventh column (colored orange) defines specific actions. Upon exceeding threshold values, monitoring data suggest that the behavior of the storage system starts to deviate from expectations. This could for

example lead to recalibration of the models, but when persisting to more stringent measures.

### Column 8

In case the monitor values exceed the threshold defined in the eighth column (colored red), the highest alert phase starts and immediate actions (or contingency measures) as defined in the second sub column of column eight are required.

Table 13-2. Summary of specific monitoring equipment and methods to be used for monitoring of certain processes.

	<b>Injection process</b>	<b>Measurement equipment / method</b>
1	Injection rate	Flow meter
2	Injection stream CO <sub>2</sub> concentration	Samples & analysis: online system
3	Injection stream composition	Samples & analysis: Additional samples for calibration
4	Water measurement	Water measurement
5	Discontinuous emissions through leakage, venting or incidents	Combination of techniques
<b>Well integrity</b>		
6	Annular pressure	Pressure device (with alarm value)
7	Well integrity	Wireline Logging (selection of tool: CBL, PMIT, EMIT, USIT, WAF, optical)
8	Well head pressure	Pressure device
9	Well head temperature	Temperature device
10	Plug integrity	Pressure test and additional inspections
<b>Reservoir integrity</b>		
11	Reservoir pressure (FBHP) (see also line 8)	pressure device
12	Reservoir Temperature (FBHT) (see also line 9)	thermometer or DTS
13	Stabilized pressure (CIBHP) (gradient) during shut-in period	pressure device combined with shut-in
14	Stabilised temperature (CIBHT) (gradient) during shut-in period	thermometer or DTS combined with shut-in
15	Suspected leakage	Surface seismic survey
<b>Environmental monitoring</b>		
16	Pockmarks at the seabed	Multi-beam echosounding
17	Presence of shallow gas or gas chimneys in the subsurface	Baseline seismic data
18	Migration pathways for gas in the shallow subsurface	Time-lapse seismic data acquisition (2D or 3D)
19	CO <sub>2</sub> in soil at pockmarks	Gas samples using vibrocore + lab analysis
20	Bubble detection at wellhead	Acoustic bubble detector
21	Microseismic monitoring	Permanent geophones or DAS in monitoring wells

### Items to be monitored

The next part of the monitoring plan describes the different items or events to be monitored (Injection process, Well integrity, Reservoir Integrity, Environmental Monitoring) and over which time frame (Pre-injection, Injection, Post-injection, etc). See Table 19-2.

It is noted that the timing for monitoring of the post injection period including the abandonment of the wells and the decommissioning of the platform and the period to the transfer of liability to the state have not been defined in this plan. The definition of these periods will be subject of discussion with State Supervision of the Mines (SodM).

#### 13.5.1 *Proposed monitoring methods*

This section provides more detailed background information on the rationale behind the selection of the proposed monitoring techniques. For each section corresponding to an identified actor in the risk analysis the primary relevant monitoring techniques are referred to between brackets by their number as appearing in the first column in Table 19-1. Monitoring techniques for contingency monitoring are not given between the brackets, this to not overcomplicate the overview below. Techniques relevant for contingency monitoring are indicated in Table 19-1.

##### 13.5.1.1 *Reservoir / injection process (1,2,3,4,5,8,9,11,12,13,14)*

The risk identified from leakage of CO<sub>2</sub> out of the reservoir / storage site where:

- Spilling (via spill point), or
- Sealing capacity of fault zone between P18-2 and P18-6.

Based on the history match of the P18-2 reservoir the field can be considered as a “tank model”, without an active aquifer drive. Therefore CO<sub>2</sub> is expected to disperse throughout the original gas reservoir.

Often – and this applies only to storage of CO<sub>2</sub> in saline aquifers - the key tool for reservoir / CO<sub>2</sub> plume imaging is 3D surface seismic, however this technique is not deemed suitable for P18-2. This is because of the considerable depth of the P18-2 storage reservoir, which renders surface seismic methods less effective. Additionally, for P18-2 the presence of (residual) gas within the reservoir makes the feasibility of repeated seismic surveys for the monitoring of CO<sub>2</sub> dispersion questionable, as seismic data cannot discern between CO<sub>2</sub> and residual gas.

The main components for monitoring deviations in expected behaviour indicating potential migration out of the reservoir or storage complex consist of pressure (and temperature) monitoring. After proper history matching, a deviation from the expected pressure trend (P/z curve) during and after the operational phase is an indicator for potential migration out of the storage complex. As for the P18-2 reservoir, pressure monitoring has the potential to be a powerful tool, since there is no strong aquifer drive masking potential deviations. A rough estimation of the threshold of the mass of CO<sub>2</sub> migration out of the reservoir that can be detected is in the order of 2-10 ktonnes of CO<sub>2</sub>. The exact value depends on the quality of the P/z curves with proper and reliable pressure measurements. Factors like water influx, communication with neighboring compartments or CO<sub>2</sub> dissolution in water

have a negative effect on the detectability. In addition, the measurement accuracy of inflow rates should be taken into account.

Proper pressure measurements can be obtained from the injection well after a shut-in, or continuously from a “monitoring” well. The latter is the preferred option allowing a continuous measurement of the reservoir pressure in equilibrium. In case the reservoir pressure is measured in the injection well after a shut-in, pressure equilibration should be measured over a time interval in the order of days. Based on the latter, the equilibrium pressure can be extrapolated (if it has not already been reached in this period).

Migration in the reservoir can be followed by additional geophysical logs (RST logs) well tests and downhole fluid samples at monitoring wells to detect CO<sub>2</sub> breakthrough. During the injection phase, microseismic monitoring and innovative pulse testing techniques may provide data on the location of the advancing CO<sub>2</sub> temperature front by detecting thermal fracturing (if any), and density/viscosity differences. The latter is not considered as an absolutely required measurement for CO<sub>2</sub> tracking, but is recommended. Furthermore the CO<sub>2</sub> can be traced as it closes in on boundary faults or moves toward spill points.

#### 13.5.1.2 *Well integrity (6,7,8,9,10,11,12,13,14,16)*

The key tool for monitoring well integrity is logging, aimed both directly at the wellbore (cement bond logging, etc.), but also at the surrounding formations (saturation logging). Pressure-temperature logging and downhole fluid chemistry are also potentially very useful. Non-well-based tools include 2D or 3D surface seismic for volumetric imaging of the overburden around the wellbores and multibeam echosounding to detect surface changes around the wellbore. During the injection stage, well-based microseismic monitoring can also provide information on flow and degradation processes around the wellbores.

#### 13.5.1.3 *Caprock/overburden (11,12,13,14,16,17,21)*

Caprock integrity is assumed intact as long as no abnormal behaviour of the pressure is observed. In case significant deviations are observed, contingency monitoring is required; potentially useful techniques include time-lapse seismic surveys to detect migration pathways (chimneys) or shallow gas accumulations. 2D surface seismic surveys may be a cost-effective alternative to full 3D, but will not provide full areal coverage of the top seal.

The threshold value of seismically detectable shallow accumulations of CO<sub>2</sub> is in the order of 10's of ktonnes under the condition that CO<sub>2</sub> accumulates as a concentrated gas pocket. The shallower the CO<sub>2</sub> accumulates, the better the chances of picking up the signal.

During the injection phase, microseismic monitoring provides data on whether the top seal is being geomechanically compromised. The feasibility of using wells as monitoring wells for microseismic monitoring has not been thoroughly explored yet, but may be regarded as a option, for example during periods when an injection well is shut in.

#### 13.5.1.4 *Faults (11,12,13,14,21)*

Thermal reactivation of faults is identified as a risk with risk classification B-2 (Section 12.3). If the cold front of the injected CO<sub>2</sub> reaches a fault, the likelihood of activation increases. In order to reduce this risk, the advancement of the cold front

from the injector wells to nearby faults needs to be managed and monitored.

Pressure and temperature monitoring data needs to be used in combination with non-isothermal reservoir simulations to assess whether the cold front stays away from the faults within and bounding reservoir compartments.

During the injection phase, microseismic monitoring as well as advanced well tests (pulse testing) may provide data on the location of the migrating CO<sub>2</sub> front. Geophysical logs would not provide reliable indications of generalized CO<sub>2</sub> migration, except where free CO<sub>2</sub> accumulates in very close proximity to the wellbores.

The threshold value of seismically detectable accumulations of CO<sub>2</sub> in the overburden is in the order of 10's of ktonnes, depending on the depth and geophysical properties of the reservoir and surrounding rocks. In the P18-2 case this is considered a contingency measurement. Just like sampling fluids of shallower aquifers can show traces of leaking CO<sub>2</sub>. To detect the absence of migration to the seabed, various types of surveys are an option. These will be able to identify pockmarks or bubbles and check for composition and origin.

#### 13.5.1.5 *Calibration of flow simulations (1,2,3,4,5,8,9,11,12,13,14)*

The calibration of flow simulations combines aspects of several of the above aims, effective reservoir management, accurate pressure and temperature monitoring and insights into fine-scale and geochemical processes. Likely tools are downhole pressure/temperature measurements, RST logs and monitoring breakthrough in monitoring wells. For P18-2 where 3D seismic imaging of CO<sub>2</sub> in the reservoir is considered difficult if not impossible, downhole pressure/temperature is the key technology. As in a number of cases above, microseismic monitoring and pulse testing (an advanced way of well testing) may be useful in the injection phase.

### 13.6 **Conclusion**

The adopted monitoring approach for CO<sub>2</sub> storage in P18-2, builds on the results of the site characterization and the risk assessment. The reservoir has been classified as suitable for CO<sub>2</sub> storage; the reservoir offers stable long-term containment. This conclusion is essentially based on a) the fact that natural gas has been contained in these reservoirs for millions of years, b) the knowledge of the reservoirs obtained during exploration and production of the fields, c) the fact that at the end of injection the pressure in the reservoir will be lower than that of surrounding formations.

The monitoring plan proposed is designed to verify CO<sub>2</sub> containment and storage reservoir integrity while and after the storage facility is in operation. This is achieved by both measuring the absence of any leakage through direct detection methods (for example at the wells), and by verifying indirectly that the CO<sub>2</sub> is behaving as expected in the reservoir by collecting pressure, temperature and injection rate data that feed in to static and dynamic modelling. The design includes therefore the collection of data such as representative storage pressures and annuli pressures, injected volumes and gas qualities, well integrity measurements, reservoir conditions, micro seismicity and sea bottom measurements.

The main component for monitoring deviations in expected behaviour indicating potential migration out of the reservoir consists of pressure and temperature monitoring. After proper history matching any deviations from the expected pressure trend (P/z curve) during and after the operational phase is a potential

indicator for migration out of the storage reservoir. Reservoir pressures will be determined regularly via shut-in of injection wells or monitoring wells. Downhole pressure tests are envisaged to verify the storage pressures and to verify the conversion of the wellhead pressures to downhole pressures.

Only in case irregularities are observed in seismicity pressure, or the temperature behaviour and when migration in the overburden is suspected, additional monitoring is proposed, like time-lapse seismic monitoring to detect possible migration pathways (chimneys) or shallow gas accumulations. The threshold value of seismically detectable accumulations of CO<sub>2</sub> is of the order of 10's of ktonnes under the likely condition that CO<sub>2</sub> accumulates as a concentrated gas pocket in shallower aquifers. The shallower the CO<sub>2</sub> accumulates, the better the chances of picking up the signal.

The key tools for monitoring well integrity consist of (repeated) logging, measuring the annuli pressures and regular analysis of the annuli fluids for the presence of gas or CO<sub>2</sub>. Prior to CO<sub>2</sub> injection a proper assessment of the current state of the existing wells is carried out, as well as work-overs. Before abandonment, wells will be suspended for a period of time to verify the quality of the plugs at caprock level by gas tests, monitoring of annuli pressures and possibly sampling of fluids from the well to monitor for the presence of CO<sub>2</sub>.

Finally, shallow monitoring, to detect the absence of migration to the seabed, in the form of multi-beam echosounding, side scanning sonar or high-resolution 3D surveys can be considered for identifying pockmarks or bubbles. Furthermore, sampling fluids in the soil at the sea bottom (via cores) can be used to verify the absence of traces of migrating CO<sub>2</sub>. The locations of the sampling will essentially be associated with the well positions, but additional locations can be selected based on multi-beam echosounding results.

In both cases, echosounding and fluid sampling, these types of monitoring should be performed when there is reason to suspect loss of containment and significant leakage out of the storage complex.

## 14 Conclusions

All risks identified that are related to the potential leakage of CO<sub>2</sub> out of the P18-2 storage site during or after CO<sub>2</sub> injection have been studied in detail and classified in a risk register. Most of the risks have been classified as 'low', with 'very low likelihood' that 'nil to negligible amount of CO<sub>2</sub> migrates out of the reservoir' (risk classification A-1). The remaining risks with slightly higher likelihood and/or consequence are related to (1) lateral CO<sub>2</sub> migration out of the storage reservoir, (2) the integrity of the wells in the field, and (3) the stability of the faults in the storage system.

- (1) Simulation of the behaviour of CO<sub>2</sub> after injection into the storage formations shows that there is a possibility for the CO<sub>2</sub> to move into the attached water-filled formation (but remain within the storage complex). Simulations show that when CO<sub>2</sub> injection is stopped before the initial reservoir pressure is reached the CO<sub>2</sub> is retained within the original gas-filled reservoir and will not leave the storage complex.
- (2) Analysis of available data on the integrity of the wells in the P18-2 field shows that a workover is required for each of the injection wells. Once these are performed, the risk of CO<sub>2</sub> leaking along wells, based on pre-injection status, is considered low.

The initial low reservoir pressure leads to low temperature of the CO<sub>2</sub> at the bottom of the well, causing significant temperature gradients in the well. These might lead to de-bonding of well liner (casing) and cement, potentially allowing leakage pathways to form (micro-annuli) for CO<sub>2</sub>. However, only when the pressure in the reservoir is above hydrostatic pressure could CO<sub>2</sub> enter these micro-annuli and potentially migrate into overlying aquifers. Therefore, the pressure in the reservoir is to be maximized at hydrostatic pressure, to reduce the likelihood of CO<sub>2</sub> flowing through these micro-annuli to small to negligible.

- (3) The cold CO<sub>2</sub> is injected into the reservoir formations, where it will create a low-temperature zone around the injection wells. If this zone could reach faults that are present in the reservoir, fault stability might be affected; however, at the same time, faults become more stable during the injection process due to increasing reservoir pressure. Monitoring of injection rate and temperature is required to track the pressure and temperature development in the reservoir and ensure that faults remain stable. All analysis points to small to negligible probability of fault reactivation; the caprock of 450 m to 750 m thick ensures that, fault destabilization, if any, will not lead to CO<sub>2</sub> movement through the caprock.

### *Recommendations*

- (1) In the study presented here the modelling of the injection process was performed with an isothermal reservoir simulator that could not simultaneously handle pressure and temperature variations in the reservoir. The impact of the low temperature of the injected CO<sub>2</sub> was estimated through the use of an additional simulator and analytical approaches and of scenarios that bring out potential effects. While the results are considered sufficient for the assessment

of the risks associated with CO<sub>2</sub> storage, detailed simultaneous modelling of pressure and temperature in the storage formations is required prior to the start of injection. This is needed for pressure and temperature predictions that are sufficiently reliable for the management of the injection process and for the interpretation of monitoring data.

- (2) The aim of the present study was to provide the basis for a storage permit application, by understanding the response of the storage formations, the caprock, the faults and the wells to the injection of CO<sub>2</sub>. The study established that conditions can be found under which CO<sub>2</sub> can be injected and stored safely and securely in the P18-2 field. The study did not aim to arrive at a complete and detailed description of these conditions. Such an 'operational plan' for CO<sub>2</sub> injection into the P18-2 field will be required prior to the start of injection, as a basis for the detailed monitoring plan and for the operational management of the injection process. The present study is the first step towards the P18-2 operational plan.

## 15 References

- Adelinet M., Nauroy J-F., Graham C.C., Cuss R.J., Wiseall A.C., Bakker E., Spiers C.J. and Hangx S.J.T. (2014). Progress report with data on processes, constitutive relations and parameters for modelling work. EU FP7 UltimateCO<sub>2</sub> Deliverable D4.5.
- Akemu O., Miersemann U., Benedictus T., Nepveu M. and Desroches J. (2011). Well integrity assessment of the P18 gas field (TAQA), CATO2 report WP3.4-D22.
- Ames R. and Farfan P.F. (1996). The environments of deposition of the Triassic Main Buntsandstein Formation in the P and Q quadrants, offshore the Netherlands. In: Rondeel H.E., Batjes D.A.J., Nieuwenhuijs W.H. (eds) *Geology of Gas and Oil under the Netherlands*. Springer, Dordrecht. pp 167-178.
- Bacci G., Korre A. and Durucan S. (2011). An experimental and numerical investigation into the impact of dissolution/precipitation mechanisms on CO<sub>2</sub> injectivity in the wellbore and far field regions. *International Journal of Greenhouse Gas control* 5, 579-588.
- Baines S.J., and Worden R.H. (2004). *Geological Storage of Carbon Dioxide*. Geological Society, London, Special Publications 233, 59-85.
- Barnes J. and Hut P. (1986). A hierarchical O(N log N) force-calculation algorithm. *Nature*, 324, 446-449.
- Bakker E., Hangx S.J.T., Niemeijer A.R. and Spiers C.J. (2016). Frictional behaviour and transport properties of simulated fault gouges derived from a natural CO<sub>2</sub> reservoir. *International Journal of Greenhouse Gas Control* 54, 70-83.
- Baumann G., Henniges J. and De Lucia M. (2014). Monitoring of saturation changes and salt precipitation during CO<sub>2</sub> injection using pulsed neutron-gamma logging at the Ketzin pilot site. *International Journal of Greenhouse Gas Control* 28, 134-146.
- Belfroid, S. (2019). Porthos – CO<sub>2</sub> injection, TNO report TNO 2019 R10335.
- BP (2007). P/18 Field Petrophysical Study. Company report, 13 p.
- Candela, T., van der Veer, E.F., Fokker, P.A. (2018). On the importance of thermo-elastic stressing in injection-induced earthquakes, *Rock Mechanics and Rock Eng.*, 51 (12), 3925-3936.
- Duguid A. and Scherer G.W. (2010). Degradation of oilwell cement due to exposure to carbonated brine. *International Journal of Greenhouse Gas Control* 4, 546-560.
- Energy Institute (2019). Hearts and Minds toolkit – Risk assessment matrix. website, version 15 Oct 2019.  
<https://publishing.energyinst.org/heartsandminds/toolkit/RAM>.
- EPA (2012). *Geologic Sequestration of Carbon Dioxide Underground Injection Control (UIC) Program Class VI Well Construction Guidance* (May 2012).
- ETS directive (2009): DIRECTIVE 2009/29/EC OF THE EUROPEAN PARLIAMENT AND OF THE COUNCIL of 23 April 2009 amending Directive 2003/87/EC so as to improve and extend the greenhouse gas emission allowance trading scheme of the Community EU Guidance Document 2 (draft 2010): Site Characterisation, CO<sub>2</sub> Stream Composition, Monitoring and Corrective Measures. Draft document for consultation version June 17, 2010.

- EU (2009): DIRECTIVE 2009/31/EC OF THE EUROPEAN PARLIAMENT AND OF THE COUNCIL of 23 April 2009 on the geological storage of carbon dioxide and amending Council Directive 85/337/EEC, European Parliament and Council Directives 2000/60/EC, 2001/80/EC, 2004/35/EC, 2006/12/EC, 2008/1/EC and Regulation (EC) No 1013/2006.
- EU (2011). Implementation of Directive 2009/31/EC on the Geological Storage of Carbon Dioxide. Guidance document 2: Characterisation of the storage complex, CO<sub>2</sub> Stream Composition, Monitoring and Corrective Measures.
- EU (2017). EU Guidance Document (MRGs); The Monitoring and Reporting Regulation – General guidance for installations; Updated November 2017.
- EU (2018). Commission Implementing Regulations (EU) 2018/2066 of 19 December 2018 on the monitoring and reporting of greenhouse gas emissions pursuant to Directive 2003/87/EC of the European Parliament and of the Council and amending Commission Regulation (EU) No 601/012.
- Fisher Q. (2013). Collection of petroleum field analogues data and description of risks of CO<sub>2</sub> leakage along faults. EU FP7 UltimateCO<sub>2</sub> Deliverable D4.1.
- Fischer, H., Orlic, B., Osinga, S., Hopmans, P., Wollenweber, J., Geel, K. (2016). Options to initiate and enhance ductile properties of shale for well bore sealing. “TKI Plugging wells by enhanced formation ductility” - Deliverable report D5.1; TNO report 2016 R10970.
- Furre, A.-K., Eiken, O., Alnes, H., Vevatne, J.N., Kiær, A.F. (2017). 20 years of monitoring CO<sub>2</sub>-injection at Sleipner, Energy Procedia, 114, 3916-3926.
- Gaus I., Zazroual M. and Czernichowski-Lauriol I. (2005). Reactive transport modelling of the impact of CO<sub>2</sub> injection on the clayey cap rock at Sleipner (North Sea). Chemical Geology 217, 319-337.
- Geel, C.R. (2016). Geological screening of ductile formations. “TKI Plugging wells by enhanced formation ductility” - Deliverable report D4.1; TNO report 2016 R10273.
- Geertsma, J. (1973). A basic theory of subsidence DUE to reservoir compaction: The homogeneous case. Verhandelingen Koninklijk Nederlandsch Geologisch Mijnbouwkundig Genootschap 2S, 43-61.
- Gilfillan S.M.V., Lollar B.S., Holland G., Blagburn D., Stevens S., Schoell M., Cassidy M., Ding Z., Zhou Z., Lacrampe-Couloume G. and Ballentine C.J. (2009). Solubility trapping in formation water as dominant CO<sub>2</sub> sink in natural gas fields. Nature 458, 2 April 2009, doi:10.1038/nature07852.
- Grude S., Landrø M. and Dvorkin J. (2014). Pressure effects caused by CO<sub>2</sub> injection in the Tubåen. Fm., the Snøhvit field. International Journal of Greenhouse Gas Control 27, 178-187.
- IEAGHG (Greenhouse Gas Programme) (2016). Impact of impurity on CO<sub>2</sub> compression, liquefaction and transportation, Report 2016/01.
- IEAGHG (2018). Well Engineering and Injection Regularity in CO<sub>2</sub> Storage wells, IEAGHG Technical Report, 2018-08.
- ISO/TC 67/SC 4 Drilling and production equipment. (2017). *ISO 16530-1:2017: Petroleum and natural gas industries - Well integrity - Part 1: Life cycle governance*. bsi.
- Kim K.-Y., Han W.S., Oh J., Kim T. and Kim J.-C. (2012). Characteristics of salt precipitation and the associated pressure build-up during CO<sub>2</sub> storage in saline aquifers. Transport in Porous Media 92, 397-418.
- Koenen M., Wasch L., Wollenweber J. and Tambach T. (2014). CATO-2 Deliverable WP3.4-D12. Experimental and modelling study into chemical

- degradation mechanisms and rates of cement subjected to aqueous and supercritical CO<sub>2</sub> at in-situ reservoir conditions.
- Koenen M. and Wasch L. (2018). The potential of CO<sub>2</sub> leakage along de-bonded cement-rock interface. 14th International Conference on Greenhouse Gas Control Technologies, GHGT-14. 21<sup>st</sup> – 25<sup>th</sup> October 2018, Melbourne, Australia.
- Kutchko B.G., Strazisar B.R., Dzombak D.A., Lowry G.V. and Thaulow N. (2007). Degradation of well cement by CO under geologic sequestration conditions. *Environmental Science and Technology* 41 (13), p4787-4792
- Loeve, D., Hofstee C. and Maas J.G.,(2014). Thermal effects in a depleted gas field by cold CO<sub>2</sub> injection in the presence of methane, *Energy Procedia*, Volume 63, p. 5378-5393.
- Mijnbouwwet, <https://wetten.overheid.nl/jci1.3:c:BWBR0014168&z=2019-04-10&g=2019-04-10>
- Mindlin, R.D. (1936). Force at a point in the interior of a semi-infinite solid, *Physics*, 7(5), 195–202.
- Miocic J.M., Gilfillan S.M.V., Frank N., Schroeder-Ritzrau A., Burnside N.M. and Haszeldine R.S. (2019). 420,000 year assessment of fault leakage rates shows geological carbon storage is secure. *Scientific Reports*, DOI:10.1038/s41598-018-36974-0.
- Miri R. and Hellevang H. (2016). Salt precipitation during CO<sub>2</sub> storage – A review. *International Journal of Greenhouse Gas Control* 51, 136-147.
- Myklestad, N.O. (1942). Two problems of thermal stress in the infinite solid, *Journal of Applied Mechanics*, 9, 136-143.
- Neele, F., Delprat-Jannaud, F., et al. (2013). Site characterization workflow, SiteChar report D1.4.
- Nepveu, M, Neele, F, Delprat-Jannaud, F, Akhurst, M, Vincké, O, Volpi, V, Lothe, A, Brunsting, S, Pearce, J, Battani, A, Baroni, A, Garcia, B, Hofstee, C, And Wollenweber, J. 2015. CO<sub>2</sub> storage feasibility: a workflow for site characterization, *Oil and Gas Science and Technology* 70, 4, 555–566.
- Nieuwland, D. A. (2012) Fault Seal Prediction in Sandstone Reservoirs - A quantitative and calibrated geomechanical method, 3rd International Conference on Fault and Top Seals - From Characterization to Modelling, Montpellier, France 1-3 October, 2012.
- NOGEP A - OPCOM. (2016, October 12). Industry Standard no. 45 - Well Decommissioning. NOGEP A.
- NORSOK. (2013). *Norsok standard D-010: Well integrity in drilling and well operations*
- North Sea Basin Task Force (NSBTF), 2009, Monitoring Verification Accrediting and Reporting (MVAR) Report for CO<sub>2</sub> storage deep under the seabed of the North Sea.
- Okada, Y. (1992). Internal deformation due to shear and tensile faults in a half-space, *Bull. Seism. Soc. Am.*, 82(2), 1018–1040.
- OSPAR (2007). OSPAR Guidelines for Risk Assessment and Management of Storage of CO<sub>2</sub> Streams in Geological Formations (Reference Number: 2007-12), Meeting of the OSPAR Commission, Ostend, 25-29 June 2007.
- Peach C.J., de Bresser J.H.P., van der Kroef R.F.M., Mols A., Verberne B.A. and Samuelson J. (2010). Site-representative caprock and fault rock samples acquired and characterised (1st Year Progress Report). CATO-2 Deliverable WP 3.03-D06.

- Pruess, K., (2011). ECO2M: A TOUGH2 Fluid Property Module for Mixtures of Water, NaCl, and CO<sub>2</sub>, Including Super- and Sub-Critical Conditions, and Phase Change Between Liquid and Gaseous CO<sub>2</sub>. LBML, Univ. Berkeley, Berkeley, CA (Updated Sept 2013).
- Rimmelé G., Barlet-Gouédard V., Porcherie O., Goffé B. and Brunet F. (2008). Heterogeneous porosity distribution in Portland cement exposed to CO<sub>2</sub>-rich fluids. *Cement and Concrete Research* 38, 1038-1048.
- ROAD (2018). Rotterdam capture and storage demonstration project, <https://ccsnetwork.eu/projects/road-project-rotterdam>.
- Roels S.M., Ott H. and Zitha P.L.J. (2014).  $\mu$ -CT analysis and numerical simulation of drying effects of CO<sub>2</sub> injection into brine-saturated porous media. *International Journal of Greenhouse Gas Control* 27, 146-154.
- Samuelson J., Spiers C., Koenen M. and Tambach T. (2012). Lab evaluation of the reactivation potential of simulated faults under CO<sub>2</sub> storage conditions – implications for system integrity and seismic risk. CATO-2 Deliverable WP 3.3 – D13.
- Shell (2015). Peterhead CCS Project, Well Technical Specification, Doc No.: PCCS-05-PT-ZW-7770-00001, 20/05/2015.
- SodM. (2019). *De integriteit van onshore putten*. SodM
- Spain D.R. and Conrad C.P. (1997). Quantitative analysis of top-seal capacity: offshore Netherlands, southern North Sea. *Geologie en Mijnbouw* 76, 217-226.
- Tambach T., van Bergen F., Gutierrez-Neri M., Hostee C., Koenen M., Kooi H., Loeve D., Maas J., Plug W.-J., Ranganathan P., Roels S., van der Meer B., Wasch L. and Zitha P. (2012). Models describing near-well clogging and mineralization to support feasibility and long-term integrity. CATO-2 Deliverable WP3.02-D13.
- Tambach T.J., Loeve D., Hofstee C., Plug W.-J. and Maas J.G. (2015a). Effect of CO<sub>2</sub> injection on brine flow and salt precipitation after gas field production. *Transport in Porous Media* 108, 171-183.
- Tambach T.J., Koenen M., Wasch L.J. and van Bergen F. (2015b). Geochemical evaluation of CO<sub>2</sub> injection and containment in a depleted gas field. *International Journal of Greenhouse Gas Control* 32, 61-80.
- TAQA (2009). CO<sub>2</sub> Offshore Storage Source to Sink. Presentation given by TAQA Energy B.V., 3 July 2009.
- TAQA (2018) Geophysical Evaluation P18. TAQA Internal report, 6 p.
- Tian H., Xu T., Zhu H., Yang C. and Ding F. (2019). Heterogeneity in mineral composition and its impact on the sealing capacity of caprock for a CO<sub>2</sub> geological storage site. *Computers and Geosciences* 125, 30-42.
- Van Balen, R.T., Van Bergen, G., De Leeuw, C., Pagnier, H.J.M., Simmelink, H., Van Wees, J.D., Verweij, J.M. (2000). Modeling the hydrocarbon generation and migration in the West Netherlands Basin, the Netherlands. *Netherlands Journal of Geosciences* 79, 29-44.
- Van Eijs, R., Kuijper, M. and Bisschop, R. (2011). Containment demonstration for the Barendrecht CO<sub>2</sub> storage project, *Energy Procedia*, 4, 4092-4099.
- Vandeweijer V. et al. (2011). Feasibility study P18 (final report). CATO2-WP3.01-D06.
- Vrålstad, T., Todorovic, J., Wollenweber, J., Abdollahi, J., Karas, D., & Buddensiek, M. (2015). *D8.1 - Description of leakage scenarios for consideration in the work in SP3*.

Williams, S., T. Carlsen, K. Constable, & A. Guldahl (2009) Identification and qualification of shale annular barriers using wireline logs during plug and decommissioning operations. SPE paper 119321, 15 p.

## 16 Appendix A. compliance with EU Storage Directive site characterisation and assessment

This appendix presents the links between the site characterisation and assessment elements in the EU Storage Directive (EU, 2009) and the site characterisation elements workflow pursued in the P18-2 feasibility study. Annex I of the EUSD is used here as a reference. This annex consists of three steps, each of which consists of a list of items. The Guidance Document #2 to the EU Storage Directive provides an explanation of all the list elements; there is no need to repeat that here. The table below is modified after the Site characterisation workflow in Appendix I of the SiteChar report D1.4 (Neele *et al.*, 2013).

### 16.1 Data collection (step 1)

	Storage Directive elements in step 1	Sections of the P18-2 feasibility study	Comments
(a)	Geology and geophysics	17 Appendix B	
(b)	Hydrogeology (in particular existence of ground water intended for consumption)	-	n.a.
(c)	Reservoir engineering (including volumetric calculations of pore volume for CO <sub>2</sub> injection and ultimate storage capacity)	17 Appendix B	
(d)	Geochemistry (dissolution rates, mineralisation rates)	-	Based on earlier studies
(e)	Geomechanics (permeability, fracture pressure)	17 Appendix B	
(f)	Seismicity	17 Appendix B	Related to fault stability in 12.3.3, 12.3.4
(g)	Presence and condition of natural and man-made pathways, including wells and boreholes which could provide leakage pathways	17 Appendix B	
(h)	Domains surrounding the storage complex that may be affected by the storage of CO <sub>2</sub> in the storage site	-	Based on earlier studies
(i)	Population distribution in the region overlying the storage site	-	n.a.
(j)	Proximity to valuable natural resources (including in particular Natura 2000 areas pursuant to Council Directive 79/409/EEC of 2 April 1979 on the conservation of wild birds(1) and Council Directive 92/43/EEC of 21 May 1992 on the conservation of natural habitats and of wild fauna and flora(2) ,	-	Addressed in EIA

	potable groundwater and hydrocarbons)		
(k)	Activities around the storage complex and possible interactions with these activities (for example, exploration, production and storage of hydrocarbons, geothermal use of aquifers and use of underground water reserves)	-	Addressed in EIA
(l)	Proximity to the potential CO <sub>2</sub> source(s) (including estimates of the total potential mass of CO <sub>2</sub> economically available for storage) and adequate transport networks	-	Not known at time of study; assumptions provided by client

## 16.2 Building the 3-D static geological earth model (step 2)

	Storage Directive elements in step 2	Sections of the P18-2 feasibility study	Comments
(a)	Geological structure of the physical trap	4.2, Appendix B: 17.1-17.5	
(b)	Geomechanical, geochemical and flow properties of the reservoir overburden (caprock, seals, porous and permeable horizons) and surrounding formations	4.2, 4.3, 4.4, 8.2, 8.3 Appendix B: 17.4	Geochemical properties based on earlier work
(c)	Fracture system characterisation and presence of any human-made pathways	4.2, 4.5, 9 Appendix B: 17.4	
(d)	Areal and vertical extent of the storage complex	10	
(e)	Pore space volume (including porosity distribution)	Appendix B: 17.4.3-17.4.5	
(f)	Baseline fluid distribution	Appendix B: 17.8	
(g)	Any other relevant characteristics	Appendix B: 17.7.5, 17.8.2, 17.8.3, 17.8.6	Gas production data, PVT, RFT and PLT data
(all)	The uncertainty associated with each of the parameters used to build the model shall be assessed by developing a range of scenarios for each parameter and calculating the appropriate confidence limits. Any uncertainty associated with the model itself shall also be assessed.	6.3.4 6.3.5 6.5.4 9.3 17.8.5	Injection rate Salt precipitation Mineral assemblage Cement bonding Well cross flow

### 16.3 Characterisation of storage dynamic behaviour, sensitivity characterisation, risk assessment (step 3)

Step 3 consists of several parts, which are discussed separately.

#### 16.3.1 Characterisation of the storage dynamic behaviour (step 3.1)

	<b>Storage Directive elements in step 3, characterisation of the storage dynamic behaviour</b>	<b>Sections of the P18-2 feasibility study</b>	<b>Comments</b>
(a)	Possible injection rates and CO <sub>2</sub> stream properties	5.2, 5.3, 6.2	
(b)	Efficacy of coupled process modelling (that is, the way various single effects in the simulator(s) interact)	6.3, 6.4 7.2, 7.3, 8.2, 8.3, 9.3	Thermohydraulic Thermomechanical
(c)	Reactive processes (that is, the way reactions of the injected CO <sub>2</sub> with in situ minerals feedback in the model)	6.5, 7.4, 9.3	
(d)	Reservoir simulator used (multiple simulations may be required in order to validate certain findings)	6.3.2, 6.4.2	
(e)	Short and long-term simulations (to establish CO <sub>2</sub> fate and behaviour over decades and millennia, including the rate of dissolution of CO <sub>2</sub> in water)	6.3 6.5	Short term Long term geochem.

#### 16.3.2 Insights from dynamic modelling (step 3.1)

	<b>Storage Directive elements in step 3, insights from dynamic modelling</b>	<b>Sections of the P18-2 feasibility study</b>	<b>Comments</b>
(f)	Pressure and temperature of the storage formation as a function of injection rate and accumulative injection amount over time	6.3, 6.4	
(g)	Areal and vertical extent of CO <sub>2</sub> vs time	6.3	
(h)	Nature of CO <sub>2</sub> flow in the reservoir, including phase behaviour	6.3, 6.4	
(i)	CO <sub>2</sub> trapping mechanisms and rates (including spill points and lateral and vertical seals)	4, 6.3, 10	
(j)	Secondary containment systems in the overall storage complex	10, 11	
(k)	Storage capacity and pressure gradients in the storage site	6.3, 6.4	
(l)	Risk of fracturing the storage formation(s) and caprock	7.2, 7.3, 8.2, 8.3, 12.2, 12.3	
(m)	Risk of CO <sub>2</sub> entry into the caprock	4.3, 8.3, 8.4, 12.2	

(n)	Risk of leakage from the storage site (for example, through abandoned or inadequately sealed wells)	12	
(o)	Rate of migration (in open-ended reservoirs)	11, 12.1	
(p)	Fracture sealing rates <sup>8</sup>	12.3.2	Qualitative; no rates
(q)	Changes in formation(s) fluid chemistry and subsequent reactions (for example, pH change, mineral formation) and inclusion of reactive modelling to assess affects	6.5, 7.4, 8.4, 9.3.4	
(r)	Displacement of formation fluids	-	
(s)	Increased seismicity and elevation at surface level	7	

### 16.3.3 Sensitivity characterisation (step 3.2)

This element of the EU Storage Directive reads: “Multiple simulations shall be undertaken to identify the sensitivity of the assessment to assumptions made about particular parameters. The simulations shall be based on altering parameters in the static geological earth model(s), and changing rate functions and assumptions in the dynamic modelling exercise. Any significant sensitivity shall be taken into account in the risk assessment.”

Sections of the P18-2 feasibility study: 6.3.4, 6.3.5, 8.4.2

Comments: Sensitivity to temperature, injection rate, mineral types

### 16.3.4 Risk assessment: hazard characterisation (step 3.3.1)

This element of the SDEU reads: “The hazard characterisation shall cover the full range of potential operating conditions to test the security of the storage complex. Hazard characterisation shall be undertaken by characterising the potential for leakage from the storage complex, as established through dynamic modelling and security characterisation described above. This shall include consideration of [the items in the table below]. The hazard characterisation shall cover the full range of potential operating conditions to test the security of the storage complex.”

	Elements of Storage Directive Risk assessment: hazard characterisation (step 3.3.1)	Sections of the P18-2 feasibility study	Comments
(a)	potential leakage pathways	9, 11, 12	
(b)	potential magnitude of leakage events for identified leakage pathways (flux rates)	7.4.4	Mostly qualitative
(c)	critical parameters affecting potential leakage (for example maximum reservoir pressure, maximum injection rate, temperature, sensitivity to various	12	

<sup>8</sup> The EU Guidance Document #2 does not offer an explanation as to the meaning of ‘fracture sealing rates’. Here, fracture sealing is assumed to be a combination of chemical reactions (resulting in mineral deposition in injection-induced fractures) and geomechanical processes (resulting in fractures closing).

	assumptions in the static geological Earth model(s))		
(d)	secondary effects of storage of CO <sub>2</sub> , including displaced formation fluids and new substances created by the storing of CO <sub>2</sub>	6.5, 7.4, 8.4	Displaced formation fluids: New substances
(e)	any other factors which could pose a hazard to human health or the environment (for example physical structures associated with the project)	-	n.a.

16.3.5 *Risk assessment: exposure assessment (step 3.3.2)*

This element of the SDEU reads: “Based on the characteristics of the environment and the distribution and activities of the human population above the storage complex, and the potential behaviour and fate of leaking CO<sub>2</sub> from potential pathways identified under Step 3.3.1.”

Sections of the P18-2 feasibility study: -

Comments: Not in scope of present study

16.3.6 *Risk assessment: effects characterisation (step 3.3.3)*

This element of the SDEU reads: “Based on the sensitivity of particular species, communities or habitats linked to potential leakage events identified under Step 3.3.1. Where relevant it shall include effects of exposure to elevated CO<sub>2</sub> concentrations in the biosphere (including soils, marine sediments and benthic waters (asphyxiation; hypercapnia) and reduced pH in those environments as a consequence of leaking CO<sub>2</sub>). It shall also include an assessment of the effects of other substances that may be present in leaking CO<sub>2</sub> streams (either impurities present in the injection stream or new substances formed through storage of CO<sub>2</sub>). These effects shall be considered at a range of temporal and spatial scales, and linked to a range of different magnitudes of leakage events.”

Sections of the P18-2 feasibility study: -

Comments: Not in scope of present study

16.3.7 *Risk assessment: risk characterisation (step 3.3.4)*

This element of the EU Storage Directive reads: “This shall comprise an assessment of the safety and integrity of the site in the short and long term, including an assessment of the risk of leakage under the proposed conditions of use, and of the worst-case environment and health impacts. The risk characterisation shall be conducted based on the hazard, exposure and effects assessment. It shall include an assessment of the sources of uncertainty identified during the steps of characterisation and assessment of storage site and when feasible, a description of the possibilities to reduce uncertainty.”

Sections of the P18-2 feasibility study: Chapter 12

Comments: Directed to characterisation of subsurface hazards

## 17 Appendix B. Subsurface model descriptions

### 17.1 Static model

#### 17.1.1 *New geological model – reasons*

Since the completion of the storage feasibility assessment for the P18-4 field (Vandeweyer et al., 2011), which produced a 3D reservoir model of all P18 fields, a number of developments necessitated the building of a new 3D reservoir model. Around 2014, the operators and co-owners of the P15-P18 blocks had the P15-P18 3D seismic survey reprocessed. A pre-stack, depth migrated (PSDM) version of the cube was now available, both in time and depth, as well as a velocity cube. An initial comparison of the Top Bunter interpreted from that cube with the one from the P18-4 study (Vandeweyer et al., 2011) revealed several important differences.

The most important differences were the location of the SW boundary fault of P18-2, particularly near the intended injector wells. In the new interpretation, the intended injector wells were at a larger distance from the fault, which might have a positive effect on the geomechanical behaviour of the fault when exposed to cold-CO<sub>2</sub> injection.

Another item that showed changes was the Top Bunter horizon, particularly in low-lying areas such as in the hanging walls of the boundary faults. Again, this might impact the geomechanical behaviour of these faults, as the vertical throw is now larger.

Further reasons for critically reviewing the P18-2 reservoir model are that in the 2011 P18-4 study (Vandeweyer et al., 2011) the emphasis was on the P18-4 compartment rather than the P18-2 compartment, and that since 2010 new production data have become available for all P18 compartments.

It was therefore decided to build a new reservoir model, based on a seismic interpretation on the new, reprocessed 3D cube.

### 17.2 Seismic interpretation

A substantial part of the Top Bunter and Top Keuper had already been interpreted by TAQA. Only a few blank areas needed to be done. After a review of the TAQA horizon and fault interpretations, the remaining blank areas of the reprocessed cube were interpreted. This was mostly the southeastern tip of the P18-2 compartment and its surroundings (Figure 17-1). In some places, TAQA's interpretation was slightly changed, e.g. Compartment 2-II of P18-2 (Well P18-02-A6ST1). This was mostly done in combination with the interpretation of the overlying Top Keuper, a conspicuous reflector.

Faults interpreted by TAQA were inspected and generally found to agree with the seismic data, although in some instances modifications were made on some of the faults. A few new faults were interpreted, mostly in the P18-2 compartment. This was partly done using the variance attribute with a 5x5x50 computing window (Figure 17-2). During the interpretation it was found that boundary fault F20 (see Figure 17-7) displaces the entire caprock, and even cuts through the Base

Cretaceous Unconformity where it displaces the Lower Cretaceous sands (Figure 17-3).

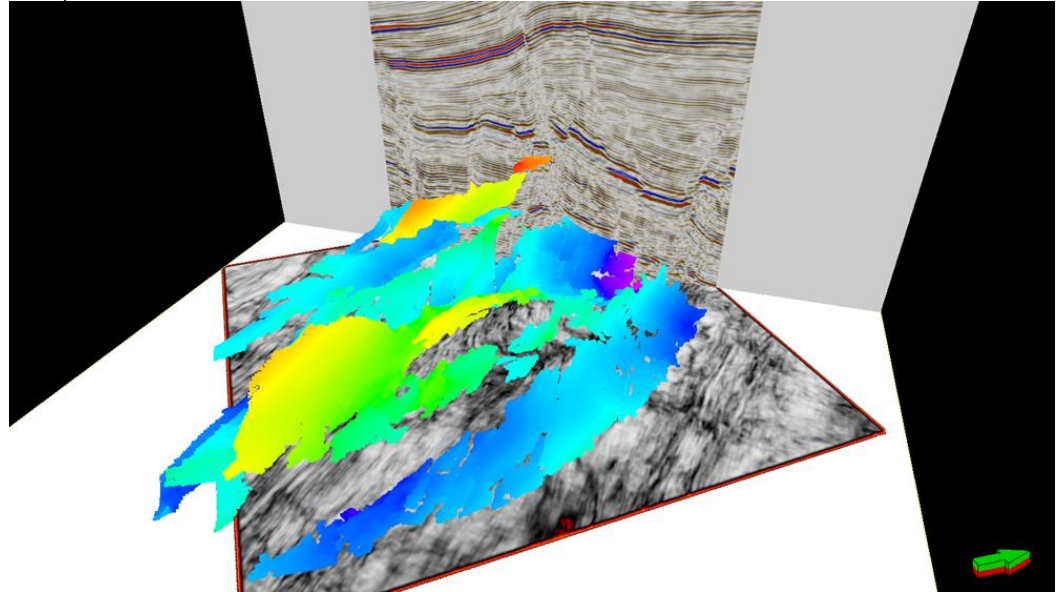


Figure 17-1: Oblique view on seismic interpretation of Top Bunter on the reprocessed P15-P18 3D cube.

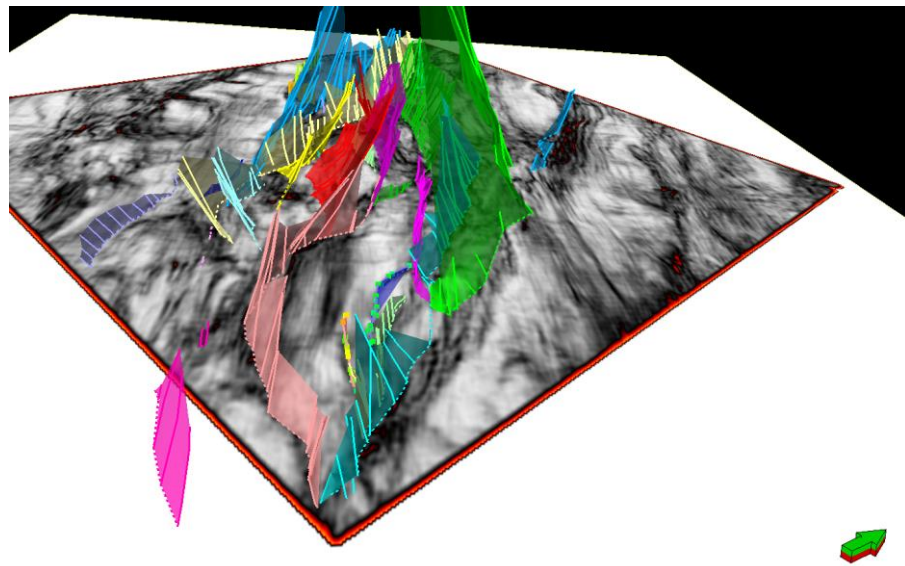


Figure 17-2: Checking existing fault interpretation and identifying additional faults with the variance attribute (5x5x50). Time slice through variance cube with interpreted faults.

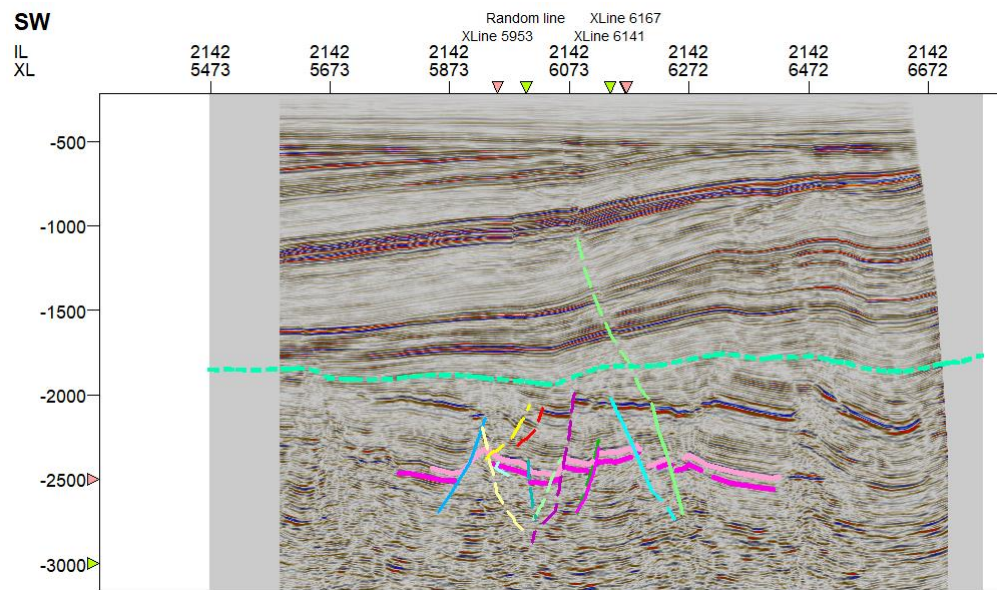


Figure 17-3: Seismic inline 2142 showing the top Bunter (purple horizon), Top Keuper (pink), and Base Cretaceous Unconformity (light green). Boundary Fault F20 (green) cuts through BCU.

### 17.3 Time-depth conversion

After consulting TAQA, it was found that the reprocessed P15-P18 cube came with a strongly improved velocity cube. It was therefore decided to adopt TAQA's velocity model which for the current project only contains two horizons: Top Keuper and Top Bunter (Table 17-1). In contrast to the velocity model that was used in the 2011 CATO study which was based on VELMOD and used six horizons, in the present model the entire overburden velocities above the Triassic are taken from the velocity cube (TAQA, 2018). For the Upper Germanic Trias itself a constant velocity of 4568 m/s was applied.

Table 17-1: Velocity model from TAQA as used in the current study

Interval	Top	Base	TZ conversion method
Overburden	MSL	Top Keuper	PSDM velocities
Upper Triassic	Top Keuper	Top Hardegsen	Constant velocity: 4568 m/s
LowerTr.-Perm.	Top Hardegsen	Top Carboniferous	Constant velocity: 4694 m/s

### 17.4 Petrel model building

Figure 17-4 shows the workflow that was followed to build the new static model. Apart from the newly interpreted faults, the horizons, and the new velocity model, all the necessary steps to build a reservoir model needed to be done. Thus, the horizons and zones were created, and a layering. For the property modelling the same procedure was followed as in the 2011 CATO model.

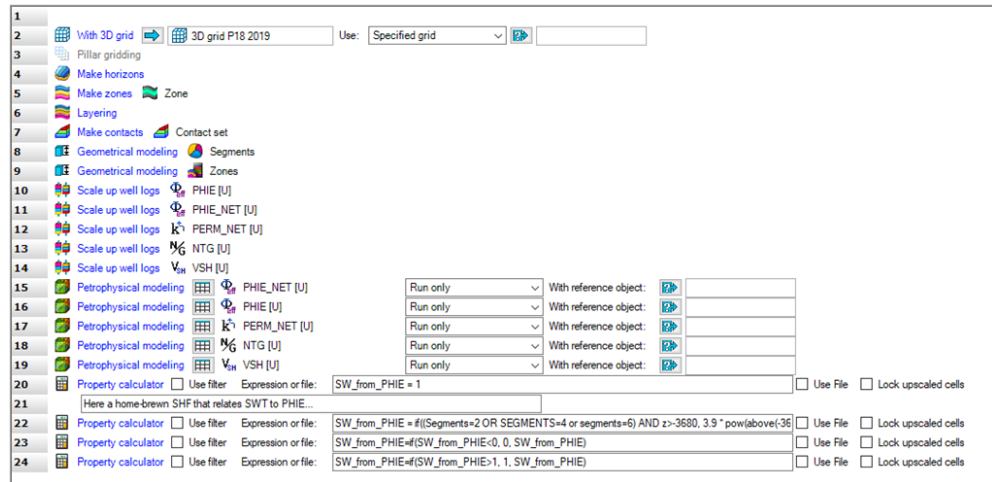


Figure 17-4: Petrel workflow that builds and populates the reservoir model.

17.4.1 *Fault model, gridding*

All depth-converted faults from TAQA were converted to model faults. However, several faults from the fault model were deleted, either because they were outside the area of interest, or because they were too small to be modelled. Quite some effort was spent on the creation of the fault model and pillar grid of the P18 area in order to ensure a smooth and regular grid that would cause as little problems in ECLIPSE as possible. Most slopes are faulting so the pillar grid needs to be vertically cut close to the base and top of the reservoir model. When the faults reach too shallow or too deep they tend to cross each other, after which Y-faults need to be constructed which usually ends in gridding and geometric problems. Figure 17-5 and Figure 17-7 show the end result of the fault construction and pillar gridding process. Names of the faults used in the current model are displayed in Figure 17-7. For the pillar gridding (Figure 17-6) an average X and Y increment of 50 m was specified.

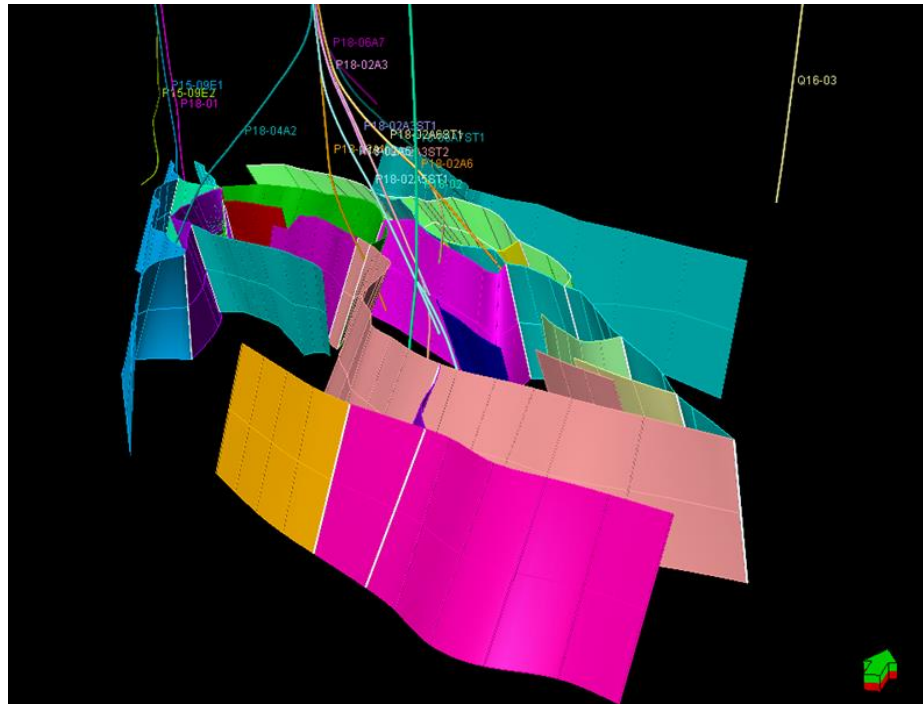


Figure 17-5: 3D view of all faults that have been incorporated in the pillar grid of the Petrel reservoir model.

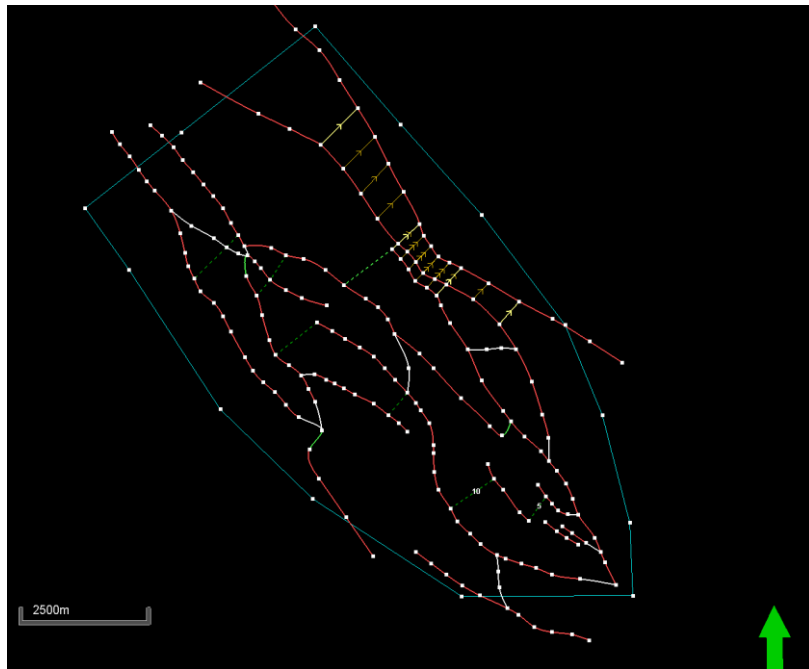


Figure 17-6: Map view of all faults and trends used in the pillar gridding.

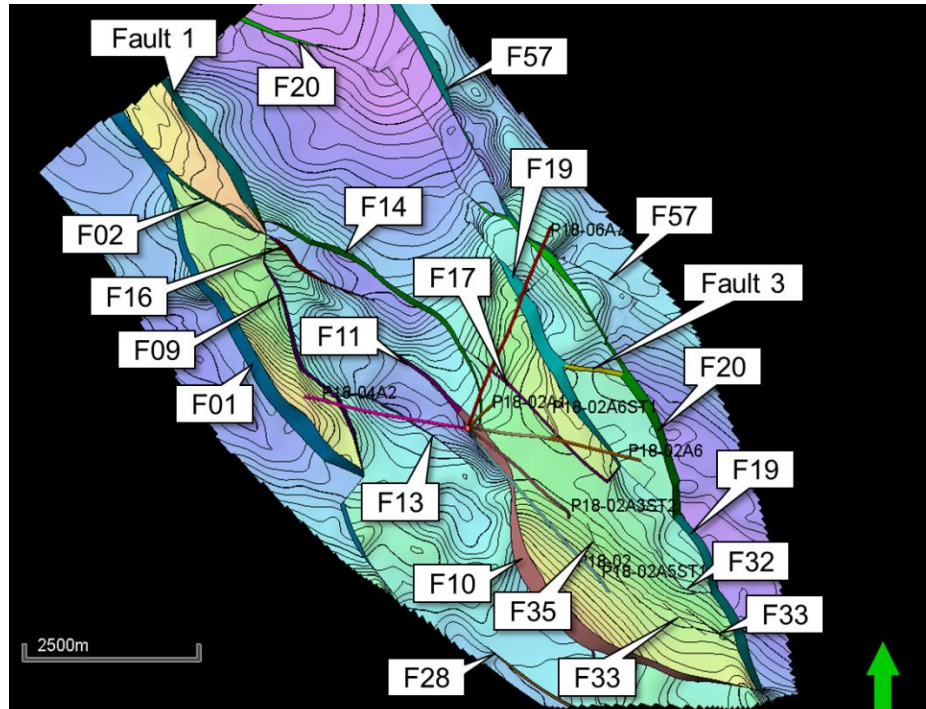


Figure 17-7: Nomenclature of all faults that have been incorporated in the pillar grid of the Petrel reservoir model.

17.4.2 *Make Horizons / Make Zones*

The new model has a different approach towards the construction of the reservoir formations compared to the P18 model from 2011. In the previous model, all Lower Triassic formation tops had a separate horizon as input in the ‘Make Horizons’ process. In combination with the many faults this led to geometrical problems such as rapidly thinning and thickening formations. The current model utilises only one horizon for the reservoir formations (Top Bunter; Figure 17-8).

The 2011 P18 model subdivision into formations was maintained, from top to base: Hardegsen, Upper Detfurth, Lower Detfurth, and Volpriehausen Formation. The rest of the horizons were created using isopachs (Figure 17-10, Figure 17-11, Figure 17-12). The result is a smooth reservoir model where formation thickness changes across the field are kept to a minimum. Figure 17-9 contains a list of all faults that have been incorporated in the pillar gridding process and subsequently in the ‘Make Horizons’ process.

The layering was done as follows: Hardegsen 5, Upper Detfurth 4, Lower Detfurth 3, and Volpriehausen 5 layers. All layers were assigned the type ‘proportional’.

Index	Horizon name	Color	Calculate	Horizon type	Conform to another horizon	Status	Smooth iterations	Use horizon fault lines	Well tops	Input #1
1	Top-Keuper		<input checked="" type="checkbox"/> Yes	Conformable	No	1 Done	5	<input checked="" type="checkbox"/> Yes	Top-Keuper (Well tops TAQA)	06_NearKeuper_P18-ctd_PSDMTime_JakuR2014_grid [Converted] [Cropped Volume for TNO] smoothed (Z)
2	Top-Bunter		<input checked="" type="checkbox"/> Yes	Conformable	No	1 Done	5	<input checked="" type="checkbox"/> Yes	Top-Bunter (Well tops TAQA)	07_TBunter_P18-ctd_SGSH_PSDMTime_JakuR2014_grid [Converted] [Cropped Volume for TNO] smoothed (Z)

Figure 17-8: Dialog box of the ‘Make Horizons’ process of the Petrel reservoir model.

Fault name	Distance	Displacement
<input type="checkbox"/> Use default	Distance: 100	Displacement: Min: 0, Max: 100
<input checked="" type="checkbox"/> Active fault	<input type="checkbox"/> Diff. sides	<input type="checkbox"/> Allow hinge
<input type="checkbox"/> Growth fault		<input checked="" type="checkbox"/> Smooth: 5
		<input type="checkbox"/> Tolerance: 1
<b>Default for all faults</b>	100	Smooth N: 5
<b>Default for each fault</b>		
P18-04 - SGS F01	100	Smooth N: 5
P18-04 - SGS F02	100	Smooth N: 5
P18-04 - SGS F09	100	Smooth N: 5
P18-04 - SGS F10	200/200	Smooth N: 5
P18-04 - SGS F11	100	Smooth N: 5
P18-04 - SGS F13	150	Smooth N: 5
P18-04 - SGS F14	100	Smooth N: 5
P18-04 - SGS F16	100	Smooth N: 5
P18-04 - SGS F17	100	Smooth N: 5
P18-04 - SGS F19	150/100	Smooth N: 5
P18-04 - SGS F20	200	Smooth N: 5
P18-04 - SGS F23	100	Smooth N: 5
P18-04 - SGS F24	100	Smooth N: 5
P18-04 - SGS F28	100	Smooth N: 5
P18-04 - SGS F32	50	Smooth N: 5
P18-04 - SGS F33	50	Smooth N: 5
P18-04 - TNO F34	50	Smooth N: 5
P18-04 - TNO F35	50	Smooth N: 5
Fault 1	100	Smooth N: 5
Fault 2	100	Smooth N: 5
Fault 3	100	Smooth N: 5
F57.xyz	100	Smooth N: 5
Top-Keuper		
Top-Bunter		

Figure 17-9: Detailed list of all faults that have been included in the 'Make Horizons' process of the Petrel reservoir model.

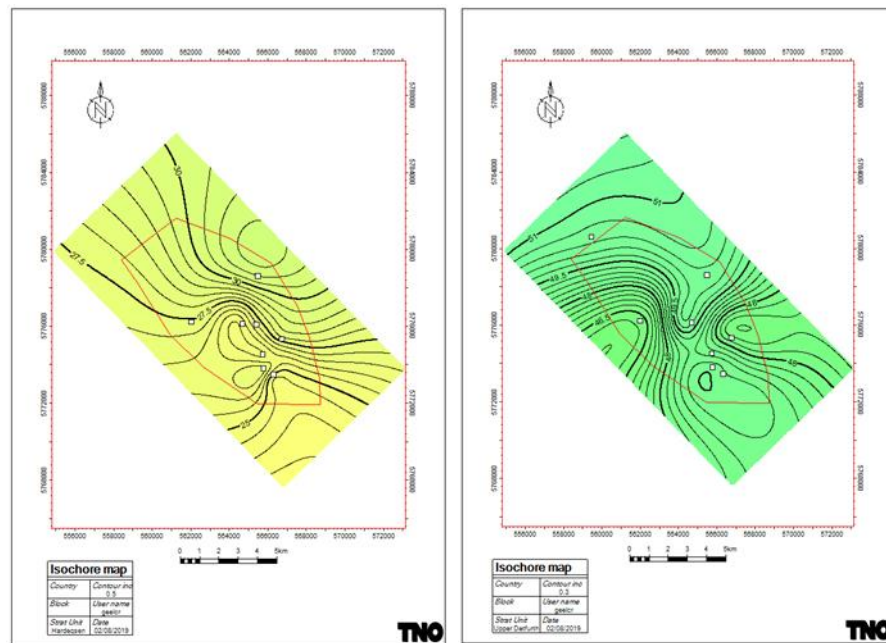


Figure 17-10: Isochore maps of the Hardegsen Fm (left) and the Upper Detfurth (right). Well values on which the isochore maps are based are shown as white squares.

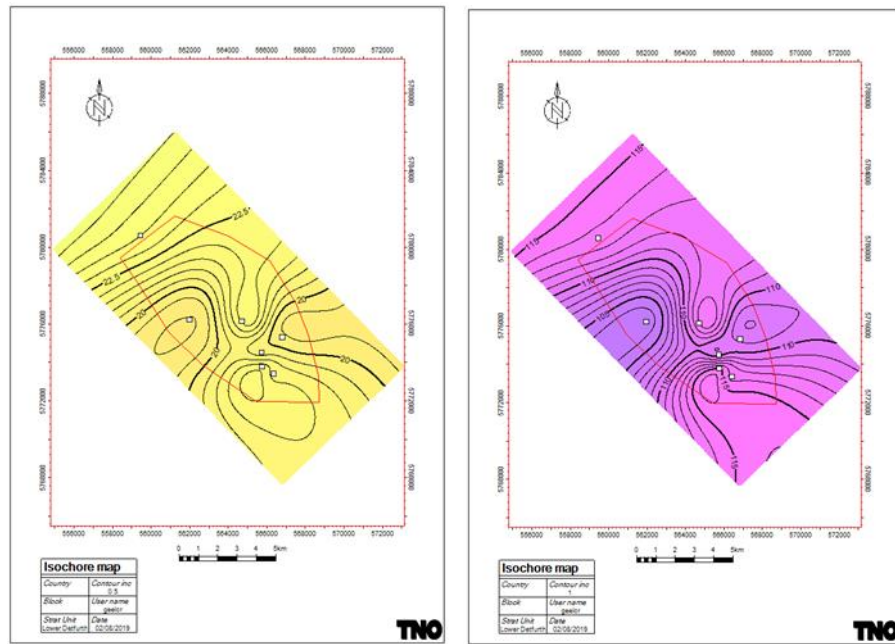


Figure 17-11: Isochore maps of the Lower Detfurth Fm (left) and the Volpriehausen Fm (right). Well values on which the isochore maps are based are shown as white squares.

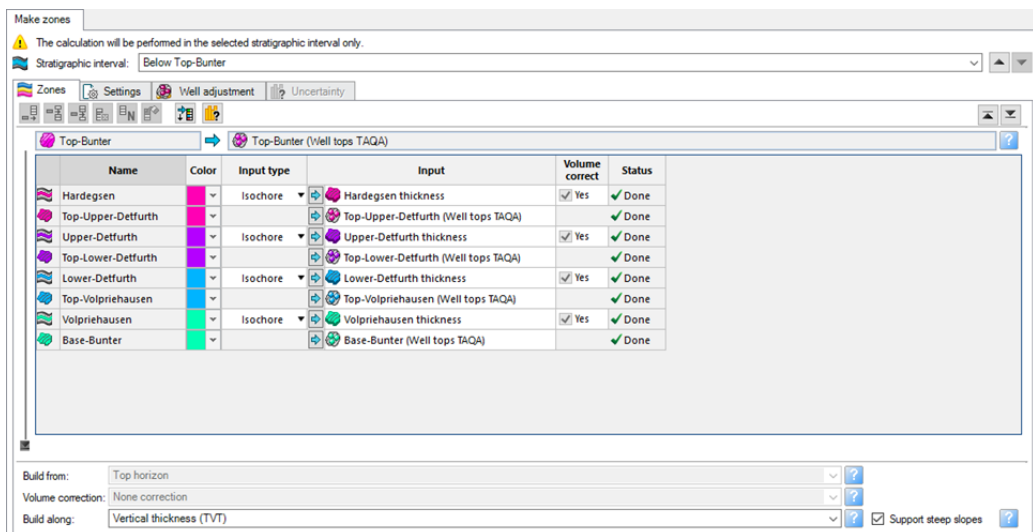


Figure 17-12: Creation of the various reservoir zones in the Petrel reservoir model.

### 17.4.3 Reservoir properties

A detailed petrophysical study on the P15-P18 area was done by BP (2007). Relationships between porosity and permeability in this study were established on the basis of rock types (lithofacies). The origin of these rock types is not readily apparent from this study but seems to have been generated by the Baker Hughes “Horizon” software package (see Ames & Farfan, 1996). On the basis of well log readings, this software package classifies depth intervals into rock types that have been calibrated against lithofacies from core descriptions.

For the P18 area these rocktypes are:

- Rock Type 1: Eolian Dune

- Rock Type 2: Interdune
- Rock Type 3: Eolian Dolomitic
- Rock Type 4: Shales

For each of these rock types a separate porosity-permeability relation has been established (BP, 2007).

- Rock Type 1:  $K_{calc} = 10^{(-3.3+0.58 \cdot PH_{calc} - 0.01229(PH_{calc})^{**2})}$
- Rock Type 2:  $K_{calc} = 10^{(-2.75+0.464 \cdot PH_{calc} - 0.011(PH_{calc})^{**2})}$
- Rock Type 3:  $K_{calc} = 10^{(-3.003+0.358 \cdot PH_{calc} - 0.0068(PH_{calc})^{**2})}$
- Rock Type 4:  $K_{calc} = 0.01$

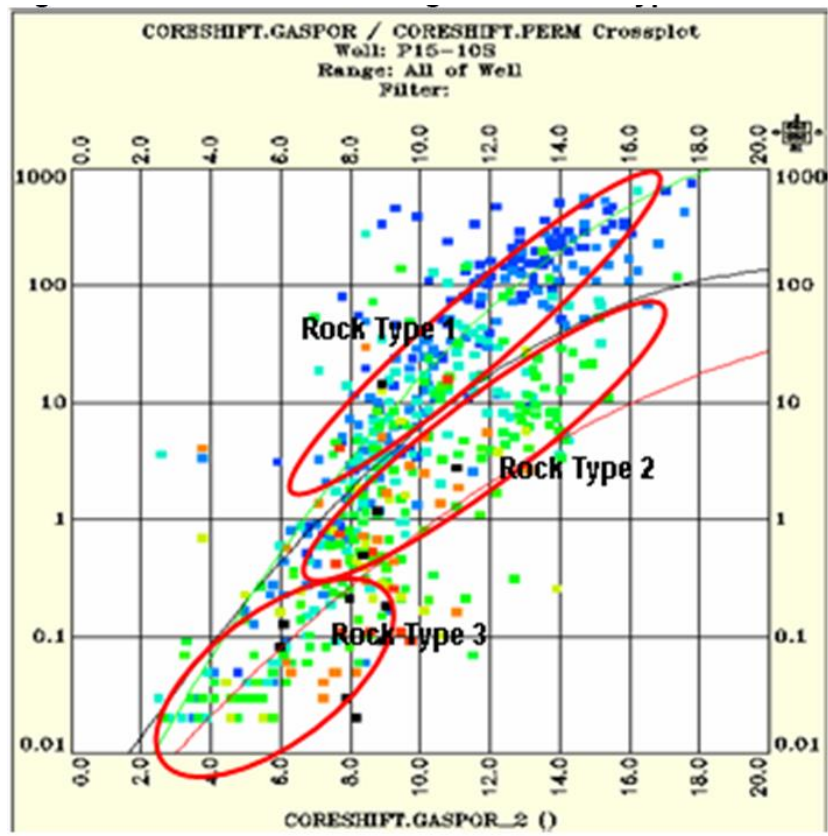


Figure 17-13: Relationship between porosity and permeability for three rock types (lithofacies):  
 1 = Aeolian Dune, 2 = Interdune, 3= Aeolian Dolomitic. Not shown in this graph is rock type 4 = shales. From BP (2007).

There are two field-wide no-flow boundaries or baffles (possibly even pressure boundaries), between Upper and Lower Detfurth Fm, and between Lower Detfurth and Volpriehausen (Figure 17-14). These have impact on pressure behaviour, as illustrated in Figure 17-15. The implementation in the reservoir model was done in ECLIPSE using reduced transmissibility multipliers between the lowermost layer of Upper Detfurth and uppermost layer of Lower Detfurth, and between the lowermost layer of Lower Detfurth and uppermost layer of Volpriehausen Fm.



- NTG (Net to gross; log is either one or zero, depending on cutoffs PHIE 8% and VSH 35%)
- PHIE\_NET (Net effective porosity. Log has the value of PHIE or is undefined, depending on the NTG log)
- PERM\_NET (Net permeability. Log has the value of PERM or is undefined, depending on the NTG log)

All properties were distributed using Kriging, with an isotropic variogram range of 5 km. In order to investigate the effect of anisotropy, a second realisation was done for the porosity and permeability using Kriging with an elongated variogram: long axis 5 km, short axis 2.5 km, long axis strikes NW-SE (135-315).

Figure 17-16 to Figure 17-19 show histograms of the distribution of porosity, permeability, and net porosity and net permeability. Ideally, all histograms should be identical. Although there are minor differences, most of the histograms are comparable.

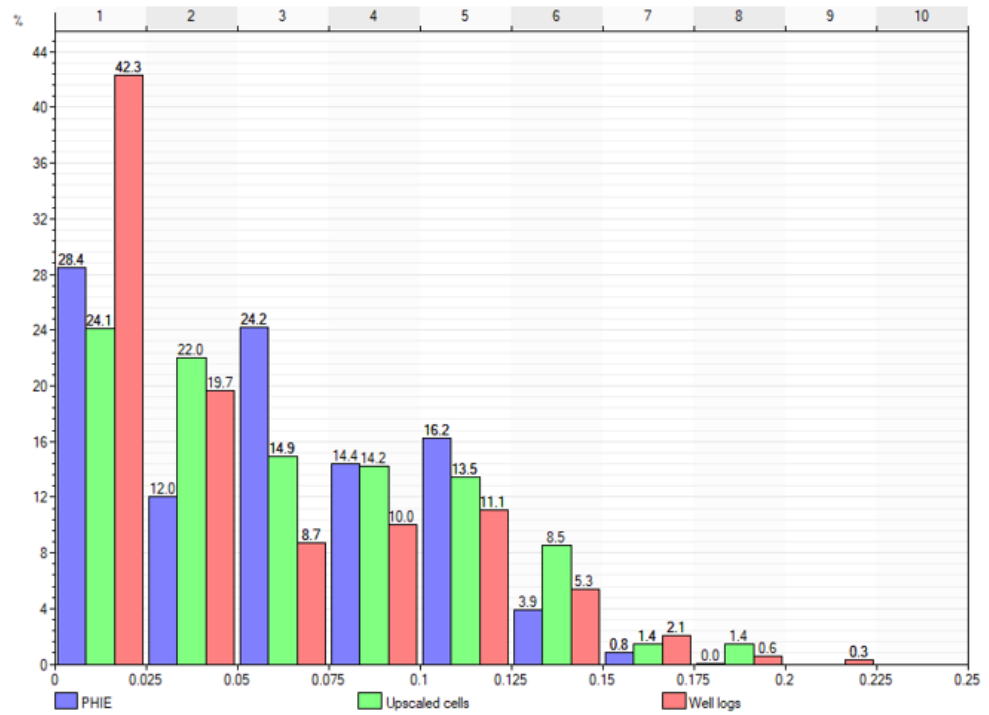


Figure 17-16: Comparison of the distributions of effective porosity (PHIE) in well logs, upscaled well logs, and as 3D property.

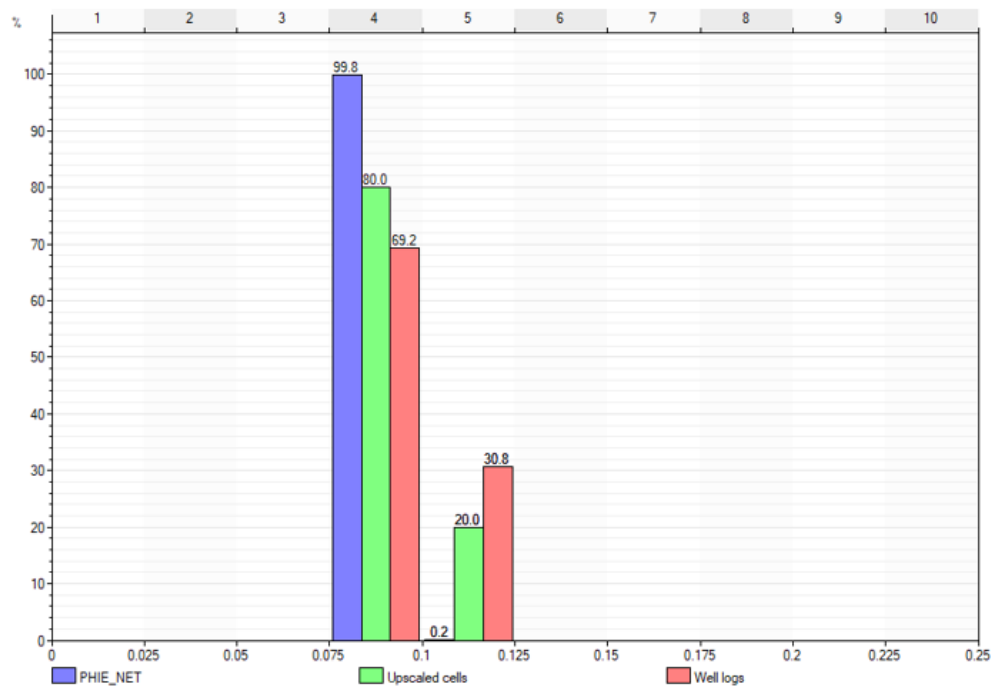


Figure 17-17: Comparison of the distributions of net effective porosity (PHIE\_NET, based on a cutoff of 8%) in well logs, upscaled well logs, and as 3D property.

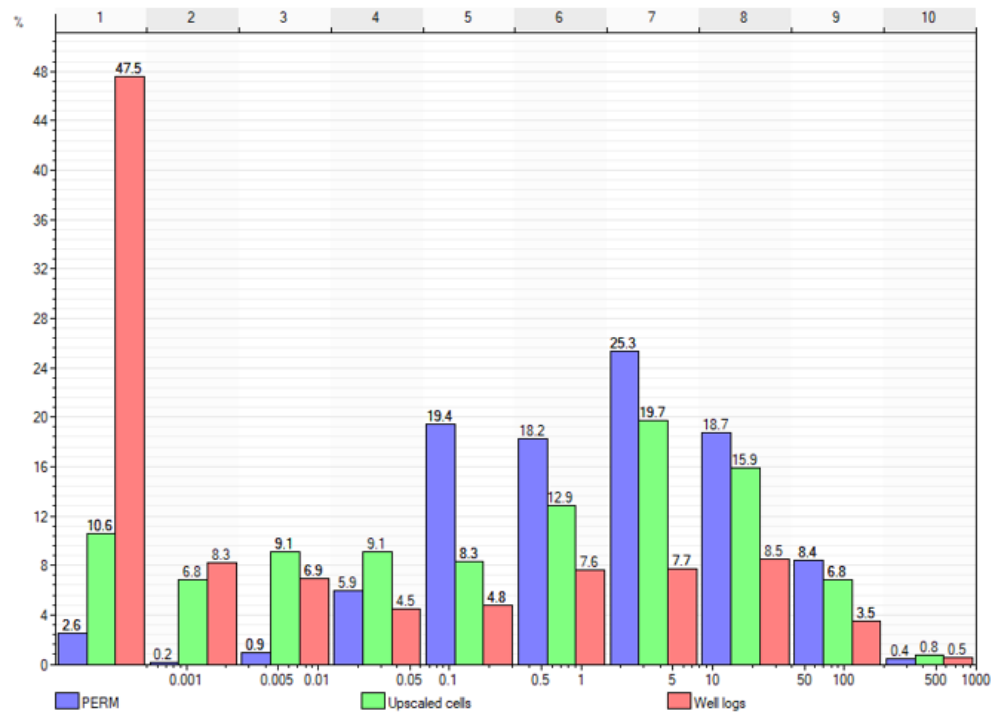


Figure 17-18: Comparison of the distributions of permeability (PERM) in well logs, upscaled well logs, and as 3D property.

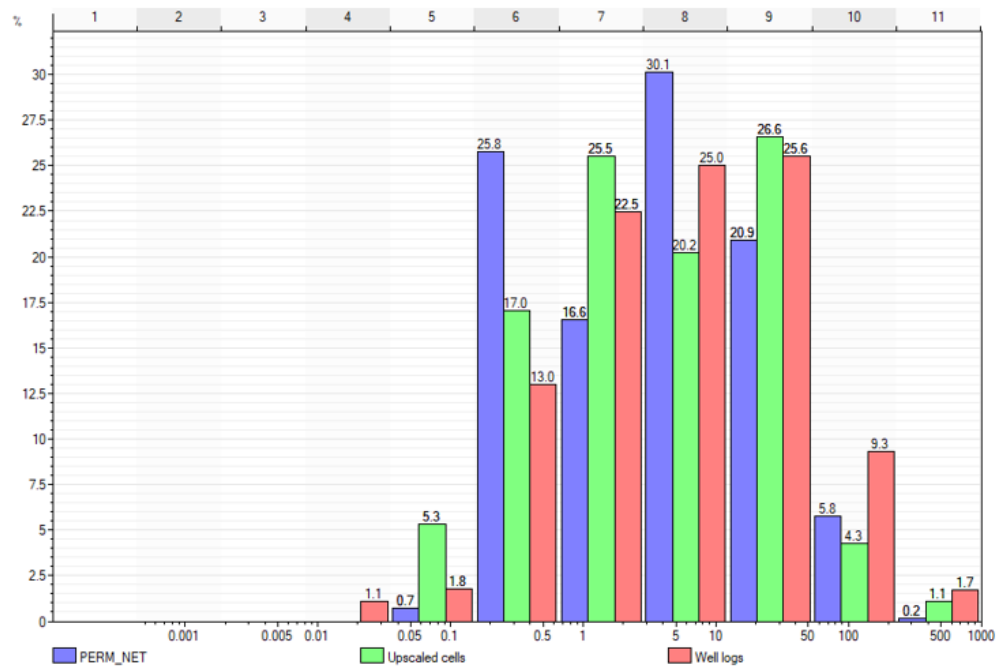


Figure 17-19: Comparison of the distributions of net permeability (PERM\_NET, based on a cutoff of 8% PHIE and 35% VSH) in well logs, upscaled well logs, and as 3D property.

In order to compare the static gas in place with the dynamic gas in place, it is necessary to calculate the water saturation in the field. A Lambda saturation-height function was developed by matching the water saturation logs from resistivity logs with a water saturation log calculated from porosity and height above free water level. The best match yielded the following Lambda saturation-height function (Figure 17-20):

$$S_w = 3.9 HAFWL^{-2.7} Phie^{-0.22}$$

Figure 17-21 and Figure 17-22 show the result of using PHIE or PHIE\_NET for calculating water saturation. In the latter case water saturations in the Volpriehausen Fm are higher. However, because the net to gross is lower the end result is a lower GIIP (see below).

Figure 17-23 to Figure 17-25 show cross plots of the upscaled well logs for water saturation. The Total Water Saturation (from the 2010 model; logs provided by TAQA) is cross plotted against TNO's saturation-height function. All cross plots show the same behaviour, with the majority of the points falling around the  $y=x$  line, and a tail towards higher water saturations for SWT. This can be easily explained by the fact that SWT is calculated for total porosity, hence represents total water saturation which includes all clay-bound water. Apart from this, the match is good, and the currently used water saturations used by TNO in the static model do not underestimate the gas in place, at least not in comparison to the original SWT.

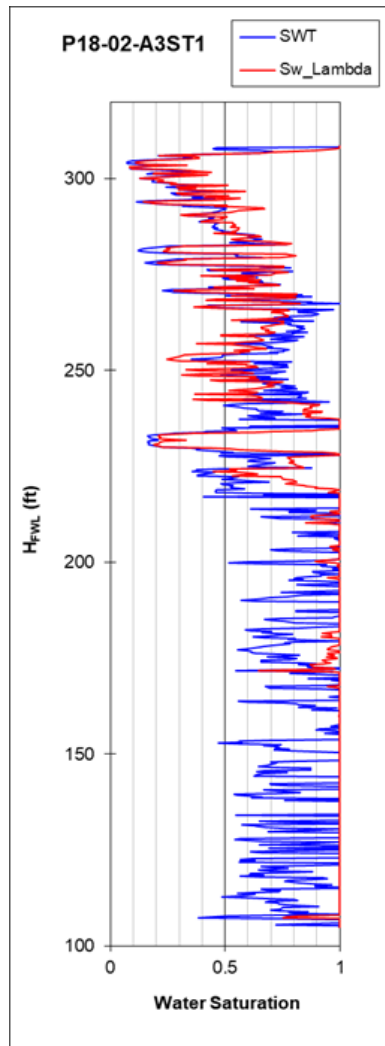


Figure 17-20: Comparison of log-derived water saturation (STW; blue line) and water saturation calculated with a saturation-height function (SW\_Lambda; red line).

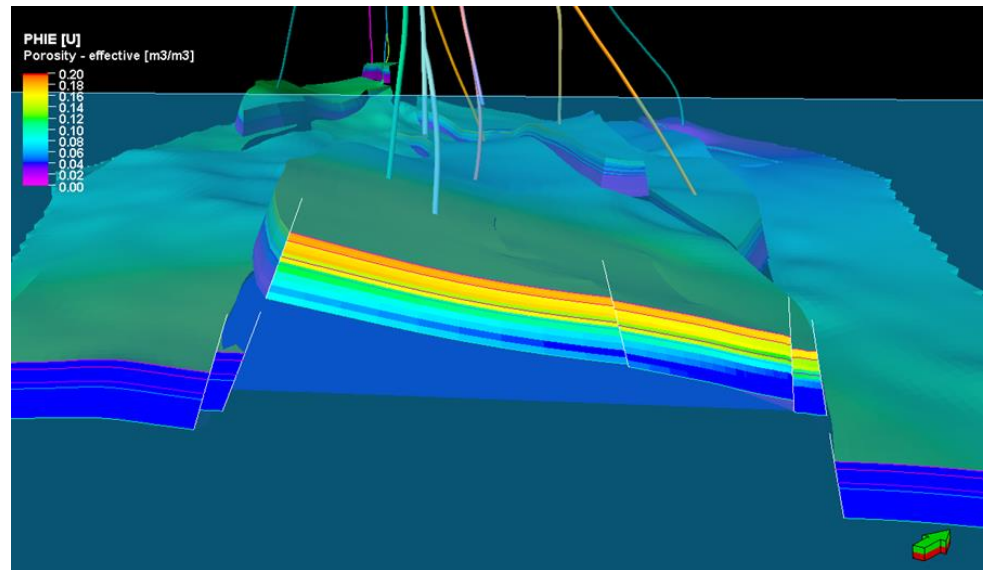


Figure 17-21: Water saturation in Compartment P18-2 without cutoffs on PHIE and VSH. Note the high water saturations in the Volpriehausen Formation. Legend as in Figure 17-22.

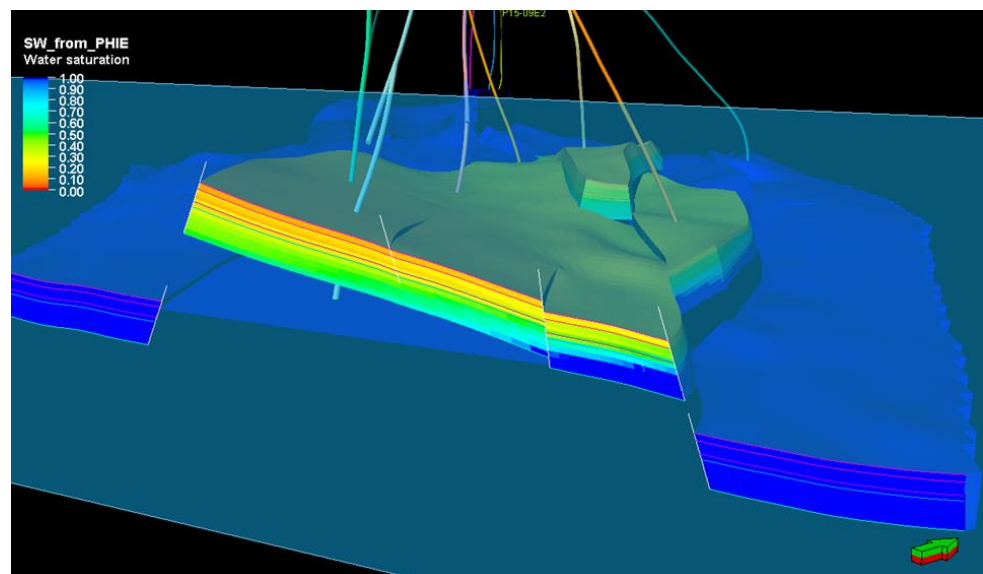


Figure 17-22: Water saturation in Compartment P18-2 with PHIE cutoff of 8% and a cutoff of 35% on VSH.

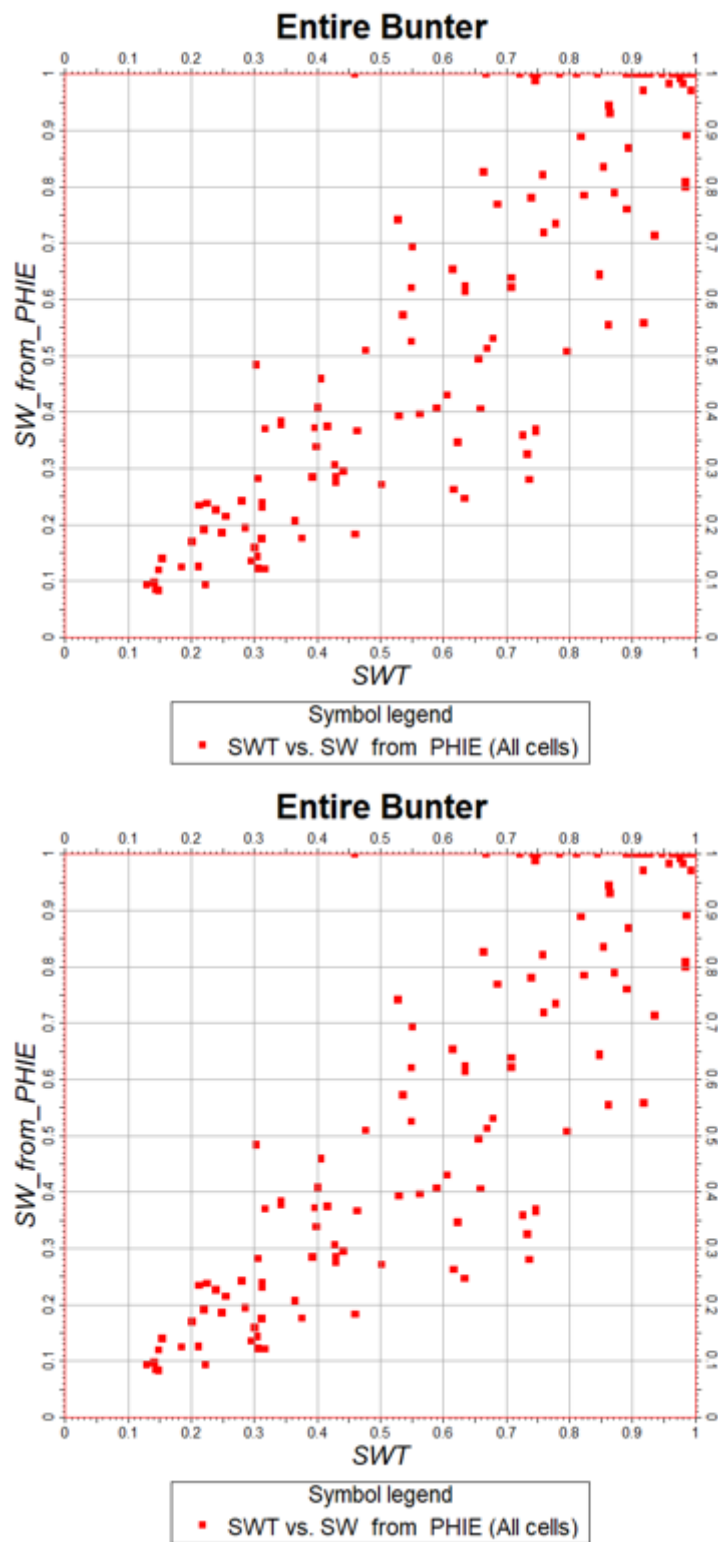


Figure 17-23: Crossplot of upscaled water saturation logs SWT (personal communication TAQA, 2010) and TNO's 2019 saturation-height function SW\_from\_PHIE, for all four Bunter formations.

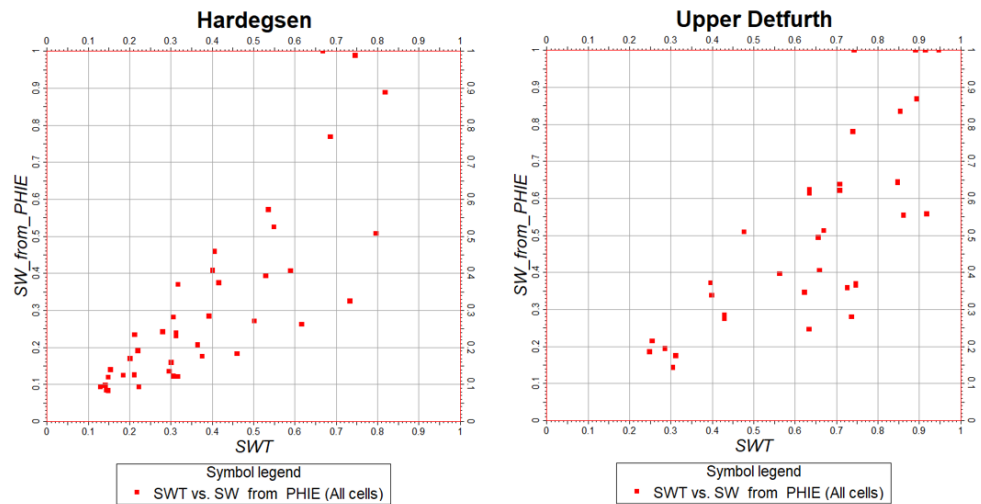


Figure 17-24: Crossplot of upscaled water saturation logs SWT (personal communication TAQA, 2010) and TNO’s 2019 saturation-height function SW\_from\_PHIE, for the Hardegsen and Upper Detfurth formations.

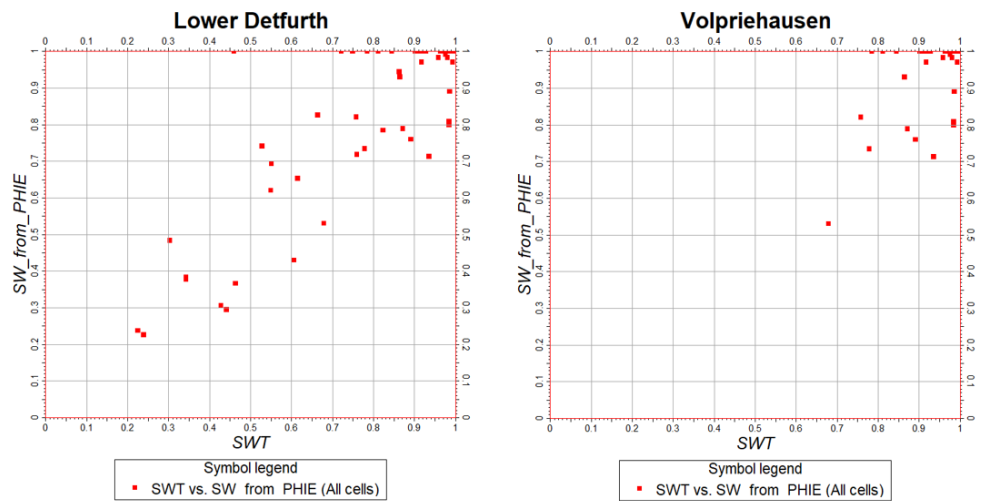


Figure 17-25: Crossplot of upscaled water saturation logs SWT (personal communication TAQA, 2010) and TNO’s 2019 saturation-height function SW\_from\_PHIE, for the Lower Detfurth and Volpriehausen Formations.

17.4.5 GIIP

The actual volumetrics are done during the ECLIPSE history match, but to see whether the geometry and properties of the reservoir model are sufficiently close, the GIIP for the various compartments was calculated.

GIIP was calculated without cutoffs on PHIE or VSH, so with a Net to Gross of 1.0, and with a cutoff on porosity and VSH. Two cutoffs on porosity were examined: 6% and 8%. VSH cutoff was set to 35%. The gas expansion factor Bg was set to 0.0040. Cutoffs of 8% and 35% were derived from BP’s petrophysical evaluation report (BP, 2007).

Table 17-2 shows the results of the GIIP calculations. A realistic scenario with a 35% cutoff on VSH and 8% cutoff on PHIE results in a total GIIP of 13 bcm, which

is on the low side in comparison to the P/Z volumes that sum up to 14.5 bcm. However, the fact that they are in the same range justifies the use of the current model for reservoir simulations. Table 17-3 compares the static volumes from the 2010 and 2019 models.

Table 17-2: Result of static GIIP calculations using various cutoffs. (N.B. for Block read Compartment in this study)

P18-2 Compartment Scenario	2-I GIIP [bcm]	2-II GIIP [bcm]	2-III GIIP [bcm]	Total [bcm]
No cutoffs	11	3	0.9	15
6% Phie, 35% Vsh	10	3	0.9	14
8% Phie, 35% Vsh	9	3	0.8	13

Table 17-3: Comparison of the volumes from the 2010 CATO models and the 2019 model. (N.B. for Compartment read Compartment in this study)

3Dmodel	Block	Bulk volume [*10 <sup>6</sup> m <sup>3</sup> ]	Net volume [*10 <sup>6</sup> m <sup>3</sup> ]	Pore volume [*10 <sup>6</sup> m <sup>3</sup> ]	HCPV gas [*10 <sup>6</sup> m <sup>3</sup> ]	GIIP [*10 <sup>6</sup> sm <sup>3</sup> ]	Total GIIP [*10 <sup>6</sup> sm <sup>3</sup> ]
2010 38 layers	Block I	1512	1245	83	37	9262	12711
	Block II	450	379	24	10	2400	
	Block III N	140	116	6	1	249	
	Block III M	199	127	8	3	718	
	Block III S	24	20	1	0	82	
2010 14 layers	Block I	1512	1246	83	36	9123	12266
	Block II	449	379	24	8	2114	
	Block III N	140	117	6	1	332	
	Block III M	199	128	8	2	620	
	Block III S	24	20	1	0	77	
2019, SW_PHIE, no cutoff	Block 2-I	2262	2262	76	42	10603	15912
	Block2-II	858	858	30	14	3444	
	Block2-III	355	355	10	4	880	
	Block2-IV	917	917	13	4	985	

## 17.5 Differences with 2010 model and implications

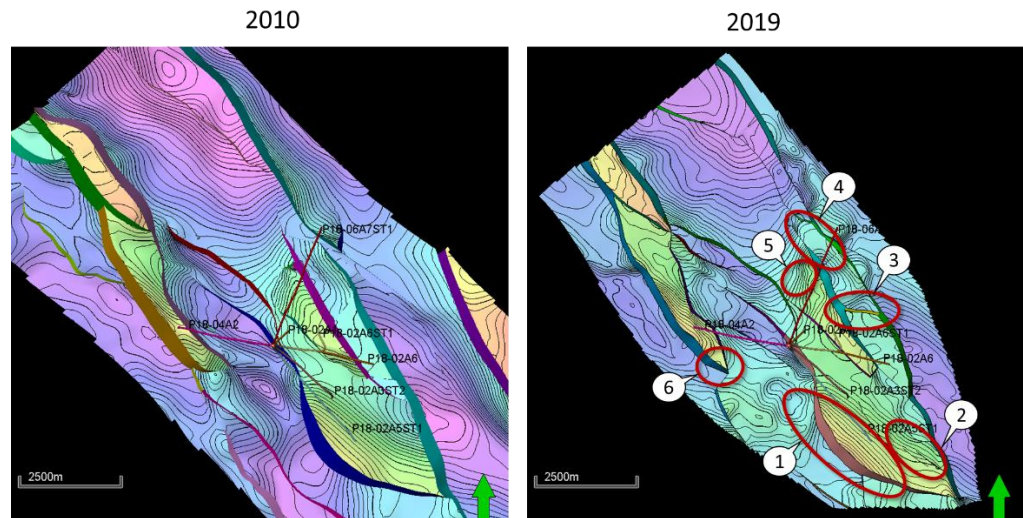


Figure 17-26: Comparison of the 2011 (left) and 2019 (right) Petrel models.

Although in the new model many faults and properties remained the same as in the 2010 TNO model (Vandeweyer et al., 2011), there a number of relevant differences.

These are highlighted in Figure 17-26 and are listed below, with their implications.

- 1) The location of the SW boundary fault (F10) has moved, so the proposed injection wells P18-02-A3 and P18-02-A5 are now further away from that fault. This probably has a positive effect on the geomechanical behaviour of the fault during CO<sub>2</sub> injection.
- 2) A number of small-offset faults are introduced. Because of the small vertical throw they are not expected to have an effect.
- 3) The internal fault in compartment 2-III now has a different orientation. Also, its throw is much larger, so that it is probably sealing.
- 4) The Top Bunter in P18-2 adjacent to P18-6 is now interpreted shallower. That means that the previous interpretation where the P18-6 reservoir was sealed off from the P18-2 reservoir by a simple juxtaposition of Upper Triassic and Alتنا shales is no longer valid. However, P18-6 is still likely to be separated from P18-2 because of a peculiar constellation of faults (Figure 17-27 to Figure 17-31). Two faults (F20 and F57, which form a synthetic-antithetic fault system) separate P18-6 and P18-2. Wherever Bunter is juxtaposed against Bunter, one of the two is invariably the low-permeable and water-filled Volpriehausen Fm, making across-fault fluid flow extremely unlikely. Fault 57 is a sinistral wrench fault, which increases the likelihood that Fault 57 contains a substantial amount of smeared Solling Clay, increasing the capillary entry pressure of that fault. Therefore, any fluid flowing across Fault 57 needs to surpass that capillary pressure.
- 5) The fault that sealed off Compartment 2-II from its downdip aquifer is no longer in the model. A small-throw fault (around 15 m) could be interpreted, but that would have little consequences for the fluid flow. This means that Compartment 2-II is in pressure communication with its downdip, lateral aquifer.

- 6) The SE tip of the P18-4 field has been slightly modified. Partly based on seismic interpretation of Top Bunter and the faults surrounding the tip, and partly on constraints by Petrel's pillar gridding.

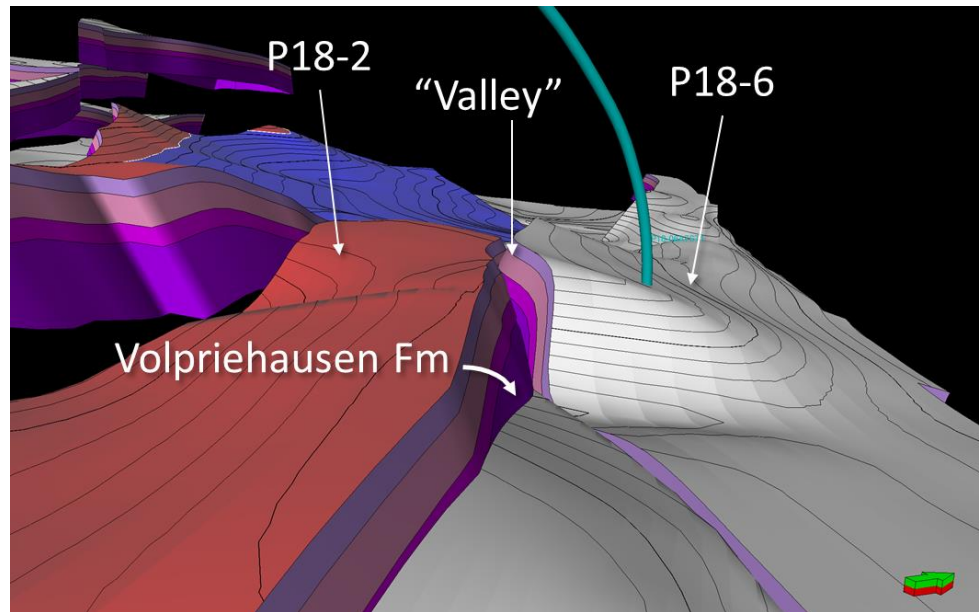


Figure 17-27: Oblique view toward the NW on the boundary between the P18-2 and P18-6 fields. Two horizontally cross-cutting faults create a "valley" between the two fields that is filled with Upper Triassic and Alتنا shales, thus providing an effective seal. Direct contact would only be through the tight Volpriehausen Fm.

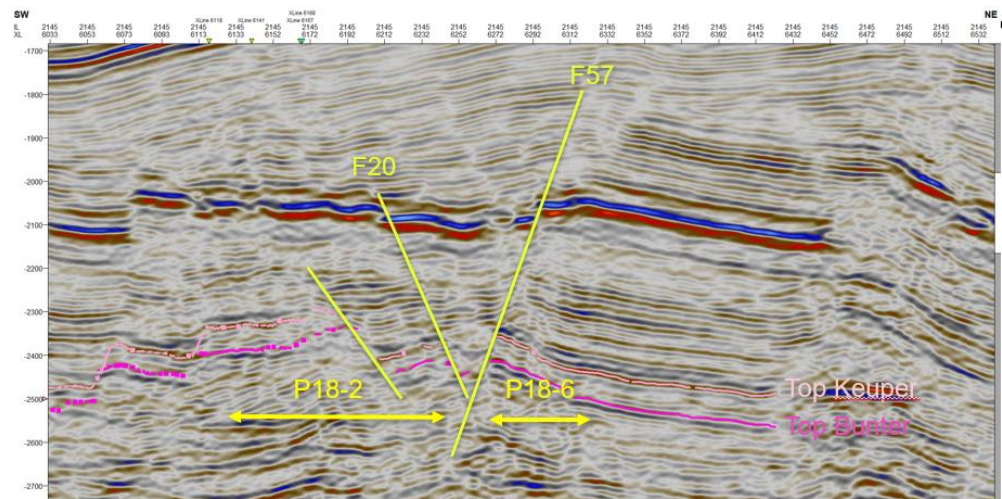


Figure 17-28: Seismic inline 2145 showing the fault configuration that separates the P18-06 accumulation from P18-02.

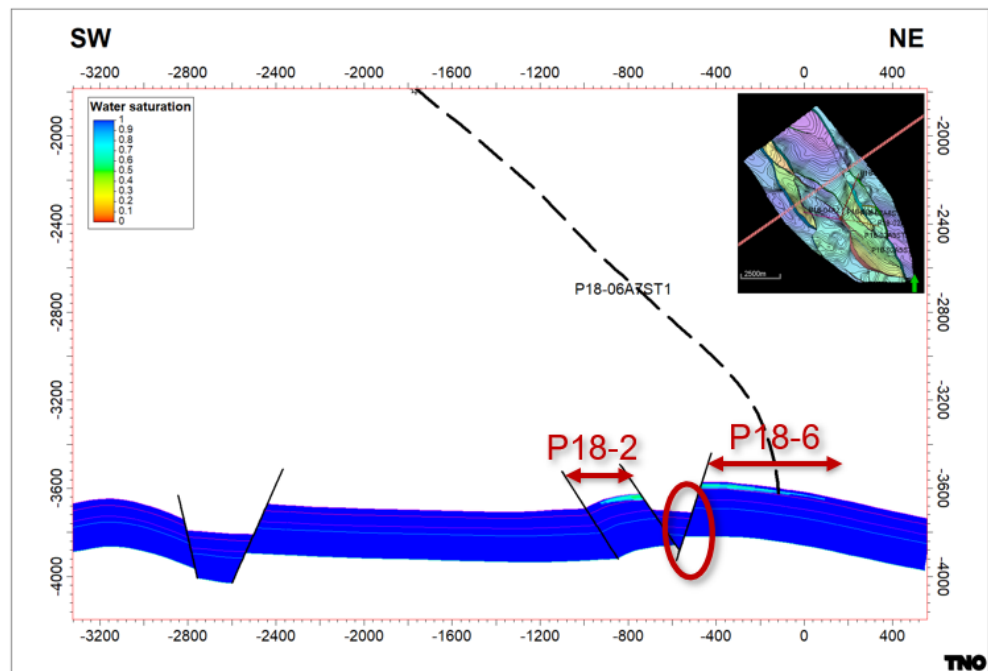


Figure 17-29: Model cross-section through P18-6 and P18-2 showing the original water saturation in the two accumulations. Note that Volpriehausen Fm in P18-6 is juxtaposed against Hardegsen and Detfurth Fm in P18-2.

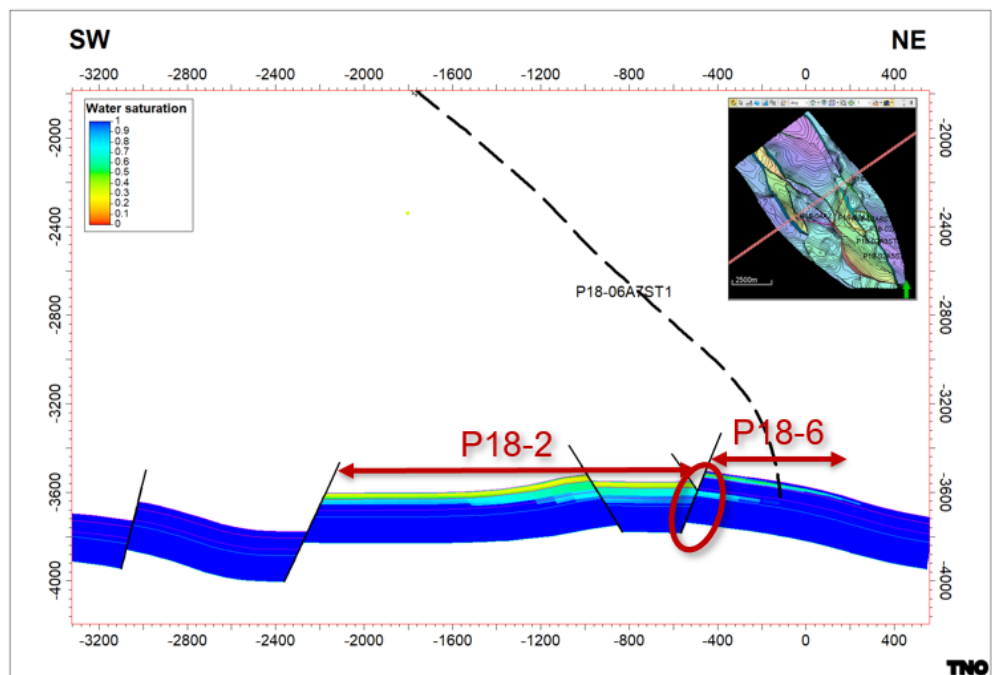


Figure 17-30: Model cross-section through P18-6 and P18-2 showing the original water saturation in the two accumulations. Note that Lower Detfurth in P18-6 is juxtaposed against Upper Detfurth in P18-2, and Hardegsen in P18-6 is juxtaposed against Upper Triassic seal in P18-2.

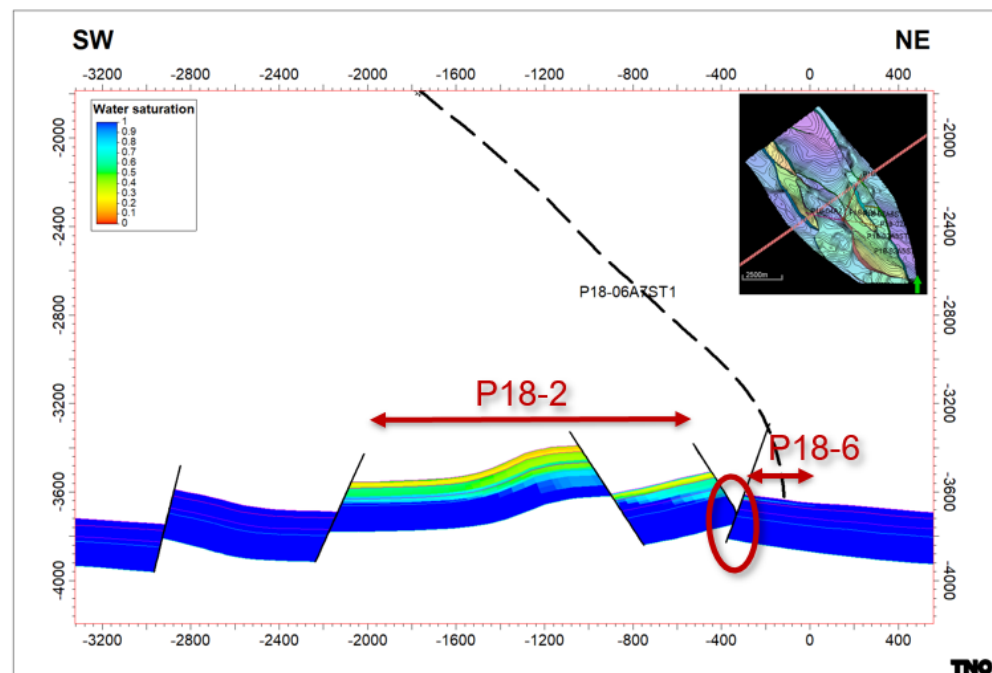


Figure 17-31: Model cross-section through P18-6 and P18-2 showing the original water saturation in the two accumulations. Bunter in P18-6 is juxtaposed against Upper Triassic seal, or Volpriehausen.

## 17.6 Adjustments made to the static model

During the history matching process and after discussions with TAQA and EBN, a modification was made in the dynamic model. A flow boundary was imposed near the GWC in Compartment 4. During the ECLIPSE simulations the question arose whether there was a possibility that Compartment 4 was not in pressure communication with the water-bearing part of Compartment 2 (indicated by "Aquifer" in Figure 17-32). Close inspection of the seismic in that area and the fact that the nearby well P18-06A07ST1 has very poor reservoir properties leads to the conclusion that the narrow passage around the GWC of Compartment 4 (red ellipse) is heavily faulted and forms therefore most likely a flow barrier to the down dip aquifer. This was implemented in the ECLIPSE grid.

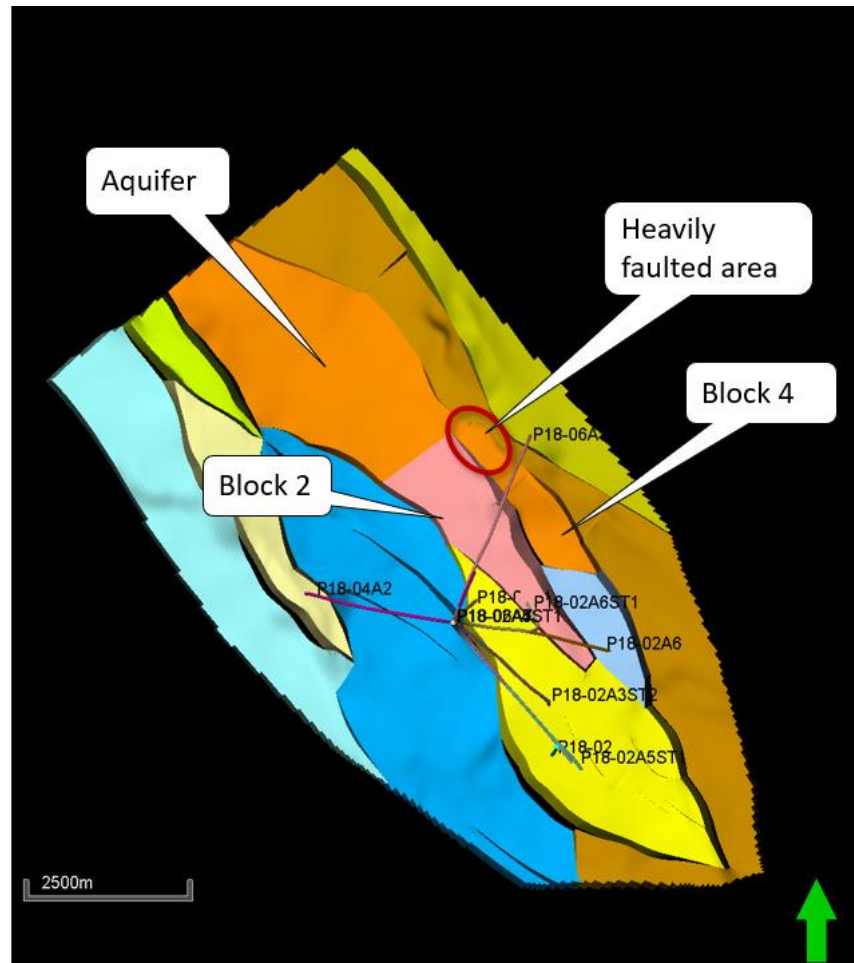


Figure 17-32: The narrow passage around the GWC of Compartment 4 (red ellipse) is heavily faulted and forms therefore most likely a flow barrier to the down dip aquifer.

## 17.7 Dynamic model

### 17.7.1 Reservoir simulator

For the dynamic modelling Eclipse 300 was used. Alternatives were to use the Eclipse 100 simulator or the Shell proprietary reservoir simulator MoReS. The compositional Eclipse simulator was used for the following reasons:

- A black oil simulator cannot handle gas to gas interactions, which is needed for CO<sub>2</sub> injection into a gas (methane) reservoir.
- MoReS was used for P18-2 and P18-4 modelling in a previous study (Vandeweyer et al (2011)). Since that study, the workflow Petrel-Eclipse-Macris has been developed and is considered to be state of the art.

### 17.7.2 Data

For any dynamic reservoir simulation, including Eclipse, the following sets of data are required:

- General run data: grid dimensions, phases present, components present.
- Grid geometry data: specification of geometry of computational grid (location of grid block corners).
- Reservoir rock properties: porosity, net-to-gross, absolute permeability in each grid block.

- PVT data: properties of reservoir and stock tank fluids such as density, viscosity and saturation pressure.
- Saturation and pressure dependent rock properties: relative permeabilities and capillary pressures as function of phase saturations, and rock compressibility.
- Initial conditions in the reservoir: pressure, temperature, phase saturations and phase compositions.
- Regions: specification of regions that splits the computational grid into regions for calculation of PVT properties, saturation properties, initial conditions, and fluids in place.
- Operations data: specification of the wells (location, productivity index, etc.) and the operations to be simulated (production and injection controls and constraints).

These data describe the dynamic characteristics of the P18 reservoir. Each of these sets of data will be discussed in the following sections

### 17.7.3 General simulation data

As mentioned in section 17.7.1 the Eclipse 300 simulator is used with two reservoir fluid phases namely water and gas, and six components namely H<sub>2</sub>O, N<sub>2</sub>, CO<sub>2</sub>, C<sub>1</sub>, C<sub>2</sub>, C<sub>3P</sub>.

The geological grid as described in Section 17.1 - 17.4 was not upscaled to the dynamic 2019 model, however directly from the logs a new dynamic grid was generated, with a cut-off of 6% of the porosity. Table 17-4 below gives an overview of the grid dimensions. The size of the grid blocks do vary in size in each individual direction but are in the order of 50x50x4m (XYZ).

Table 17-4 – Overview of grid dimensions in the geological model and in the simulation model. The '2010 model' refers to the model used in Vanderweijer et al. (2011).

	Number grid blocks x-direction NX	Number grid blocks y-direction NY	Number grid blocks z-direction NZ	Total number of grid blocks	Number active grid blocks
<b>Geological grid 2010 model</b>	51	149	38	3472820	n/a
<b>Simulation grid 2019 model</b>	63	170	17	182070	118504

### 17.7.4 Reservoir Rock properties

This is described in previous sections of Section 17.

### 17.7.5 PVT data

#### 17.7.5.1 Gas PVT data

An equation of state is generated for Eclipse 300 with the composition at 1 m depth listed in Table 17-5.

Table 17-5 – Overview of composition at 1 m depth.

	Composition
N <sub>2</sub>	0.01508
CO <sub>2</sub>	0.01288

C <sub>1</sub>	0.9411
C <sub>2</sub>	0.02376
C <sub>3P</sub>	0.0718

#### 17.7.5.2 Water PVT data

The water formation volume factor is 1.0223 m<sup>3</sup>/Sm<sup>3</sup> at a reference pressure of 215 bar. The water compressibility is 4.1483·10<sup>-5</sup>/bar and water viscosity is 0.32929 cP, also at reference pressure of 215 bar.

#### 17.7.6 Saturation and pressure dependent rock properties

Relative permeability and capillary pressure (Special Core Analysis - SCAL - data) are not available for P18 field. In this study the final parameters used to describe the individual curves are described see Table 17-6 and Figure 17-33 and was part of the history match study. Previous saturation curves used in the CATO-2 study showed the GWC was rising to fast and the water was penetrating from compartment II to compartment-I. The high water saturation basically was disconnecting the two individual compartments, which was in reality not the case. The final parameters used showed a slower movement of the GWC and therefore a improved history match

The most used description of the relative permeability curves is the Corey parametrization according to equation (17-1):

$$k_{r,i}(S_i) = k_{r,end,i} \left( \frac{(S_i - S_{irr,i})}{(1 - S_{irr,i} - S_{irr,j})} \right)^{n_i} \quad (17-1)$$

Where

- $k_{r,i}$  = relative permeability of phase  $i$
- $k_{r,end,i}$  = end-point relative permeability of phase  $i$
- $S_i$  = saturation of phase  $i$
- $S_{irr,i}$  = irreducible or connate saturation of phase  $i$
- $n_i$  = Corey exponent for phase  $i$

The values used to describe the relative permeabilities are listed in Table 17-6.

Table 17-6 – Parameters for calculation of gas-water relative permeabilities

Parameter	Description	Value used in dynamic model
$S_{wc}$	Connate water saturation	0.13
$S_{grw}$	Residual gas saturation in gas/water system	0.20
$n_w$	Corey exponent for water	3.5
$n_o$	Corey exponent for gas	1.5
$k_{rwor}$	Water end-point relative permeability	0.35
$k_{rgcw}$	Gas end-point relative permeability	1

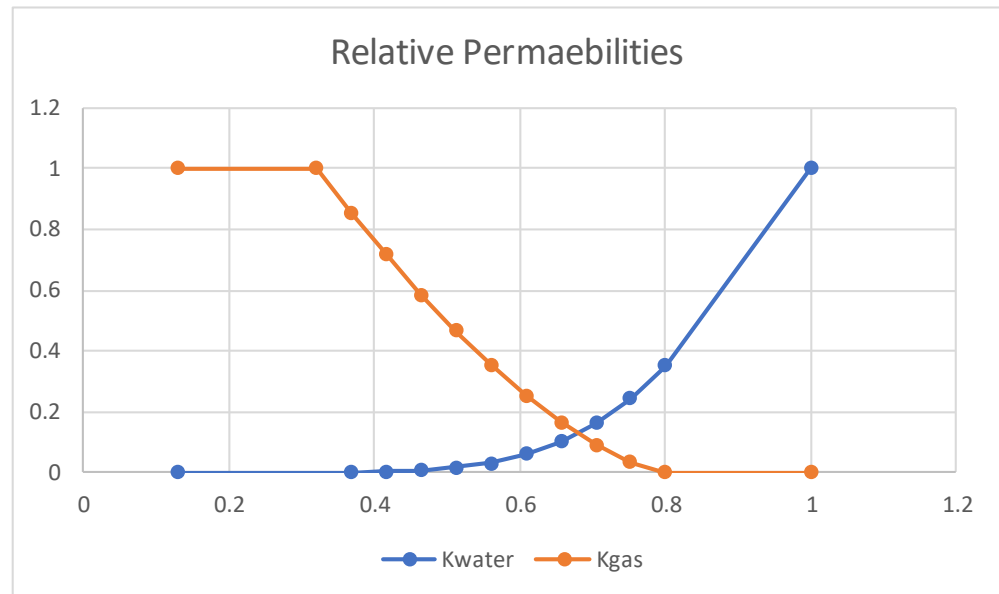


Figure 17-33: Relative permeabilities used in the P18-2 study.

The capillary pressure curves were based on a J-function corresponding to equation 17-2. The J-function itself was provided by TAQA. The reason for using the J-function rather than the saturation height functions from the static model is described in section 17.8.5. Capillary pressure is given by

$$P_c = J(s) \cdot ST \cdot \left( \frac{por}{perm} \right)^{\frac{1}{2}} \cdot U_{cons} \quad 17-2$$

Where

$P_c$  = capillary pressure

$J(s)$  = J-function (shown in Figure 17-34)

ST = surface tension (water gas) set to 76 dynes/cm (typical value for water gas system, petrowiki)

Por = porosity

Perm = permeability

$U_{cons}$  = constant depending on the unit system (Eclipse reference manual)

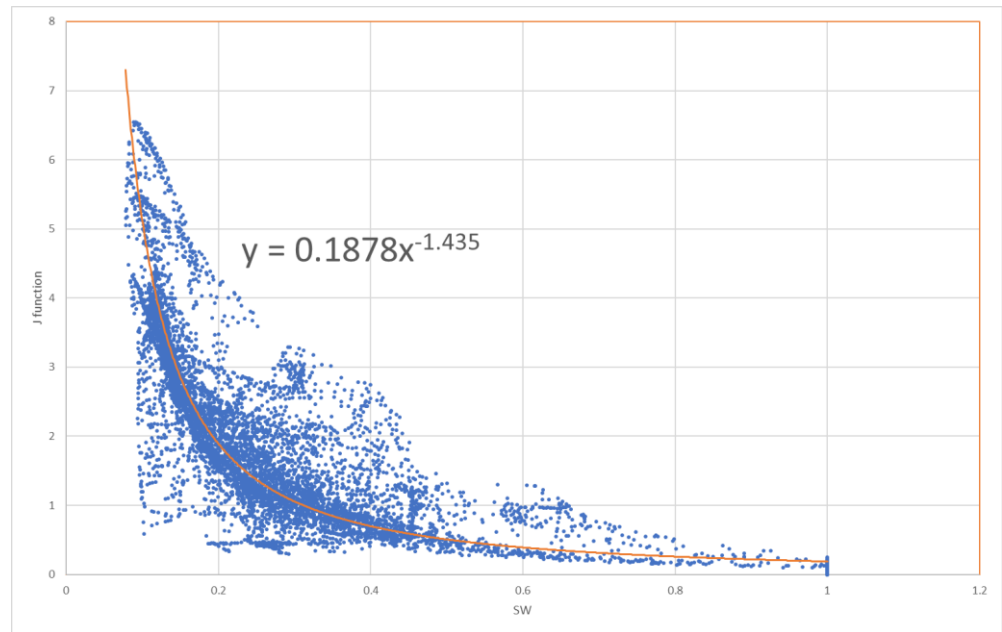


Figure 17-34: The J-function used (orange line) and the saturations of the P18 reservoir (blue dots).

After initialisation with these saturation functions the modelled water saturations were compared to the saturations based on the logs (Figure 17-35). Based on the comparison there is room for improvement, however note that the logs visualise the total water saturation and not the effective water saturation.

figure

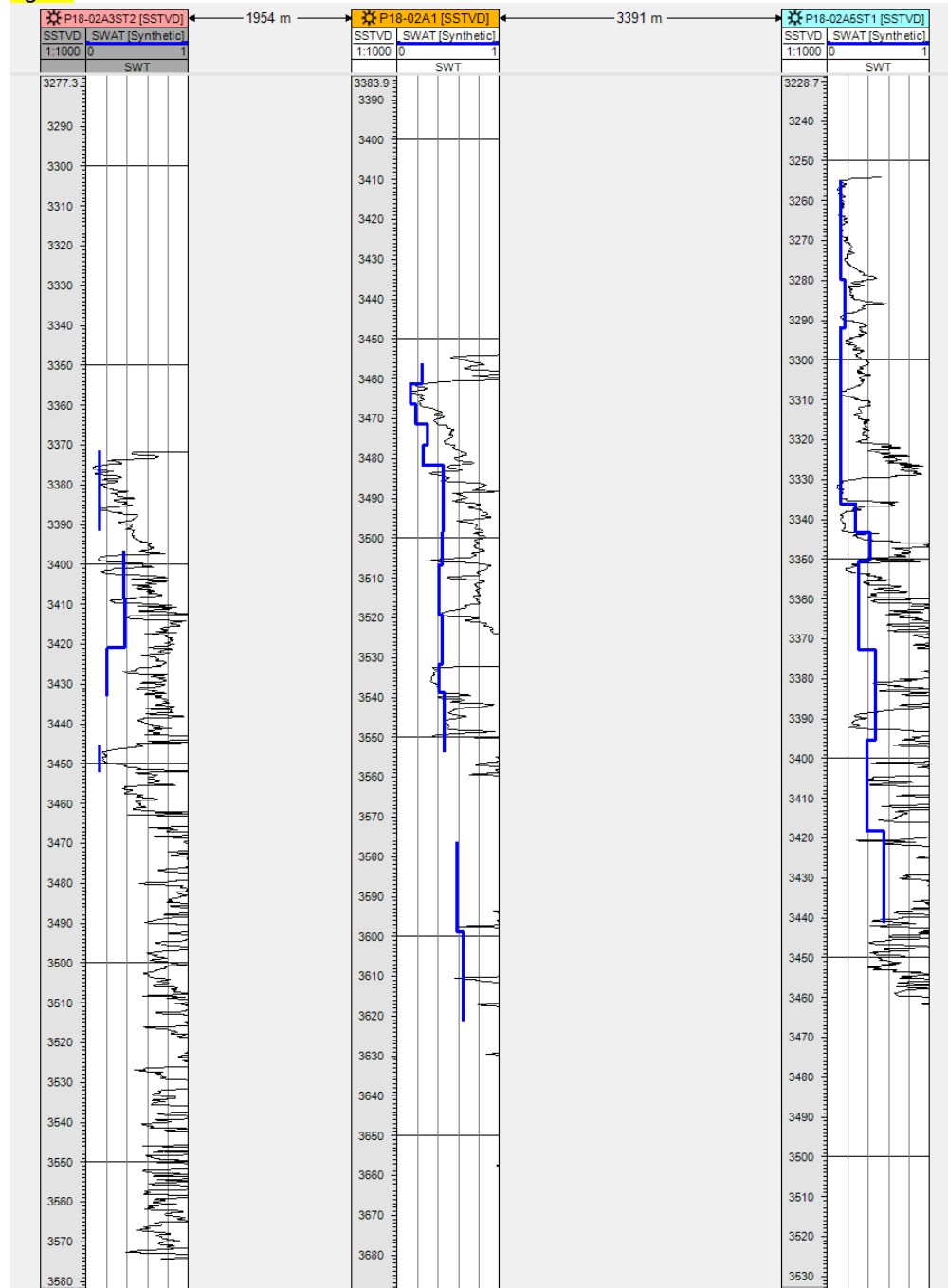


Figure 17-35: total water saturation based on logs (black) and synthetic log based on the jfunction (blue).

17.7.7 Pore compressibility

As no pore compressibility measurements are available for the P18-2 field, a correlation is used<sup>9</sup>. The compressibility is (also) dependent on the porosity according to:

$$Cr(\Phi) = 7.248 \cdot 10^{-6} / (\Phi + 0,000001) - 0.26 \cdot 10^{-5}$$

<sup>9</sup> Personal communication, NAM.

Where

$C_r$  = pore compressibility,

$\Phi$  = porosity.

### 17.7.8 Regions

In the dynamic model regions are specified based on porosity classes for rock properties described in section 17.7.6. and to split the computational grid into regions for calculation. Furthermore regions are used to evaluate the gas initial in place (GIIP) for the different compartments separated by faults or boundaries (see Figure 17-36) .

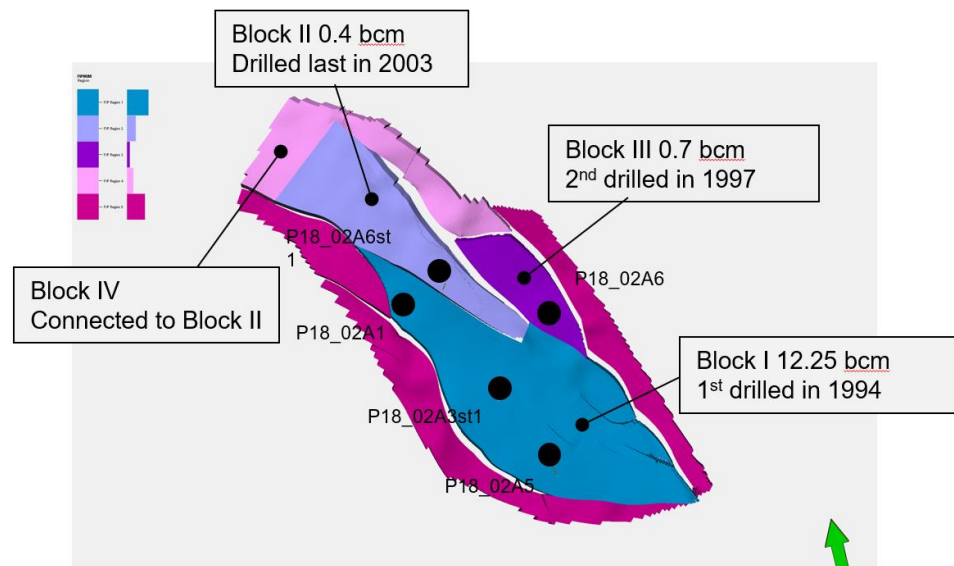


Figure 17-36: Four different regions specified to evaluate GIIP. (N.B. for Block read Compartment in this study)

### 17.7.9 Initial condition in the reservoir

The reservoir is a mechanical and thermodynamic system and hence its (initial) conditions are fully defined by the following state variables at any point in the reservoir or grid block in the simulator:

- Temperature;
- Pressure;
- phase compositions;
- phase saturations.

Initialization of these variables is discussed below.

#### 17.7.9.1 Temperature

An isothermal model is used, all temperature dependent fluid and rock properties are assume to be specified at reservoir temperature of 126 °C degrees.

#### 17.7.9.2 Pressure

The initial (gas) reservoir pressure is 375 bar at datum depth 3150 m. It is important to note that in fact each phase has its own pressure and that each phase pressure

is assumed to be in hydrostatic equilibrium. Phase pressures and phase saturations are coupled through capillary pressure between phases. The capillary pressure is based on the J-function defined in equation 17-2.

#### 17.7.9.3 Gas water Contact

The gas water contact (taken as free water level, i.e.  $P_c = 0$ ) is at 3680 m depth.

#### 17.7.10 General remarks

Petrel 2018 was used to generate an input deck for dynamic model the reservoir engineering module offers options such as specification of fluid and rock properties, specification of historic production data.

There a few manual adaptations in the input files:

- PVT data generated by Petrel are overwritten by TNO's PVT data, in other words an equation of state is used;
- Saturation functions generated by Petrel are overwritten by TNO's saturation functions;
- History match multipliers.

### 17.8 History Match of the dynamic model

#### 17.8.1 Introduction

In the previous chapter the data required to describe the reservoir have been described. In this chapter the data required to define the operations and resulting reservoir behavior will be discussed. These data are:

- Specification of wells: location, trajectory, casing data, perforation data, productivity index, etc.;
- Production and injection data:
  - Water and gas production rates;
  - Bottom hole pressures;
  - Reservoir pressures.

Next the adaption of the reservoir parameters to arrive at an acceptable history match is discussed in detail.

#### 17.8.2 Well data and production data

##### 17.8.2.1 Well Location and trajectory

For all wells well head coordinates and deviation data have been received and imported in Petrel. (see section 17.4).

##### 17.8.2.2 Well completions and perforations

Based on the received well test reports the completion perforation and skin data was gathered shown in Table 17-7.

Table 17-7 - Well test, completion and perforation data.

Well name	Completion size (inch)	Productivity index (Nm <sup>3</sup> /day)/bar	Perforations (m)	KH (mDm) from well test	Skin from well test
P18-02-A-01	4 ½	26.72	3580-3695	1847	0.6-0.9
P18-02-A-03S2	4 ½	31.89	4070-4209	-	2.1-3.3
P18-02-A-05S1	7	37.33	4798-4980	25249	3.19
P18-02-A-06	4 ½	14	4488-4633	3686	2
P18-02-A-06ST1	4 ½	22.28	3376-3936	-	-
P18-4A-02	4 ½	40.95	4085-4199	8208	-
P18-6A-07	4 ½	6.83	4975-5065	-	-

### 17.8.2.3 RFT and PLT data

For well P18-02-A-6ST1 (Figure 17-37) and for well P18-2-A-05st1(Figure 17-38) RFT are available; for the latter also PLT data (Table 17-8) was available.

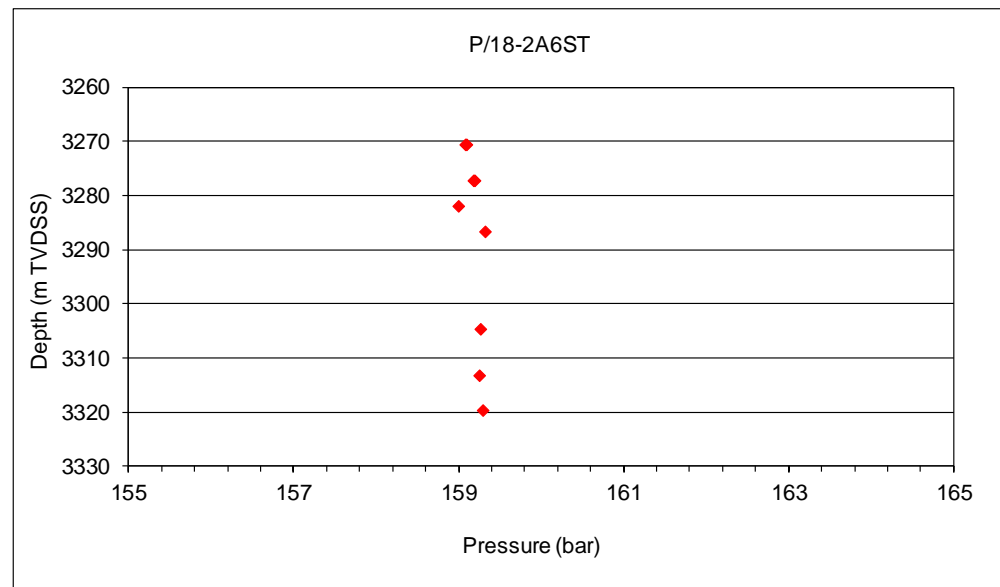


Figure 17-37: RFT data of P18-2-A-6ST1.

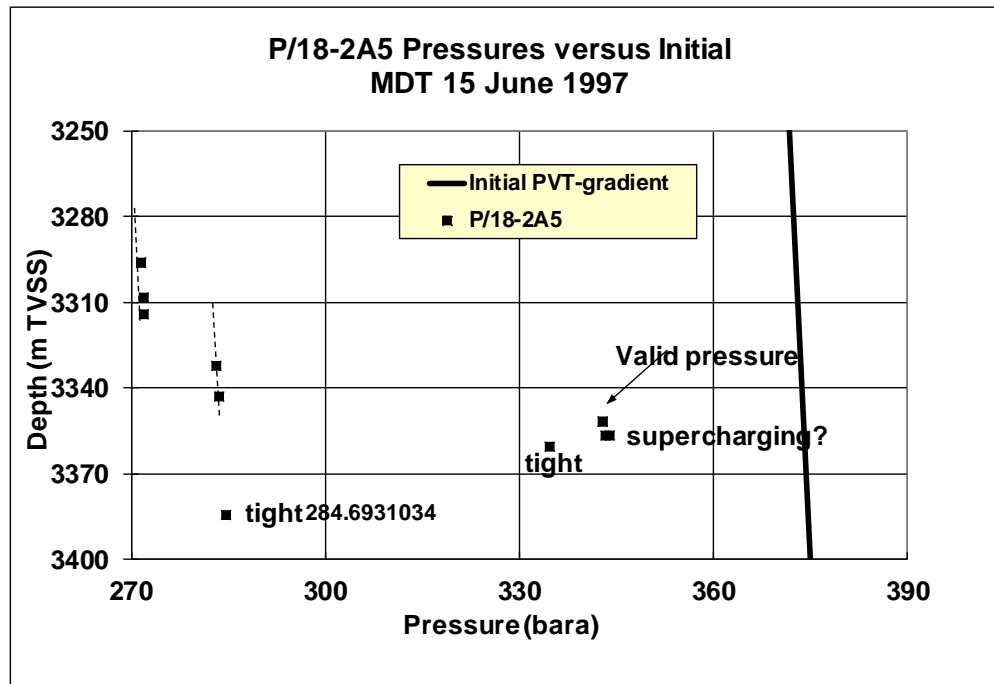


Figure 17-38: RFT data of P18-A-6ST1, note that the vales in the Volpriehausen formation (between 3350-3400 m depth) are more uncertain since the values of the measured pressure values broad range.

Table 17-8: PLT results of P18-2-A5ST1.

Formation	P18-2-A5ST1 (%)
Hardeggen	83
Detfurth Claystone	4
Lower Detfurth Sandstone	13
Volpriehausen	< 1

17.8.2.4 Historic Well Production data

Daily gas and condensate production data was provided by the operator for each individual well.

In Figure 17-39 to Figure 17-43 the daily gas production data of production wells is shown. The received data was improved and used after the following manual editing:

- Daily production data from well P18-02-A-01 and P18-02-A-03ST2 are considered unreliable in the period between 1993 and 1997 → decided to use average production rate for these wells within this particular period.
- In 2003 a sidetrack was drilled from P18-02-A-06 and all production data was assigned to the new production well P18-2-A-06ST1 only. However in 2005 the whipstock is perforated and the production data is not only from P18-02-A-06ST1 but also from P18-02-A-06, therefore crossflow is allowed in this well. From 2005 on the pressure values have to be interpreted with special care since the pressure measurement is a result of two wells drilled and perforated in different compartments in the P18-2 reservoir.

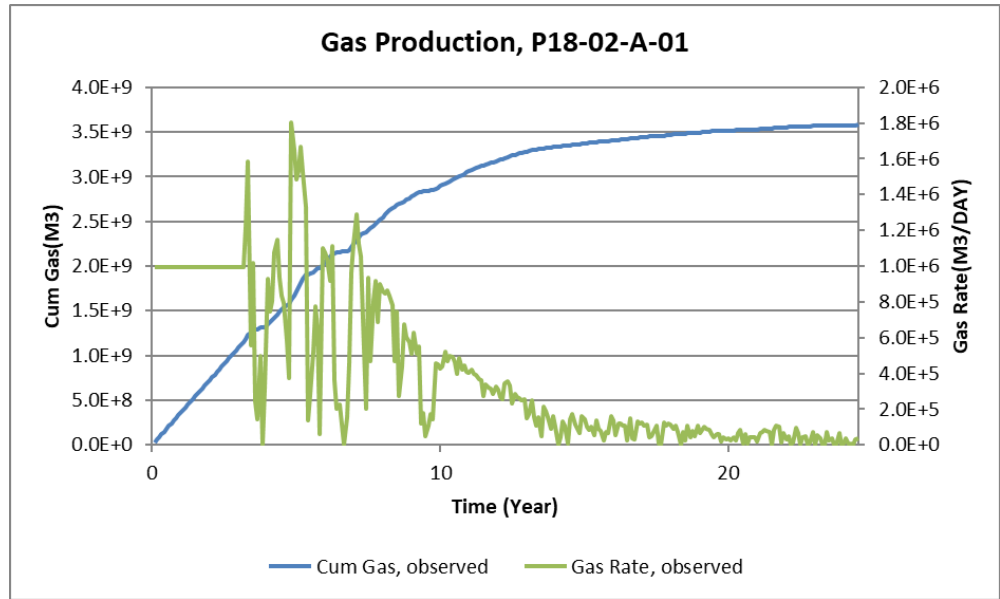


Figure 17-39: Gas production of well P18-02-A-01.

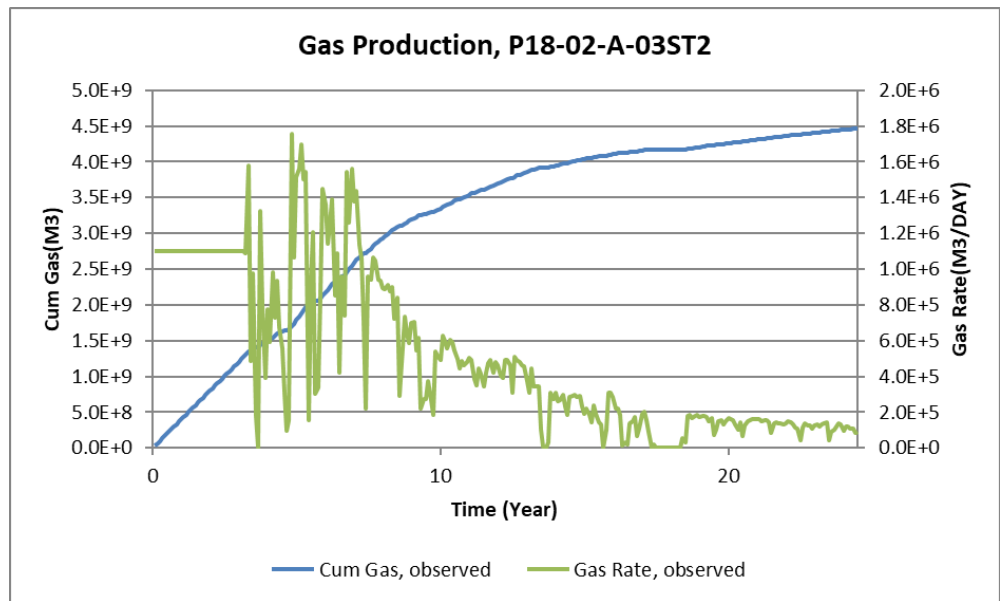


Figure 17-40: Gas production of well P18-02-A-03ST2.

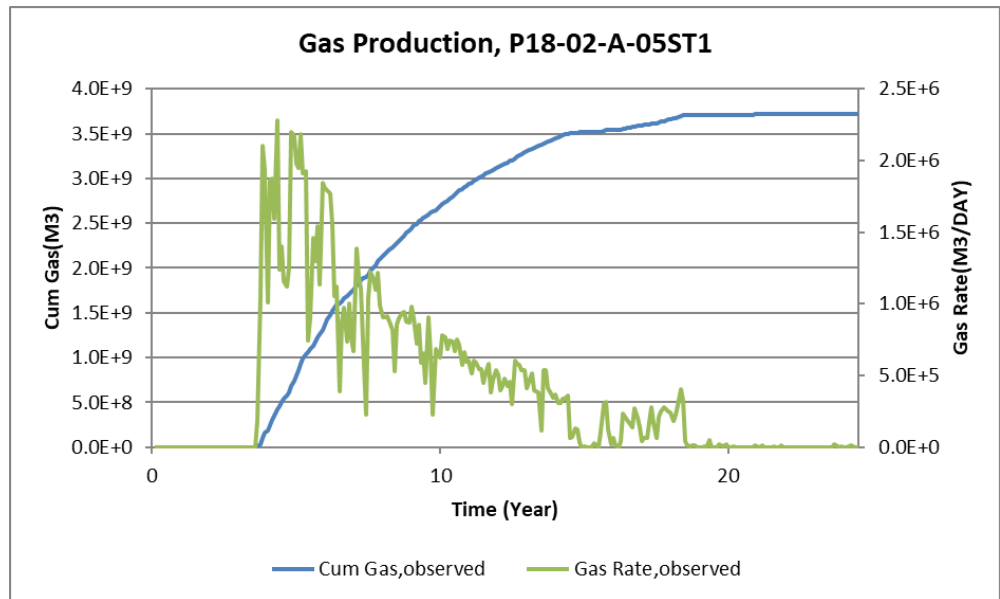


Figure 17-41: Gas production of well P18-02-A-05ST1.

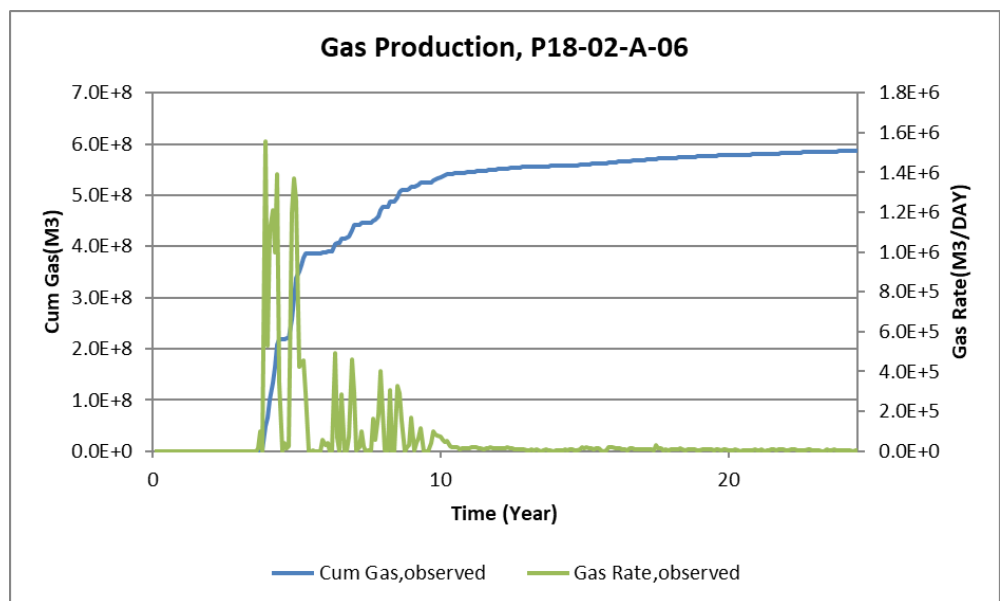


Figure 17-42: Gas production of well P18-02A6.

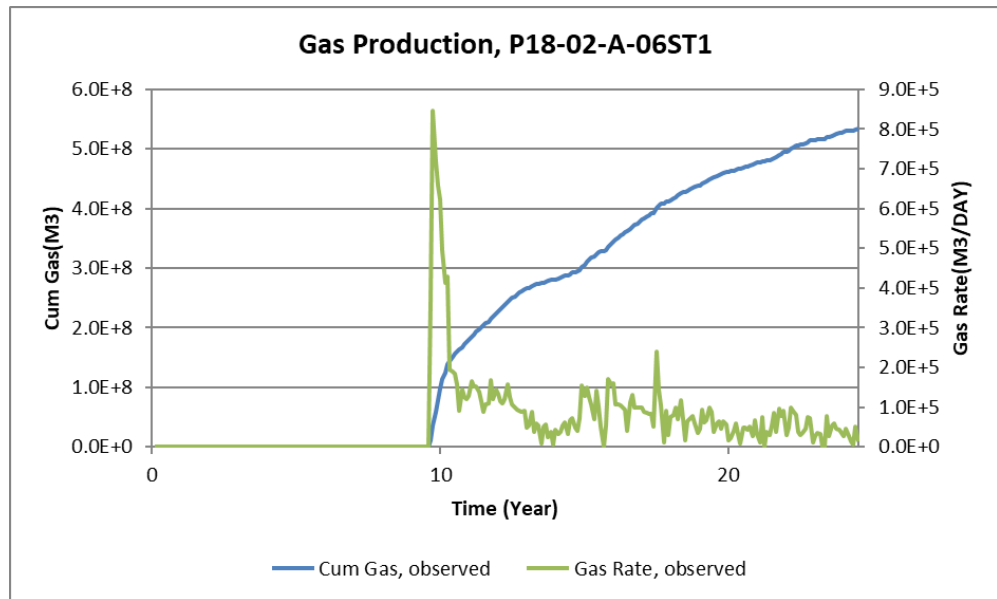


Figure 17-43: Gas production of well P18-02-A-06ST1.

17.8.2.5 Historic pressure data

Daily tubing head pressure (THP) data and on irregular basis shut in pressure data was provided. A bottom hole pressure (BHP) is generally not measured directly. Instead, the (THP) is measured and BHP is calculated from this THP and reported production or injection rates using a well bore flow model. To be able to calculate the BHP from the THP a number of parameters, including completion data and production rates, have to be accurately known by absence of Vertical Lift Performance Relationship (VLP) of each production well the opportunity to convert THP to BHP is not performed.

The measured pressure data (Figure 17-44) suggests a clear communication between compartment I, II and IV, therefore an open fault between compartment I and II is assumed. However compartment III (well P18-02-A-06) has no pressure communication to the other P18 compartments.

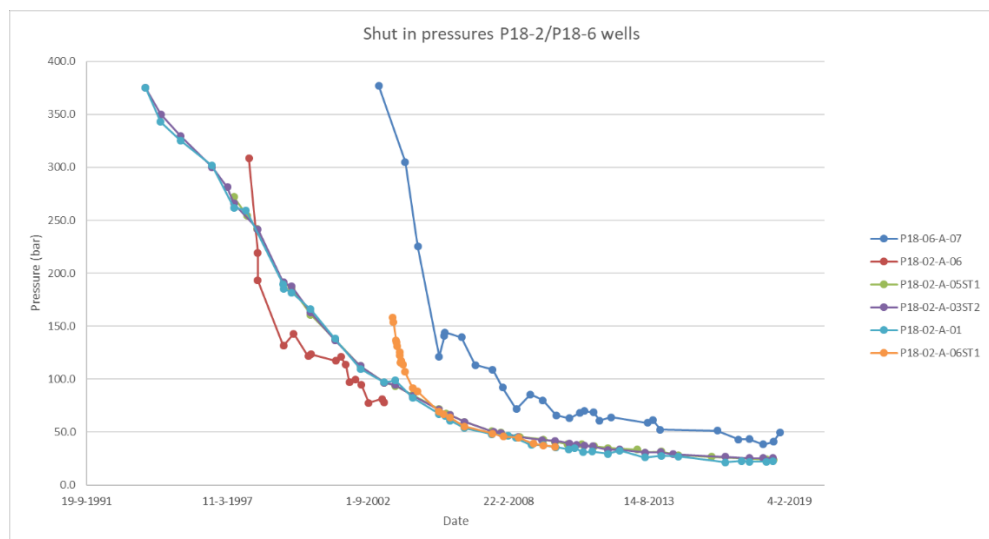


Figure 17-44: Pressure profiles of the five production wells over time.

17.8.3 *P/Z curves*

The standard method to estimate the GIIP and driving mechanism (e.g. natural water drive, volumetric depletions) is material balance analysis applied on the production and pressure history. The most used method is the p/z plot shown in

Figure 17-45 and Figure 17-46, which shows a linear profile corresponding to volumetric depletion driving mechanism.

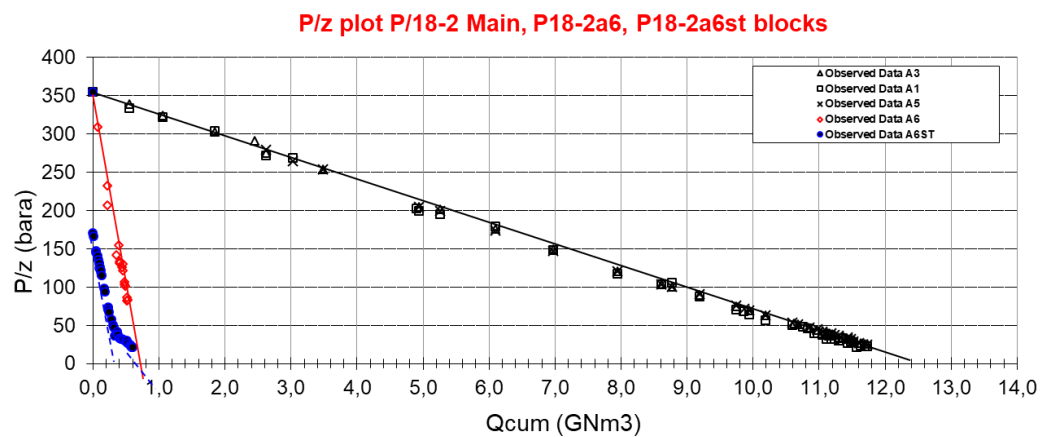


Figure 17-45: P/Z curves of P18-2 field.

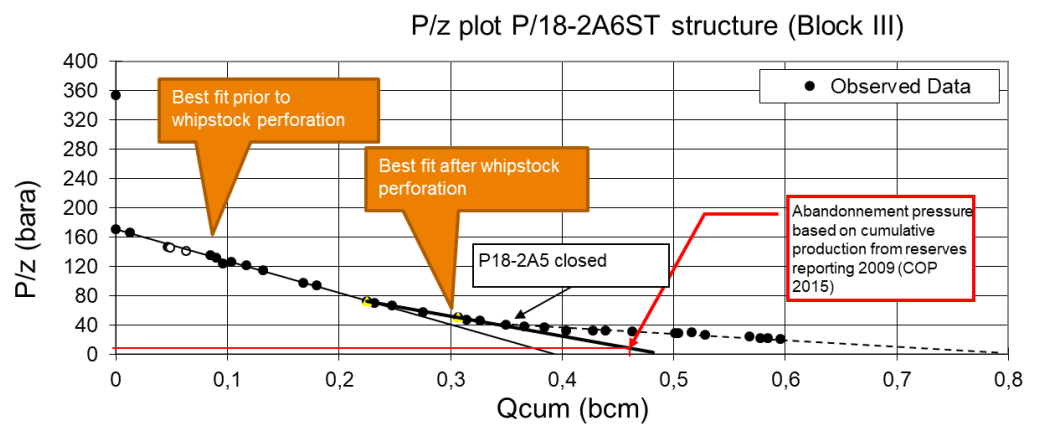


Figure 17-46: P/Z curve of P18-2 compartment, compartment III.

17.8.4 *History matching approach*

As discussed in a previous section (17.8.2.5) no BHP observations are available, therefore the measured shut-in pressures is matches with the 9-point pressure of each individual well. The history match approach is done according to the following procedure:

- The simulations was performed under rate constraint conditions
- Change the GIIP of the individual compartments by a pore volume multiplier (if needed)
- Change the permeability of the dynamic model based on porosity – permeability relationship, since the well logs and well test data (KH) do not match.

- Match the measured shut-in pressures with the 9-point pressure of each individual well.

#### 17.8.4.1 History Match of GIIP

The result of the history matching the GIIP is summarized in Table 17-9. The base case is the model without any pore volume multipliers, but with the baffle and adjusted permeability to fit the well test KH as described in 0. The base case model is already close to the GIIP estimated by P/Z analysis, however to improve the pressure behaviour of the different production wells, multipliers in the main compartment (compartment I) and in compartment III are used. Especially the multiplier used in compartment III could indicate further compartmentalisation needed to match. In the HM case the following pore volume multipliers for the different compartments are used:

- Compartment I: 1.10;
- Compartment II: 1.00;
- Compartment III: 0.75;
- Compartment IV: 1.00.

For completeness all volumes for the base case and the HM case are summarised in Table 17-10.

Table 17-9: GIIP results.

	Volume in Compartment I, II and IV (GSm <sup>3</sup> )	Volume in Compartment III (GSm <sup>3</sup> )	Total Volume (GSm <sup>3</sup> )	GWC (m)
P/Z	12.65	0.7	13.35	3680
Base case	12.30	0.97	13.27	3680
HM case	13.2	0.73	13.93	3680

Table 17-10: Overview of the pore volume, Hydrocarbon volume (HC) and GIIP of the base case and History Match case of all compartments in P18-2 reservoir.

		pore volume (10 <sup>6</sup> rm <sup>3</sup> )		HC pore volume (10 <sup>6</sup> rm <sup>3</sup> )		GIIP (10 <sup>6</sup> Sm <sup>3</sup> )	
		static	dynamic	static	dynamic	static	dynamic
Base case	P18-2-compartment-I	46	46	36	37	9.1·10 <sup>3</sup>	9.1·10 <sup>3</sup>
	P18-2-compartment-II	22	22	12	12	3.0·10 <sup>3</sup>	3.0·10 <sup>3</sup>
	P18-2-compartment-III	5	5	4	4	9.0·10 <sup>2</sup>	9.7·10 <sup>2</sup>
	P18-2-compartment-IV	47	47	0	1	1.1·10 <sup>2</sup>	1.9·10 <sup>2</sup>
	Total	120	121	52	54	1.3·10 <sup>4</sup>	1.3·10 <sup>4</sup>
Hm case	P18-2-compartment-I	46	51	36	40	9.1·10 <sup>3</sup>	1.0·10 <sup>4</sup>
	P18-2-compartment-II	22	22	12	12	3.0·10 <sup>3</sup>	3.0·10 <sup>3</sup>
	P18-2-compartment-III	5	4	4	3	9.0·10 <sup>2</sup>	7.3·10 <sup>2</sup>
	P18-2-compartment-IV	47	47	0	1	1.1·10 <sup>2</sup>	1.9·10 <sup>2</sup>

	Total	120	124	52	56	1.3·10 <sup>4</sup>	1.4·10 <sup>4</sup>
--	-------	-----	-----	----	----	---------------------	---------------------

17.8.4.2 History match on pressure data

Not only the GIP is adjusted by the static model also the permeability, which are based on logs and porosity/permeability relationship. However based on the well-test higher values for the permeability are expected (see Table 17-7). Therefore porosity-permeability relationship should be re-evaluated. This porosity-permeability relationship from the BP petrophysical report is based on three rock types based on cores of the Detfurth formation alone. Therefore it is difficult to adjust the relationship for the higher porosities alone. To adjust the relationship the following strategy was used:

- A multiplier of 2 on the permeability of the entire P18-reservoir.
- Since the Hardegsen formation has higher quality than the Detfurth (see PLT) a multiplier of 4 on top of the previous multiplier is used. The permeability of the Hardegsen is probably underestimated because of upscaling process and more importantly the absence of cores from the Hardegsen itself.

Table 17-11 shows the comparison between KH (product of permeability and formation thickness) from well test data and dynamic model; Figure 17-47 shows the distribution of permeability in the P18-2 dynamic model.

Table 17-11: Comparison of model KH and the KH estimated from the well test.

Well Name	Perforations (m)	KH (mDm) based on well test	KH (mDm) in dynamic model 2019
P18-02-A-01	3580-3695	1847	1548
P18-02-A-03ST2	4070-4209	-	1572
P18-02-A-05ST1	4798-4980	25249	15696
P18-02-A-06	4488-4633	3686	3660
P18-02-A6ST1	3376-3936	-	14493

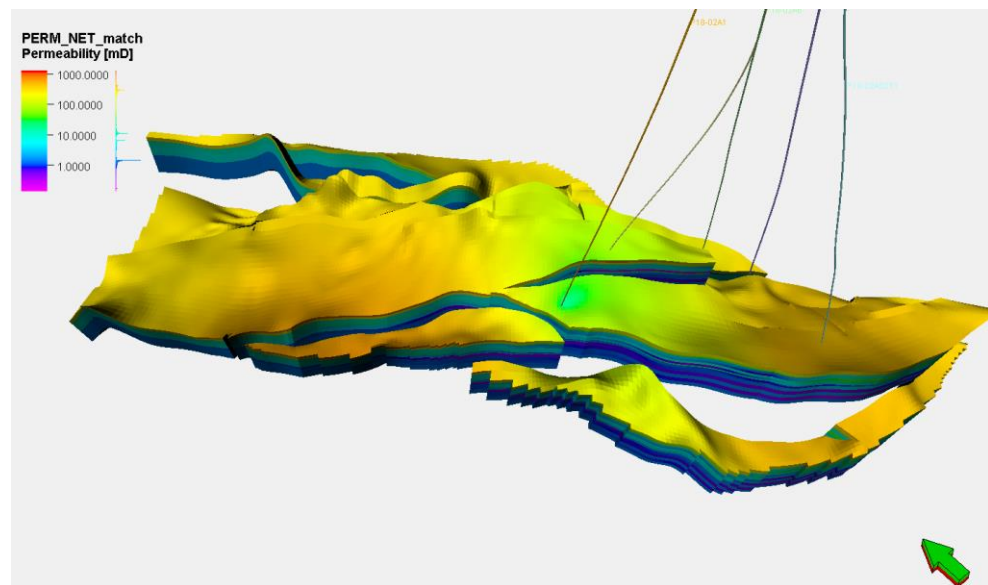


Figure 17-47: Permeability distribution in the P18-2 field.

Based on the pressure data (Figure 17-44) a clear pressure difference is observed between compartment I and compartment II, which suggest a baffle between both compartments. This baffle was modelled by a transmissibility multiplier on the fault between the two compartments with a value of 0.04.

#### 17.8.5 Result of the history match

Based on the parameters described in the previous section the following production and pressure match is achieved (Figure 17-48 through Figure 17-55). In the figures both the base case and the history matched model are presented. The base case have the same volume as the static model, but the baffle between compartment I and II is implemented). In general the match of the production and pressure of all the wells are achieved. The production rate of well P18-02-A-03ST2 is not maintained in the base case, which was the reason (together with the modelled pressures, which were too low) to increase the GIIP by 10% in compartment I.

In particular the match of well P18-02-06ST1 was problematic. From the RFT data which show that the pressure in compartment II had decreased to 159 bar (Table 17-13), it was clear that there is a baffled connection between compartments I and II. This was represented by a multiplier of 0.04. However, the connection between the compartments changes over time due to water inflow at the Hardeggen-Hardeggen juxta-position of the fault between compartments I and II. The dynamic model was mostly able to reproduce the pressure profile of well P18-02-A-06 and P18-02-06ST1 located in compartment II (see Figure 17-55). However, if water inflow is too strong and decreases the transmissibility between the compartments too fast, the pressure match deteriorates. It was found that calculation of the capillary pressure with a J-function gave a better representation of the water saturation and water inflow than the saturation-height function.

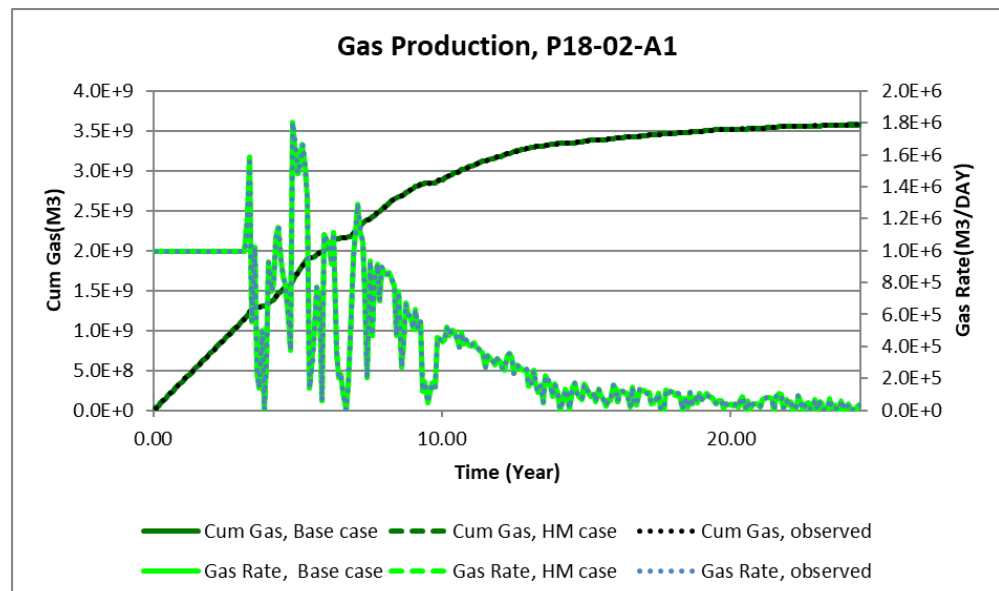


Figure 17-48: History matched production data well P18-02-A-01.

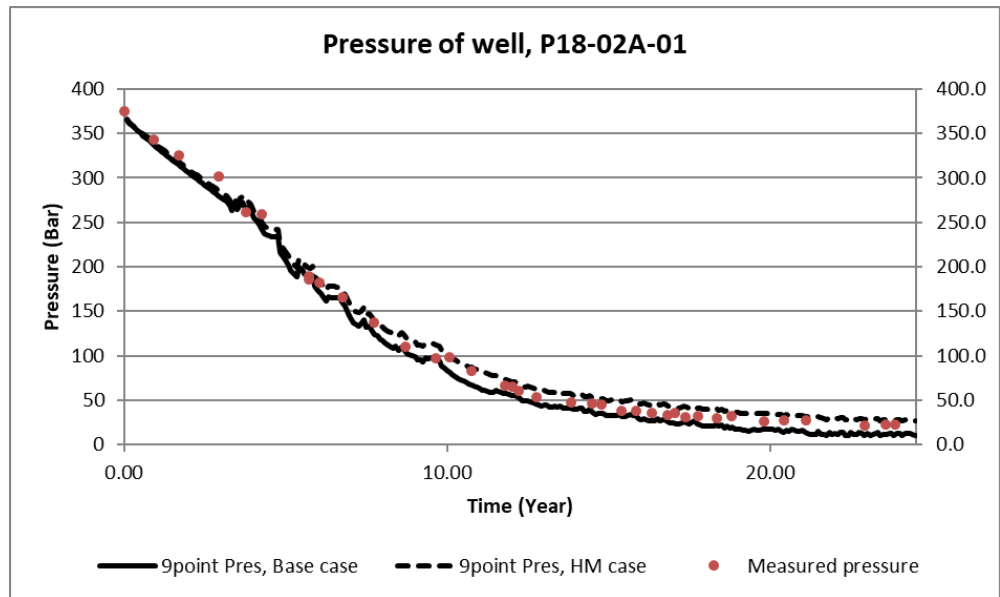


Figure 17-49: History matched pressure data well P18-02-A-01.

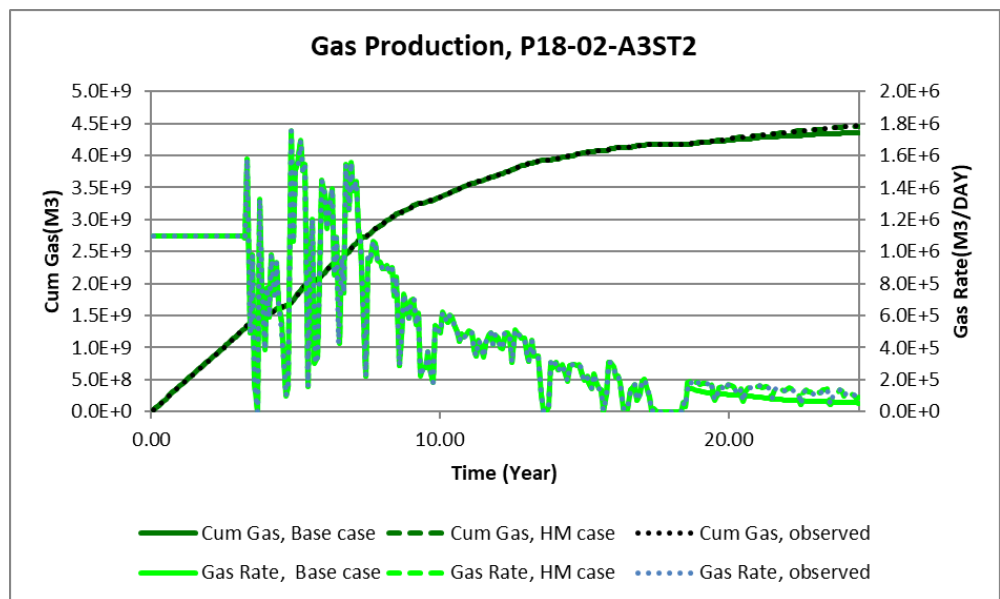


Figure 17-50: History matched production data well P18-02-A3ST2.

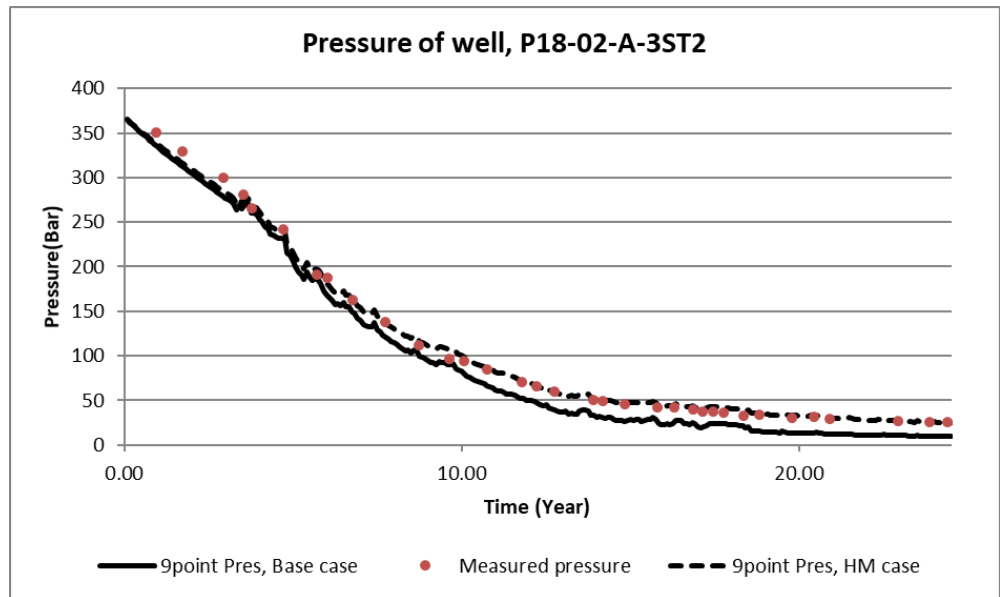


Figure 17-51: History matched pressure data well P18-02-A-03ST2.

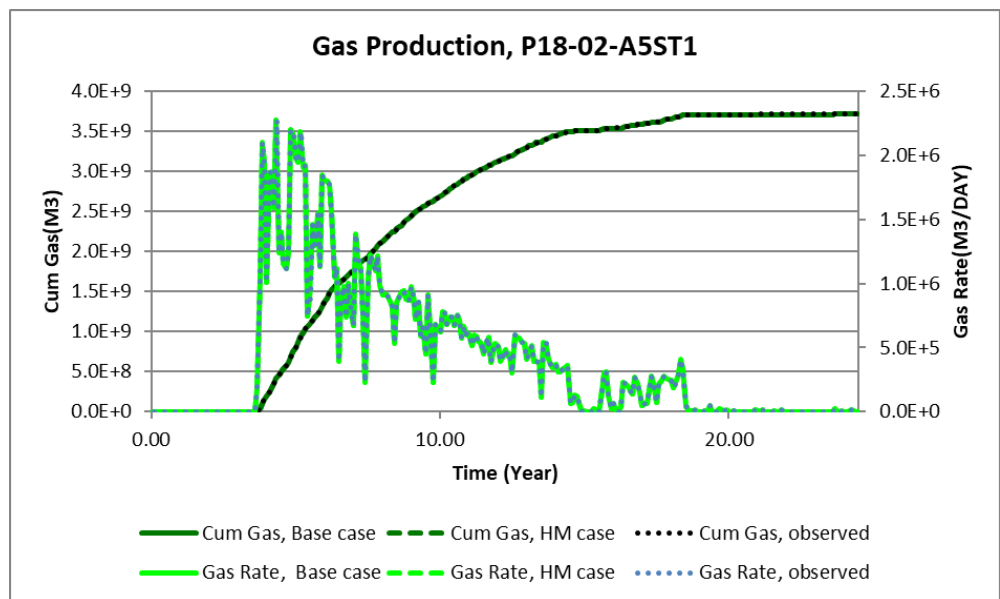


Figure 17-52: History matched production data well P18-02-A-05ST1.

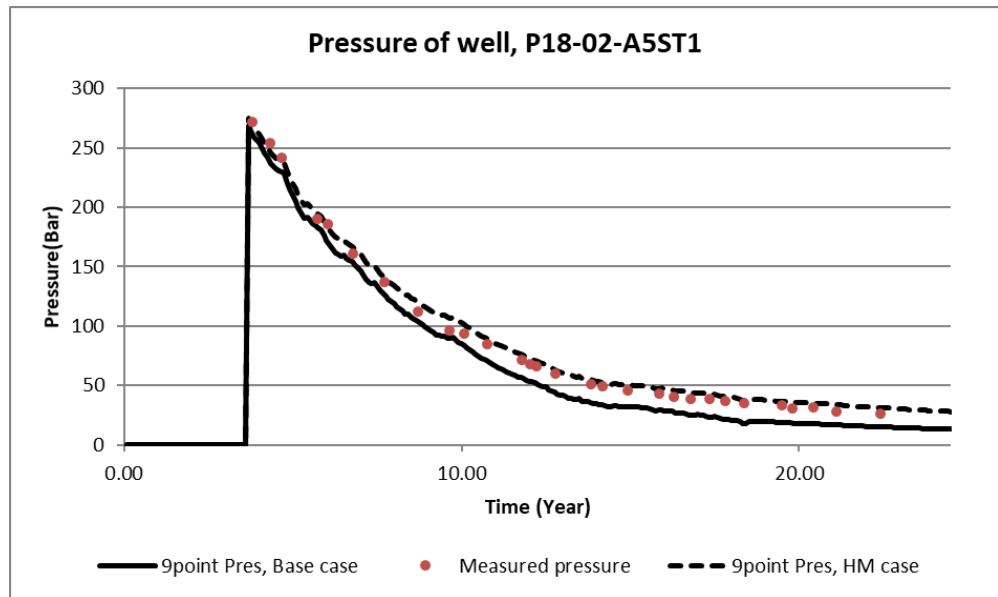


Figure 17-53: History matched pressure data well P18-02-A-05ST1.

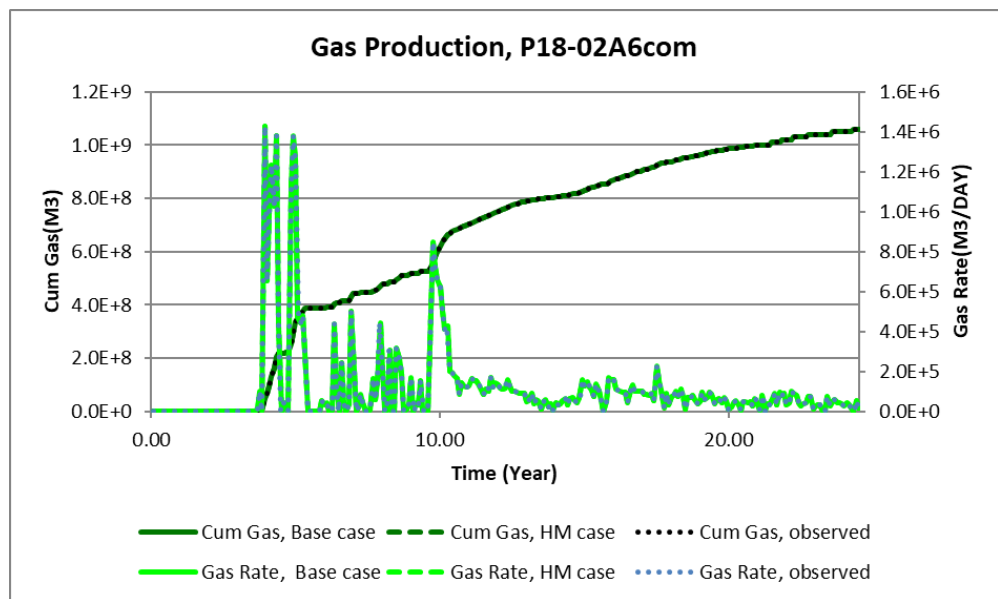


Figure 17-54: History matched production data well P18-02A6 and P18-02-A6ST1.

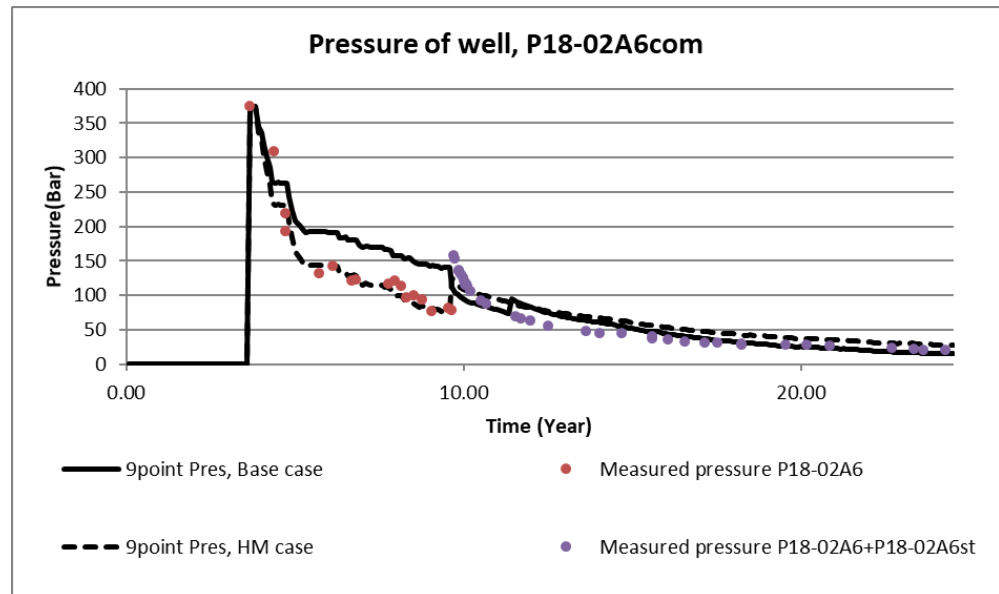


Figure 17-55: History matched pressure data for wells P18-02A6 and P18-02A6st. Note in 2003 (after 10 years the well P18-02A6 is closed and P18-02A6st is opened. In 2005 (after 12 years) the whipstock is perforated and production is from both wells at the same time. The pressure measurements from 2005 (after year 12 in the figure) and later are difficult to interpret because of simultaneous production from the two compartments.

17.8.6 History Match on RFT and PLT data

The modelled and observed RFT data from well P18-02-A5ST1 are in agreement, although it was difficult to obtain a match for P18-02-A6ST1. The reservoir model allows for crossflow between the wells P18-02-A6ST1 and P18-02-A6, but the rate of crossflow is highly uncertain. A better match was obtained with a model without crossflow.

Table 17-12: PLT results of P18-2-A5ST1.

Formation	P18-2-A5-str1 measured (%)	P18-2-A5-str1 modelled (%)
Hardegsen	83	84
Detfurth Claystone	4	13
Lower Detfurth Sandstone	13	2
Volpriehausen	< 1	1

Table 17-13: RFT data observed and modelled, for wells P18-02-A5ST1 and P18-02-A6ST1.

Formation	RFT P18-02-A5ST1		RFT P18-02-A6ST1		TNO model without crossflow (bar)
	Observed (bar)	TNO model (bar)	Observed (bar)	TNO model with crossflow (bar)	
Hardegsen		275	159	127	136
Upper Detfurth	270	276	159	127	136
Lower Detfurth	280	277	159	127	136
Volpriehausen	340*	280	159	127	136

#### 17.8.7 *History match conclusion*

- The dynamic model reproduces production rates and most of the pressure data. The start of P18-02-A-6ST1 well was more difficult to capture in this model.
- Compartment I and II are partly connected.
- Compartment III is likely to be disconnected and probably further compartmentalized.
- A pressure measurement in the well P18-02-A6ST1 should make clear whether crossflow happened. For the purpose of this study we assumed the model with crossflow, which is the basis for the injection scenarios.
- The dynamic model reproduces the pressure behaviour of the proposed injection wells, despite the unknown parameters (compressibility, saturation curves).

### 17.9 **Geomechanical model**

#### 17.9.1 *MACRIS – Poro-elastic model*

We detail here the TNO-developed semi-numerical approach (MACRIS, Mechanical Analysis of Complex Reservoirs for Induced Seismicity) to handle pressure effects along multiple faults. More specifically MACRIS is designed to compute 3D stress changes along faults induced by: (1) poro-elastic effect (contraction/inflation of the reservoir due to fluid pressure depletion/injection), (2) direct pressure effect (changes of the fluid pressure intra-faults can induce changes in effective normal stress), (3) differential compaction effect due to the fault offset.

MACRIS is a mesh-free approach where there is no need to build a dedicated grid for the geomechanical analysis. MACRIS takes directly as input the grid of the reservoir flow simulation; in our case: the 3D pressure fields of the P18-2 field at a yearly sampling rate. Each grid block of the reservoir flow simulation is considered as a compacting nucleus of strain (center of compression; Mindlin 1936; Geertsma, 1973; Okada, 1992). The contribution of each of these nuclei is integrated to compute the poro-elastic stress changes along each fault of the P18-2 field with a meter-scale spatial resolution. The restriction that we presently still have is that only one-way coupling is considered. We deem this acceptable for gas reservoirs, where the effect of compaction on the gas pressures in the pores is small. The Barnes-Hut algorithm (Barnes and Hut, 1986) is used for re-discretizing the initial reservoir grid for two purposes: (i) clustering the nuclei of strain close to the faults in order to increase the spatial stress resolution, and (ii) shortening the computation time.

MACRIS thus computes the poro-elastic normal and shear stress changes induced by the reservoir compaction for every observation point along each fault.

Observation points are placed on fault pillars (i.e. sub-vertical lines along the fault dip direction), which in turn make up the 3D geometry of a fault (see Figure 17-56).

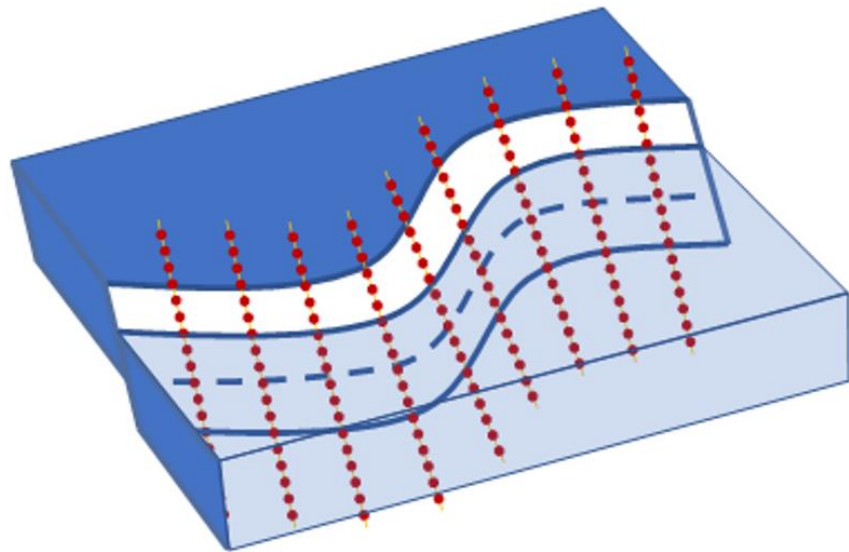


Figure 17-56: Schematic of the distribution of the observation points (where the stress solution is evaluated) along fault pillars.

In order to account for the direct pressure effect, we still need to define the pore pressure changes inside the faults to calculate the effective normal stress changes and derive the Coulomb stress changes. This intra-fault pore pressure is defined as the average fluid pressure between the two juxtaposed reservoir compartments.

MACRIS has been validated by comparison with relatively slow finite-element (FE) numerical computations (DIANA), with excellent results (van Wees et al., 2018). This benchmarking exercise has been carried on using single-fault tank models; for MACRIS it was a 3D model and for DIANA it was a 2D plane strain model. For the present study we extended this benchmarking exercise by comparing the 3D MACRIS model with this time a full 3D DIANA model. Results of this exercise are presented in Figure 17-57. The 3D single-fault model mimics the P18-2 field at the end of the depletion period, that is with an initial pressure of 330 bars and a decrease of pressure of -300bars at the end of the depletion period. The MACRIS results closely match the FE DIANA solution. Deviations between both solutions are less than 3%.

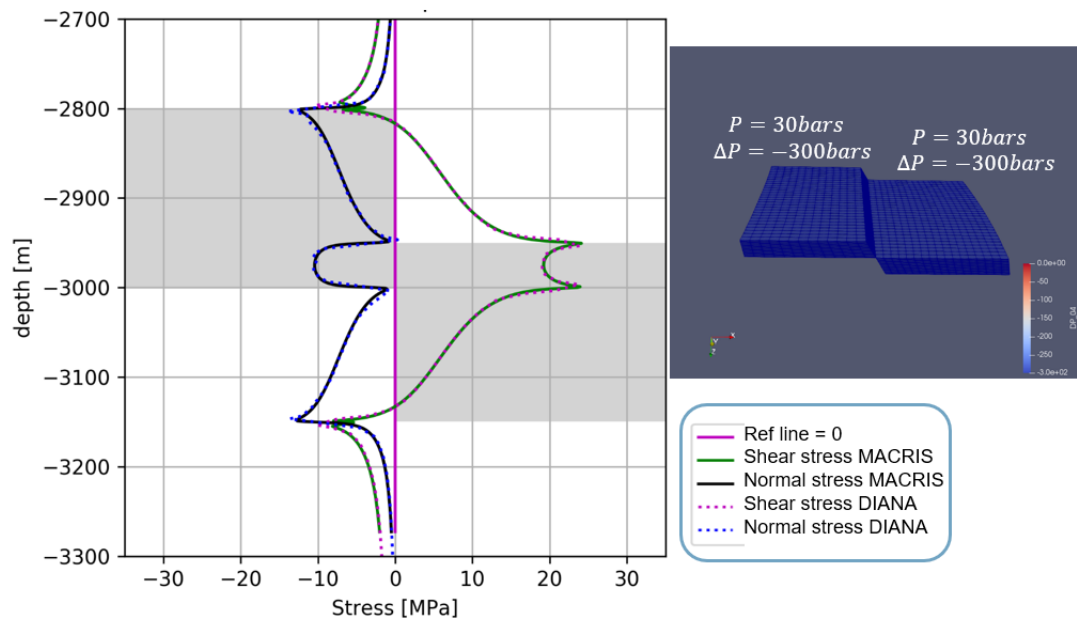


Figure 17-57: Comparison MACRIS vs. Diana FEM package. Right: 3D single-fault model with offset. Both compartments start with the same initial pressure (330 bars) and are depleted of the same amount (-300 bars). Left: Stress solution along the central pillar of the model. The changes in shear and normal stresses induced by the poro-elastic effect are almost identical between both solutions. For this particular example, the pore pressure inside the fault remains at the initial pore pressure.

### 17.9.2 Thermo-elastic model

The TNO-developed semi-analytical approach to model thermo-elastic stresses due changes in temperature of reservoir rock is based on Myklestad (1942). Myklestad (1942) derived equations for all the components of the stress tensor as induced by heating a semi-infinite cylinder to a constant temperature difference with respect to the ambient reservoir temperature using elliptical integrals in a cylindrical coordinate system. Candela et al. (2018) contains all the details of the derivation.

This approach gives us the tensor of stress changes inside and outside the reservoir in the cylindrical coordinate system. This tensor of stress changes thus needs to be translated to Cartesian coordinates using standard cylindrical coordinate transformation. The initial stress state is then added to the tensor of stress changes to obtain the stress tensor in Cartesian coordinates (see Figure Figure 17-58 and Figure 17-59).

We consider faults uniformly distributed in our model. In other words, each location inside and outside the reservoir (in the caprock) can potentially host a fault. More specifically, from the stress tensor, at each location, one can calculate the Coulomb stress changes for any fault plane orientations.

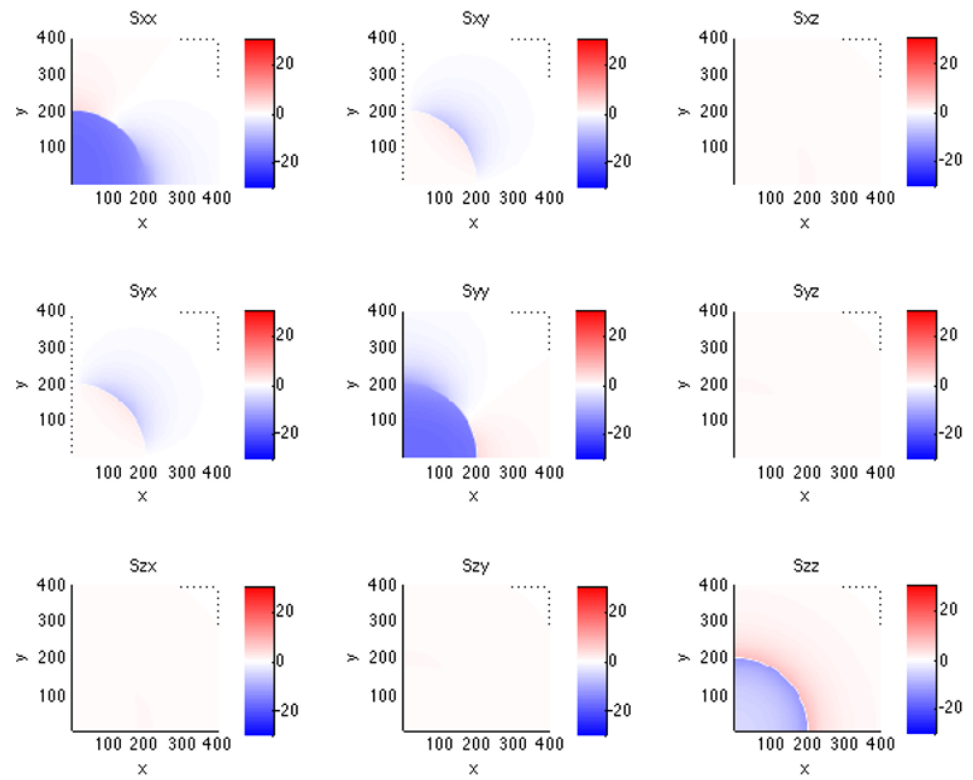


Figure 17-58: Horizontal [XY] spatial distribution of each component of the tensor of stress changes.

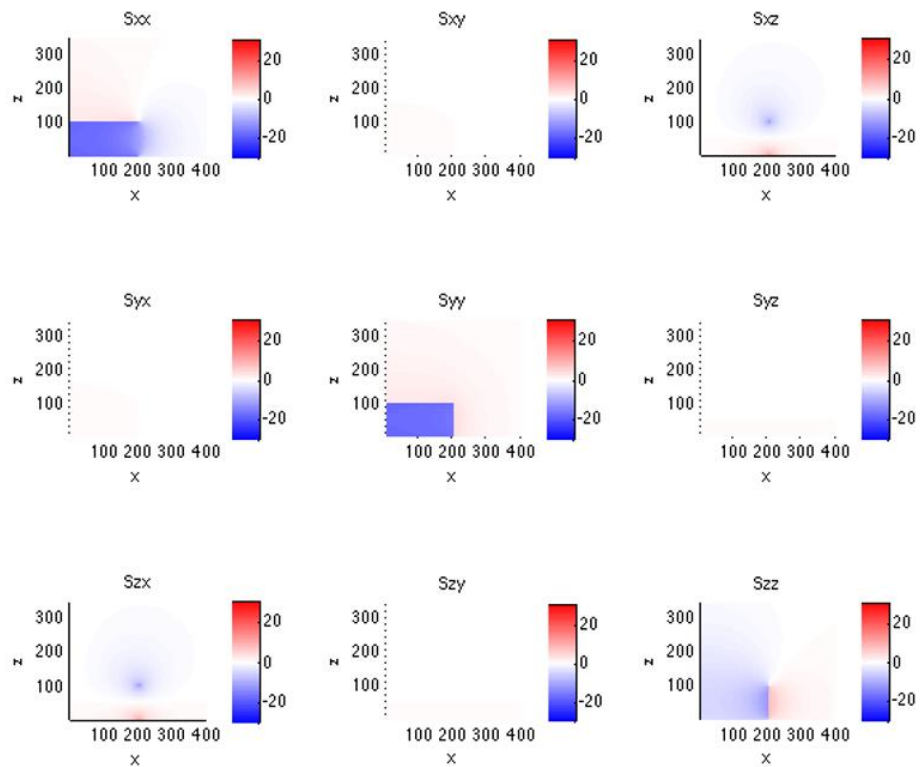


Figure 17-59: Vertical [XZ] spatial distribution of each component of the tensor of stress changes.

### 17.10 Well degradation model

The nonlinear finite element simulator DIANA<sup>10</sup> is used to generate meshes for 2D numerical models of the well system and run structural and heat transfer simulations. The workflow is automated by a dedicated user interface DIANA SEALEC: the user-defined input and model parameters are used to generate meshes and define the complete non-linear (phased, staggered) analysis, which mimics the different loads acting on the well system throughout the entire lifetime of a well, from the drilling phase, well completion, testing, operations and abandonment (Figure 17-60).

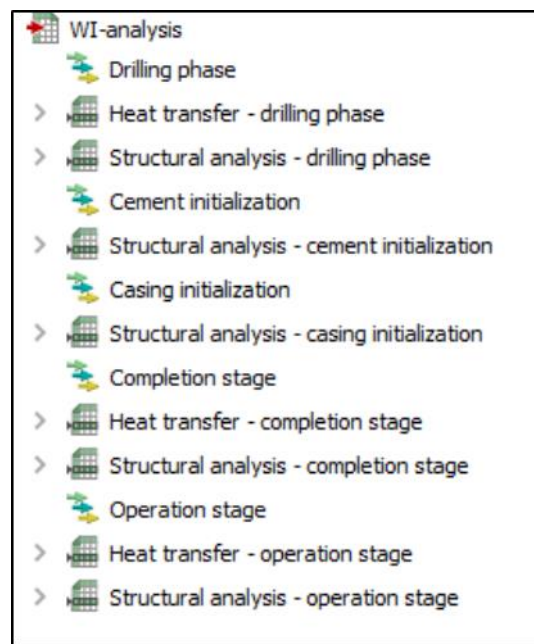


Figure 17-60: Example of steps in the wellbore integrity analysis.

The model of the well system, representing a cross-section normal to the well axis, comprises the casing, the cement and the surrounding rock formation. The chosen 2D modelling approach is computationally efficient and simulations can easily be repeated for various depths along the wellbore. Complete plane strain elements are used for bulk materials. Zero-thickness interface elements are used for the casing-cement and the cement-formation interfaces. The well materials can be modelled with different constitutive models; for example a von Mises elasto-plastic material model for the steel casing; a combination of the Mohr-Coulomb elasto-plastic model and the multi-directional fixed crack model for the cement; a Mohr-Coulomb elasto-plastic model for the rock formation; and the Coulomb friction model with a tension cut-off for the interfaces between materials. Different failure modes can be simulated, for example: plastic deformation of casing, plastic deformation and cracking of the cement sheath, plastic deformation of formation and debonding of cement interfaces (Figure 17-61). Specific deformational behaviour of materials can be modelled such as shrinkage of cement and the creep behaviour of viscous rock salt formation.

<sup>10</sup> See [dianafea.com](http://dianafea.com).

Structural, heat transfer and fluid flow analyses are typically needed for wellbore integrity assessment. Results from finite element analyses are typically displacements, stresses and strains in different formulations.

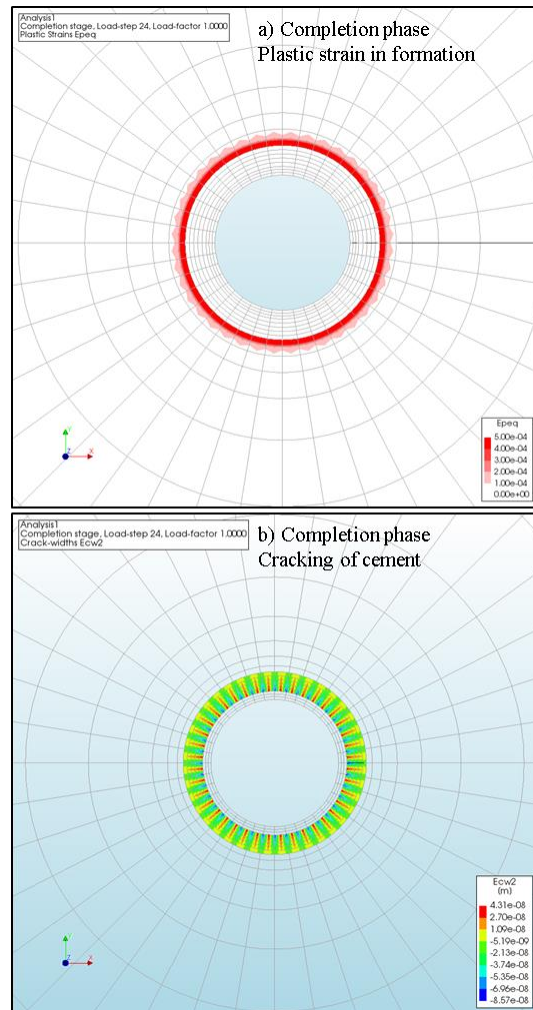


Figure 17-61: (a) Plastic strain in the formation and (b) cracking of annular cement in the completion phase.

## 18 Appendix C. Risk Register

## Caprock

Identified risk	Description	Positive evidence for integrity	Risk reduction measures	Risk characterisation	Risk classification
Initial condition	Impermeable shales of the Upper Triassic and Altona Groups overlie the P18-02 reservoir, which represent a good seal for the natural gas reservoir.	Effective seal as evidenced by the presence of gas in reservoir below the seal; 50 m of primary caprock and 100s of metres of secondary caprock; gas column of 581 m	Reservoir pressure after CO2 injection equal to or lower than initial gas reservoir pressure	As the evidence for the initial sealing of the gas reservoir is very strong, it is a good seal for CO2 storage as well and consequently the risk of migration out of the reservoir is low to even negligible when the pressure is kept at or below the initial reservoir pressure.	A-1
Fracturing	Fractures in the seal may be caused by local stress variations due to initial gas production, subsequent CO2 injection and associated pressure and temperature changes. Fractures represent a potential conduit for CO2 loaded fluids depending on their connectivity and continuity (see also Fault zone)	Semi-analytic modelling has shown that Coulomb stresses as a consequence of pressure build-up due to injection quickly decay on top of the reservoir inside the caprock. The pressure effect is thus not expected to contribute to the risk of fault reactivation in the caprock. New fractures or faults will not be generated as they would require even higher Coulomb stresses. This is confirmed by earlier mechanical analysis of seal and fault based on P18-2; no critical factors identified (Vandeweyer et al., 2011: ch6, par 6.7, p108). Although temperature-induced positive Coulomb stresses occur in the caprock near the edges of the cooling front, they are not sufficiently large to re-activate faults in the caprock nor will they result in new fractures in the caprock. The likelihood of re-activating a pre-existing fault in the caprock is thus very low. A similar conclusion was drawn for P18-4 at a depth 3190 m (Peters et al., 2014).	Keep the pressure below fracturing condition and appropriate management of thermal effects	If fracturing due to pressure increase and/or temperature drop will occur, this will only result in local effects if any. Considering the huge thickness of the caprock, the likelihood of fracturing the complete caprock is nil and consequently the risk is low (to even negligible).	A-1
Chemical degradation	CO2 if dissolved may react with minerals in the caprock near the interface with the CO2 reservoir.	Since the caprock has proven to be a seal for gas, the only way of upward migration is by diffusion of dissolved CO2, which is a very slow process. Chemical interaction between dissolved CO2 and caprock minerals is very slow and has minor effects on porosity and permeability. Hence, no migration path is expected to form. The affected zone of migration of dissolved CO2 and chemical interaction is in the order of several meters in thousands of years (Gaus et al., 2004; Tambach et al., 2012).	Reservoir pressure after CO2 injection at or lower than initial gas reservoir pressure, to prevent CO2 from entering the caprock in gaseous/supercritical state thereby enhancing geochemical reactions.	Chemical degradation will only marginally influence the sealing properties of the caprock and thus will the overall integrity of the caprock stay intact. The likelihood of degrading the caprock is very low and its consequence will be nil or negligible.	A-1

**Fault zone**

Identified risk	Description	Positive evidence for integrity	Risk reduction measures	Risk characterisation	Risk classification
Initial condition	Sealing capacity of reservoir boundary faults determined by juxtaposed claystone and reservoir rocks (Vandeweyer et al., 2011: par3.5.1, p20 and Fig. 3:8 on p23)	Bounding faults F19/F20 and F40 are effective seals as evidenced by presence of juxtaposed gas reservoirs and sealing rock. In two cases reservoir rocks can be juxtaposed over a very small section on both sides of faults but in these cases reservoir rock with very low permeability (< 1mD) is present on one or both sides of the fault (see also discussion on communication between P18-2 and P18-6 for the reservoir compartment).	Manage pressure gradient across fault	As reservoir rocks next to bounding faults are sealed off by very low permeable rocks on the other side of the fault zone, it has a very low likelihood that a negligible amount of CO2 will migrate across or along the fault and sealing rock.	A-1
Chemical degradation	Chemical degradation of material in fault zone	Currently, there is no evidence for gas migration from the P18-02 reservoir along the faults to overlying formations. In general, the geochemical reactions between CO2, formation water and fault gouge mineralogy will result in precipitation of carbonate minerals. On the longer term, silicate minerals might react, providing additional cations for carbonate precipitation. Porosity and hence permeability effects are predicted to be negligible. Increase of carbonate content in the fault gouge is known to increase the friction coefficient and to decrease potential for fault re-activation.		Chemical degradation leads to lowering of the porosity and permeability of the fault gouge and increases the friction coefficient of faults. Therefore it is highly unlikely that chemical degradation in itself leads to the migration of CO2 across the fault zone.	A-1
Pressure re-activation	Due to pressure changes during production and/or injection faults may be re-activated (Vandeweyer et al., 2011: par 6.7, p109) and potentially act as conduits for CO2.	No seismic activity was encountered during production, based on the KNMI database (Vandeweyer et al., 2011) Semi-analytic modelling has shown that at the end of the injection period most (if not all) of the areas where positive Coulomb stresses which are present at the end of depletion, have disappeared. The faults are thus expected to be stable at the end of the injection period.	Injection of CO2 is a mitigation measure in itself as it reduces the underpressure in the reservoir and consequently the risk of fault re-activation.	Based on the results from the semi-analytic modelling it appears to be highly unlikely that faults will be re-activated due to the increased pressure by CO2 injection and consequently will not lead to migration of CO2 along the fault.	A-1
Thermal re-activation	Cold injection stream could re-activate a nearby fault and change its fluid transport properties.	TOUGH2 simulations have shown that the cooling front could extend to 300 m from the injector after 15 years of injection. Semi-analytic modelling indicates that the Coulomb stresses rapidly decay to around 2.5 MPa at a distance of 100 m from the cooling front. Thus injection wells at less than 300 to 400 m from a fault may thermomechanically influence its stability.	Managing the advancement of the cold front near faults by adjusting the injection rates of wells which are within a distance of 300 to 400 m from a major fault. More detailed thermomechanical assessment may reduce the uncertainty in the consequence of cooling for fault re-activation.	With inclusion of proper management of the injection rates in wells nearby faults the likelihood of thermomechanical fault re-activation leading to the migration of a very small amount of CO2 out of the reservoir will be low.	B-2

Cont. improvement
ALARP
Intolerable

**Reservoir**

Identified risk	Description	Positive evidence for integrity	Risk reduction measures	Risk characterisation	Risk classification
Spilling NW of compartment II	Overfilling could lead to lateral migration (spilling) of CO2 to neighbouring Buntsandstein aquifers and gas reservoirs. Subsequently, CO2 may migrate to Lower Cretaceous or Lower Tertiary aquifers in case the wells are not well isolated. A potential spill zone is identified at the NW edge of compartment II of the reservoir near Fault 1.	The final pressure state of the reservoir will be at or below the initial pressure. A simulation scenario with strong overpressurization during injection does not show spilling.	Spilling prevented by keeping the reservoir pressure at or below the initial pressure and limiting the total mass of injected CO2. Proper zonal isolation of wells and preventing re-activation of faults to avoid vertical migration (see also Fault compartment)	Keeping the average reservoir pressure at or below the initial pressure at the end of injection and the robustness of flow simulations indicate a very low likelihood that a negligible amount of CO2 migrates out of the reservoir.	A-1
Spilling NW of compartment I	Overfilling could lead to lateral migration (spilling) of CO2 to neighbouring Buntsandstein gas reservoirs and aquifers. Subsequently, CO2 may migrate to Lower Cretaceous or Lower Tertiary aquifers via non isolated wells or permeable faults if any. A second small potential spill zone is identified at the NW edge of compartment I (across fault F14) of the reservoir. Low permeable sandstones of the Volpriehausen Formation (< 1 MD) and permeable sandstones of the Hardegsen Formation are juxtaposed across fault F14.	The final pressure state of the reservoir will be at or below the initial reservoir pressure. The potential spill point is very likely not leading to migration of CO2 out of the reservoir as the very low permeable Volpriehausen (< 1 MD) and Hardegsen are juxtaposed hampering the flow of CO2.	Spilling prevented by keeping the reservoir pressure at or below the initial pressure and limit the total mass of injected CO2. Proper zonal isolation of wells and preventing re-activation of faults to avoid vertical migration (see also Fault zone compartment)	The very low permeability of the Volpriehausen Sandstone on the other side of Fault 14 prevents lateral migration of CO2 out of the P18-2 reservoir. This implies that there is a very low likelihood that a small amount of CO2 migrates out of the reservoir.	A-3
Flow between P18-2 and P18-6 reservoirs	Over a small section across the fault zone between the P18-2 and P18-6 reservoirs, reservoir rocks of the Volpriehausen Sandstone are juxtaposed, which may lead to migration of CO2 from P18-2 to P18-6.	As the permeability of the Volpriehausen Sandstone is very low, the migration and pressure equilibration will be very slow. An assessment of the fault zone indicates that there is a very high probability of an impermeable gouge being present in the fault zone (Nieuwland, 2011). The pressure in P18-6 was at 378 bar before starting injection whereas at the same time pressure has dropped to about 100 bar in the producing P18-2 reservoir (June 2003). Apparently, this enormous pressure difference could exist indicating that there is virtually no flow and pressure equilibration between the two reservoirs on production time scales. Geological information indicates that compartment 2-IV, which is directly adjacent to the P18-6 reservoir is a separate hydraulic unit.		The pressure difference of about 278 bar between the two reservoirs, the very low permeability of the Volpriehausen Sandstone and the hydraulic isolation of compartment 2-IV show that the likelihood of a negligible amount of CO2 migrating from P18-2 to P18-6 is very low.	A-1

Low: Cont. improvement
Medium: ALARP
High: Intolerable

**Wells**

Well	Evaluation of integrity	Risk characterisation (before application of measures)	Risk classification (before application of measures)	Risk reduction measures	Risk characterisation (after application of measures)	Risk classification (after application of measures)
P18-02	P18-02 well is suspended and left with a mud line suspension in place to allow potential re-entry. The well is plugged at various depths with a total of 4 plugs. Several barrier elements for this suspended well could not be validated.	A medium likelihood that deficiencies in the cement bond and the quality of the plug will lead to migration out of the reservoir and partly out of the storage complex	C-3	Re-assessment of the cement and plug and restore the P&A plug integrity for CO2 storage conditions if needed	Re-assessment and adequate restoration of the plug integrity will prevent leakage of CO2. The likelihood is low that a negligible amount of CO2 will migrate out of the reservoir.	B-1
P18-2A-01	Information from available cement bond logs suggests poor casing-cement bond across part of 7" liner; production packer is set across a zone with poor bonding.	Low likelihood that CO2 migrates along the well and partly ends up outside the storage complex.	B-3	Replace packer in casing or liner section with good cement bond. After definite cessation of injection the well will be plugged according to existing p&a standards.	With the implementation of the proposed workover activities leakage from the well will be prevented. The likelihood is low that a negligible amount of CO2 will migrate out of the reservoir.	B-1
P18-2A-03/-S1/-S2	All primary and secondary barrier elements have been validated and thus pose no significant risk for CO2 leaking out of the well. Mother borehole and S1 do not end in reservoir and thus do not pose a problem for CO2 migration from the reservoir.	Low likelihood that CO2 migrates along the well and partly ends up outside the storage complex.	B-3	After definite cessation of injection the well will be plugged according to existing p&a standards.	With the implementation of the proposed workover activities leakage from the well will be prevented. The likelihood is low that a negligible amount of CO2 will migrate out of the reservoir.	B-1
P18-2A-05/-S1	The mother bore was drilled to about 200 m TVD above the reservoir. Then the well was side tracked. As the mother borehole does not end in reservoir, this does not increase the likelihood of CO2 migration out of the reservoir. Sustained casing pressure was measured in production casing.	Medium likelihood that a small amount of CO2 migrates along the well and ends up outside the storage complex	C-3	Investigate and if required repair source of sustained pressure in production casing. After definite cessation of injection the well will be plugged according to existing p&a standards.	With the implementation of the proposed risk reduction measures leakage from the well will be prevented. The likelihood is low that a negligible amount of CO2 will migrate out of the reservoir.	B-1
P18-2A-06/-S1	The producing reservoir formations from the side track and the mother bore connect at the side track window, which is not isolated.	Medium likelihood that a small amount of CO2 migrates along the well and ends up outside the storage complex	C-3	The integrity of the well barriers in the mother bore and the sidetrack window has to be restored. Most likely to be done by plug and abandonment (P&A) of the side track and installing a cemented scab or tie back liner to restore the mother bore integrity. After definite cessation of injection the well will be plugged according to existing p&a standards.	With the implementation of the proposed workover activities leakage from the well will be prevented. The likelihood is low that a negligible amount of CO2 will migrate out of the reservoir.	B-1
All anticipated injector wells: cooling	Injection of cold CO2 leads to the creation of a micro-annulus well at the casing-cement interface which may be enhanced by chemical interaction with CO2.	A medium likelihood exists that a small amount of CO2 migrates along the micro-annulus and partly ends up outside the storage complex.	C-3	Keeping the max average reservoir pressure below the hydrostatic pressure. Monitoring during operations and appropriate plugging after ceasing injection.	Low likelihood remains that a negligible amount of CO2 migrates out of the reservoir	B-1
All anticipated injector wells: status of casing in conductor	Condition of outer casing inside conductor may be reduced due to external corrosion and fatigue due to me to seismic movement. This may jeopardize the integrity of the primary and secondary well barriers.	A medium likelihood exists that a small amount of CO2 migrates along the micro-annulus and partly ends up outside the storage complex.	C-3	External surface casing corrosion log to confirm remaining load capacity of surface casing for CO2 injection load case and if necessary perform necessary workover activities	After the corrosion logging and optional workover activities leakage from the well will be prevented. The likelihood is low that a negligible amount of CO2 will migrate out of the reservoir.	B-1

Low: Cont. improvement
Medium: ALARP
High: Intolerable

# 19 Appendix D. Monitoring Plan

Table 19-1

No.	Parameter to be Monitored*	Proposed Technique adopted	Category of monitoring	Project phase and frequency	Location	Normal situation	Alert value	Contingency value
			Contingency Required (preliminary estimation) EU directive Mandatory according to	Pre-inj inj Post-inj Post-inj (abandonment) Long-term stewardship		Expectation value Accuracy	> Threshold 1 Action**	> Threshold 2 Contingency measures***
	<b>Injection proces</b>							
1	Injection rate	Flow meter	x	Cont	Near well head or Compressor station	Max rate = 285 ton CO2/uur (80 kg/s or 2.5 Mton CO2/year) and no fluctuations at constant pressure, expected value t.b.d.	Fluctuations at constant pressure or value above max. rate	Fluctuations at constant pressure or value above max. safety margins Find cause, solve problem and if necessary reduce injection until flow < threshold 1 value again
2	Injection stream CO2 concentration	Samples & analysis: online system	x	Cont or 1-3 hourly sampling combined with online analysis system Quarterly	Near well head or Compressor station	Defined % for the CO2 concentration of the stream	Allowed fluctuations reached	Above allowed fluctuations Adapt stream composition, reduce injection temporarily
3	Injection stream composition	Samples & analysis: Additional samples for calibration	x	Quarterly	Near well head or Compressor station	Defined % for the composition of the gas	Allowed fluctuations reached	Above allowed fluctuations Find cause, adapt stream composition, potentially reduce or stop injection temporarily
4	Water measurement	Water measurement	x	Cont	Near well head or Compressor station	Specification value	In case specification value is reached	In case value is above specification value and creates a safety issue Stop CO2 delivery, investigate at the CO2 provider, check dehydration system Stop CO2 delivery, investigate at the CO2 provider, check dehydration system
5	Discontinuous emissions through leakage, venting or incidents	Combination of techniques	x	Yearly	Potential leakage points like joints or ventstacks			Stop CO2 delivery, investigate at the CO2 provider, check dehydration system Stop CO2 delivery, investigate at the CO2 provider, check dehydration system

No.	Parameter to be Monitored*	Proposed Technique adopted	Category of monitoring	Project phase and frequency	Location	Normal situation	Alert value	Contingency value
			Mandatory according to EU directive	Pre-inj Inj Post-Inj (abandonment) Post-Inj (abandonment) Long-term stewardship	Expectation value Accuracy		> Threshold 1	> Threshold 2
			Contingency Required (preliminary estimation)					Contingency measures**
	<b>Well integrity</b>							
6	Annular pressure	Pressure device (with alarm value)	x	Baseline date prior to operations Continuously with remote system for online reading	At the well head	Constant pressure	Increase or decrease in pressure within safety margins Additional measurements like logging or sampling + analysis of fluids to detect CO2	Increase or decrease in pressure above safety margins Investigate causes (sampling) and options to remediate (in the extreme case well abandonment)
7	Well integrity	Wireline Logging (selection of tool: CBL, PMIT, EMIT, USIT, WAF, optical)	x	Baseline Every 5 years. If advanced technology is available, more measurements are aimed for.	Well	Measurements within the expected range	Measurements above expectation values Additional measurements (such as repeat) to corroborate observations, potentially seismic contingency measurements in case values large enough to be detected by seismic	Measurements significantly above expectation values Stop injection, additional measurements and seismic contingency measurements to identify shallow gas accumulations, investigate options to remediate (in the extreme case well abandonment)
8	Well head pressure	Pressure device	x	Baseline Continuous Continuous Continuous	At the well head (injection skid)	Measurements within the expected range, no large fluctuations expected at constant flow rates	Loss or increase of pressure with respect to expected values Additional measurements to determine the cause	No recovery of injection pressure after lowering or increasing injection flow Stop injection, investigate the cause and evaluate whether conditions are safe
9	Well head temperature	Temperature device	x	Baseline Continuous Continuous Continuous	At the well head (injection skid)	Determine operational limits for temperature range	In case temperature reaches the determined operational limits (high or low) Additional measurements to determine the cause	In case temperature reaches the determined operational limits Stop injection until the cause of the temperature change is clarified and safe
10	Plug integrity	Pressure test and inspection	x	Test during abandonment to assess the quality of the plug	In the well above the plug	No pressure changes	Minimal pressure changes Investigate cause with other measurements (e.g. check wellbore, fluid sample)	Significant pressure changes Redo the plug

No.	Parameter to be Monitored*	Proposed Technique adopted	Category of monitoring	Project phase and frequency	Location	Normal situation	Alert value	Contingency value
			Mandatory according to EU directive Required (preliminary estimation) Contingency	Pre-inj Inj Post-inj Post-inj (abandonment) Long-term stewardship		Expectation value Accuracy	> Threshold 1 Action**	> Threshold 2 Contingency measures**
	<b>Reservoir integrity</b>							
11	Reservoir pressure (FBHP) (see also line 8)	pressure device	(x)	Baseline data Cont. (TH cont. BH cont. or monthly in case memory gauges) Cont. (TH cont. BH cont. or monthly in case memory gauges) as long as the well is not suspended	Calculated from FTHP continuous, AND downhole permanent sensor (large risk of failure) OR downhole memory gauges	Flowing bottomhole pressure in agreement with simulations	Deviation from expected values Recalibration of the reservoir simulation model until satisfactory history match	Significant deviation from expected values Re-evaluate reservoir model, in case no explanation can be provided, stop injection
12	Reservoir Temperature (FBHT) (see also line 9)	thermometer or DTS	(x)	Baseline data Cont. (TH cont. BH cont. or monthly in case memory gauges) as long as the well is not suspended	Calculated from FHT AND potentially downhole permanent sensor /same	Flowing bottomhole temperature in agreement with well model	Deviation from expected values Recalibration of the well model until satisfactory history match	Significant deviation from expected values Re-evaluate well model, in case no explanation can be provided, stop injection
13	Stabilized pressure (CIBHP) (gradient) during shut-in period	pressure device combined with shut-in	x	Baseline data Every year Every year as long as the well is not suspended	Calculated from THP, AND permanent downhole sensor (large risk of failure) or downhole memory gauges, combined with shut-in	Pressure data in agreement with expected simulation model and P/z curve	Deviation from expected values Recalibration of the reservoir simulation model until satisfactory history match	Significant deviation from expected values Re-evaluate reservoir model, in case no explanation can be provided, stop injection
14	Stabilised temperature (CIBHT) (gradient) during shut-in period	thermometer or DTS combined with shut-in	x	Baseline data Every year Every year as long as the well is not suspended	DTS for permanent installation or memory gauges combined with shut-in AND if available in monitoring well	Temperature data in agreement with expected well model	Deviation from expected values Recalibration of the well model until satisfactory history match	Significant deviation from expected values Re-evaluate well model, in case no explanation can be provided, stop injection
15	Suspected leakage	Surface seismic survey	x	Baseline data Other monitoring indicates leakage Only when other monitoring indicates leakage Only when other monitoring indicates leakage Survey can be considered for the transfer of liability	Marine vessel (seismic acquisition using streamers)	No changes in the presence of shallow gas pockets or gas chimneys	Shallow gas pockets Determine the origin of the gas	

No.	Parameter to be Monitored*	Proposed	Category of	Project phase and frequency					Location	Normal situation	Alert value		Contingency value
				Pre-inj	Inj	Post-Inj (abandonment)	Post-Inj (stewardship)	Accuracy			> Threshold 1	> Threshold 2	
Environmental monitoring													
16	Pockmarks at the seabottom	Multi-beam echosounding	Mandatory according to EU directive Required (preliminary estimation) Contingency	Pre-inj	Inj	Post-Inj (abandonment)	Post-Inj (stewardship)	Marine vessel	No pockmarks	Expectation value	> Threshold 1	> Threshold 2	Contingency measures***
17	Presence of shallow gas or gas chimneys in the subsurface	Baseline seismic data	x	Baseline	Contingency	Contingency	Contingency	Marine vessel (seismic acquisition using streamers)	No bright spots or chimneys in the subsurface		Bright spots and/or gas chimneys	Bright spots and/or gas chimneys to the surface	Additional gas sampling + analysis to identify the origin of potential seepage or leakage. In case of leakage, identify the pathway with time-lapse seismic data. Mitigation to potential leaks.
18	Migration pathways for gas in the shallow subsurface	Time-lapse seismic data acquisition (2D or 3D)	x	Contingency	Contingency	Contingency	Contingency	Marine vessel	No changes in bright spots or chimneys in the subsurface		Changes in bright spots and/or gas chimneys	Changes in bright spots and/or gas chimneys to the surface	Additional gas sampling + analysis to identify the origin of potential seepage or leakage. In case of leakage, identify the pathway with time-lapse seismic data. Mitigation to potential leaks.
19	CO2 in soil at pockmarks	Gas samples using vibrocore + lab analysis	x	Contingency	Contingency	Contingency	Contingency	Sampling from a marine vessel			In case of leakage detection at the seabottom by geophysical methods	In case of leakage detection at the seabottom by geophysical methods	Investigate origin of the gas, in case a leakage pathway is suspected, apply time-lapse seismic data
20	Bubble detection at wellhead	Acoustic bubble detector	x	Contingency	Contingency	Contingency	Contingency	Install at the seabottom	No bubbles		In case of few bubbles	Significant bubble stream	Well remediation (workover)
21	Microseismic monitoring	Permanent geophones or DAS in monitoring wells	x	Baseline data	Cont	Cont	Cont	Injection well at caprock and reservoir level	No large events in caprock or at faults (re-activation)		Large events in the caprock or at faults	Very large events in the caprock or at faults	If considered a safety issue then stop injection, additional measurements and seismic contingency measurements to identify shallow gas accumulations, evaluate whether injection can be continued safely

\*Follows from the risk assessment  
 \*\* t.b.d. by operator, examples are updating model, additional monitoring, ...  
 \*\*\* t.b.d. by operator, examples are stop injection, back-production, well workover, contingency monitoring



